USGS
science for a changing world

Techniques of Water-Resources Investigations
of the United States Geological Survey

CHAPTER D1

APPLICATION OF SURFACE GEOPHYSICS TO GROUND-WATER INVESTIGATIONS

By A. A. R. Zohdy, G. P. Eaton,
and D. R. Mabey

BOOK 2
COLLECTION OF ENVIRONMENTAL DATA

DEPARTMENT OF THE INTERIOR
MANUEL LUJAN, Jr., *Secretary*

U.S. GEOLOGICAL SURVEY
Dallas L. Peck, *Director*

First printing 1974
Second printing 1980
Third printing 1984
Fourth printing 1990

UNITED STATES GOVERNMENT PRINTING OFFICE: 1974

For sale by the Books and Open-File Reports Section, U.S. Geological Survey,
Federal Center, Box 25425, Denver, CO 80225

PREFACE

The series of manuals on techniques describes procedures for planning and executing specialized work in water-resources investigations. The material is grouped under major subject headings called "Books" and further subdivided into sections and chapters. Section D of Book 2 is on surface geophysical methods.

The unit of publication, the chapter, is limited to a narrow field of subject matter. This format permits flexibility in revision and publication as the need arises. "Application of surface geophysics to ground-water investigations" is the first chapter to be published under Section D of Book 2.

CONTENTS

FIGURES

Metric Units of Measurement

Many of the analyses and compilations in this report were made in metric units of measurements. The equivalent English units are given in the text and illustrations where appropriate. To convert metric units to English units, the following conversion factors should be used:

Metric units	Conversion factor	English units
Length in centimeters (cm) ----	×0.394	=inches
in meters (m) ----	×3.281	=feet
in kilometers (km) ----	×0.6214	=miles
Area in square kilometers (km^2) ----	×0.386	= square miles
Slope in meters per kilometer (m/km) ----	×5.28	=feet per mile

APPLICATION OF SURFACE GEOPHYSICS TO GROUND-WATER INVESTIGATIONS

By A. A. R. Zohdy, G. P. Eaton, and D. R. Mabey

Abstract

This manual reviews the standard methods of surface geophysics applicable to ground-water investigations. It covers electrical methods, seismic and gravity methods, and magnetic methods.

The general physical principles underlying each method and its capabilities and limitations are described. Possibilities for non-uniqueness of interpretation of geophysical results are noted. Examples of actual use of the methods are given to illustrate applications and interpretation in selected geohydrologic environments.

The objective of the manual is to provide the hydrogeologist with a sufficient understanding of the capabilities, limitations, and relative cost of geophysical methods to make sound decisions as to when use of these methods is desirable. The manual also provides enough information for the hydrogeologist to work with a geophysicist in designing geophysical surveys that differentiate significant hydrogeologic changes.

Introduction

This manual is a brief review of the standard methods of surface geophysical exploration and their application in ground-water investigations. It explains the capabilities of exploration geophysics and, in a general way, the methods of obtaining, processing, and interpreting geophysical data. A minimum of mathematics is employed, and the scope is limited to an elementary discussion of theory, a description of the methods, and examples of their applications. It is in no sense intended as a textbook on applied geophysics. Rather its aim is to provide the hydrogeologist with a rudimentary understanding of how surface geophysical measurements may be of help to him. Many of the standard methods of geophysical exploration are described, but those used most extensively in ground-water investigations are stressed. The rapidly developing techniques of geophysical exploration involving measurements in the microwave, infrared, and ultraviolet portions of the electromagnetic spectrum are not included. The application of these "remote sensors" to ground-water investigations is in an early stage of development and testing; thus, their eventual importance cannot be appraised at this time. Borehole geophysical techniques will not be discussed here except as they relate to surface or airborne surveys.

In the discussions that follow each of the major geophysical methods will be briefly described with emphasis on the applications and limitations in ground-water investigations. A few examples of successful application of each method will be described.

Design of Geophysical Surveys

Geophysical surveys can be useful in the study of most subsurface geologic problems. Geophysics also can contribute to many investigations that are concerned primarily with surface geology. However, geophysical surveys are not always the most effective method of obtaining the information needed. For example, in some areas auger or drill

holes may be a more effective way of obtaining near-surface information than geophysical surveys. In some investigations a combination of drilling and geophysical measurements may provide the optimum cost-benefit ratio. Geophysical surveys are not practical in all ground-water investigations, but this determination usually can be made only by someone with an understanding of the capabilities, limitations, and costs of geophysical surveys.

A clear definition of the geologic or hydrologic problem and objectives of an investigation is important in determining whether exploration geophysics should be used and also in designing the geophysical survey. The lack of a clear definition of the problem can result in ineffective use of geophysical methods. The proper design of a geophysical survey is important not only in insuring that the needed data will be obtained but also in controlling costs, as the expense of making a geophysical survey is determined primarily by the detail and accuracy required.

Collection and Reduction of Geophysical Data

Some simple geophysical surveys can be made by individuals with little previous experience and with an investment in equipment of only a few hundred dollars. Other surveys require highly skilled personnel working with complex and expensive equipment. Good equipment and technical expertise are essential to a high quality survey. Attempts to use obsolete or "cook-book" interpretation methods in geophysical surveys often increase the total cost of the survey and result in an inferior product.

Some geophysical data can be used directly in geologic interpretations. Other geophysical data require considerable processing before the data can be interpreted, and the cost of data reduction is a major part of the total cost of the survey. Many data processing operations in use today require the use of electronic computers.

Interpretation

Interpretation of geophysical data can be completely objective or highly subjective. It can range from a simple inspection of a map or profile to a highly sophisticated operation involving skilled personnel and elaborate supporting equipment. Some interpretations require little understanding of the geology, but the quality of most interpretations is improved if the interpreter has a good understanding of the geology involved. Although some individuals are both skilled geophysicists and geologists, a cooperative effort between geologists and geophysicists is usually the most effective approach to the interpretation of geophysical data.

The Literature of Exploration Geophysics

The science, technology, and art of geophysical exploration have undergone explosive growth in the last two decades and with this growth has come an increasing degree of specialization in all subdisciplines of the field. The literature indicates an increasing trend in this direction and the geologist or engineer interested in applications of geophysics to problems with which he is concerned is faced with a growing array of books and periodicals. With the idea that interested readers of this manual may want to pursue specific subjects, a list of the more readily available texts and periodicals published in English follows. Some of them date back as many as 30 years, and parts of these are outdated. Nevertheless, much of the theory presented in them is still valid today.

Elementary Textbooks of a General Nature

Dobrin, M. B., 1960, Introduction to Geophysical Prospecting: Second ed., McGraw-Hill Book Co., Inc., New York, 446 p.

Eve, A. S., and Keys, D. A., 1956, Applied Geophysics in the Search for Minerals: Fourth ed., Cambridge University Press, London, 382 p.

Griffiths, D. H., and King, R. F., 1965, Applied Geophysics for Engineers and Geologists: Pergamon Press, London, 223 p.

Nettleton, L. L., 1940, Geophysical Prospecting for Oil: McGraw-Hill Book Co., Inc., New York, 444 p.

Parasnis, D. S., 1962, Principles of Applied Geophysics: Methuen, London, 176 p.

Advanced Textbooks of a General Nature

Grant, F. S., and West, G. F., 1965, Interpretation Theory in Applied Geophysics: McGraw-Hill Book Co., Inc., New York, 581 p.

Heiland, C. A., 1940, Geophysical Exploration, Reprinted 1963: Hafner, New York, 1,013 p.

Jakosky, J. J., 1950, Exploration Geophysics: Second ed., Trija, Los Angeles, 1,195 p.

Landsberg, H. E., ed., Advances in Geophysics: vols. 1–13, Academic Press, New York.

Books Emphasizing the Electrical Methods

Bhattacharya, P. K., and Patra, H. P., 1968, Direct Current Geoelectric Sounding—Principles and Interpretation: Elsevier, Amsterdam, 135 p.

Hansen, D. A., Heinrichs, W. E., Jr., Holmer, R. C., MacDougall, R. E., Rogers, G. R., Sumner, J. S., and Ward, S. H., eds., 1967, Mining Geophysics, Vol. II, Theory, Chapter II: Soc. Explor. Geophysicists, Tulsa, 708 p.

Keller, G. V., and Frischknecht, F. C., 1966, Electrical Methods in Geophysical Prospecting: Pergamon Press, Oxford, 517 p.

Kunetz, Geza, 1966, Principles of Direct Current Resistivity Prospecting: Gebruder Bornträeger, Berlin, 103 p.

Books Emphasizing the Seismic Method

Dix, C. H., 1952, Seismic Prospecting for Oil: Harper, New York, 414 p.

Musgrave, A. W., ed., 1967, Seismic Refraction Prospecting: Soc. Explor. Geophyisists, Tulsa, 604 p.

Slotnick, M. M., 1959, Lessons in Seismic Computing: Soc. Explor. Geophysicists, Tulsa, 268 p.

White, J. E., 1965, Seismic Waves—Radiation, Transmission, and Attenuation: McGraw-Hill Book Co., Inc., New York, 302 p.

Books Emphasizing the Magnetic Method

Hansen, D. A., Heinrichs, W. E., Jr., Holmer, R. C., MacDougall, R. E., Rogers, G. R., Sumner, J. S., and Ward, S. H., eds., 1967, Mining Geophysics, Vol. II, Theory, Chapter III: Soc. Explor. Geophysicists, Tulsa, 708 p.

Nagata, Takesi, 1961, Rock Magnetism: Rev. ed., Maruzen, Tokyo, 350 p.

Case History Compilations

European Association of Exploration Geophysicists, 1958, Geophysical Surveys in Mining, Hydrological and Engineering Projects: European Association of Exploration Geophysicists, The Hague, The Netherlands, 270 p.

Lyons, P. L., ed., 1956, Geophysical Case Histories: Vol. II–1956, Soc. Explor. Geophysicists, Tulsa, 676 p.

Nettleton, L. L., ed., 1949, Geophysical Case Histories: Vol. 1–1948, Soc. Explor. Geophysicists, Tulsa, 671 p.

Woollard, G. P., and Hanson, G. F., 1954, Geophysical Methods Applied to Geologic Problems in Wisconsin: Univ. Wisconsin, Madison, 255 p.

Periodicals

"Geoexploration," published by the Elsevier Publishing Company, Amsterdam, The Netherlands.

"Geophysics," published by the Society of Exploration Geophysicists, Tulsa, Okla.

"Geophysical Abstracts," previously published by the U.S. Geological Survey, Washington, D.C. (Publication ceased in 1971)

"Geophysical Prospecting," published by the European Association of Exploration Geophysicists, The Hague, The Netherlands.

Electrical Methods

By A. A. R. Zohdy

The electrical properties of most rocks in the upper part of the Earth's crust are dependent primarily upon the amount of water in the rock, the salinity of the water, and the distribution of the water in the rock. Saturated rocks have lower resistivities than unsaturated and dry rocks. The higher the porosity of the saturated rock, the lower its resistivity, and the higher the salinity of the saturating fluids, the lower the resistivity. The presence of clays and conductive minerals also reduces the resistivity of the rock.

Two properties are of primary concern in the application of electrical methods: (1) the ability of rocks to conduct an electric current, and (2) the polarization which occurs when an electrical current is passed through them (induced polarization). The electrical conductivity of Earth materials can be studied by measuring the electrical potential distribution produced at the Earth's surface by an electric current that is passed through the Earth or by detecting the electromagnetic field produced by an alternating electric current that is introduced into the Earth. The measurement of natural electric potentials (spontaneous polarization, telluric currents, and streaming potentials) has also found application in geologic investigations. The principal methods using natural energy sources are (1) telluric current, (2) magnetotelluric, (3) spontaneous polarization, and (4) streaming potential.

Telluric Current Method

Telluric currents (Cagniard, 1956; Berdichevskii, 1960; Kunetz; 1957) are natural electric currents that flow in the Earth's crust in the form of large sheets, and that constantly change in intensity and in direction. Their presence is detected easily by placing two electrodes in the ground separated by a distance of about 300 meters (984 feet) or more and measuring the potential difference between them. The origin of these telluric currents is believed to be in the ionosphere and is related to ionospheric tidal effects and to the continuous flow of charged particles from the Sun which become trapped by the lines of force of the Earth's magnetic field.

If the ground in a given area is horizontally stratified and the surface of the basement rocks is also horizontal, then, at any given moment, the density of the telluric current is uniform over the entire area. In the presence of geologic structures, however, such as anticlines, synclines, and faults, the distribution of current density is not uniform over the area. Furthermore, current density is a vector quantity, and the vector is larger when the telluric current flows at right angles to the axis of an anticline than when the current flows parallel to the axis (fig. 1). By plotting these vectors we obtain ellipses over anticlines and synclines and circles where the basement rocks are horizontal. The longer axis of the ellipse is oriented at right angles to the axis of the geologic structure.

The measurement of telluric field intensity is relatively simple. Four electrodes, M, N, M′, and N′ are placed on the surface of the ground at the ends of two intersecting perpendicular lines (fig. 2), and the potential differences are recorded on a potentiometric chart recorder or on an x-y plotter (Yungul, 1968). From these measurements two components E_x and E_y of the telluric field can

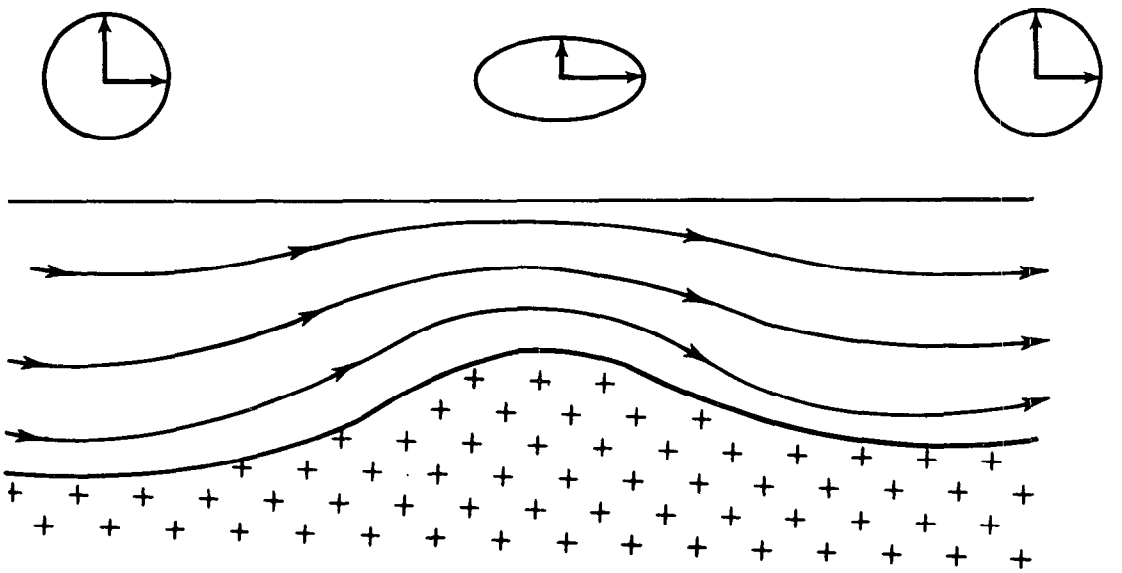

Figure 1.—Flow of telluric current over an anticline. Ellipse and circles indicate telluric field intensity as a function of direction with respect to axis of anticline.

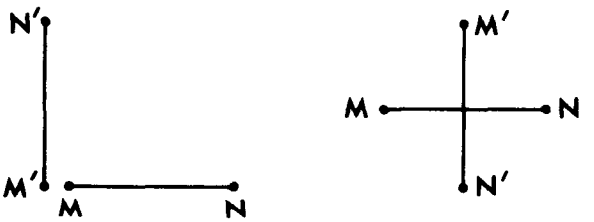

Figure 2.—Examples of electrode arrays for measuring x and y components of telluric field. M, M', N, and N' are potential electrodes.

be computed, and the total field obtained by adding E_x and E_y vectorially.

The intensity and direction of the telluric current field vary with time; therefore, measurements must be recorded simultaneously at two different stations to take into account this variation. One station is kept stationary (base station), and the other is moved to a new location in the field (field station) after each set of measurements. The ratio of the area of the ellipse at the field station to the area of a unit circle (Keller and Frischknecht, 1966) at the base station is calculated mathematically. When a contour map of equal elliptical areas is prepared (Migaux, 1946, 1948; Migaux and others, 1952; Migaux and Kunetz, 1955; Schlumberger, 1939) it reflects the major geologic structures of the basement rocks in very much the same manner as a gravity map or magnetic map. However, a telluric map (fig. 3) delineates rock structure based on differences in electrical resistivity rather than on differences in density or magnetic susceptibility.

Magneto-Telluric Method

The magneto-telluric method (Berdichevskii, 1960; Cagniard, 1953) of measuring resistivity is similar to the telluric current method but has the advantage of providing an estimate of the true resistivity of the layers. Measurements of amplitude variations in the telluric field E_x and the associated magnetic field H_y determine earth resistivity. Magneto-telluric measurements at several frequencies provide information on the variation of resistivity with depth because the depth of penetration of electromagnetic waves is a function of frequency. A limitation of the method is the instrumental difficulty of measuring rapid fluctuations of the magnetic field. Interpretation techniques usually involve comparisons of observed data with theoretical curves. The method is useful in exploration to depths greater than can be

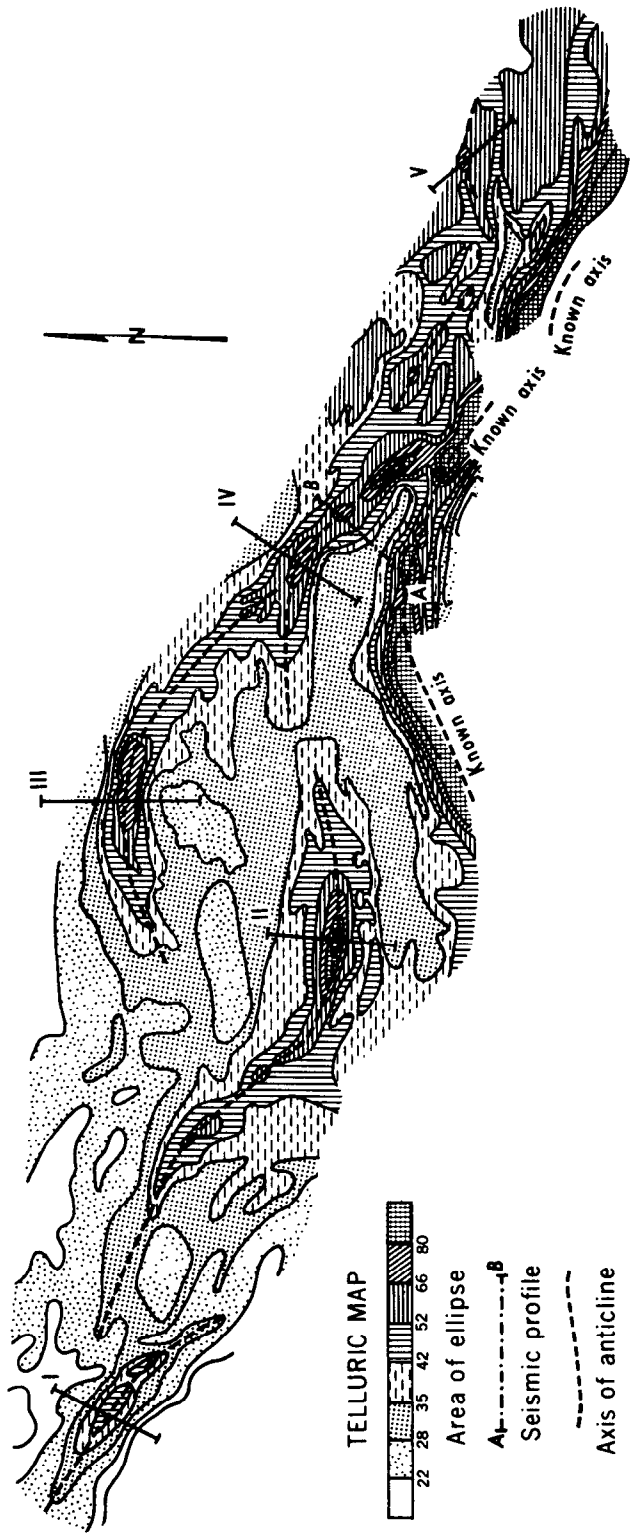

Figure 3.—Telluric map of the Aquitaine basin, France.

reached effectively by methods using artificially induced currents.

To the author's knowledge the telluric and magneto-telluric methods have not been used extensively in the Western Hemisphere; however, the methods have been used extensively in the Eastern Hemisphere by French and Russian geophysicists in petroleum exploration. The use of the methods in ground-water exploration is recommended at present only for reconnaissance of large basins.

Spontaneous Polarization and Streaming Potentials

Spontaneous polarization or self-potential methods involve measurement of electric potentials developed locally in the Earth by electro-chemical activity, electrofiltration activity, or both. The most common use of self-potential surveys has been in the search for ore bodies in contact with solutions of different compositions. The result of this contact is a potential difference and current flow which may be detected at the ground surface. Of more interest to ground-water investigations are the potentials generated by water moving through a porous medium (streaming potentials). Measurements of these potentials have been used to locate leaks in reservoirs and canals (Ogilvy and others, 1969).

Spontaneous potentials generally are no larger than a few tens of millivolts but in some places may reach a few hundred millivolts. Relatively simple equipment can be used to measure the potentials, but spurious sources of potentials often obscure these natural potentials. Interpretation is usually qualitative although some quantitative interpretations have been attempted.

Direct Current-Resistivity Method

In the period from 1912 to 1914 (Dobrin, 1960) Conrad Schlumberger began his pioneering studies which lead to an understanding of the merits of utilizing electrical resistivity methods for exploring the subsurface (Compagnie Générale de Géophysique, 1963). According to Breusse (1963), the real progress in applying electrical methods to ground-water exploration began during World War II. French, Russian, and German geophysicists are mainly responsible for the development of the theory and practice of direct-current electrical prospecting methods.

Definition and Units of Resistivity

It is well known that the resistance R, in ohms, of a wire is directly proportional to its length L and is inversely proportional to its cross-sectional area A. That is:

$$R \propto L/A,$$

or

$$R = \rho \frac{L}{A}, \qquad (1)$$

where ρ, the constant of proportionality, is known as the electrical resistivity or electrical specific resistance, a characteristic of the material which is independent of its shape or size. According to Ohm's law, the resistance is given by

$$R = \Delta V/I, \qquad (2)$$

where ΔV is the potential difference across the resistance and I is the electric current through the resistance.

Substituting equation 1 in equation 2 and rearranging we get

$$\rho = \frac{A}{L}\frac{\Delta V}{I}. \qquad (3)$$

Equation 3 may be used to determine the resistivity ρ of homogeneous and isotropic materials in the form of regular geometric shapes, such as cylinders, parallelopipeds, and cubes. In a semi-infinite material the resistivity at every point must be defined. If the cross-sectional area and length of an element within the semi-infinite material are shrunk to infinitesimal size then the resistivity ρ may be defined as

$$\rho = \frac{\lim_{L \to 0} (\Delta V/L)}{\lim_{A \to 0} (I/A)}$$

or

$$\rho = \frac{E_L}{J} \qquad (4)$$

where E_L is the electric field and J is the current density. To generalize, we write

$$\rho = \frac{E}{J}. \qquad (5)$$

Equation 5 is known as Ohm's law in its differential vectorial form.

The resistivity of a material is defined as being numerically equal to the resistance of a specimen of the material of unit dimensions. The unit of resistivity in the mks (meter-kilogram-second) system is the ohm-meter. In other systems it may be expressed in ohm-centimeter, ohm-foot, or other similar units.

Rock Resistivities

The resistivity ρ of rocks and minerals displays a wide range. For example, graphite has a resistivity of the order of 10^{-6} ohm-m, whereas some dry quartzite rocks have resistivities of more than 10^{12} ohm-m (Parasnis, 1962). No other physical property of naturally occurring rocks or soils displays such a wide range of values.

In most rocks, electricity is conducted electrolytically by the interstitial fluid, and resistivity is controlled more by porosity, water content, and water quality than by the resistivities of the rock matrix. Clay minerals, however, are capable of conducting electricity electronically, and the flow of current in a clay layer is both electronic and electrolytic. Resistivity values for unconsolidated sediments commonly range from less than 1 ohm-m for certain clays or sands saturated with saline water, to several thousand ohm-m for dry basalt flows, dry sand, and gravel. The resistivity of sand and gravel saturated with fresh water ranges from about 15 to 600 ohm-m. Field experience indicates that values ranging from 15 to 20 ohm-m are characteristic of aquifers in the southwestern United States, whereas in certain areas in California the resistivity of fresh-water bearing sands generally ranges from 100 to 250 ohm-m. In parts of Maryland resistivities have been found to range between about 300 and 600 ohm-m, which is about the same range as that for basaltic aquifers in southern Idaho. These figures indicate that the geophysicists should be familiar with the resistivity spectrum in the survey area before he draws conclusions about the distribution of fresh-water aquifers.

Principles of Resistivity Method

In making resistivity surveys a commutated direct current or very low frequency (<1 Hz) current is introduced into the ground via two electrodes. The potential difference is measured between a second pair of electrodes. If the four electrodes are arranged in any of several possible patterns, the current and potential measurements may be used to calculate resistivity.

The electric potential V at any point P caused by a point electrode emitting an electric current I in an infinite homogeneous and isotopic medium of resistivity ρ is given by

$$V = \frac{\rho I}{4\pi R}, \qquad (6)$$

where $R = \sqrt{x^2 + y^2 + z^2}$.

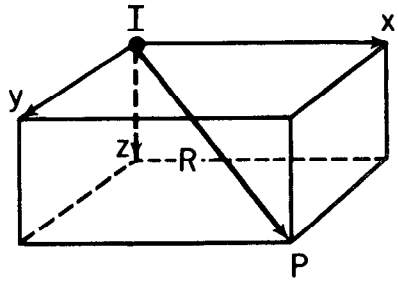

Figure 4.—Diagram showing the relationship between a point source of current I (at origin of coordinates) in an isotropic medium of resistivity ρ and the potential V at any point P. $V = \frac{\rho I}{4\pi R}$, where $R = \sqrt{x^2 + y^2 + z^2}$.

For a semi-infinite medium, which is the simplest Earth model, and with both current and potential point-electrodes placed at the Earth surface ($z = 0$), equation 6 reduces to

$$V = \frac{\rho I}{2\pi\sqrt{x^2 + y^2}} = \frac{\rho I}{2\pi \overline{AM}} \qquad (7)$$

where $\overline{AM}$ is the distance on the Earth surface between the positive current electrode A and the potential electrode M. When two current electrodes, A and B, are used and the potential difference, ΔV, is measured between two measuring electrodes M and N, we get

$V_M^A = \frac{\rho I}{2\pi}\frac{1}{\overline{AM}}$ = potential at M due to positive electrode A,

$V_N^A = \frac{\rho I}{2\pi}\frac{1}{\overline{AN}}$ = potential at N due to positive electrode A,

$V_M^B = \frac{\rho I}{2\pi}\frac{1}{\overline{BM}}$ = potential at M due to negative electrode B,

$V_N^B = \frac{\rho I}{2\pi}\frac{1}{\overline{BN}}$ = potential at N due to negative electrode B,

$V_M^{A,B} = \frac{\rho I}{2\pi}\left(\frac{1}{\overline{AM}} - \frac{1}{\overline{BM}}\right)$ = total potential at M due to A and B,

$V_N^{A,B} = \frac{\rho I}{2\pi}\left(\frac{1}{\overline{AN}} - \frac{1}{\overline{BN}}\right)$ = total potential at N due to A and B,

and, therefore, the net potential difference is:

$$\Delta V_{MN}^{A,B} = V_M^{A,B} - V_N^{A,B} =$$

$$\frac{\rho I}{2\pi}\left(\frac{1}{\overline{AM}} - \frac{1}{\overline{BM}} - \frac{1}{\overline{AN}} + \frac{1}{\overline{BN}}\right). \qquad (8)$$

Rearranging equation 8, we express the resistivity ρ by:

$$\rho = \left(\frac{2\pi}{\frac{1}{\overline{AM}} - \frac{1}{\overline{BM}} - \frac{1}{\overline{AN}} + \frac{1}{\overline{BN}}}\right)\frac{\Delta V}{I}. \qquad (9)$$

Equation 9 is a fundamental equation in direct-current (d-c) electrical prospecting.

The factor $\dfrac{2\pi}{\frac{1}{\overline{AM}} - \frac{1}{\overline{BM}} - \frac{1}{\overline{AN}} + \frac{1}{\overline{BN}}}$ is called the geometric factor of the electrode arrangement and generally is designated by the letter K. Therefore,

$$\rho = K\frac{\Delta V}{I}. \qquad (10)$$

If the measurement of ρ is made over a semi-infinite space of homogeneous and isotropic material, then the value of ρ computed from equation 9 will be the true resistivity of that material. However, if the medium is inhomogeneous and (or) anisotropic then the resistivity computed from equation 9 is called an apparent resistivity $\bar{\rho}$.

The value of the apparent resistivity is a function of several variables: the electrode spacings $\overline{AM}$, $\overline{AN}$, $\overline{BM}$, and $\overline{BN}$, the geometry of the electrode array, and the true resistivities and other characteristics of the subsurface materials, such as layer thicknesses, angles of dip, and anisotropic properties. The apparent resistivity, depending on the electrode configuration and on the geology, may be a crude average of the true resistivities in the section, may be larger or smaller than any of the true resistivities, or may even be negative (Al'pin, 1950; Zohdy, 1969b).

Electrode Configurations

The value of $\bar{\rho}$ (eq. 9) depends on the four distance-variables $\overline{AM}$, $\overline{AN}$, $\overline{BM}$, and $\overline{BN}$. If $\bar{\rho}$ is made to depend on only one distance-variable the number of theoretical curves can be greatly reduced. Several electrode arrays have been invented to fulfill this goal.

Wenner Array

This well-known array was first proposed for geophysical prospecting by Wenner (1916). The four electrodes A, M, N, and B are placed at the surface of the ground along a straight line (fig. 5) so that $\overline{AM} = \overline{MN} = \overline{NB} = a$.

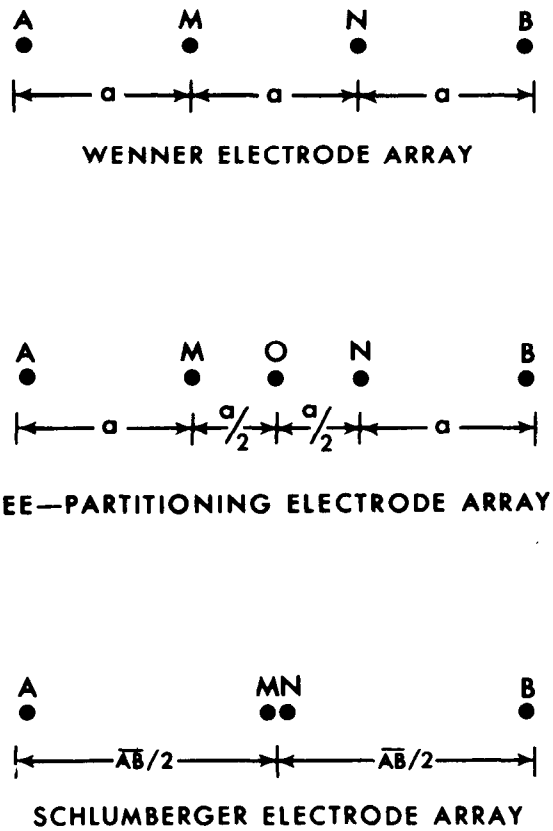

Figure 5.—Wenner, Lee-partitioning, and Schlumberger electrode arrays. A and B are current electrodes, M, N, and O are potential electrodes; a and $\overline{AB}/2$ are electrode spacings.

For the Wenner array, equation 9 reduces to:

$$\bar{\rho}_w = 2\pi a \frac{\Delta V}{I}. \qquad (11)$$

Thus the resistivity $\bar{\rho}_w$ is a function of the single distance-variable, a. The Wenner array is widely used in the Western Hemisphere.

Lee-Partitioning Array

This array is the same as the Wenner array, except that an additional potential electrode O is placed at the center of the array between the potential electrodes M and N. Measurements of the potential difference are made between O and M and between O and N. The formula for computing the Lee-partitioning apparent resistivity is given by

$$\bar{\rho}_{L.P.} = 4\pi a \frac{\Delta V}{I}$$

where ΔV is the potential difference between O and M or O and N. This array has been used extensively in the past (Van Nostrand and Cook, 1966).

Schlumberger Array

This array is the most widely used in electrical prospecting. Four electrodes are placed along a straight line on the Earth surface (fig. 5) in the same order, AMNB, as in the Wenner array, but with $\overline{AB} \geqq 5\overline{MN}$. For any linear, symmetric array AMNB of electrodes, equation 9 can be written in the form:

$$\bar{\rho} = \pi \frac{(\overline{AB}/2)^2 - (\overline{MN}/2)^2}{\overline{MN}} \frac{\Delta V}{I}, \qquad (12)$$

but if $\overline{MN} \to 0$, then equation 12 can be written as

$$\bar{\rho}_s = \pi (\overline{AB}/2)^2 \frac{E}{I} \qquad (13)$$

where $E = \lim_{\overline{MN} \to 0} \frac{\Delta V}{\overline{MN}}$ = electric field.

Conrad Schlumberger defined the resistivity in terms of the electric field E rather than the potential difference ΔV (as in the Wenner array). It can be seen from equation 13 that the Schlumberger apparent resistivity $\bar{\rho}_s$ is a function of a single distance-variable $(\overline{AB}/2)$. In practice it is possible to measure $\bar{\rho}_s$ according to equation 13, but only in an approximate manner. The apparent resistivity $\bar{\rho}_s$ usually is calculated by using equation 12 provided that $\overline{AB} \geqq 5\overline{MN}$ (Deppermann, 1954).

Dipole-Dipole Arrays

The use of dipole-dipole arrays in electrical prospecting has become common since the 1950's, particularly in Russia, where Al'pin (1950) developed the necessary theory. In a dipole-dipole array, the distance between the current electrodes A and B (current dipole) and the distance between the potential

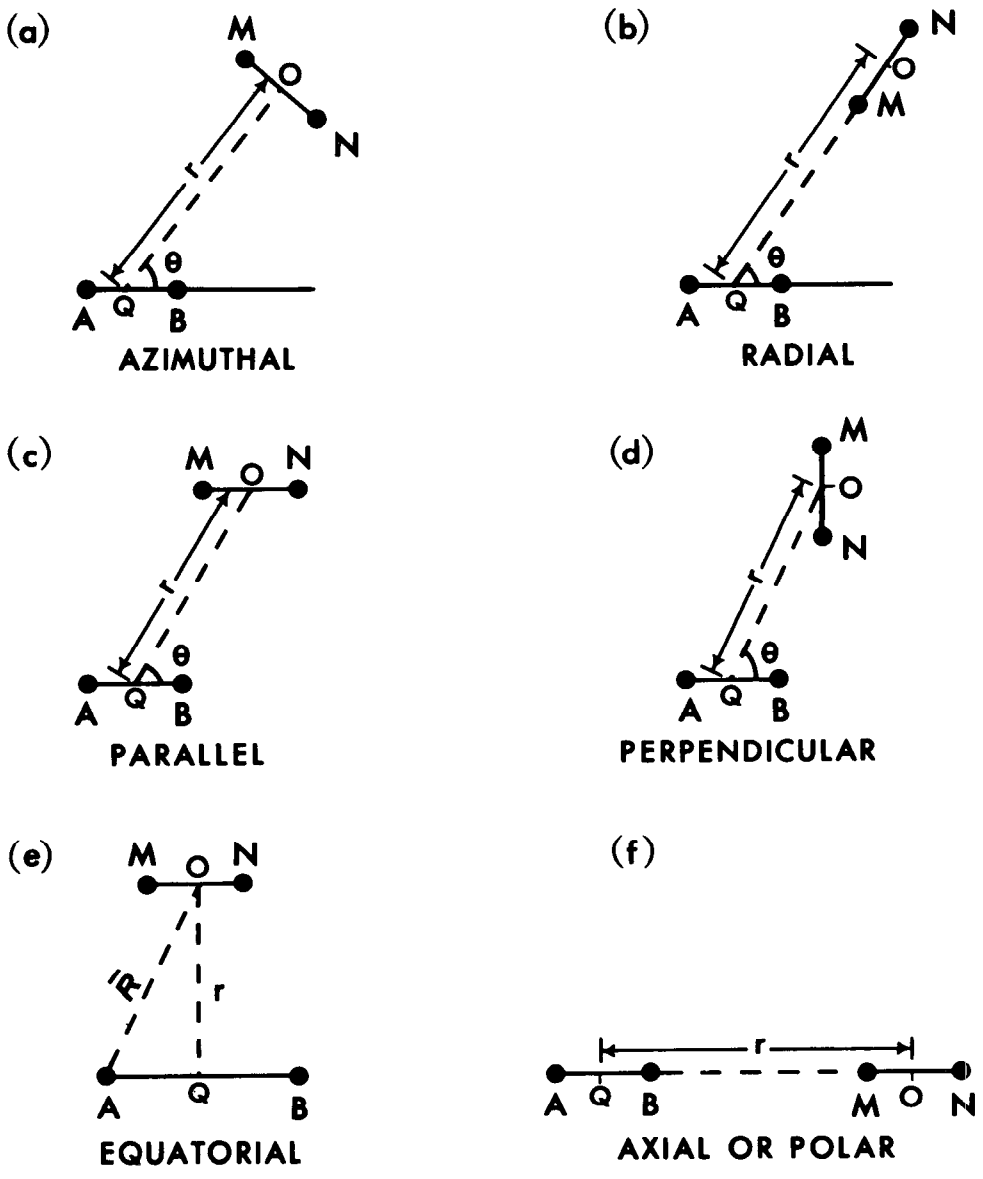

Figure 6.—Dipole-dipole arrays. The equatorial is a bipole-dipole array because AB is large.

electrodes M and N (measuring dipole) are significantly smaller than the distance r, between the centers of the two dipoles. Figure 6 (a, b, c, and d) shows the four basic dipole-dipole arrays that are recognized: azimuthal, radial, parallel, and perpendicular. When the azimuth angle θ formed by the line r and the current dipole AB equals $\frac{\pi}{2}$, the azimuthal array and the parallel array reduce to the equatorial array, and when $\theta = 0$ the parallel and radial arrays reduce to the polar (or axial) array. It can be shown (Al'pin, 1950; Bhattacharya and Patra, 1968; Keller and Frischknecht, 1966) that the electric field due to a dipole at a given point is inversely proportional to the cube of the distance r and that for a given azimuth angle θ the value of the apparent resistivity $\overline{\rho}$ is a function of the single distance-variable r.

Of the various dipole-dipole arrays, the equatorial array in its bipole-dipole form ($\overline{AB}$

is large and $\overline{MN}$ is small) has been used more often than the other dipole-dipole arrays. By enlarging the length of the current dipole, that is, by making it a bipole, the electric current required to generate a given potential difference ΔV at a given distance r from the center of the array, is reduced. Furthermore the apparent resistivity remains a function of the single distance variable, $\overline{R} = \sqrt{(\overline{AB}/2)^2 + r^2}$, (Berdichevskii and Petrovskii, 1956). The equatorial array has been used extensively by Russian geophysicists in petroleum exploration (Berdichevskii and Zagarmistr, 1958). Recently it has been used in ground-water investigations in the United States (Zohdy and Jackson, 1968 and 1969; Zohdy, 1969a).

Electrical Sounding and Horizontal Profiling

Electrical sounding is the process by which depth investigations are made, and horizontal profiling is the process by which lateral variations in resistivity are detected. However, the results of electrical sounding and of horizontal profiling often are affected by both vertical and horizontal variations in the electrical properties of the ground.

If the ground is comprised of horizontal, homogeneous, and isotropic layers, electrical sounding data represent only the variation of resistivity with depth. In practice, however, the electrical sounding data are influenced by both vertical and horizontal heterogeneities. Therefore, the execution, interpretation, and presentation of sounding data should be such that horizontal variations in resistivity can be distinguished easily from vertical ones.

The basis for making an electrical sounding, irrespective of the electrode array used, is that the farther away from a current source the measurement of the potential, or the potential difference, or the electric field is made, the deeper the probing will be. It has been stated in many references on geophysical prospecting that the depth of probing depends on how far apart two current electrodes are placed, but this condition is not necessary for sounding with a dipole-dipole array. Furthermore, when sounding with a Wenner or Schlumberger array, when the distance between the current electrodes is increased, the distance between the current and the potential electrodes, at the center of the array, is increased also. It is this latter increase that actually matters.

In electrical sounding with the Wenner, Schlumberger, or dipole-dipole arrays, the respective electrode spacing a, $\frac{\overline{AB}}{2}$, or r, is increased at successive logarithmic intervals and the value of the appropriate apparent resistivity, $\overline{\rho}_w$, $\overline{\rho}_s$, or $\overline{\rho}_D$, is plotted as a function of the electrode spacing on logarithmic-coordinate paper. The curve of $\overline{\rho} = f\left(a, \frac{\overline{AB}}{2}, \text{or } r\right)$ is called an electrical sounding curve.

In horizontal profiling, a fixed electrode spacing is chosen (preferably on the basis of studying the results of electrical soundings), and the whole electrode array is moved along a profile after each measurement is made. The value of apparent resistivity is plotted, generally, at the geometric center 0 of the electrode array. Maximum apparent resistivity anomalies are obtained by orienting the profiles at right angles to the strike of the geologic structure. The results are presented as apparent resistivity profiles (fig. 7) or apparent resistivity maps (fig. 8), or both. In making horizontal profiles it is recommended that at least two different electrode spacings be used, in order to aid in distinguishing the effects of shallow geologic structures from the effects of deeper ones (fig. 9). In figure 9, the effect of shallow geologic features is suppressed on the profile made with the larger spacing, whereas the effect of deeper features is retained.

In certain surveys, the two current electrodes may be placed a large distance apart (1—6 km) and the potential electrodes moved along the middle third of the line AB. This method of horizontal profiling has been

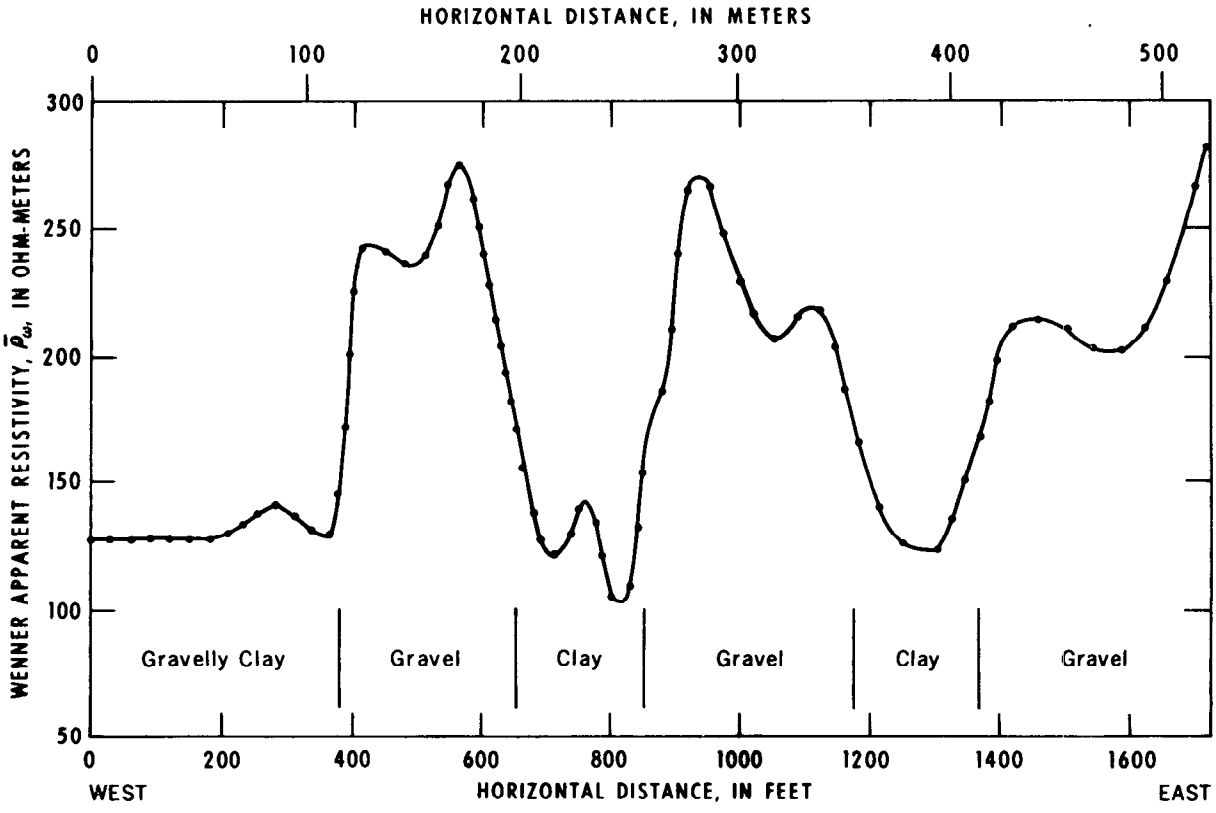

Figure 7.—Horizontal profile and interpretations over a shallow gravel deposit in California (Zohdy, unpub. data, 1964; Zohdy, 1964) using Wenner array at a = 9.15 meters.

called the Schlumberger AB profile (Kunetz, 1966; Lasfargues, 1957); in Canada and in parts of the United States it is referred to sometimes as the "Brant array" (fig. 10a). A modification of this procedure where the potential electrodes are moved not only along the middle third of the line AB but also along lines laterally displaced from and parallel to AB (fig. 10b) is called the "Rectangle of Resistivity Method" (Breusse and Astier, 1961; Kunetz, 1966). The lateral displacement of the profiles from the line AB may be as much as $\frac{\overline{AB}}{4}$.

Another horizontal profiling technique, used by many mining geophysicists, has been given the name "dipole-dipole" method, although it does not approximate a true dipole-dipole. The lengths of the current and potential "dipoles" are large in comparison to the distance between their centers. This arrangement introduces an extra variable in the calculation of theoretical curves and makes quantitative interpretation of the results difficult.

Practically all types of the common electrode arrays have been used in horizontal profiling, including pole-dipole (Hedstrome, 1932; Logn, 1954) and dipole-dipole arrays (Blokh, 1957 and 1962).

The interpretation of horizontal profiling data is generally qualitative, and the primary value of the data is to locate geologic structures such as buried stream channels, veins, and dikes. Quantitative interpretation can be obtained by making a sufficient number of profiles with different electrode spacings and along sets of traverses of different azimuths. Best interpretative results are obtained generally from a combination of horizontal profiling and electrical sounding data.

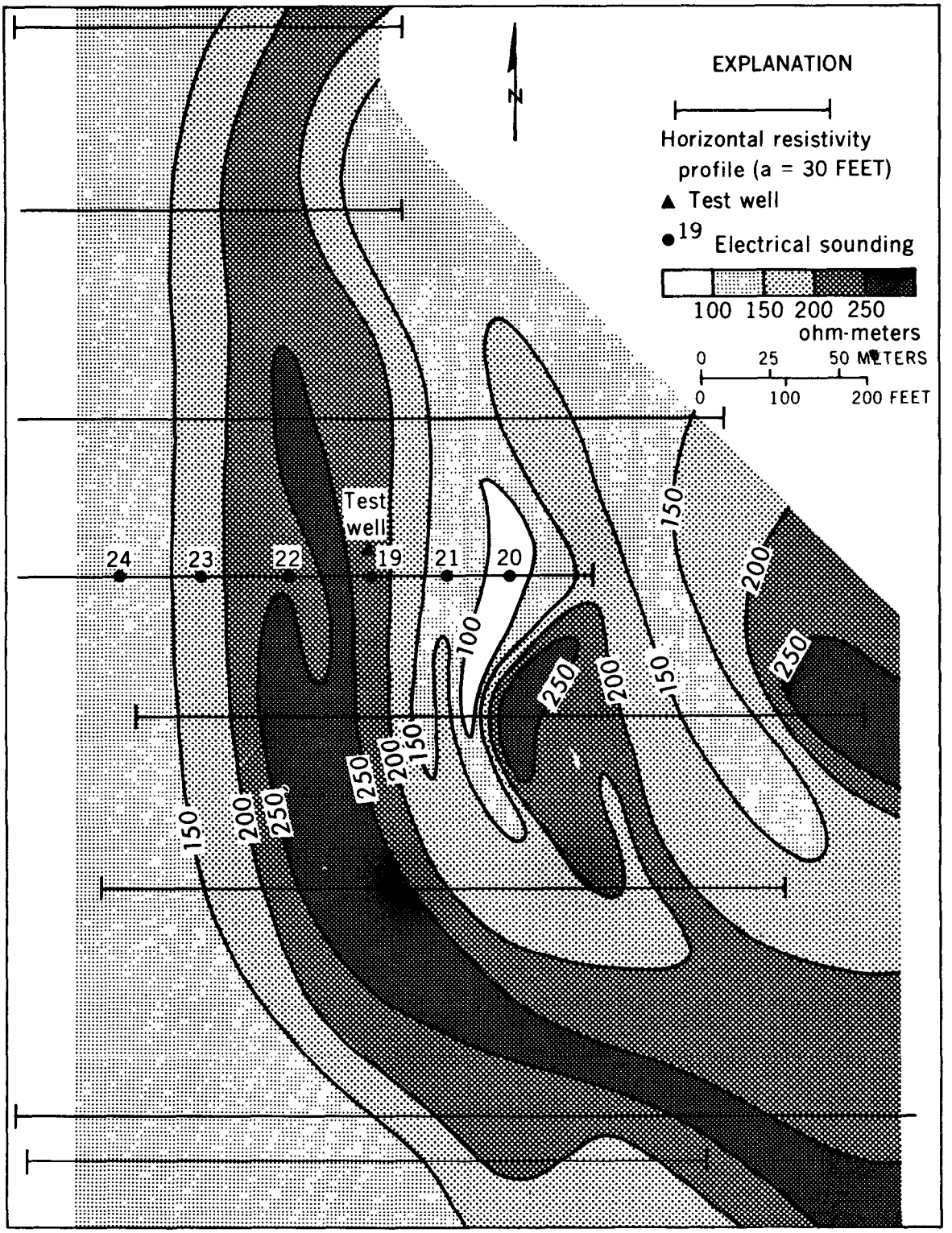

Figure 8.—Apparent-resistivity map near Campbell, Calif. Unpublished data obtained by Zohdy (1964) using Wenner array. Crosshatched areas are buried stream channels containing thick gravel deposits. Stippled areas are gravelly clay deposits.

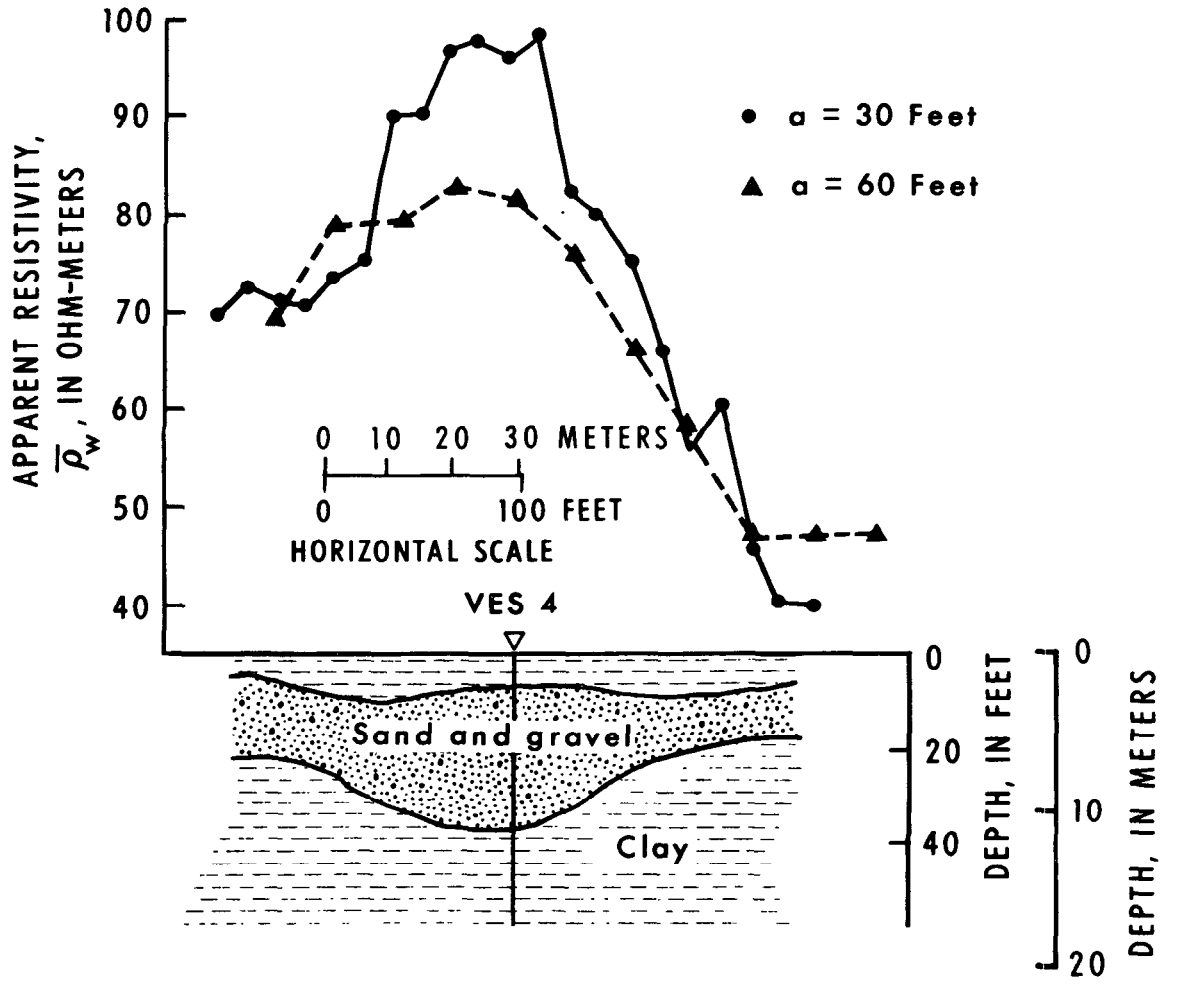

Figure 9.—Horizontal profiles over a buried stream channel using two electrode spacings: a = 9.15 meters (30 feet) and a = 18.3 meters (60 feet) (after Zohdy, 1964). VES 4 marks the location of an electrical sounding used to aid in the interpretation of the profiles.

Comparison of Wenner, Schlumberger, and Dipole-Dipole Measurements

The Schlumberger and the Wenner electrode arrays are the two most widely used arrays in resistivity prospecting. There are two essential differences between these arrays: (1) In the Schlumberger array the distance between the potential electrodes $\overline{MN}$ is small and is always kept equal to, or smaller than, one-fifth the distance between the current electrodes $\overline{AB}$; that is, $\overline{AB} \geq 5\overline{MN}$. In the Wenner array $\overline{AB}$ is always equal to $3\overline{MN}$. (2) In a Schlumberger sounding, the potential electrodes are moved only occasionally, whereas in a Wenner sounding they and the current electrodes are moved after each measurement.

As a direct consequence of these two differences the following facts are realized:

1. Schlumberger sounding curves portray a slightly greater probing depth and resolving power than Wenner sounding curves for equal AB electrode spacing. The maximum and the minimum values of apparent resistivity on a theoretical Schlumberger curve ($\overline{MN} \rightarrow 0$) appear on the sounding

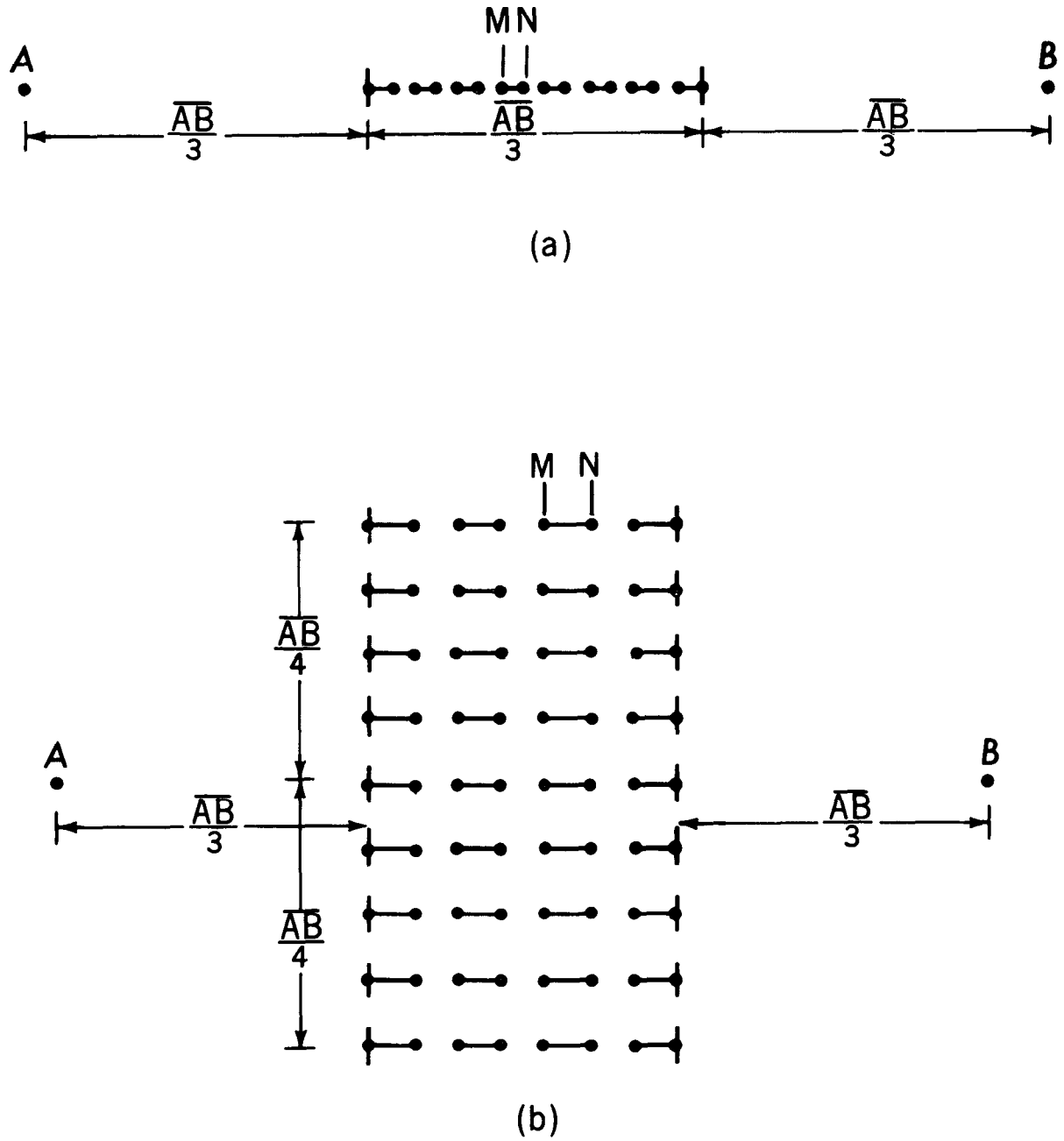

Figure 10.—Electrode arrays, for (a) Schlumberger $\overline{AB}$ profile, also called Brant array and (b) rectangle of resistivity.

curve at shorter electrode spacings and are slightly more accentuated than on a Wenner curve (fig. 11). This fact was proved theoretically by Depperman (1954), discussed by Unz (1963), and practically illustrated by Zohdy (1964). A true comparison between the two types of sounding curves is made by standardizing the electrode spacing for the two arrays; that is, both apparent resistivities $\overline{\rho}_w$ and $\overline{\rho}_s$ should be plotted as a function of $\overline{AB}/2$, or $\overline{AB}/3$, or $\overline{AB}$.

2. The manpower and time required for mak-

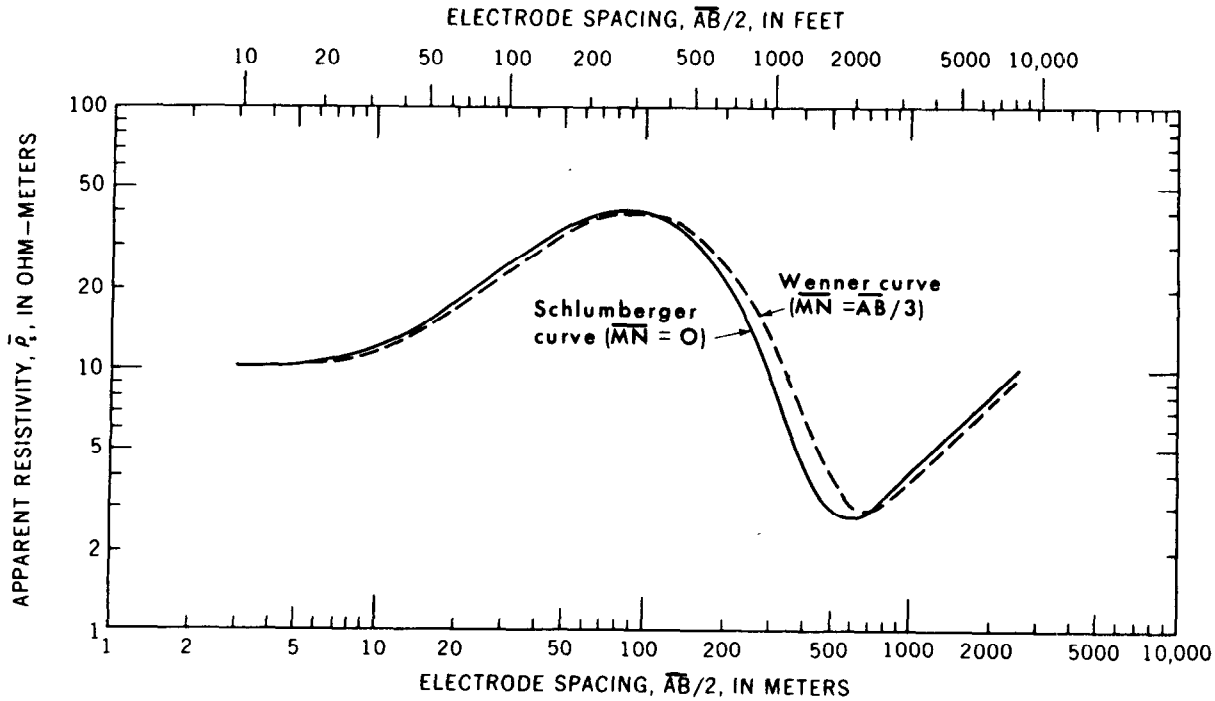

Figure 11.—Comparison between four-layer Schlumberger and Wenner sounding curves. Electrode spacing is $\overline{AB}/2$ for both curves.

ing Schlumberger soundings are less than that required for making Wenner soundings.

3. Stray currents in industrial areas and telluric currents that are measured with long spreads affect measurements made with the Wenner array more readily than those made with the Schlumberger array.
4. The effects of near-surface, lateral inhomogeneities are less apt to affect Schlumberger measurements than Wenner measurements. Furthermore, the effect of lateral variations in resistivity are recognized and corrected more easily on a Schlumberger curve than on a Wenner curve.
5. A drifting or unstable potential difference is created upon driving two metal stakes into the ground. This potential difference, however, becomes essentially constant after about 5–10 minutes. Fewer difficulties of this sort are encountered with the Schlumberger array than with the Wenner array.
6. A Schlumberger sounding curve, as opposed to a theoretical curve, is generally discontinuous. The discontinuities result from enlarging the potential electrode spacing after several measurements. This type of discontinuity on the Schlumberger sounding field curve is considered as another advantage over Wenner sounding field curves, because if the theoretical assumption of a horizontally stratified laterally homogeneous and isotropic Earth is valid in the field, then the discontinuities should occur in a theoretically prescribed manner (Depperman, 1954). The Schlumberger curve then can be rectified and smoothed accordingly as shown in figure 12. Any deviation of the Schlumberger sounding field curve from the theoretically prescribed pattern of discontinuities would indicate lateral inhomogeneities or errors in measurements. The effect of lateral inhomogeneities on a Schlumberger curve can be removed by shifting the displaced segments of the curve upward or downward to where they should be in relation to the other segments of the curve. Such information is usually unobtainable from Wenner sounding curves and there is no systematic way of smoothing the ob-

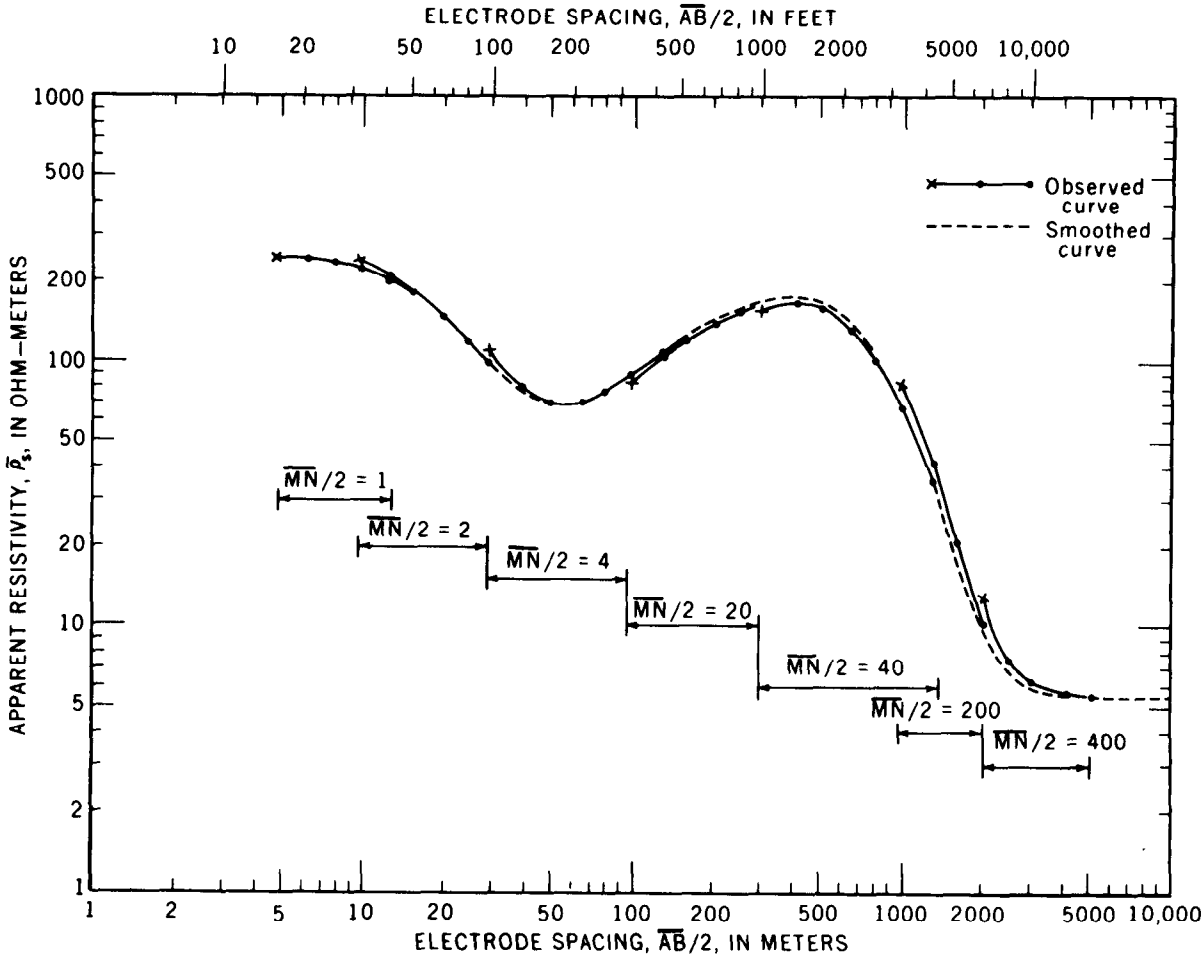

Figure 12.—Correct displacements on a Schlumberger sounding curve and method of smoothing.

served data. With the Lee-partitioning method, it is possible to obtain an indication of lateral changes in subsurface conditions or of errors in measurements, but there is no simple method that would reduce the observed data so that it would correspond to a horizontally homogeneous Earth.

The advantages of the Wenner array are limited to the following: (1) The relative simplicity of the apparent resistivity formula $\bar{\rho}_w = 2\pi a\ (\Delta V/I)$, (2) the relatively small current values necessary to produce measurable potential differences, and (3) the availability of a large album of theoretical master curves for two-, three-, and four-layer Earth models (Mooney and Wetzel, 1956).

The above comparison indicates that it is advantageous to use the Schlumberger array rather than the Wenner array for making electrical resistivity soundings. The use of the Schlumberger array is recommended not only because of the above listed advantages but also, and perhaps more important, because the interpretation techniques are developed more fully and they are more diversified for Schlumberger sounding curves than for Wenner sounding curves.

With the invention of dipole-dipole arrays and their use in the Soviet Union and the United States, their following advantages over the Schlumberger array became recognized: (1) Relatively short AB and MN lines are used to explore large depths, which reduces field labor and increases productivity, (2) problems of current leakage (Dakhnov, 1953; Zohdy, 1968b) are reduced to a mini-

mum, (3) bilateral investigations are possible and therefore more detailed information on the direction of dip of electrical horizons is obtainable, and (4) problems of inductive coupling and associated errors are minimized.

Among the disadvantages of dipole methods are: (1) The requirement of a large generator to provide ample amounts of current, especially in deep exploration, and (2) special knowledge and special theoretical developments and materials are required to interpret most of the data obtained by dipole-dipole arrays. Generally one cannot use the experience gained in using Schlumberger or Wenner arrays to obtain or to interpret dipole sounding data in a straightforward way.

Problem of Defining Probing Depth

A favorite rule-of-thumb in electrical prospecting is that the electrode spacing is equal to the depth of probing. This rule-of-thumb is wrong and leads to erroneous interpretations. Its origin probably stems from the fact that when using direct current in probing a homogeneous and isotropic semi-infinite medium, there is a definite relation between the spacing $\overline{AB}$ separating the current electrodes and the depth to which any particular percentage of the current penetrates. For example, 50 percent of the current penetrates to a depth equal to $\overline{AB}/2$ and 70 percent to a depth equal to $\overline{AB}$. Therefore the greater the current electrode separation, the greater the amount of current that penetrates to a given depth. This relation is governed by the equation (Weaver, 1929; Jakosky, 1950)

$$I_z/I_t = \frac{2}{\pi} \tan^{-1}(2z/\overline{AB}),$$

where I_z = current confined between depth 0 and z,

I_t = total current penetrating the ground, and

$\overline{AB}$ = distance separating current electrodes.

This current-depth relation for a homogeneous and isotropic Earth cannot be used as a general rule-of-thumb to establish a so-called "depth of penetration" or "probing depth" that also applies to a stratified or an inhomogeneous Earth. For an inhomogeneous medium the percentage of the total current that penetrates to a given depth z depends not only upon the electrode separation but also upon the resistivities of the Earth layers. This fact was discussed by Muskat (1933), Muskat and Evinger (1941), Evjen (1944), Orellana (1960), 1961), and others. Furthermore, the above relation does not include the apparent resistivity nor the true resistivity (or resistivities) of the medium. Consequently it is of no value in interpreting apparent resistivity data. In fact, in resistivity interpretation we do not care about the percentage of current that penetrates to a given depth or the percentage of current that exists at a given distance as long as we can make measurements of the total current I_t and of the potential difference ΔV from which the apparent resistivity can be calculated.

Many investigators, however, still use the above rule-of-thumb in making their interpretations, with variable degrees of fortuitous success and more often failure. Perhaps this rule-of-thumb is of some value when the geophysicist has to decide on an electrode spacing for horizontal profiling over a buried structure, but a better choice can be made after making a few soundings in the area.

Advantages of Using Logarithmic Coordinates

Electrical sounding data should be plotted on logarithmic coordinates with the electrode spacing on the abscissa and the apparent resistivity on the ordinate. The advantages of plotting the sounding data on logarithmic coordinates are:

1. Field data can be compared with precalculated theoretical curves for given

Earth models (curve-matching procedure).

2. The form of an electrical sounding curve does not depend on the resistivity and thickness of the first layer provided that the ratios $\frac{\rho_2}{\rho_1}, \frac{\rho_3}{\rho_1}, \ldots, \frac{\rho_n}{\rho_1}$, and the ratios $\frac{h_2}{h_1}, \frac{h_3}{h_1}, \ldots, \frac{h_n}{h_1}$, remain constant from model to model, where $\rho_1, \rho_2, \rho_3, \ldots, \rho_n$, are the resistivities and $h_1, h_2, h_3, \ldots, h_n$, are the thicknesses of the first, second, third, and n^{th} layers, respectively. When the absolute values of ρ and h change but the ratios $\frac{\rho_i}{\rho_1}$ and $\frac{h_i}{h_1}$, where $i = 2, 3, \ldots, n$, remain constant, the position of the curve is merely displaced vertically for changes in ρ, and horizontally for changes in h (fig. 13). Consequently, two curves with different values of ρ, and h, (but with the same values of $\frac{\rho_2}{\rho_1}$ and $\frac{h_2}{h_1}$) can be superposed by translating one curve on top of the other (while the ordinate and abscissa axes remain parallel). This is the essence of the curve-matching method. Furthermore, in the computation of theoretical sounding curves the thickness and resistivity

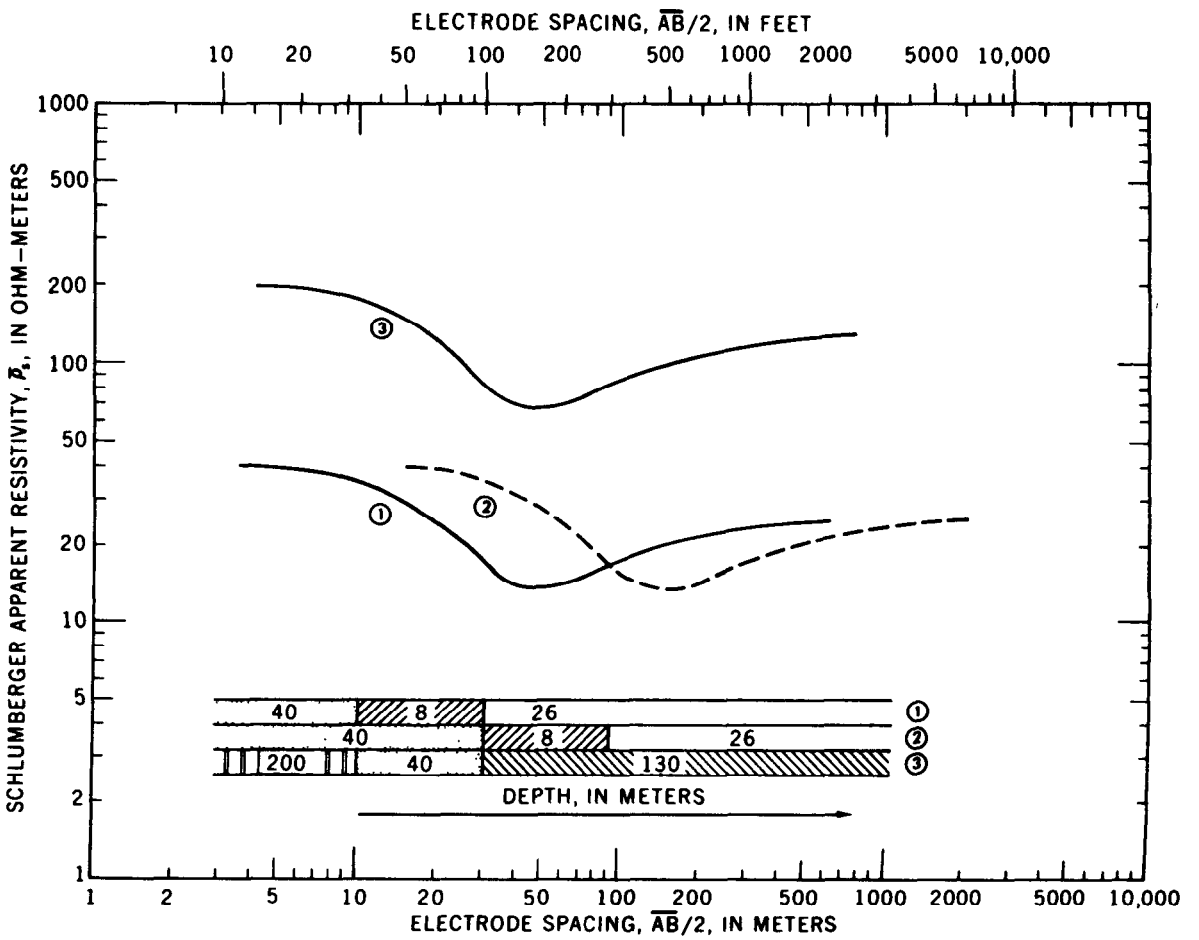

Figure 13.—Logarithmic plot of sounding curves. The layers in model 2 are three times as thick as model 1; the layer resistivities in model 3 are five times as large as model 1; however, the shapes of all three curves are identical.

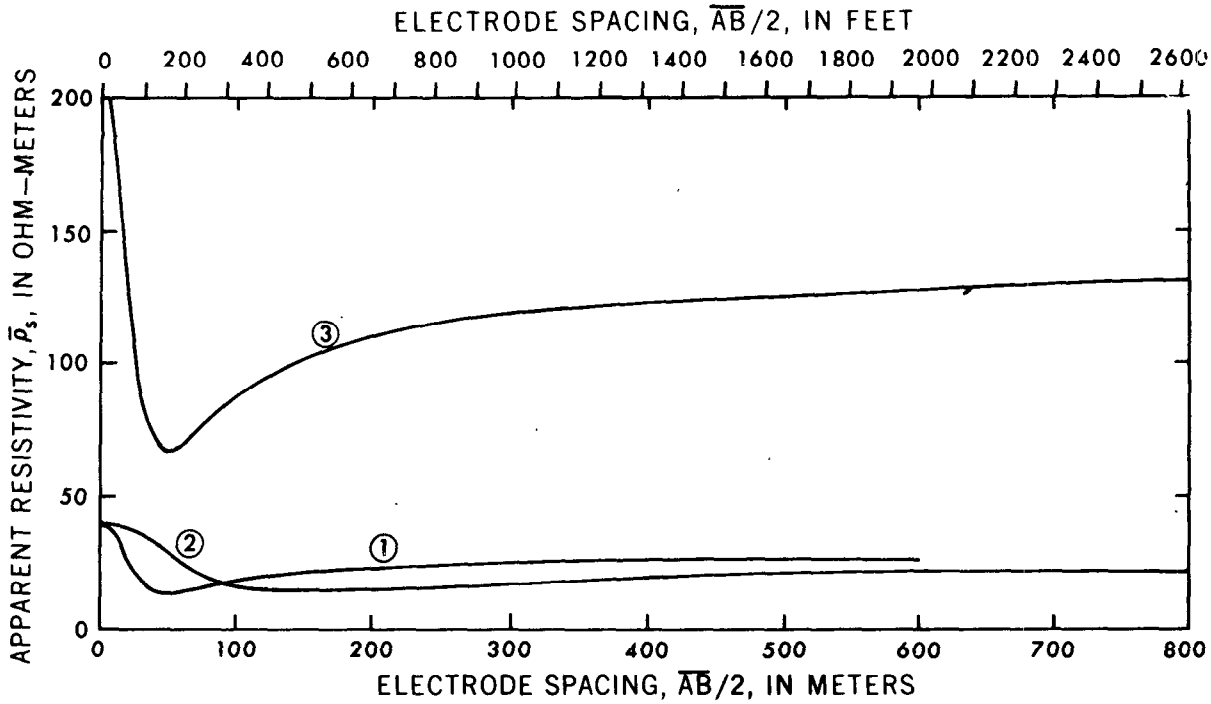

Figure 14.—Linear plot of sounding curves. Earth models are the same as in figure 13. Curve form is not preserved.

of one of the layers can be assumed equal to unity, which eliminates two parameters in the calculation of a sounding curve for a given Earth model.

When sounding curves are plotted on linear coordinates, the form, as well as the position, of the curve varies as a function of ρ_1 and h_1, even when the ratios $\frac{\rho_2}{\rho_1}$ and $\frac{h_2}{h_1}$ remain constant (fig. 14).

3. The use of logarithmic coordinates, on the one hand, suppresses the effect of variations in the thickness of layers at large depths, and it also suppresses variations of high resistivity values. On the other hand, it enhances the effect of variations in the thickness of layers at shallow depths, and it enhances the variations of low resistivity values. These properties are important because the determination of the thickness of a layer to within ±10 meters (±32.8 feet) when that layer is at a depth of several hundred meters is generally acceptable, whereas a precision to within one meter is desirable when the layer is at a depth of only a few tens of meters. Similarly, the determination of the resistivity of a conductive layer (less than about 20 ohm-m) to the nearest ohm-m is necessary for determining its thickness accurately, whereas for a resistive layer (more than about 200 ohm-m), the determination of its resistivity to within one ohm-m is unimportant.
4. The wide spectrum of resistivity values measured under different field conditions and the large electrode spacings necessary for exploring the ground to moderate depths make the use of logarithmic coordinates a logical choice.

Geoelectric Parameters

A geologic section differs from a geoelectric section when the boundaries between geologic layers do not coincide with the boundaries between layers characterized by

different resistivities. Thus, the electric boundaries separating layers of different resistivities may or may not coincide with boundaries separating layers of different geologic age or different lithologic composition. For example, when the salinity of ground water in a given type of rock varies with depth, several geoelectric layers may be distinguished within a lithologically homogeneous rock. In the opposite situation layers of different lithologies or ages, or both, may have the same resistivity and thus form a single geoelectric layer.

A geoelectric layer is described by two fundamental parameters: its resistivity ρ_i and its thickness h_i, where the subscript i indicates the position of the layer in the section ($i = 1$ for the uppermost layer). Other geoelectric parameters are derived from its resistivity and thickness. These are:

1. Longitudinal unit conductance, $S_i = h_i/\rho_i$,
2. Transverse unit resistance, $T_i = h_i\rho_i$,
3. Longitudinal resistivity, $\rho_L = h_i/S_i$,
4. Transverse resistivity, $\rho_t = T_i/h_i$, and
5. Anisotropy, $\lambda = \sqrt{\rho_t/\rho_L}$.

For an isotropic layer $\rho_t = \rho_L$ *and* $\lambda = 1$. These secondary geoelectric parameters are particularly important when they are used to describe a geoelectric section consisting of several layers.

For n layers, the total longitudinal unit conductance is

$$S = \sum_{i=1}^{n} \frac{h_i}{\rho_i} = \frac{h_1}{\rho_1} + \frac{h_2}{\rho_2} + \ldots \frac{h_n}{\rho_n};$$

the total transverse unit resistance is

$$T = \sum_{i=1}^{n} h_i\rho_i = h_1\rho_1 + h_2\rho_2 + \ldots + h_n\rho_n;$$

the average longitudinal resistivity is

$$\rho_L = \frac{H}{S} = \frac{\sum_{1}^{n} h_i}{\sum_{1}^{n} \frac{h_i}{\rho_i}};$$

the average transverse resistivity is

$$\rho_t = \frac{T}{H} = \frac{\sum_{i}^{n} h_i\rho_i}{\sum_{i}^{n} h_i};$$

and the anisotropy is

$$\lambda = \sqrt{\frac{\rho_t}{\rho_L}} = \frac{\sqrt{TS}}{H}.$$

The parameters S, T, ρ_L, ρ_t, and λ are derived from consideration of a column of unit square cross-sectional area (1×1 meter) cut out of a group of layers of infinite lateral extent (fig. 15). If current flows vertically only through the column, then the layers in the column will behave as resistors connected in series, and the total resistance of the column of unit cross-sectional area will be:

$$R = R_1 + R_2 + R_3 + \ldots + R_n,$$

or

$$R = \rho_1 \frac{h_1}{1\times1} + \rho_2 \frac{h_2}{1\times1} + \ldots + \rho_n \frac{h_n}{1\times1} = \sum_{i}^{n} \rho_i h_i = T.$$

The symbol T is used instead of R to indicate that the resistance is measured in a direction transverse to the bedding and also because

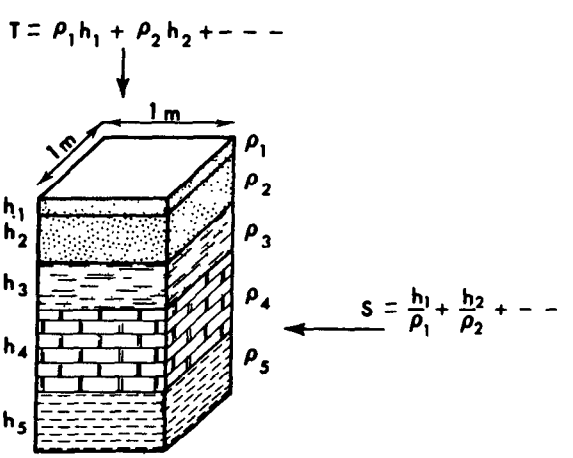

Figure 15.—Columnar prism used in defining geoelectric parameters of a section. Patterns are arbitrary. ρ = resistivity, h = thickness, S = total longitudinal conductance, T = total transverse resistance.

the dimensions of this "unit resistance" are usually expressed in ohm-m^2 instead of ohms.

If the current flows parallel to the bedding, the layers in the column will behave as resistors connected in parallel and the conductance will be

$$S = \frac{1}{R} = \frac{1}{R_1} + \frac{1}{R_2} + \ldots + \frac{1}{R_n},$$

or

$$S = \frac{1 \times h_1}{\rho_1 \times 1} + \frac{1 \times h_2}{\rho_2 \times 1} + \ldots + \frac{1 \times h_n}{\rho_n \times 1} = \frac{h_1}{\rho_1} + \frac{h_2}{\rho_2} + \ldots + \frac{h_n}{\rho_n}.$$

The dimensions of the longitudinal unit conductance are m/ohm-m = 1/ ohm = mho. It is interesting to note that the quantity $S_i = \frac{h_i}{\rho_i} = \sigma_i h_i$, where σ_i is the conductivity (inverse of resistivity), is analogous to transmissivity $T_i = K_i b_i$ used in ground-water hydrology, where K_i is the hydraulic conductivity of the i^{th} layer and b_i is its thickness.

The parameters T and S were named the "Dar Zarrouk" parameters by Maillet (1947).

In this manual we shall refer to T and S as the transverse resistance and the longitudinal conductance; the word "unit" is omitted for brevity.

In the interpretation of multilayer electrical sounding curves, the evaluation of S or T is sometimes all that can be determined uniquely. There are simple graphical methods for the determination of these parameters from sounding curves. The study of the parameters S, T, ρ_L, ρ_t, and λ is an integral part of the analysis of electrical sounding data and also is the basis of important graphical procedures (for example, the auxiliary point method) for the interpretation of electrical sounding curves (Kalenov, 1957; Orellana and Mooney, 1966; Zohdy, 1965).

Types of Electrical Sounding Curves Over Horizontally Stratified Media

The form of the curves obtained by sounding over a horizontally stratified medium is a function of the resistivities and thicknesses of the layers, as well as of the electrode configuration.

Homogeneous and isotropic medium.—If the ground is composed of a single homogeneous and isotropic layer of infinite thickness and finite resistivity then, irrespective of the electrode array used, the apparent resistivity curve will be a straight horizontal line whose ordinate is equal to the true resistivity ρ_1 of the semi-infinite medium.

Two-layer medium.—If the ground is composed of two layers, a homogeneous and isotropic first layer of thickness h_1 and resistivity ρ_1, underlain by an infinitely thick substratum ($h_2 = \infty$) of resistivity ρ_2, then the sounding curve begins, at small electrode spacings, with a horizontal segment ($\bar{\rho} \cong \rho_1$). As the electrode spacing is increased, the curve rises or falls depending on whether $\rho_2 > \rho_1$ or $\rho_2 < \rho_1$, and on the electrode configuration used. At electrode spacings much larger than the thickness of the first layer, the sounding curve asymptotically approaches a horizontal line whose ordinate is equal to ρ_2. The electrode spacing at which the apparent resistivity $\bar{\rho}$ asymptotically approaches the value ρ_2 depends on three factors: the thickness of the first layer h_1, the value of the ratio ρ_2/ρ_1, and the type of electrode array used in making the sounding measurements.

The dependence of the electrode spacing on the thickness of the first layer is fairly obvious. The larger the thickness of the first layer, the larger the spacing required for the apparent resistivity to be approximately equal to the resistivity of the second layer. This is true for any given electrode array and for any given resistivity ratio. However, for most electrode arrays, including the conventional Schlumberger, Wenner, dipole equatorial and dipole polar arrays, when $\rho_2/\rho_1 > 1$, larger electrode spacings are required for $\bar{\rho}$ to be approximately equal to ρ_2 than when $\rho_2/\rho_1 < 1$. Figure 16 shows a comparison between two Schlumberger sounding curves obtained over two-layer Earth models in which $h_1 = 1$ meter (3.28 feet), $\rho_2/\rho_1 = 10$, and $\rho_2/\rho_1 = 0.1$. Figure 17 shows the dif-

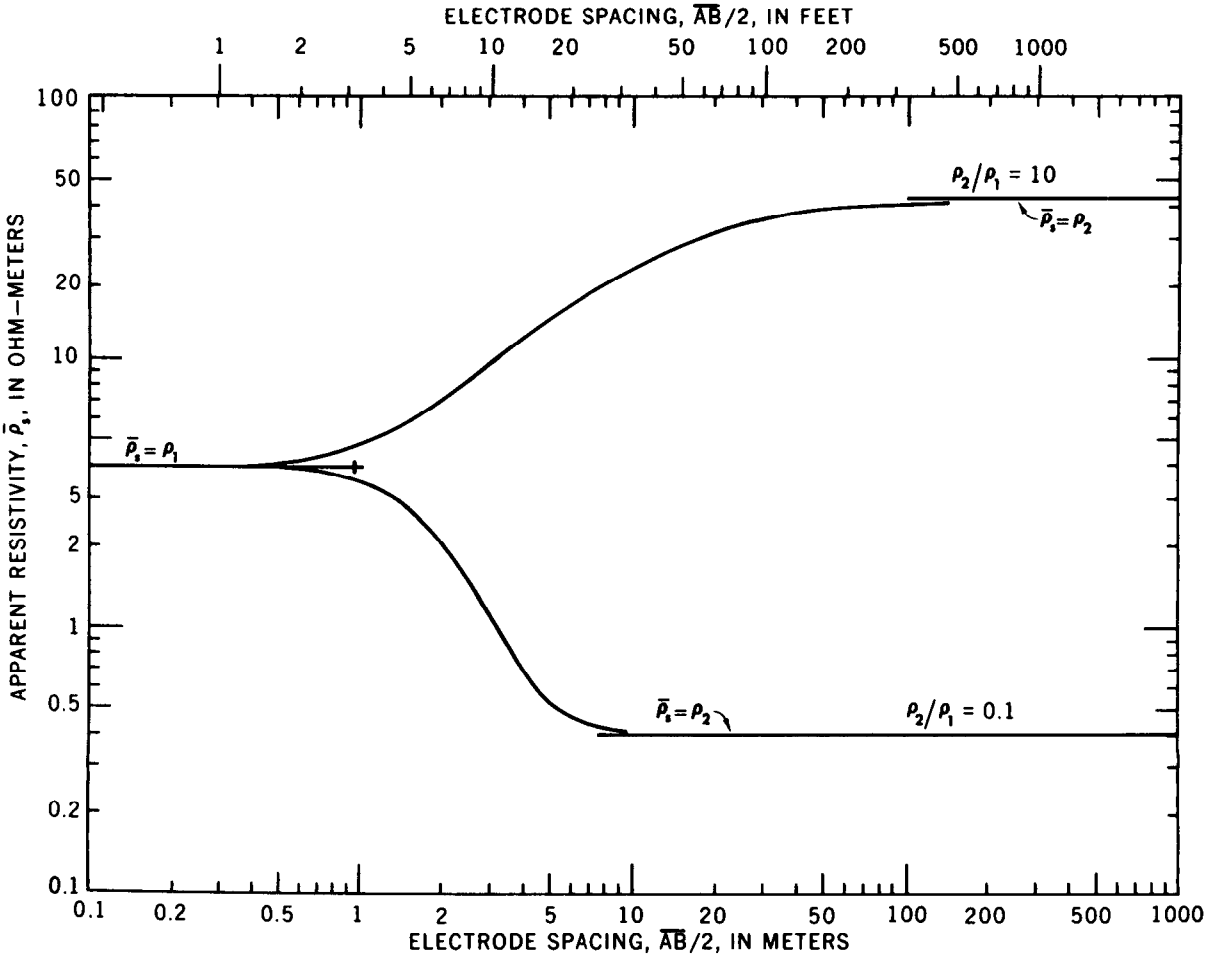

Figure 16.—Comparison between two-layer Schlumberger curves for $\rho_2/\rho_1 = 10$ and 0.1; $h_1 = 1$ meter (3.28 feet) for both curves.

ference in the form of sounding curves, and the asymptotic approach of $\bar{\rho}$ to ρ_1 and to ρ_2 as a function of electrode array for $h_1 = 1$ meter, $\rho_2/\rho_1 = 9$, and $\rho_2/\rho_1 = 0.2$. The comparison is made between equatorial and polar-dipole sounding curves.

Three-layer medium.—If the ground is composed of three layers of resistivities ρ_1, ρ_2, and ρ_3, and thicknesses h_1, h_2, *and* $h_3 = \infty$, the geoelectric section is described according to the relation between the values of ρ_1, ρ_2, and ρ_3. There are four possible combinations between the values of ρ_1, ρ_2, and ρ_3. These are:

$\rho_1 > \rho_2 < \rho_3$ ____H-type section,
$\rho_1 < \rho_2 < \rho_3$ ___A-type section,
$\rho_1 < \rho_2 > \rho_3$ ____K-type section,
$\rho_1 > \rho_2 > \rho_3$ ____Q-type section.

The use of the letters H, A, K, and Q to describe the relation between ρ_1, ρ_2, and ρ_3 in the geoelectric section is very convenient and also is used to describe the corresponding sounding curves. For example, we talk about an H-type electrical sounding curve to indicate that it is obtained over a geoelectric section in which $\rho_1 > \rho_2 < \rho_3$. H-, A-, K-, and Q-type Schlumberger sounding curves are shown in figure 18.

Multilayer-medium.— If the ground is composed of more than three horizontal layers of resistivities ρ_1, ρ_2, ρ_3, . . . ρ_n and thicknesses h_1, h_2, h_3, . . . $h_n = \infty$, the geoelectric section is described in terms of relationship between the resistivities of the layers, and the letters H, A, K, and Q are

used, in combination, to indicate the variation of resistivity with depth. In four-layer geoelectric sections, there are eight possible relations between ρ_1, ρ_2, ρ_3, and ρ_4:

$\rho_1 > \rho_2 < \rho_3 < \rho_4$ ----HA-type section,
$\rho_1 > \rho_2 < \rho_3 > \rho_4$ ----HK-type section,
$\rho_1 < \rho_2 < \rho_3 < \rho_4$ ----AA-type section
$\rho_1 < \rho_2 < \rho_3 > \rho_4$ ----AK-type section,
$\rho_1 < \rho_2 > \rho_3 < \rho_4$ ----KH-type section,
$\rho_1 < \rho_2 > \rho_3 > \rho_4$ ----KQ-type section,
$\rho_1 > \rho_2 > \rho_3 < \rho_4$ ----QH-type section,
$\rho_1 > \rho_2 > \rho_3 > \rho_4$ ----QQ-type section.

Examples of Schlumberger electrical sounding curves for three of these eight types of four-layer models are shown in figure 19.

For a five-layer geoelectric section there are 16 possible relationships between ρ_1, ρ_2, ρ_3, ρ_4, and ρ_5, and, therefore, there are 16 types of five-layer electrical sounding curves. Each of these 16 geoelectric sections may be described by a combination of three letters. For example, an HKH section is one in which $(\rho_1 > \rho_2 < \rho_3 > \rho_4 < \rho_5)$. In general, an n-layer section (where $n \geq 3$) is described by (n-2) letters.

Electrical Sounding Over Laterally Inhomogeneous Media

Lateral inhomogeneities in the ground affect resistivity measurements in different ways. The effect depends on (1) the size of the inhomogeneity with respect to its depth of burial, (2) the size of the inhomogeneity with respect to the size of the electrode array, (3) the resistivity contrast between the inhomogeneity and the surrounding media, (4) the type of electrode array used, (5) the geometric form of the inhomogeneity, and (6) the orientation of the electrode array with respect to the strike of the inhomogeneity.

The simplest type of a lateral inhomogeneity, from the geometric and mathematical points of view, is that of a vertical plane boundary separating two homogeneous and isotropic media of resistivities ρ_1 and ρ_2. Although this Earth model is ideal and does not exist commonly in nature, its study serves to illustrate the general form of the resistivity anomaly to be expected over a

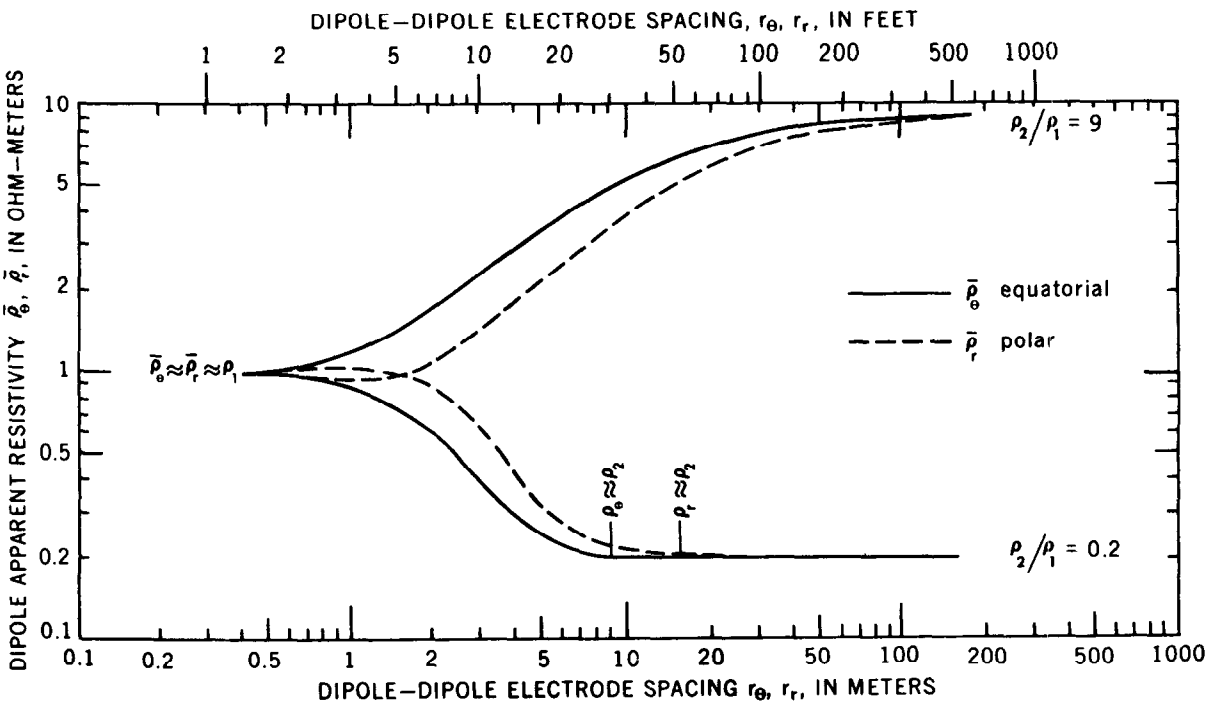

Figure 17.—Comparison between two-layer azimuthal (or equatorial) and radial (or polar) sounding curves ($h_1 = 1$ meter (3.28 feet), $\rho_2/\rho_1 = 9$ or 0.2).

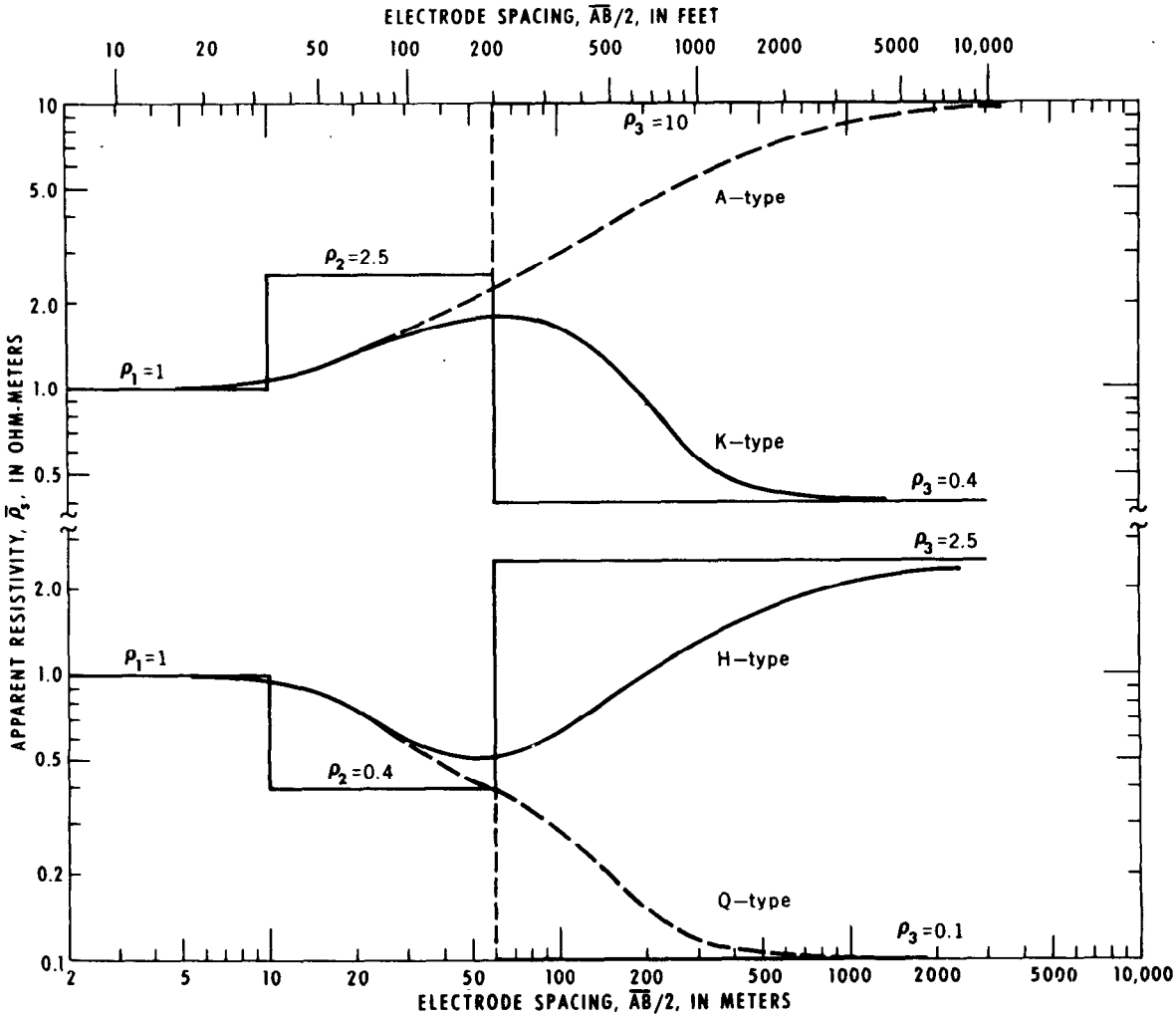

Figure 18.—Examples of the four types of three-layer Schlumberger sounding curves for three-layer Earth models.

large variety of more complicated lateral inhomogeneities.

The electrical sounding curves obtained with an ideal Schlumberger array ($\overline{MN}\rightarrow 0$) oriented at different angles to the surface trace of a vertical contact (Zohdy, 1970) are shown in figure 20. The most important feature on the sounding curves that indicates the presence of the lateral inhomogeneity is the formation of a cusp which is well developed whenever the sounding line makes an azimuth angle close to 90° with the surface trace of the vertical plane boundary. The Wenner sounding curves for azimuth angles of 0° to 90° are shown in figure 21. The Wenner curves are more complicated than the Schlumberger curves because a potential electrode crosses the contact. The effects of such things as dipping, vertical and horizontal contacts, and pipe lines have been described in the literature for different electrode arrays (Kunetz, 1966; Al'pin and others, 1966).

Limitations of the Resistivity Method

The interpretation of a multilayer sounding curve generally is not unique. This means that a given electrical sounding curve can correspond to a variety of subsurface distributions of layer thicknesses and resistivities. Furthermore, several other limitations

are inherent in the conventional methods of electrical sounding and these are considered in the following sections.

Equivalence of K-type curves.—Consider two three-layer sections of the K type ($\rho_1 < \rho_2 > \rho_3$). If ρ_1 in one section equals ρ_1' in the other section, $\rho_3 = \rho_3'$, and $T_2 = \rho_2 h_2 = T_2' = \rho_2' h_2'$, then the sounding curves for both sections will be practically identical (fig. 22, curves a and b).

This type of equivalence is known as equivalence by T and it also applies approximately to Q-type curves.

Equivalence of H-type curves.— Consider two three-layer sections of the H type ($\rho_1 > \rho_2 < \rho_3$). If ρ_1 in one section equals ρ_1' in the other section, $\rho_3 = \rho_3'$ and $S_2 = h_2/\rho_2 = S_2' = h_2'/\rho_2'$, then the sounding curves for both sections (fig. 22, curves c and d) will be practically identical (equivalence by S). The equivalence by S also applies to sounding curves of the A type ($\rho_1 < \rho_2 < \rho_3$).

For both equivalence by T and equivalence by S, there is a certain range, depending on the ratios ρ_2/ρ_1 and h_2/h_1, where the two sounding curves coincide very closely. Special nomograms published by Pilayev (1948) define this range, which is referred to as the domain of the principle of equivalence. These charts were published in the books of Bhattacharya and Patra (1968), Dakhnov (1953), Golovtsin (1963), Kalenov (1957),

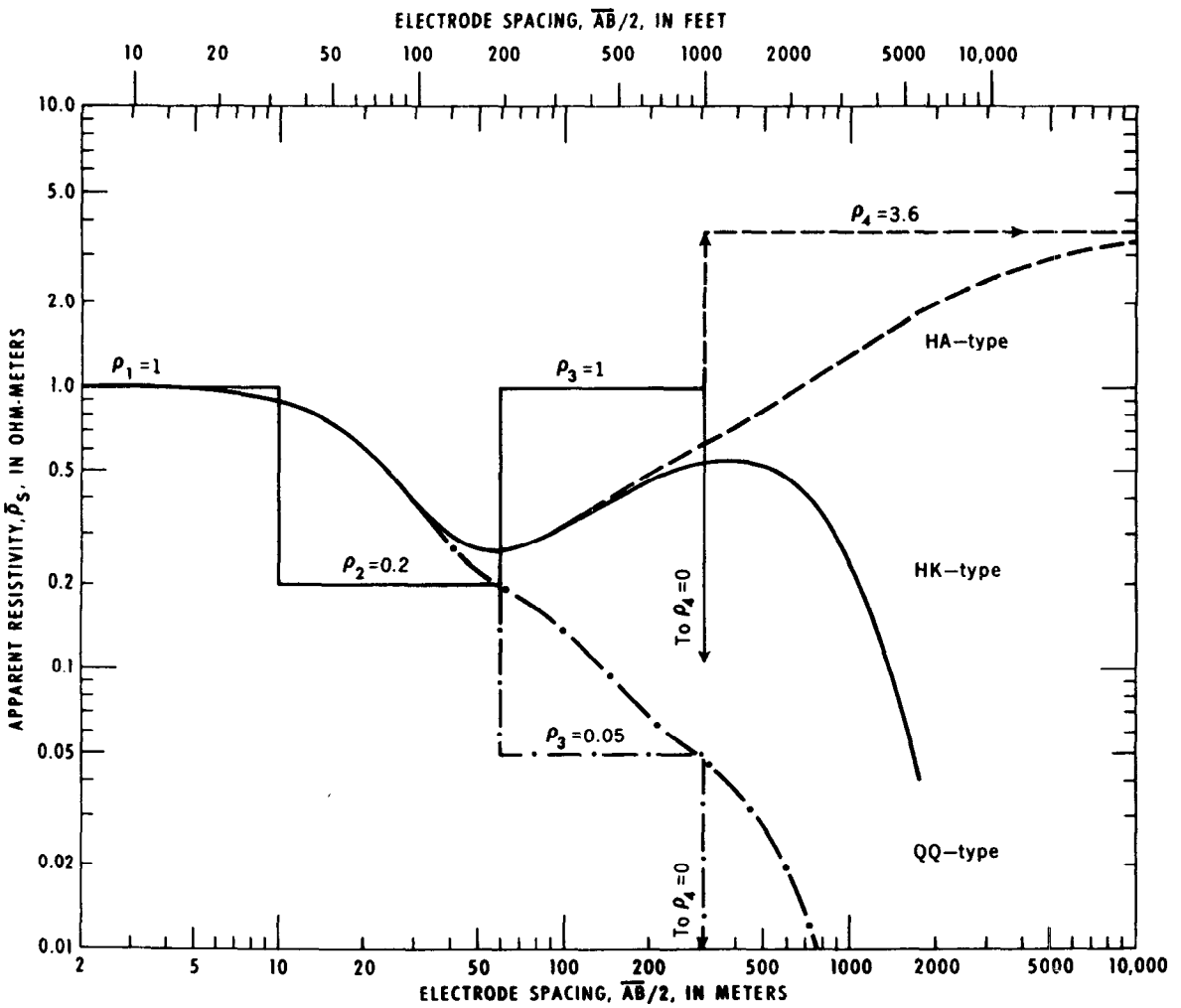

Figure 19.—Examples of three of the eight possible types of Schlumberger sounding curves for four-layer Earth models.

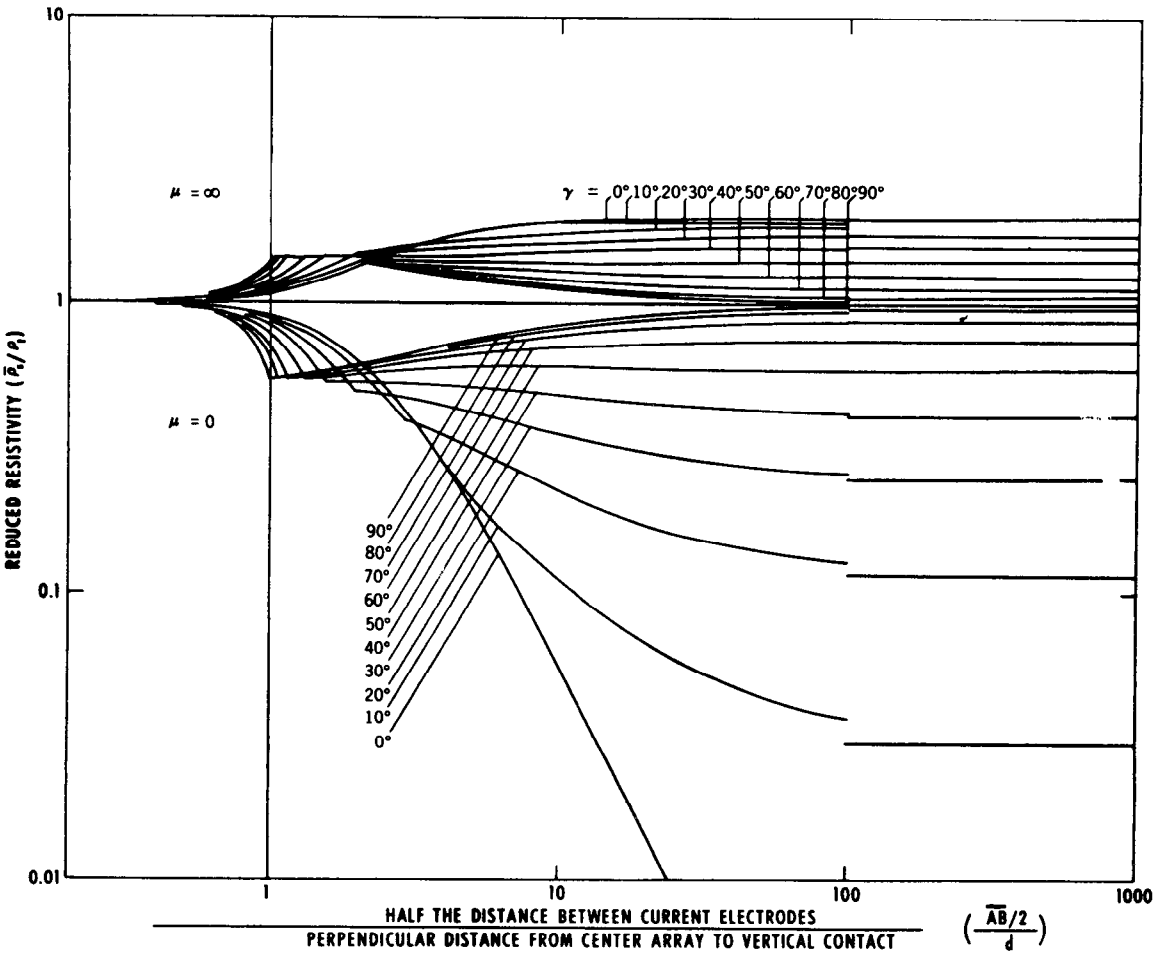

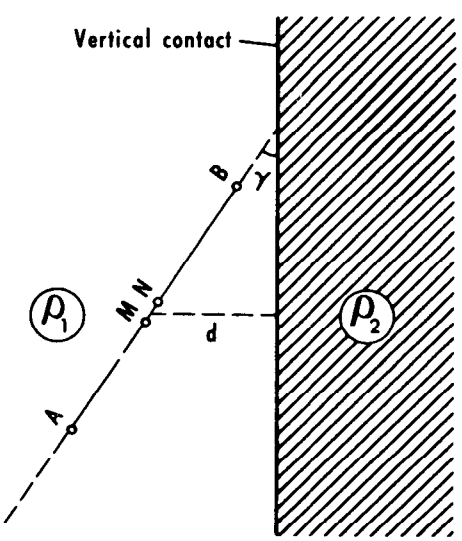

Figure 20.—Examples of the variation of Schlumberger sounding curves across a vertical contact at various azimuths. $\overline{AB}/2$, electrode spacing; d, perpendicular distance from center of array 0 to surface trace of vertical contact; $\bar{\rho}$, apparent resistivity; ρ, true resistivity; γ, azimuth angle (after Zohdy, 1970).

and Keller and Frischknecht (1966).

Approximate equivalence of sounding curves of sections with horizontal or vertical contacts, or both, to sounding curves of sections with horizontal boundaries only.— The form of sounding curves obtained over sections with horizontal and (or) vertical or inclined contacts can be quite similar to curves obtained over sections with horizontal contacts only. This is true when the sounding line is parallel to the strike of the vertical (or inclined) contact. Depending on the ratio d/h of the perpendicular distance from the center of the sounding line to the surface trace of the vertical contact d to the thickness of the top layer h, one may obtain sounding curves that are equivalent to curves obtained over a three, or more, horizontally-layered Earth model (fig. 22, curves e and f). This type of equivalence is resolved easily by making crossed soundings (soundings having the same center but expanded at right angles to one another). The forms of the two sounding curves are so different from one another that it is easy to realize the presence of a lateral heterogeneity in the ground (see curve e', fig. 22). The expansion of the Lee-partitioning array parallel to the strike of a vertical or inclined contact does not yield data that are indicative of the presence of the lateral heterogeneity, and the making of a crossed sounding is required.

Approximate equivalence between two multilayer sections.—A sounding curve obtained over a four- or five-layer section may be nearly equivalent to one obtained over a three-layer section. Generally this is attributed to the so-called principle of suppression (Maillet, 1947). The error, caused by the effect, in interpreting the depth of contacts is sometimes referred to as pseudoanisotropy (Genslay and Rouget, 1937; Flathe, 1955, 1963). An example of this type of equivalence is shown in figure 22, curves g and h.

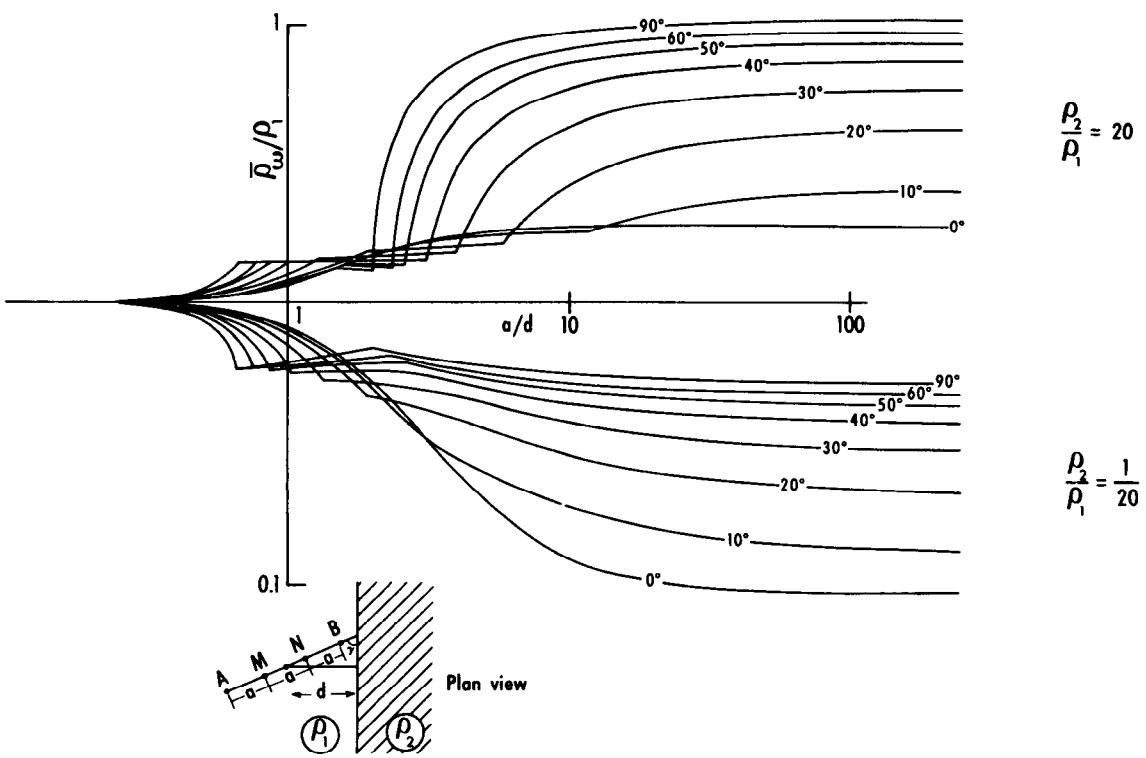

Figure 21.—Examples of the variation of Wenner sounding curves across a vertical contact at various azimuths. Unpublished data calculated by Zohdy, 1970. a, Wenner spacing; d, perpendicular distance from center of array to surface trace of vertical contact; $\overline{\rho}$, apparent resistivity; ρ, true resistivity.

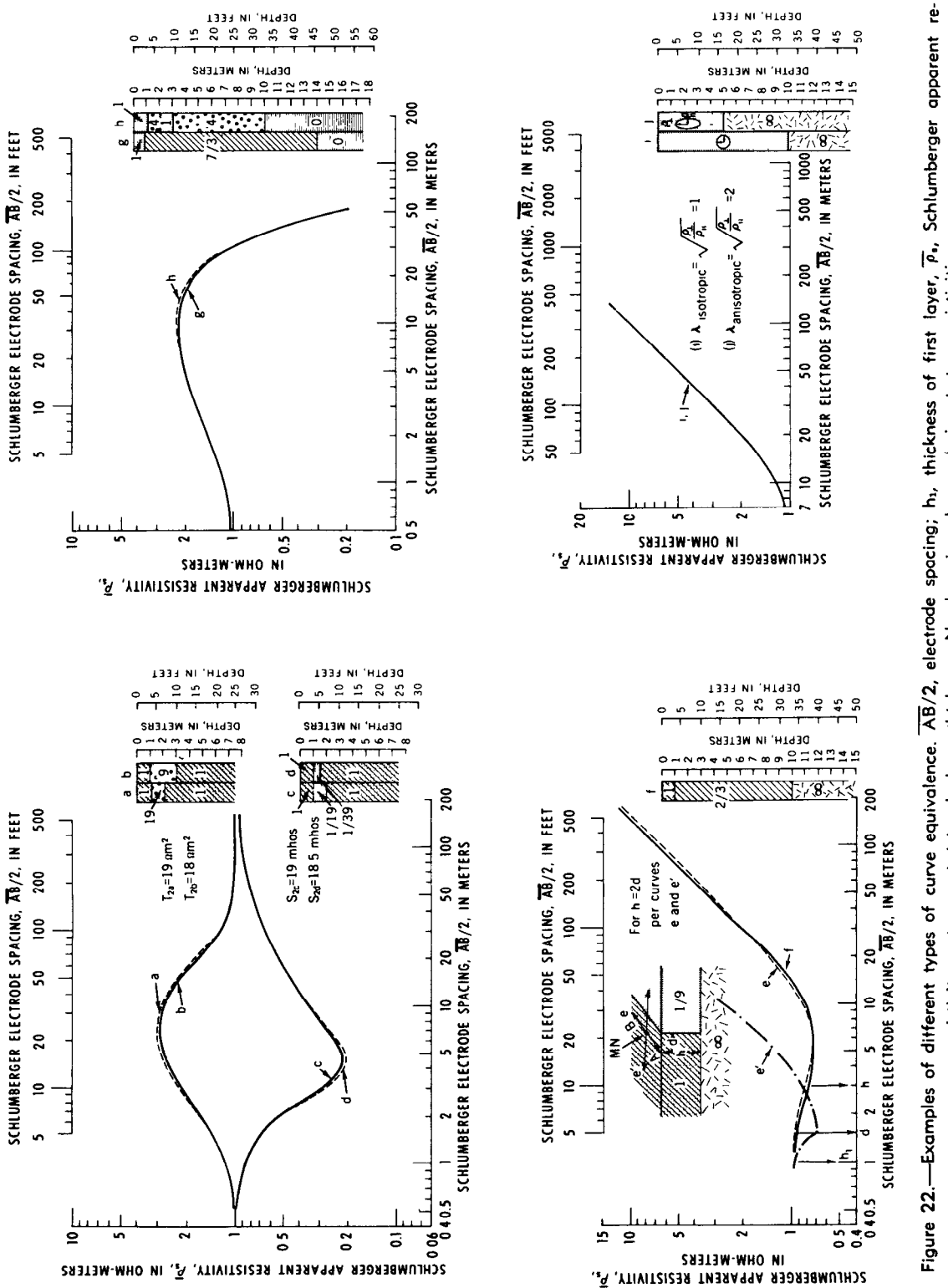

Figure 22.—Examples of different types of curve equivalence. $\overline{AB}/2$, electrode spacing; h_1, thickness of first layer, $\overline{\rho}_a$, Schlumberger apparent resistivity; ρ, true resistivity; h, layer thickness. Numbers in columns designate true resistivities.

Equivalence between isotropic and anisotropic media.—The equivalence between an isotropic layer and an anisotropic layer is exact when the equivalent layer has microanisotropic properties. In practice, depths are generally overestimated by a factor equal to the coefficient of anisotropy $\lambda = \sqrt{\frac{\rho_\perp}{\rho_\parallel}}$, where $\rho_\perp$ and $\rho_\parallel$ are the resistivities perpendicular to, and parallel to, the bedding, respectively (fig. 22, curves i and j). Values of λ generally range from 1.1 to 1.3 and rarely exceed 2.

Monotonic change in resistivity.—When the resistivity of the subsurface layers increases or decreases monotonically (A-, AA-, Q-, or QQ-type sections), the sounding curve may resemble a curve of a simple two-layer Earth model (principle of suppression), unless the thicknesses of the layers increase significantly with depth. Recently, two new methods for making so-called differential soundings have been introduced (Rabinovich, 1965; Zohdy, 1969) whereby the resolving power of the sounding curve is greatly improved for A- and Q-type sections.

Relative thickness of a layer.—The detectability of a layer of given resistivity depends on its relative thickness, which is defined as the ratio of the bed thickness to its depth of burial. The smaller the relative thickness of a given layer, the smaller the chance of its detectability on a sounding curve. In four-layer (or more) Earth models the so-called "effective relative thickness" of a layer (Flathe, 1963), which is defined as the ratio of the layer thickness to the product of the pseudoanisotropy, and the total thickness of the layers above it must be considered. For example, a layer 50 meters (164 feet) thick at a depth of 10 meters (32.8 feet) has a relative thickness of 5, which is quite favorable for its detection on a sounding curve. However, if the top 10 meters (32.8 feet) are composed of two layers of thicknesses of 2 meters (6.56 feet) and 8 meters (26.2 feet) and resistivities of 10 ohm-m and 1,000 ohm-m, respectively, then the pseudoanisotropy λ of the top two layers is 4.1. Therefore, the effective relative thickness is $50/(4.1\times10) \cong 1.22$, which is considerably smaller than the relative thickness of 5 previously calculated. The resistivity of the 50 meter (164 feet) third layer and of the underlying layers also play an important role in the detectability of the layer on the sounding curve.

The limitations to interpretation mentioned above should not be discouraging to the geophysicist nor should they persuade the reader to consider the interpretation of sounding data as an entirely hopeless endeavor. All geophysical methods that are based on potential theory (electrical, gravity, and magnetic methods) lack unique solutions. In practice, it is by correlation of several sounding curves, by making crossed soundings, by sounding with different arrays, by traversing the area with horizontal resistivity profiles, by knowledge of its general geology, and by recognition of the electrical properties of the rocks in the studied area that correct interpretations are achieved. When drilling information is available it is advisable to make parametric electrical soundings near the wells in order to determine the resistivity parameters of the layers using accurately determined layer thicknesses. Then using these known resistivity parameters, we can determine the layer thicknesses in areas where drilling information is lacking.

Analysis of Electrical Sounding Curves

When an area is investigated, the sounding curves generally are not all of the same type (H, A, K, Q, and HA, for example). Furthermore, all the curves may not be interpretable in terms of horizontally stratified media. In this section we shall describe some of the qualitative and quantitative methods of interpretation of electrical sounding data.

Qualitative Interpretation

The qualitative interpretation of sounding data involves the following:

1. Study of the types of the sounding curves obtained and notation of the areal distribution of these types on a map of the survey area.
2. Preparation of apparent-resistivity maps. Each map is prepared by plotting the apparent resistivity value, as registered on the sounding curve, at a given electrode spacing (common to all soundings) and contouring the results (fig. 23).
3. Preparation of apparent-resistivity sec-

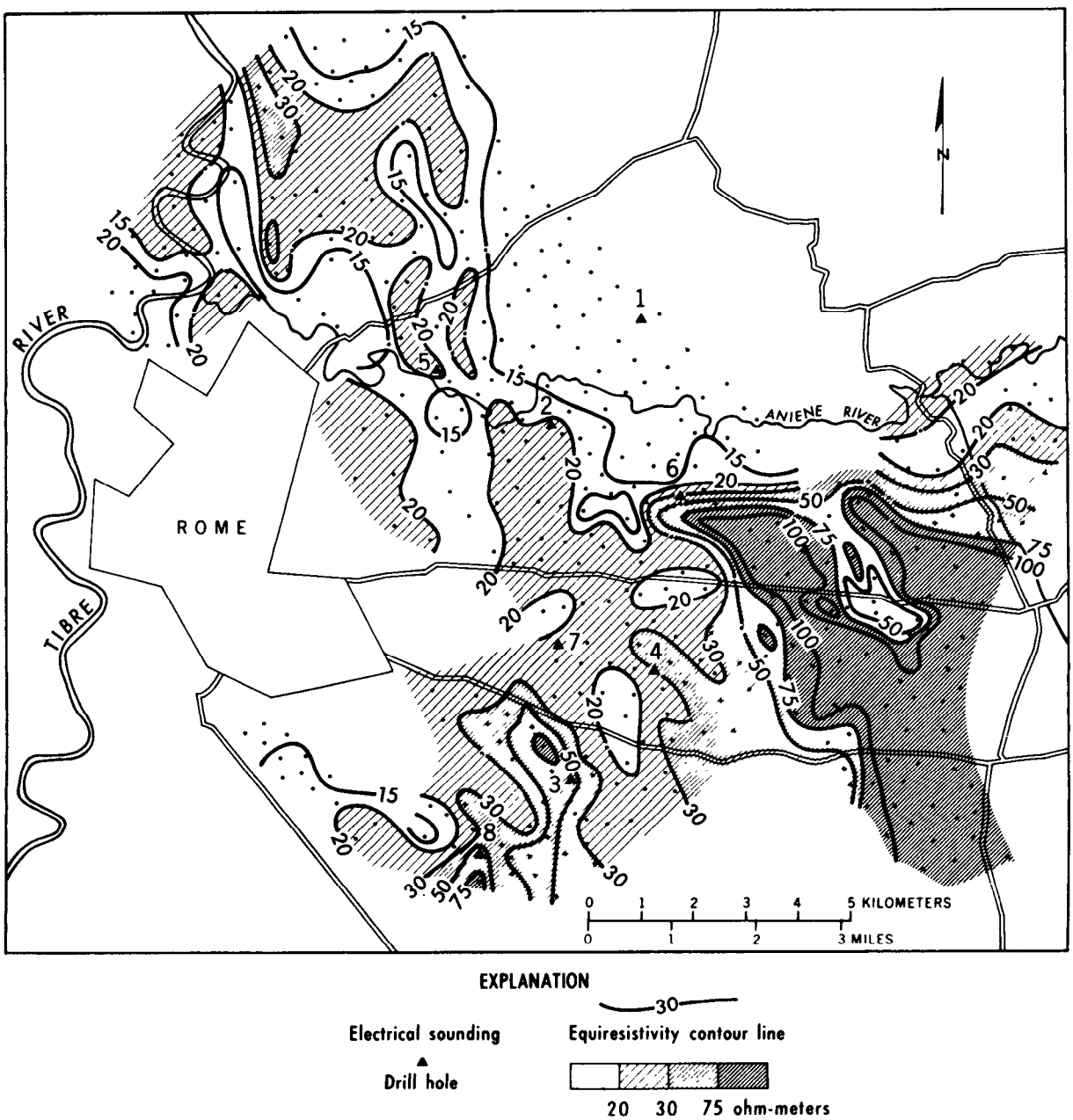

Figure 23.—Map of apparent resistivity near Rome, Italy (after Breusse, 1961a).

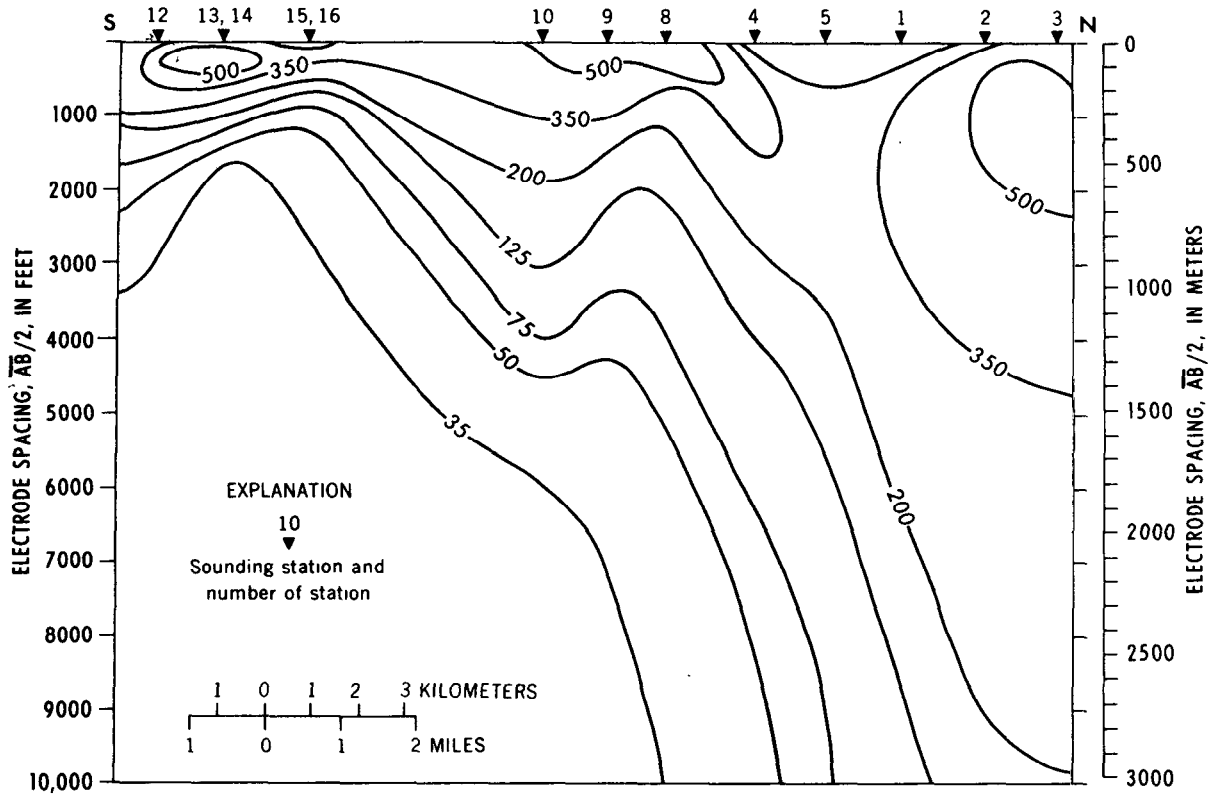

Figure 24.—Section of apparent resistivity near Minidoka, Idaho. Values on contour lines designate apparent resistivities in ohm-meters. Snake River basalt thickens toward the north.

tions. These sections are constructed by plotting the apparent resistivities, as observed, along vertical lines located beneath the sounding stations on the chosen profile. The apparent resistivity values are then contoured (fig. 24). Generally a linear vertical scale is used to suppress the effect of near-surface layers.

4. Preparation of profiles of apparent-resistivity values for a given electrode spacing, profiles of the ordinate or abscissa of the values of the minimum point $\overline{\rho}_{min}$ for H-type sections, profiles of the ordinate or absicissa of the maximum point $\overline{\rho}_{max}$ for K-type sections, profiles of ρ_L values, and profiles of S and T values.

These maps, sections, and profiles constitute the basis of the qualitative interpretation which should precede quantitative interpretation of the electrical sounding data. It should be noted, however, that an apparent resistivity map for a given electrode spacing (fig. 23) does not represent the areal variation of resistivity at a depth equal to that electrode spacing, it merely indicates the general lateral variation in electrical properties in the area. For example, an area on the map having high apparent resistivity values may correspond to a shallow high resistivity bedrock, it may indicate thickening in a clean sand and gravel aquifer saturated with fresh water, or it may indicate the presence of high resistivity gypsum or anhydrite layers in the section.

Determination and Use of Total Transverse Resistance, T, from Sounding Curves

In three-layer sections of the K type, the value of transverse resistance of the second layer can be determined approximately from a Schlumberger sounding curve (fig. 25) by multiplying the ordinate value of the maxi-

mum point ($\overline{\rho_s}_{max}$) by the corresponding abscissa value of $\overline{AB}/2$ (Kunetz, 1966). The value of T_2' thus determined generally is underestimated (fig. 25), especially when the real value T_2' is large and is approximately equal to the total transverse resistance of the upper two layers $T = T_1 + T_2 \cong T_2$, (with, $T_1 \leq 10\%\ T_2$).

The total transverse resistance of the upper two layers $T = T_1 + T_2 = \rho_1 h_1 + \rho_2 h_2$ is determined approximately by another graphical technique (Dzhavarof and Biramova, 1965). The intercept of a straight line tangent to the Schlumberger sounding curve and inclined to the abscissa axis at an angle of 135° (or -45°) with the horizontal line for $\overline{\rho}=1$ ohm-m is approximately equal to T (fig. 25). The value of $T' \cong T$ by this graphical method generally is overestimated. Therefore, for large values of T and where $T_2 \cong T$, the average of the values of T'_2 and T' is close to the true value of T (fig. 25). This is especially true when $\rho_3/\rho_1 << 1$. Where the value of T increases from one sounding station to the next, this generally means that the thickness of the resistive layer in the section (gravel, basalt, etc.) also increases. However the increase in T might be caused also by an increase in the resistivity values. A north-south profile of graphically determined values of total transverse resistance east of Minidoka, Idaho, (fig. 26) is an excellent qualitative indication that the Snake River basalt increases in thickness appreciably from south to north.

Determination of Total Longitudinal Conductance, S, From Sounding Curves

In H, A, KH, HA, and similar type sections the terminal branch on the sounding curve often rises at an angle of 45°. This usually indicates igneous or metamorphic rocks of very high resistivity (>1,000 ohm-m). However, in the presence of conductive sedimentary rocks saturated with salt water (ρ<5 ohm-m) the so-called "electric basement" of high resistivity rocks may correspond to sandstones or limestones having resistivities of only 200–500 ohm-m. The total longitudinal conductance S is determined

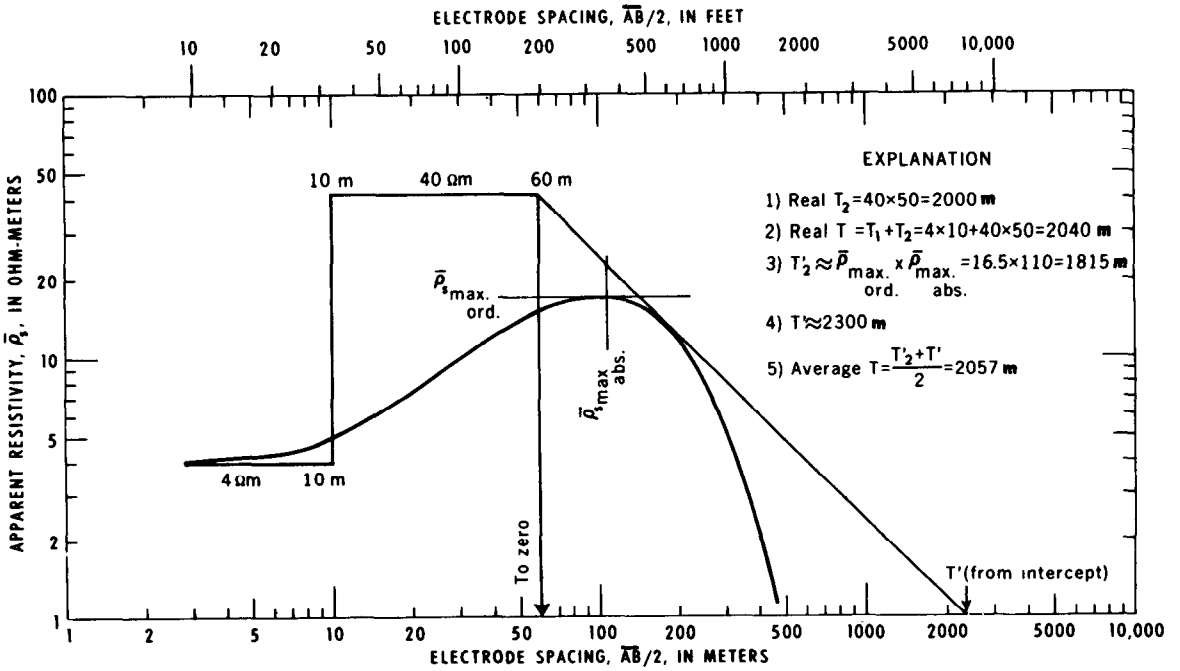

Figure 25.—Graphical determination of total transverse resistance from a K-type Schlumberger sounding curve. ρ_1 = 4 ohm-meters, ρ_2 = 40 ohm-meters, ρ_3 = 0 ohm-meters, h_1 = 10 meters (32.8 feet), h_2 = 50 meters (164 feet), $h_3 = \infty$.

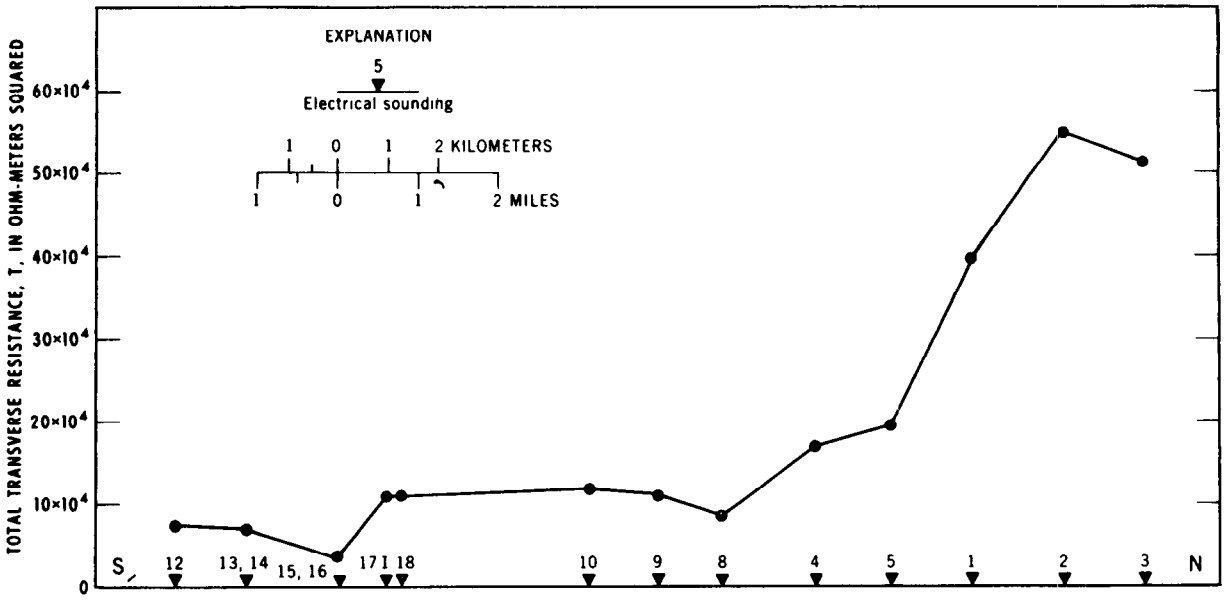

Figure 26.—Profile of total transverse resistance values, T, in ohm-meters squared, near Minidoka, Idaho. High values indicate thickening of basalt layers. Data obtained by Zohdy (1969).

from the slope of the terminal branch of a Schlumberger curve, rising at an angle of 45° (here called the *S*-line). It should be remembered that the slope of a rectilinear branch inclined to the abscissa at 45° is not necessarily equal to unity when the curve is plotted on logarithmic paper. The value of *S* is numerically equal to the inverse of the slope of this line (Kalenov, 1957; Keller and Frischknecht, 1966), and it is usually determined, very quickly, by the intercept of the extension of the *S*-line with the horizontal line, $\overline{\rho}_s = 1$ ohm-m (fig. 27). The determination of *S* by this method is as accurate as a graphical procedure can be, and is valid irrespective of the number of layers that overlie the high resistivity layer provided the terminal branch rises at an angle of 45°. When the resistivity of the bottom layer is not sufficiently high to make the terminal branch rise at an angle of 45°, other methods are used for the graphical determination of *S* (Berdichevskii, 1957; Orellana, 1966; Orellana and Mooney, 1966; Zohdy, 1968). Increases in the value of *S* from one sounding station to the next indicate an increase in the total thickness of the sedimentary section, a decrease in average longitudinal resistivity (ρ_L), or both.

Determination of Average Longitudinal Resistivity, ρ_L, from a Sounding Curve

As the value of longitudinal conductance *S* can be determined easily from a Schlumberger sounding curve, graphical methods for the evaluation of average longitudinal resistivity (ρ_L) from the sounding curve were sought so that the total depth *H* to the high resistivity bedrock could be calculated from the simple relation $H = S\rho_L$. It was found (Zagarmistr, 1957) that for three-layer sections of the H type, the value of the apparent resistivity at the minimum point ($\overline{\rho}_{r\,min}$) on a polar dipole-dipole curve is approximately equal to ρ_L, provided that the thickness of the middle low resistivity layer is at least 3 times as large as the thickness of the first layer ($h_2 \geq 3h_1$). This was found to be valid for all values of $\mu = \frac{\rho_2}{\rho_1}$ (Zagarmistr, 1957; Berdichevskii and Zagarmistr, 1958). Using formulas developed by Al'pin and by Tsekov (Al'pin, 1958; Zagarmistr, 1957; Zohdy, 1969a), Schlumberger and equatorial sounding curves can be transformed into polar dipole sounding curves (fig. 28). The average longitudinal resistivity then can be determined and the thickness of the section can be calculated.

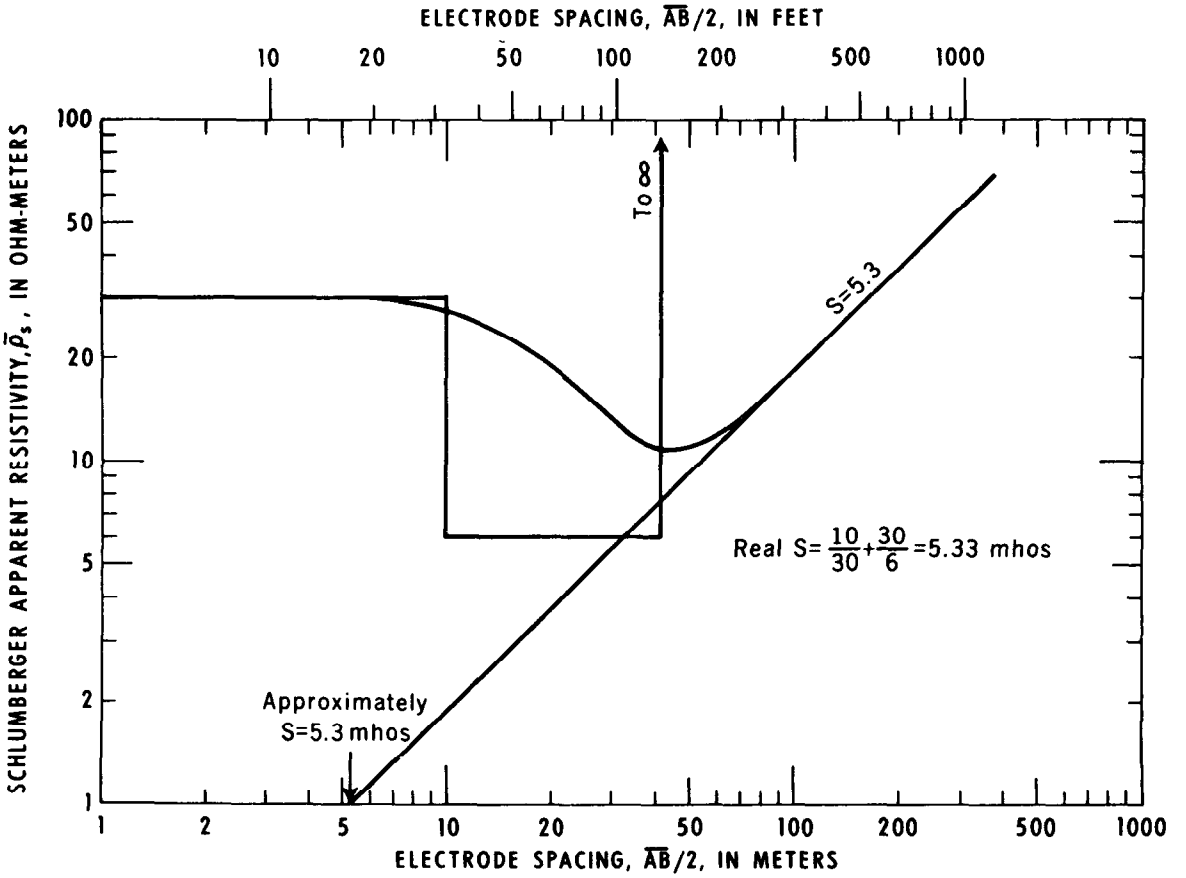

Figure 27.—Graphical determination of total longitudinal conductance S from an H-type Schlumberger sounding curve.

Average longitudinal resistivity also may be determined from borehole induction logs of wells in the area.

Distortion of Sounding Curves by Extraneous Influences

Electrical sounding curves may be distorted by lateral inhomogeneities in the ground, by errors in measurements, or by equipment failure. It is important to realize the cause of various common distortions on sounding curves.

Formation of cusps.—The formation of a cusp on a Schlumberger sounding curve generally is caused by a lateral heterogeniety, by current leakage from poorly insulated cables, by electrode spacing errors, or by errors in calculation (Zohdy, 1968b). When plotting data in the field, it is advisable to check for current leakage whenever a cusp is formed on the sounding curve. A resistive lateral inhomogeneity, in the form of a sand lens or a near-surface caliche layer, produces a cusp like the one shown in curve *A*, figure 29; and a conductive inhomogeneity, in the form of a buried pipe or a clay pocket, produces a cusp as the one shown in curve *B*, figure 29.

Sharp maximum.—The maximum or peak value on a K-type sounding curve is always gentle and broad, and should never have a sharp curvature where the ground is horizontally homogeneous. The formation of a sharp peak (fig. 30) generally is indicative of the limited lateral extent of the buried (middle) resistive layer (Alfano, 1959).

Curve discontinuities.—Two types of discontinuities are observed on Schlumberger sounding curves. The first type is observed when the spacing $\overline{MN}$ is enlarged (with $\overline{AB}$

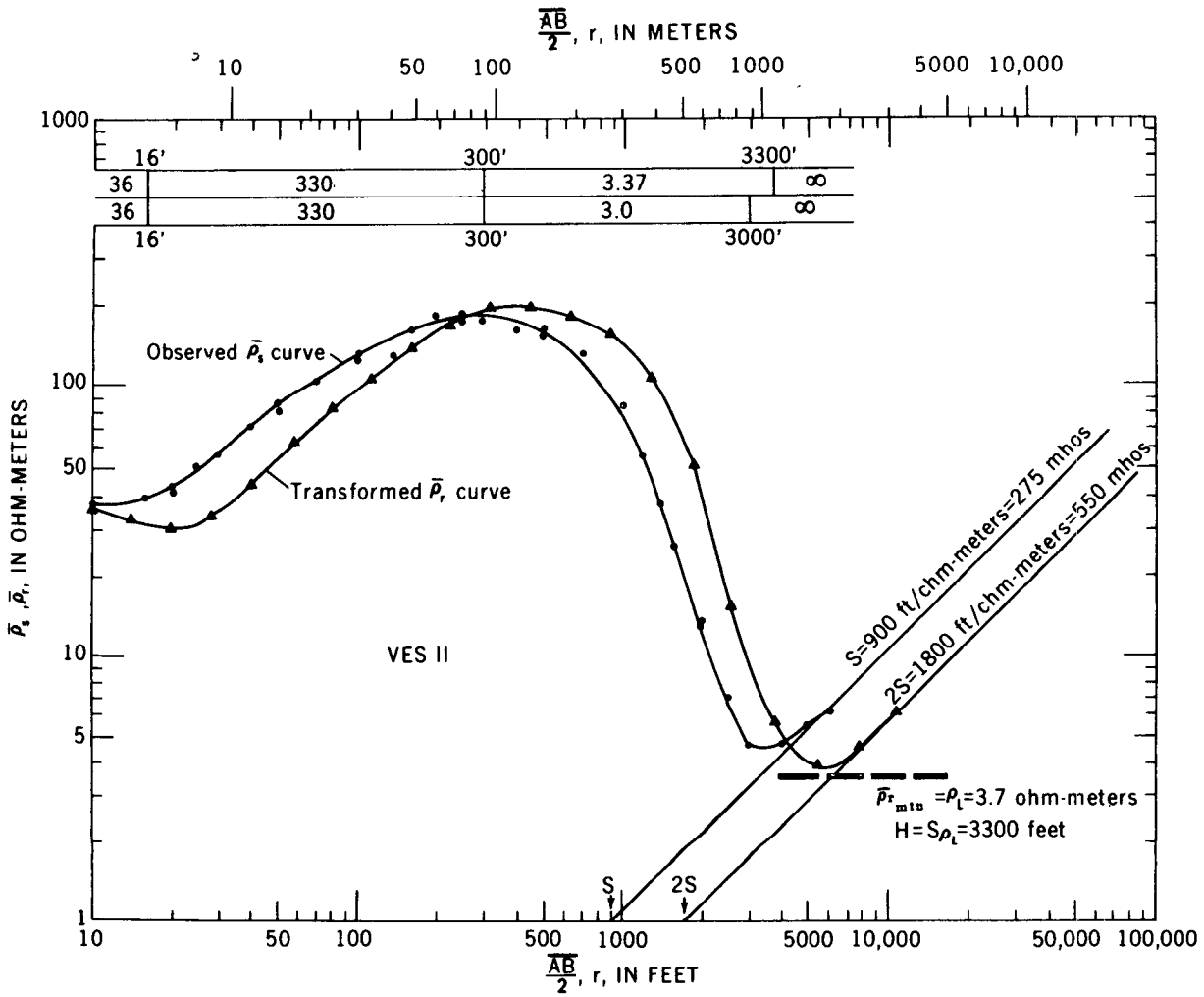

Figure 28.—Transformation of a Schlumberger KH-type curve into a polar dipole-dipole curve to evaluate $\bar{\rho}_{r_{min}} = \rho_L$ and $H = S\rho_L$ (after Zohdy, 1969a). Reproduced with permission of "Geophysics."

constant) and the value of the apparent resistivity, for the larger $\overline{MN}$ spacing, does not conform to the theoretical magnitude for such a change in $\overline{MN}$ (Deppermann, 1954). The repetition of such a discontinuity when $\overline{MN}$ is changed to a larger spacing for the second time indicates a lateral inhomogeneity of large dimensions. This type of discontinuity also may indicate current leakage, electrode spacing errors (Zohdy, 1968b), or that the input impedance of the potential-difference measuring device is not sufficiently high. Examples of the discontinuities that are not in conformity with the assumption of a horizontally homogenous Earth are shown in figure 31. When the discontinuities are not severe, the curve can be corrected easily by shifting the distorted segment of the curve vertically to where it should be.

The second type of discontinuity is less common and occurs during the expansion of the current electrode spacing $\overline{AB}$ when sounding with a Schlumberger array. In general, the curve is displaced downward, that is, the value of the apparent resistivity at the larger AB is much less than the previous reading (fig. 32). This type of discontinuity generally is caused by a narrow, shallow, dike-like structure which is more resistant than

the surrounding media and whose width is small in comparison to the electrode spacing (Kunetz, 1955, 1966; Zohdy, 1969a). The abscissa value at which the discontinuity on the sounding curve occurs is equal to the distance from the sounding center to the dike-like structure.

Quantitative Interpretation

Several methods are used in the quantitative interpretation of electrical sounding curves. These methods are classified as analytical methods, semiempirical methods, and empirical methods.

Analytical Methods of Interpretation

The analytical methods are based on the calculation of theoretical sounding curves that match the observed curves. There are several catalogues of theoretical master curves calculated for a variety of Earth structures, most of which represent horizontally stratified media. Mooney and Wetzel (1956) published an extensive catalogue of master curves for Wenner soundings over two-, three-, and four-layer Earth models. The Mooney-Wetzel album, now out of print, has several shortcomings that limit its usefulness (Zohdy, 1964).

Two problems are encountered in the calculation of theoretical sounding curves and in their application for the interpretation of field data. First, the calculation of the apparent resistivity value at each electrode spacing involves the evaluation of a difficult integral (Stefanesco and others, 1930) or the summation of an infinite series (Hummel, 1929). Thus the use of a high speed digital computer is almost always necessary for the calculation of theoretical sounding curves.

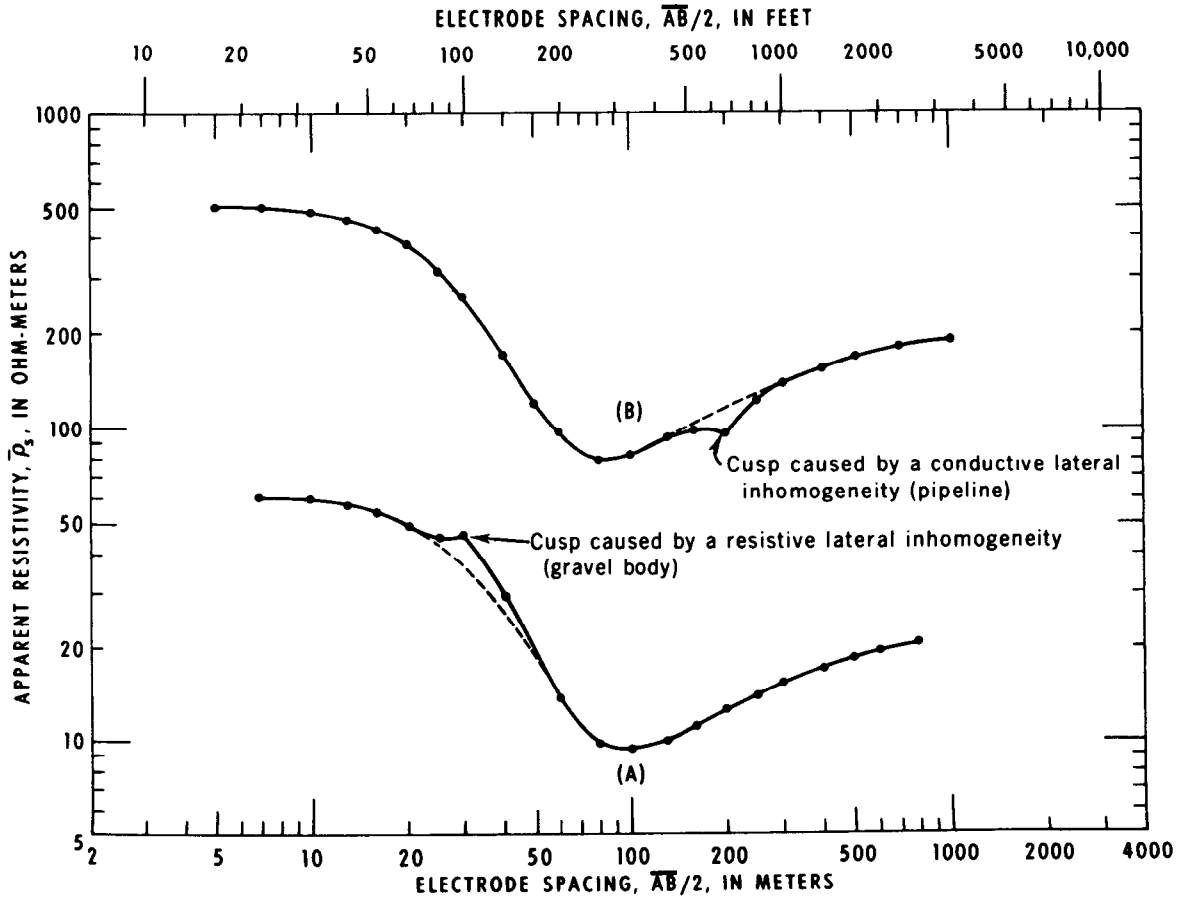

Figure 29.—Distortion of sounding curves by cusps caused by lateral inhomogeneites.

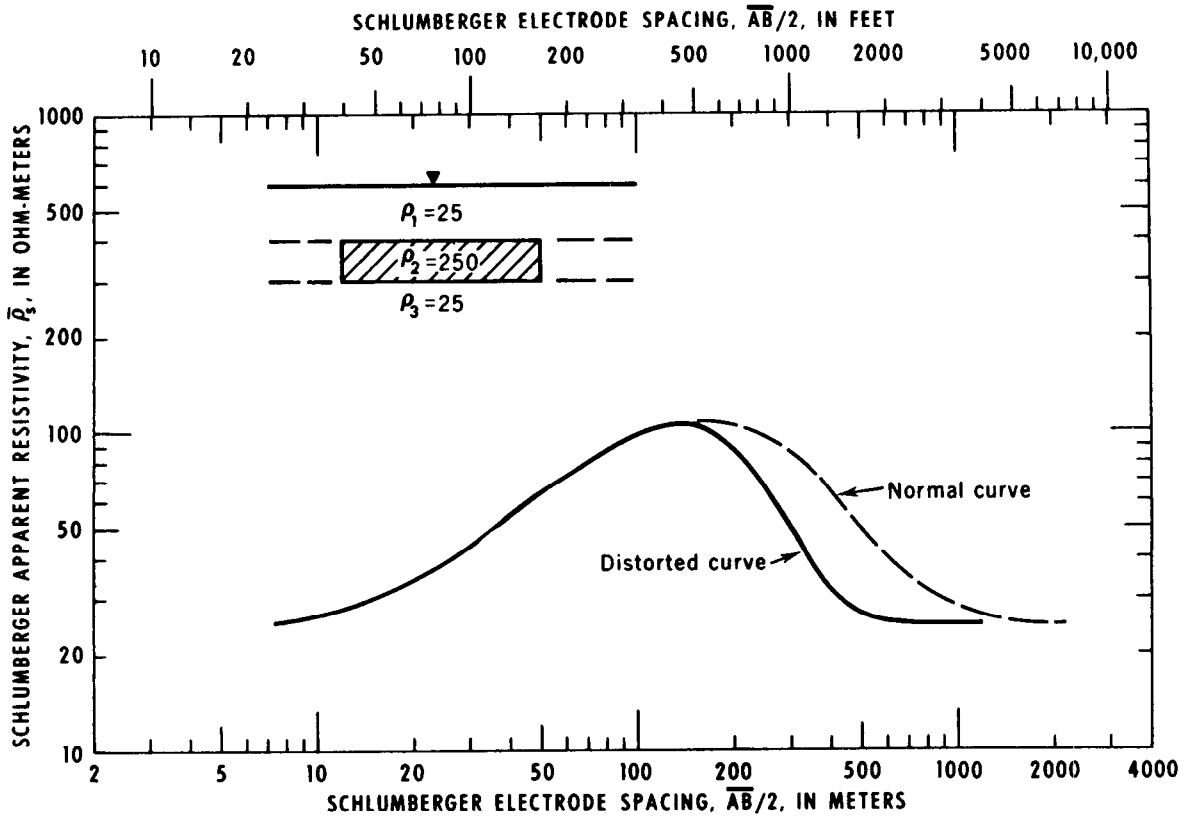

Figure 30.—Example of a narrow peak on a K-type curve, caused by the limited lateral extent of a resistive middle layer (after Alfano, 1959). Reproduced with permission of "Geophysical Prospecting."

Recently, however, the calculation of VES (vertical electrical sounding) curves of the Schlumberger type for horizontally stratified media was simplified and greatly accelerated through the use of the method of convolution (Ghosh, 1971).

The second difficulty in the calculation of theoretical curves is that in multilayer Earth models, the possible combinations of resistivity contrasts and layer thicknesses are infinite. Even in a simple two-layer Earth model, there are three variable parameters, ρ_1, ρ_2, and h_1. With ρ_1, ρ_2, and h_1 as variables there are an infinite number of possible sounding curves for the two-layer geoelectric section. However, by considering the resistivity and thickness of the first layer as unity and by plotting the theoretical sounding curves on a set of logarithmic coordinates with the dimensionless variables $\overline{AB}/2\ h_1$ (Schlumberger), a/h_1 (Wenner), or r/h_1 (dipole-dipole), on the abscissa; and $\bar{\rho}_s/\rho_1$, $\bar{\rho}_w/\rho_1$, or $\bar{\rho}_d/\rho_1$ on the ordinate, a simple family of curves is obtained. These two-layer curves vary in shape, in a unique manner, and in accordance with the infinite number of values that the ratio ρ_2/ρ_1 may attain. A set of two-layer master curves for the Schlumberger array is shown in figure 33; two-layer master sets of other arays may be different in shape.

In three-layer Earth models, there are five variable parameters: ρ_1, ρ_2, ρ_3, h_1, and h_2. By using the dimensionless variables

$$\mu_1 = \rho_2/\rho_1,\ \mu_2 = \rho_3/\rho_1,\ \upsilon_1 = \frac{h_2}{h_1}$$

and by plotting the theoretical sounding curves on logarithmic coordinates, the result is still an infinite number of curves (Cagniard, 1952).

The limitations on the calculation and application of theoretical sounding curves should not discourage their use. Several

graphical methods have been devised for the construction of electrical sounding curves of $\mu_1 = \rho_2/\rho_1$, $\mu_2 = \rho_3/\rho_1$, and $v_1 = h_2/h_1$ that have not been thoretically calculated (Kalenov, 1957; Matveev, 1964). The graphical construction of a given sounding curve is done by using the available theoretically calculated curves in conjunction with special nomograms. The graphical interpretation of sounding curves often is checked by calculating the exact sounding curve for the derived model on a digital computer.

Before interpretation is made with the master sets for horizontal layers, the interpreter must be satisfied with the form of the sounding curve, in that it is sufficiently smooth and not severely distorted by sharp cusps or discontinuities. A certain amount of smoothing generally is required. The type of curve (such as H, A, K, Q, HA, HK) and the minimum number of layers it seems to represent can be determined by visual inspection. Because of the principles of suppression and equivalence, certain three-layer curves may resemble two-layer ones and four-layer curves may resemble three-layer curves. The estimated number of layers is generally considered to be the minimum number.

Two-layer Interpretation

If the field curve, which is plotted on logarithmic transparent paper of the same module as the master curves, seems to represent a two-layer Earth model, we superpose the transparent sheet with the field curve over the two-layer master set, and move the transparent paper up, down, right, or left (maintaining the coordinate axes of the two sheets parallel) until a best fit of the field curve against one of the theoretical curves is obtained. Occasionally the field curve may have to be matched by interpolation between two of the master curves.

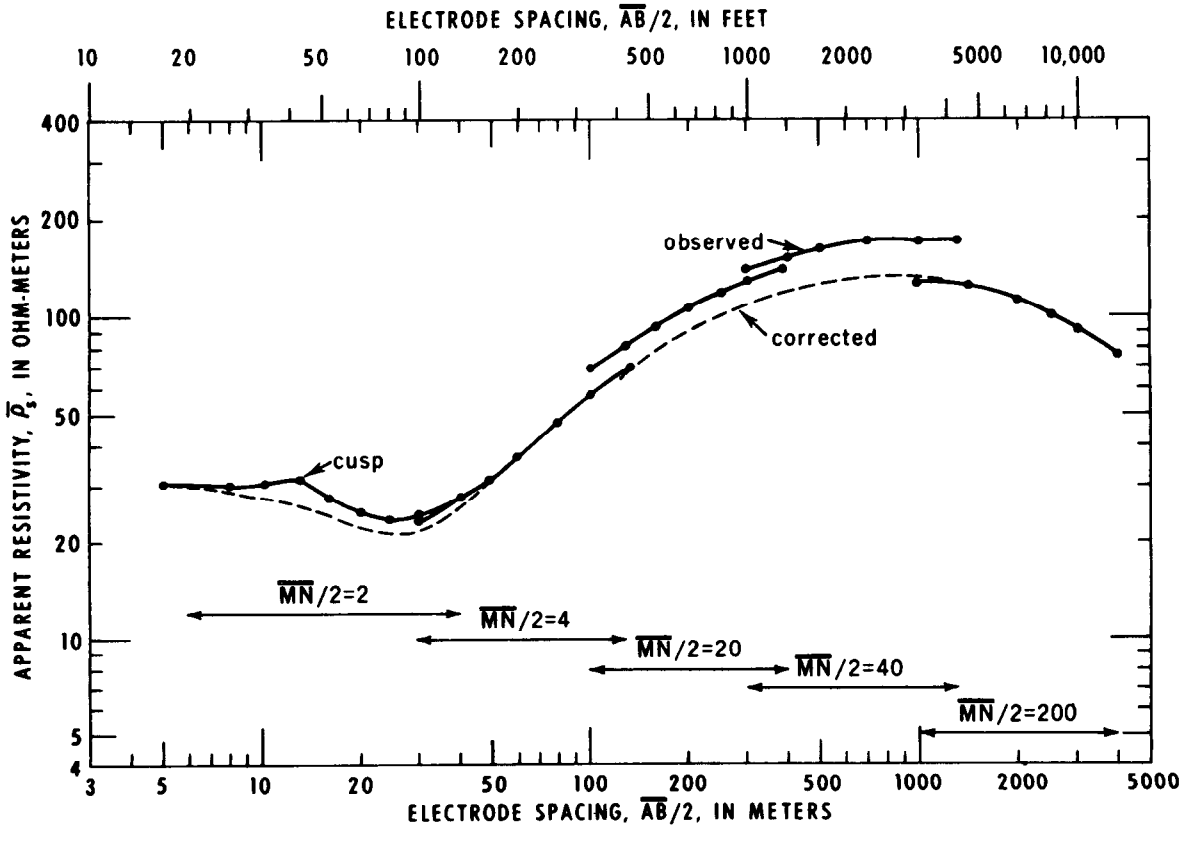

Figure 31.—Example of a distorted HK-Schlumberger curve and the method of correction.

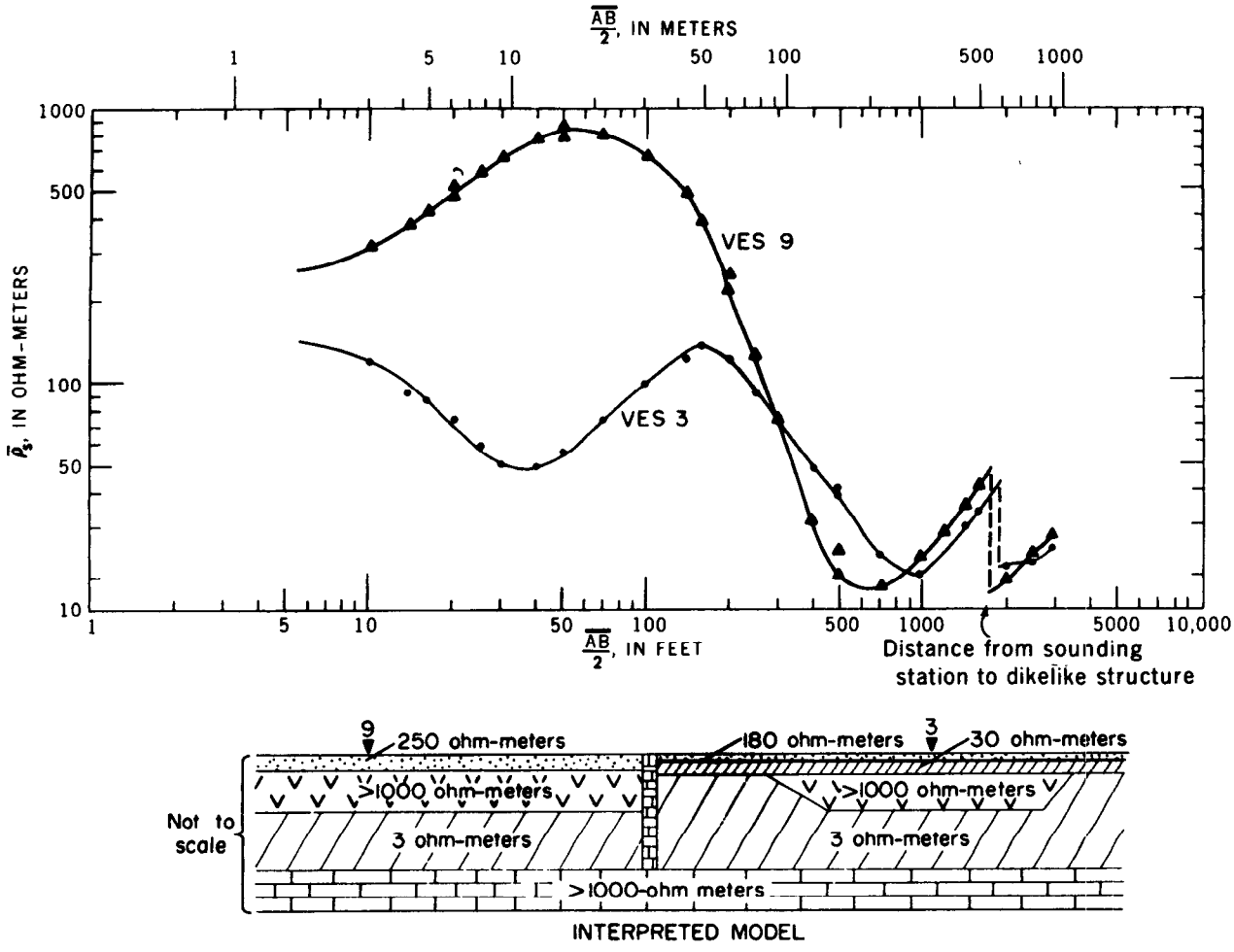

Figure 32.—Examples of tares (discontinuities) on Schlumberger curves caused by a near vertical dikelike structure. (after Zohdy, 1969a). Reproduced with permission of "Geophysics."

Determine the position of the cross, which is the origin of coordinates of the theoretical curve, and trace it on the sheet of the field curve. Also determine the resistivity of the second layer (ρ_2) by tracing the asymptote to the theoretical two-layer curve.

The abscissa value ($\overline{AB}/2$, a, or r) of the "cross" equals the thickness of the first layer and the ordinate value ($\bar{\rho}$) of the "cross" equals the true resistivity, ρ_1, of the first layer. The trace of the asymptote to ρ_2 on the field sheet equals the true resistivity, ρ_2, of the second layer (fig. 34).

Three-layer Interpretation

Determine the type of three-layer curve (H, A, K, Q) by inspection and select the applicable set of theoretical master curves.

Although one of the values of $\mu_1 = \rho_2/\rho_1$ in a set of theoretical curves may correspond to the real value of $\mu_1 = \rho_2/\rho_1$ of the field curve (or although a value of $\mu_1 = \rho_2/\rho_1$ in the album fits the observed curve through the principle of equivalence by T or by S), the value of $\mu_2 = \rho_3/\rho_1$ for the field curve may not be among those for which the theoretical curves were computed. Therefore, the first closest fit of the field curve should not be relied on. Better interpretations generally are obtained by enveloping the field curve between two three-layer curves having the same value of $\mu_1 = \rho_2/\rho_1$ and the same value of $\nu = h_2/h_1$ but different values of $\mu_2 = \rho_3/\rho_1$ (fig. 35). If the values of $\mu_2 = \rho_3/\rho_1$ for

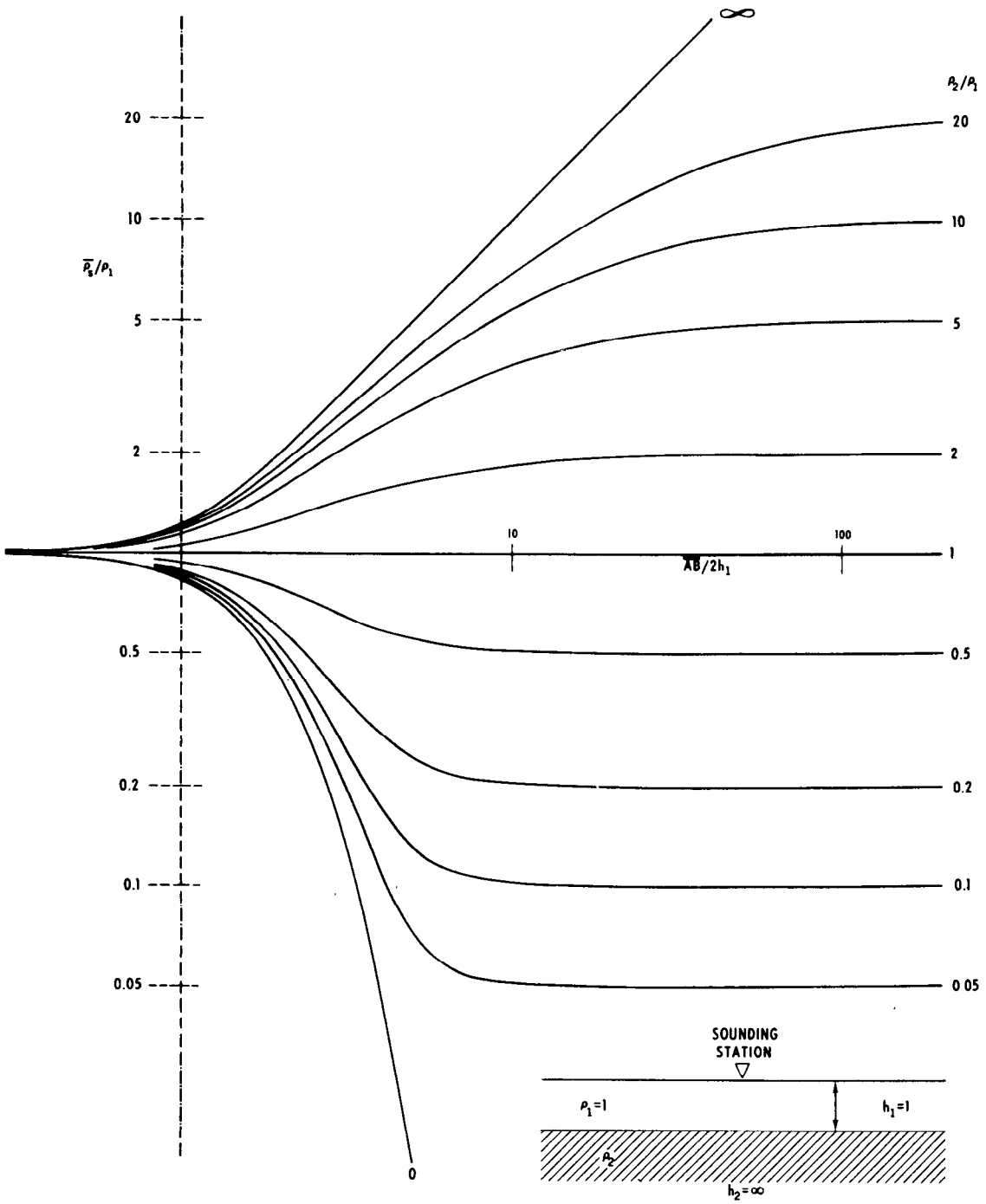

Figure 33.—Two-layer master set of sounding curves for the Schlumberger array (adapted from Orellana and Mooney, 1966).

the field curve and the theoretical curve are equal, then complete curve matching may be attained.

Maintaining parallelism between the axes of the field curve and the theoretical curve, determine the position of the cross on the field curve, note the value of $v_1 = h_2/h_1$ designating the theoretical curve, and note the values of $\mu_1 = \rho_2/\rho_1$ and $\mu_2 = \rho_3/\rho_1$.

Knowing h_1 and ρ_1 from the abscissa and ordinate of the cross, the values of ρ_2, h_2, and ρ_3 can be calculated from the values of $\mu_1 = \rho_2/\rho_1$, $v_1 = h_2/h_1$, and $\mu_2 = \rho_3/\rho_1$, respectively. The determined values of h_2 and ρ_2 may not be equal to the real values in the geologic section because of the principle of equivalence. Consequently the Pylaeve equivalency diagram (Dakhnov, 1953; Kalenov, 1957; Keller and Frischknecht, 1966; Bhattacharya and Patra, 1968) should be consulted for the section (H, A, K, or Q) under consideration, and the minimum and maximum values of h_2 and ρ_2 determined.

If a satisfactory match between the field curve and a theoretical three-layer curve is impossible, then either the curve represents more than three layers, or it is a three-layer curve with a large value of $v = h_2/h_1$ and values of $\mu_1 = \rho_2/\rho_1$ or $\mu_2 = \rho_3/\rho_1$ that are not in the album. The interpretation then is made using the two-layer curves in conjunction with auxiliary point diagrams (Orellana and Mooney, 1966; Zohdy, 1965) or by graphically constructing (Bhattacharya and Patra, 1968; Matveev, 1964; Kalenov, 1957) or numerically calculating (Ghosh, 1971) sets of three-layer master curves for the required values of v_1, μ_1, and μ_2.

Four-layer (or more) Interpretation

In practice, especially with large spacings, four or more layers may be distinctly reflected on the curve. The maximum number of layers detected by the curve with the electrode spacing $\overline{AB}/2$ of as much as 10,000 m (32,800 feet) generally does not exceed eight layers. Four- and five-layer curves are often encountered. The graphical interpretation (fig. 36) of multilayer sounding curves is made by using the three-layer curves and the auxiliary point diagrams (Bhattacharya and Patra, 1968; Kalenov, 1957; Orellana and

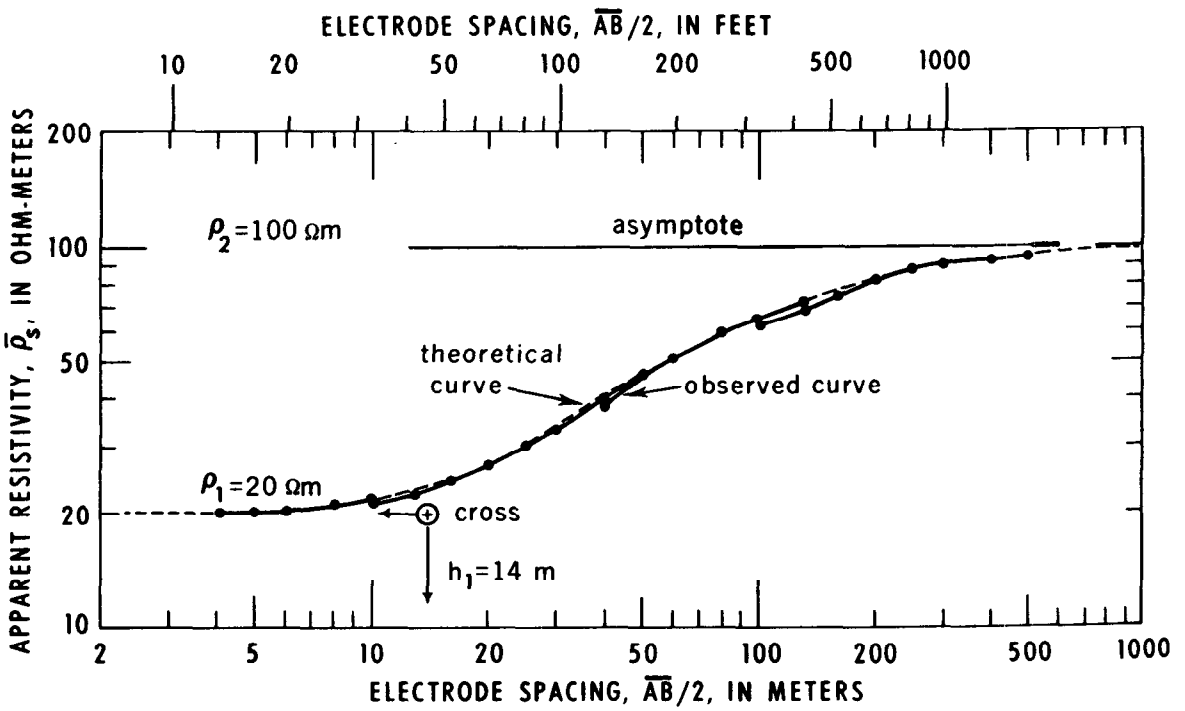

Figure 34.—Interpretation of a two-layer Schlumberger curve ($\rho_2/\rho_1 = 5$).

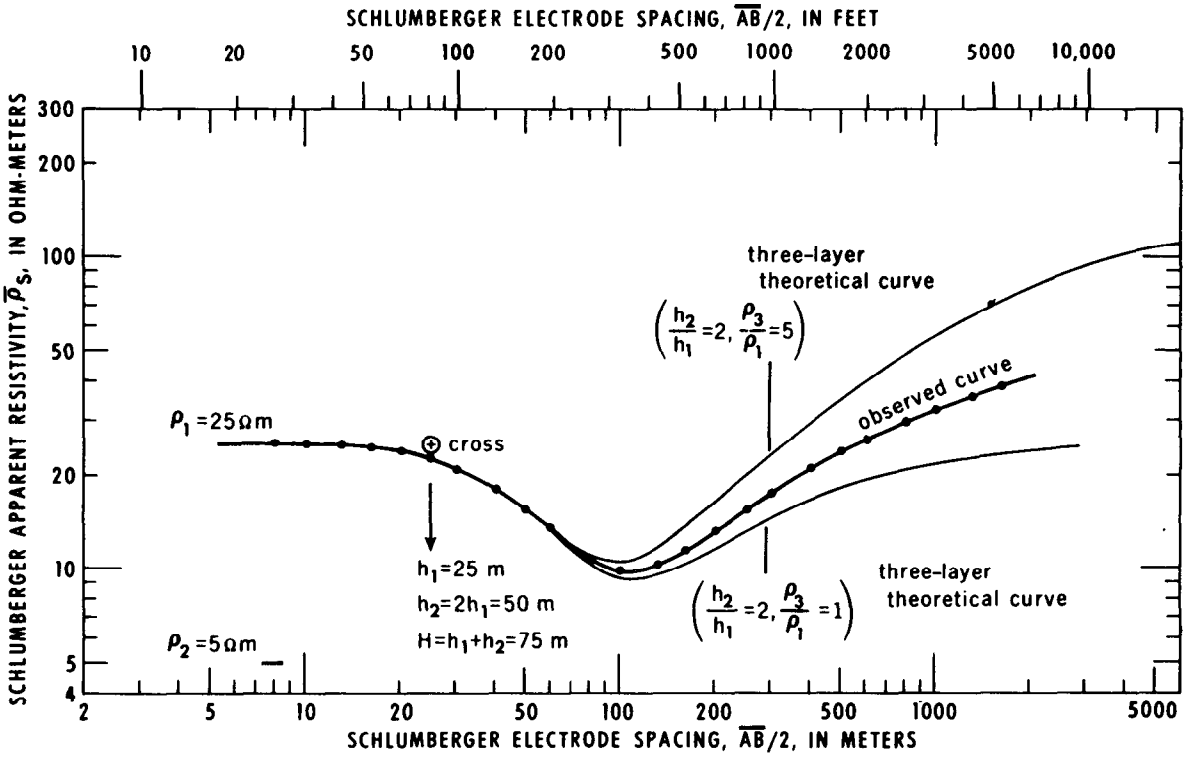

Figure 35.—Interpretation of a three-layer Schlumberger H-type curve.

Mooney, 1966; Zohdy, 1965). The accuracy of the interpretation depends on the effective relative thickness of the layers and the experience of the interpreter. It is suggested that the interpreted model be checked by (1) reconstructing the curve graphically using the method described by Matveev (1964), (2) reconstructing the first part of the curve by graphical methods and calculating the second part of the curve using the methods of Flathe (1955), Van Dam (1964, 1965), or Tsekov (1957), or (3) calculating the entire curve on a high-speed digital computer.

Empirical and Semiempirical Methods of Interpretation of Sounding Curves

Several empirical methods were invented because of the lack of calculated sets of master curves and these methods are still used by some investigators.

Moore's Cumulative Resistivity Method

Moore (1945, 1951) developed the so-called "Cumulative resistivity method," which is an empirical method for determining the depth (but not the resistivity) to horizontal layers from Wenner soundings. The method has been the subject of much discussion and has received both praise and condemnation (Muskat, 1945; Wantland, 1951).

The cumulative resistivity curve is constructed by plotting

$$\sum_{a=a_1}^{a=n} \bar{\rho}_w(a)$$

as a function of the Wenner electrode spacing a. The points on the curve will have the coordinates $(\bar{\rho}_w(a_1), a_1)$; $(\bar{\rho}_w(a_1) + \bar{\rho}_w(a_2), a_2)$; $(\bar{\rho}_w(a_1) + \bar{\rho}_w(a_2) + \bar{\rho}_w(a_3), a_3)$; . . . ; $(\bar{\rho}_w(a_1) + \rho_w(a_2) + \ldots + \rho_w(a_n), a_n)$, where $a_2 - a_1 = a_3 - a_2 = a_n - a_{n-1} =$ contant. This curve consists of straight line segments intersecting at points where the abscissa values, according to Moore are equal to the depths of horizontal boundaries. The method can be tested easily by using the theoretical data published in the Orellana-Mooney tables (Orellana and

Mooney, 1966) for Wenner curves. However, interpolation between the values given in the tables is necessary because the tables are based on electrode spacing values that increase at a logarithmic rate (1, 1.2, 1.4, 1.6, 2, 2.5, 3, 4, . . .), whereas Moore's method assumes a constant linear increase (1, 1.1, 1.2, 1.3, 1.4, 1.5, 1.6, 1.7, . . .). It is found that for horizontal two-layer Earth models the method gives reasonably accurate results provided the contrast in resistivity is moderate. If the contrast is large $(\rho_2/\rho_1) \rightarrow \infty$ or 0, the depth to the interface is underestimated by as much as 50 percent, whereas if the contrast is small, $(\rho_2/\rho_1) \cong 1$, the depth is overestimated by as much as 50 percent. This explains why Moore's method seems to work in certain areas and fails in other areas. The use of the method to interpret three-, or more, layer curves is highly questionable. Furthermore, the method does not give an estimate of the resistivities of the layers.

Barnes' Layer Method

Barnes (1952, 1954) developed an empirical method for the interpretation of electrical sounding data. The method, now known as "Barnes' layer method," is based on the erroneous assumption that the electrode spacing in the Wenner array is equal to the layer thickness. The "layer resistivity" as defined by Barnes, however, has interesting possibilities, especially if the Schlumberger array is used in lieu of the Wenner array, and provided curve-matching interpretation is used in lieu of Barnes' empirical approach (Keller, 1968).

All empirical methods either are rejected or improved by testing them with theoreti-

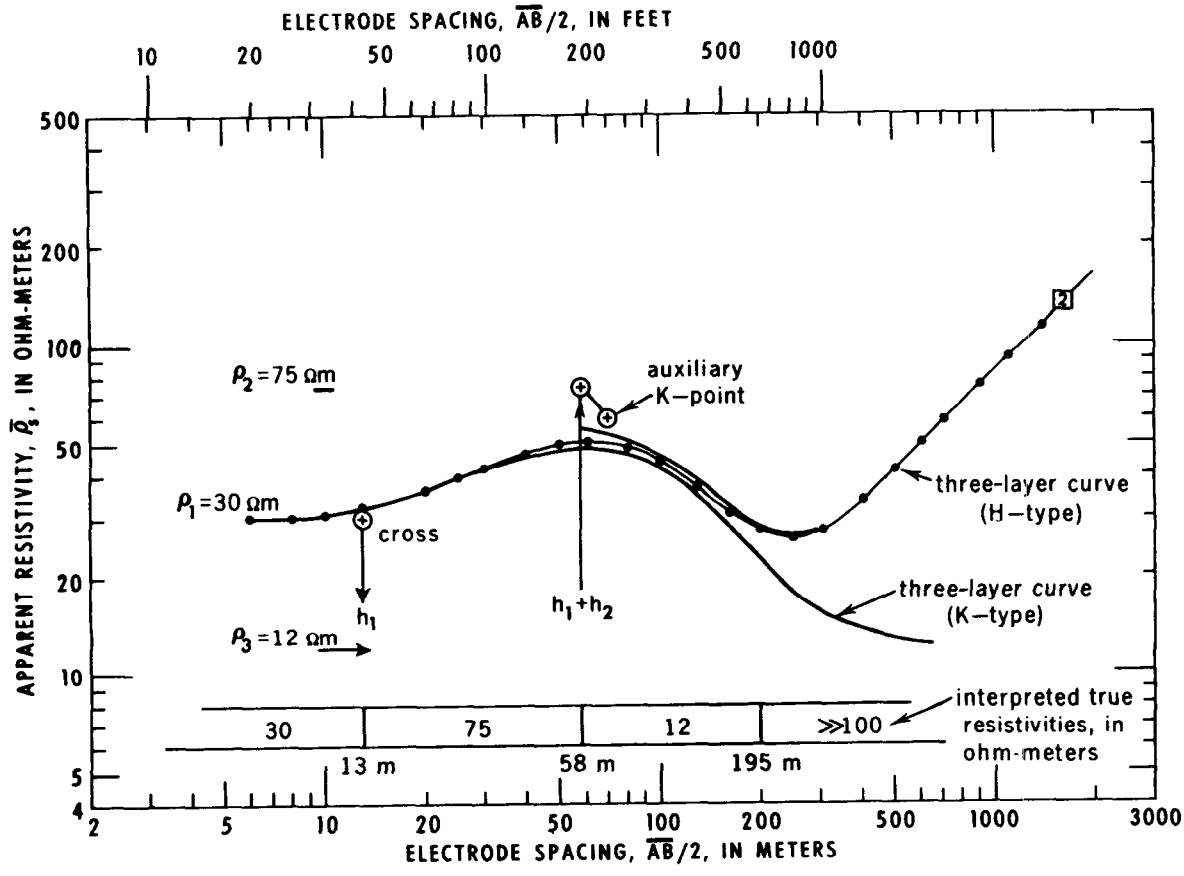

Figure 36.—Interpretation of a four-layer Schlumberger curve by the auxiliary point method using two three-layer curves. The numeral 2 on the upper curve indicates that the thickness of the third layer is twice as great as the abscissa of the auxiliary K point. (For details of method, see Bhattacharya and Patra, 1968; Zohdy, 1965.)

cally exact calculations. By testing empirical methods against tested theoretical curves, semiempirical methods are evolved. The conditions for which such semiempirical relations are valid generally are well defined, and for many of these relations rigorous mathematical formulations proving their approximate validity can be derived. Examples of these methods are: the determination of the value of T from K-type Schlumberger sounding curves, and the evaluation of ρ_L from polar dipole-dipole sounding curves. The Russian literature is richly endowed with such methods (Abdullaev and Dzhafarov, 1964; Kalenov, 1957). Many of these methods resulted in the development of useful nomograms. The general goal of all such methods is to avoid complete curve-matching procedures; consequently, only a part of the information contained in a sounding curve is utilized in interpretation, and large errors sometimes occur. Semiempirical methods, however, are useful in preliminary interpretations and in supplementing the final interpretation.

The empirical and semiempirical methods of interpretation are not recommended except in the preliminary examination of sounding curves. Considerable work has been done using these methods and some of it has been effective in ground-water studies. However, in almost every survey where the interpretation has been based on empirical and semiempirical methods only, more complete and accurate information could have been obtained using analytical methods.

Applications of Resistivity Surveys in Ground-Water Studies

In ground-water studies, the resistivity method can furnish information on subsurface geology which might be unattainable by other geophysical methods. For example, electrical methods are unique in furnishing information concerning the depth of the fresh-salt water interface, whereas neither gravity, magnetic, nor seismic methods can supply such information. A thick clay layer separating two aquifers usually can be detected easily on a sounding curve but the same clay bed may be a low velocity layer in seismic refraction surveys and cause erroneous depth estimates.

Mapping Buried Stream Channels

Buried stream channels, which often can be mapped accurately by the resistivity method, are favored targets for exploration. Horizontal profiling, electrical soundings, or both are used in their mapping.

In the San Jose area, California (fig. 37), knowledge of the presence and extent of shallow permeable layers is important in planning ponds for artificial recharge of ground water. Several buried stream channels were discovered by Zohdy (1964, 1965) and by Page (1968), using the combined techniques of horizontal profiling using the Wenner array and electrical sounding using the Schlumberger and Wenner arrays. Some of these channels were also investigated by use of induced polarization (Bodmer and others, 1968).

The buried stream channel in the Peñitencia area was discovered by making a few electrical soundings, the curves of which were distorted by the effect of lateral heterogeneities. The area was covered then by horizontal profiling using a Wenner electrode spacing of $a = 6.1$ m (20 feet). The result was an isoresistivity map (fig. 38) that clearly delineated the course of the buried channel. A cross section based on the interpretation of four sounding curves, the apparent resistivity profile, and subsequent drilling data are shown in figure 39.

According to information from the Santa Clara Valley Water Conservation District, the water table at one well near the percolation ponds subsequently developed in this area rose from a depth of about 73 m (240 ft) to a depth of about 37 m (130 ft) in two years.

In the area near Campbell, Calif., an apparent-resistivity map (fig. 40) was drawn on the basis of horizontal profiling using the Wenner array with spacing of $a = 9.15$

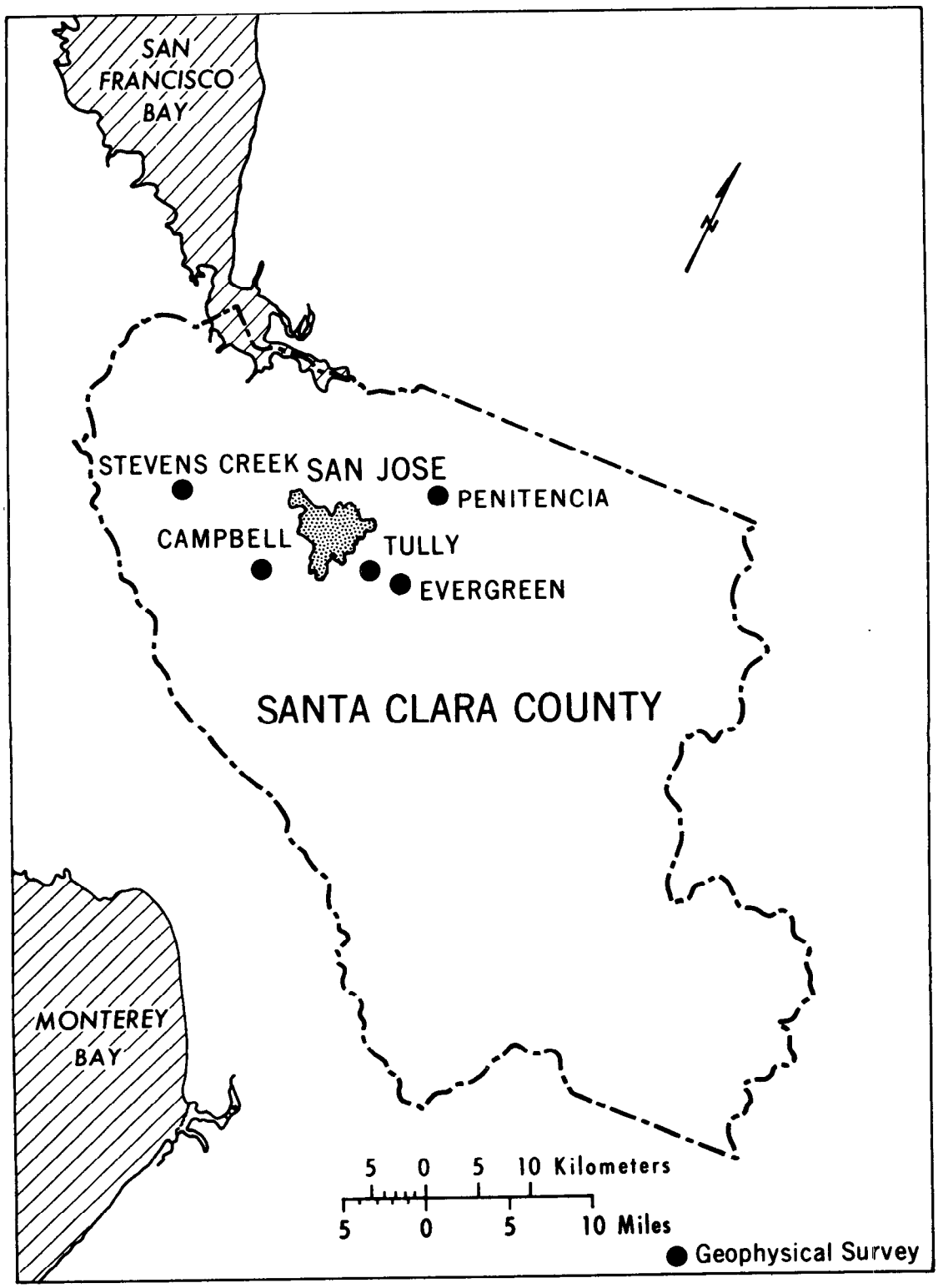

Figure 37.—Map of San Jose area, California, showing areas studied.

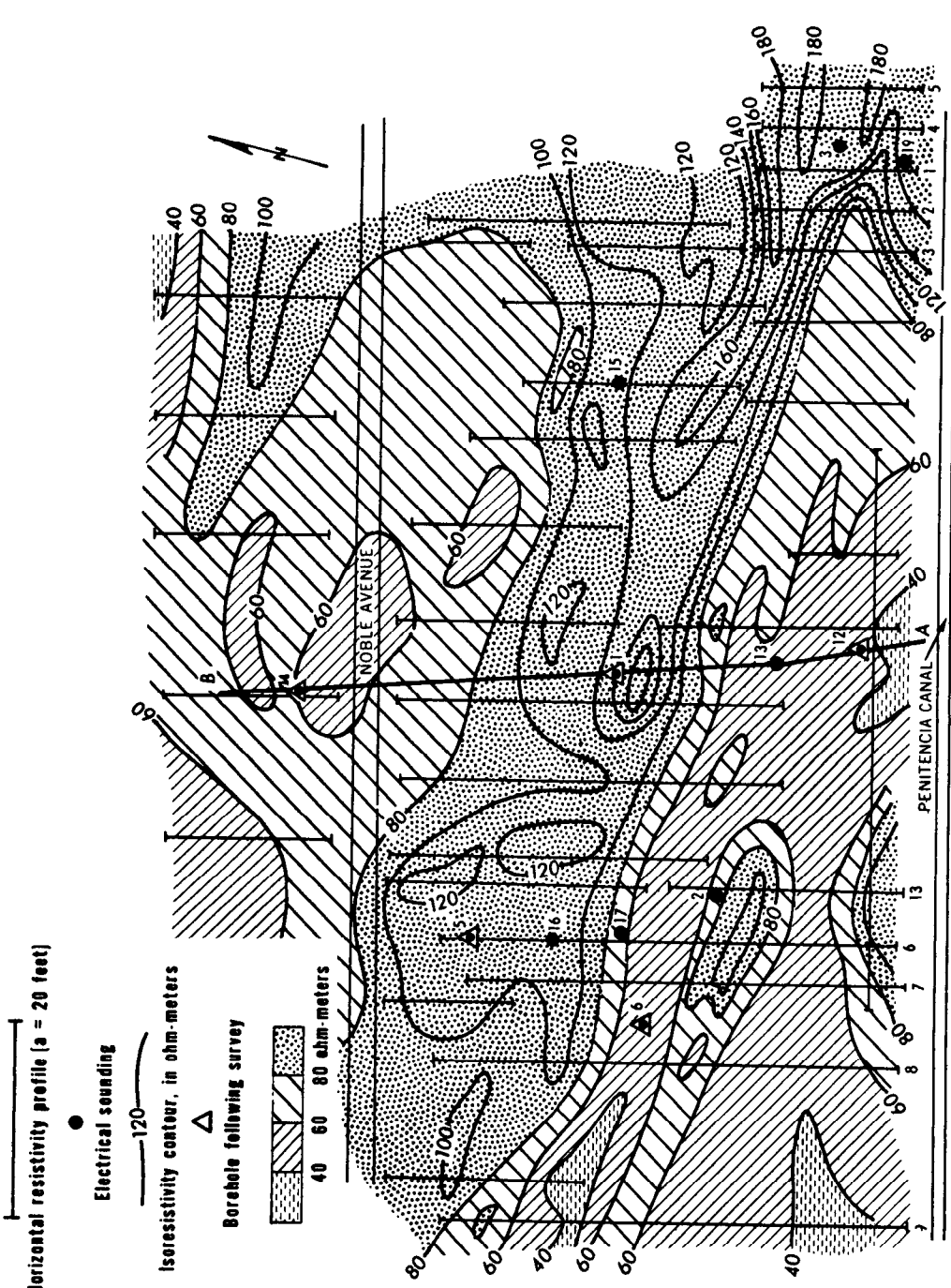

Figure 38.—Apparent-resistivity map, Penitencia, Calif. (after Zohdy, 1964, 1965), showing location of resistivity profile and geologic section, AB.

m (30 feet). The map indicated the presence of high resistivity layers at shallow depth but did not delineate the trend of a buried stream channel as directly and as clearly as in the Penitencia area. A cross-section based on the interpretation of electrical sounding data is shown in figure 41. The drilling of a well by the Santa Clara Water Conservation District near sounding 5 proved that the interpretation of the sounding curves was in excellent agreement with observed geologic conditions.

A buried stream channel saturated with fresh water was discovered near Salisbury, Md., by drilling (Hansen, 1966; Weaver and Hansen, 1966). A resistivity survey was made in the area of the channel using Schlumberger soundings and horizontal profiling ($\overline{AB}$ = 122 m (400 feet), $\overline{MN}$ = 24.4 m (80 feet)). A remarkable anomaly was obtained by horizontal profiling at right angles to the known strike of the channel (fig. 42). The interpretation of depth from the electrical soundings was in general agreement with drilling data.

From these three examples, we may conclude that, in shallow exploration, horizontal profiling can furnish information on the presence or absence of shallow buried stream channels and that elcctrical soundings for the determination of depth should precede and follow the horizontal profiling survey.

There are several examples in the literature (Denozier and others, 1961; Hallenbach, 1953) where courses of buried channels were mapped on the basis of electrical soundings and were subsequently verified by drilling. A map of interpreted true resistivities at a depth of 40 meters (131.2 ft) obtained north of Bremerhaven, West Germany, is shown in figure 43. The map was constructed on the basis of the interpretation of Schlumberger electrical soundings.

Geothermal Studies

In the Bad-Krozingen, Baden geothermal area in West Germany (Breusse and Astier, 1961) electrical soundings and horizontal profiling were made to delineate a fault zone where steam can be tapped for energy. An apparent-resistivity map was obtained

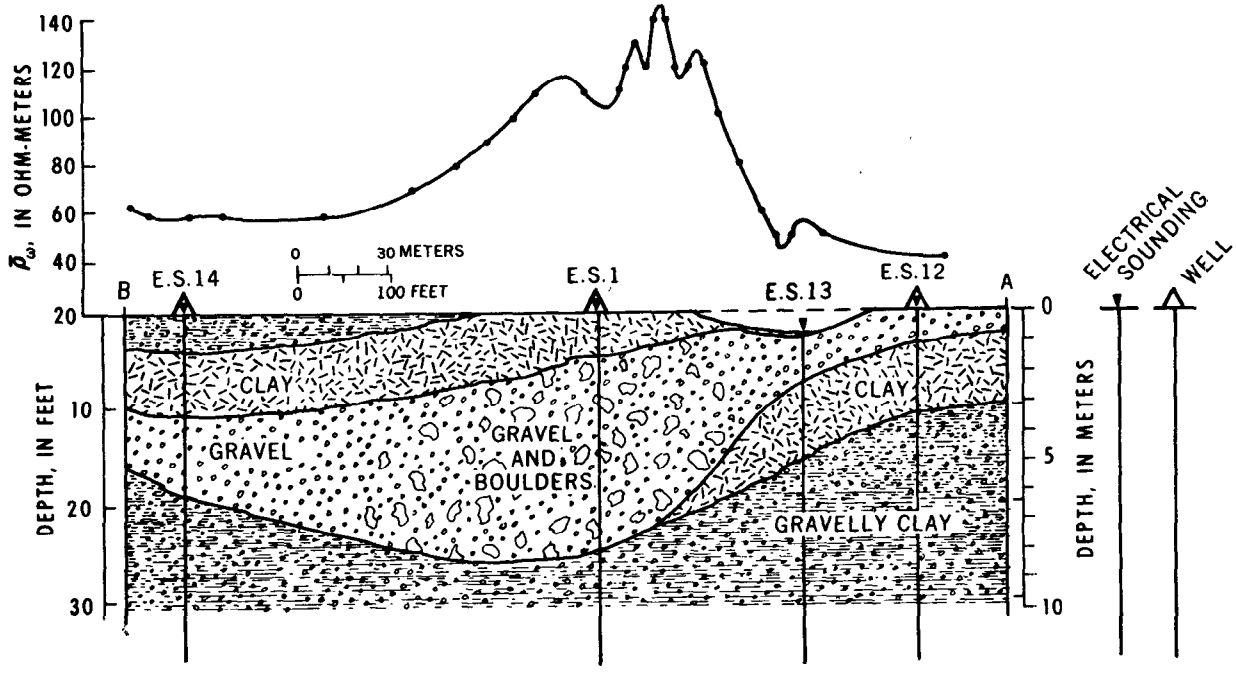

Figure 39.—Resistivity profile and geologic section, Penitencia, Calif. (after Zohdy, 1964, 1965). Horizontal profile obtained using Wenner array with electrode spacing a = 6.1 m (20 feet).

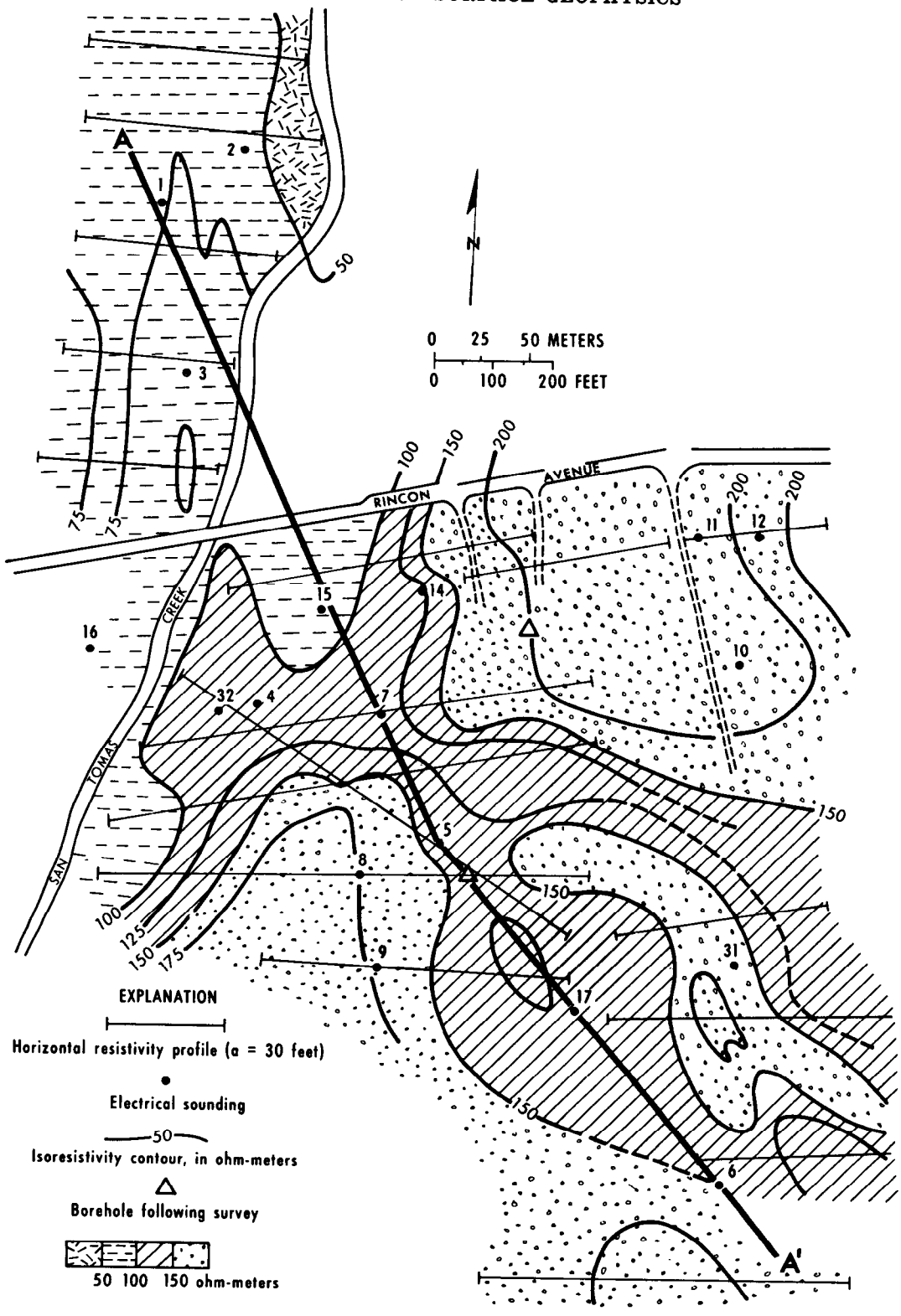

Figure 40.—Map of apparent resistivity near Campbell, Calif., obtained with Wenner array at a = 9.15 m (30 feet) and showing location of section AA'. (Unpub. data obtained by Zohdy, 1964.)

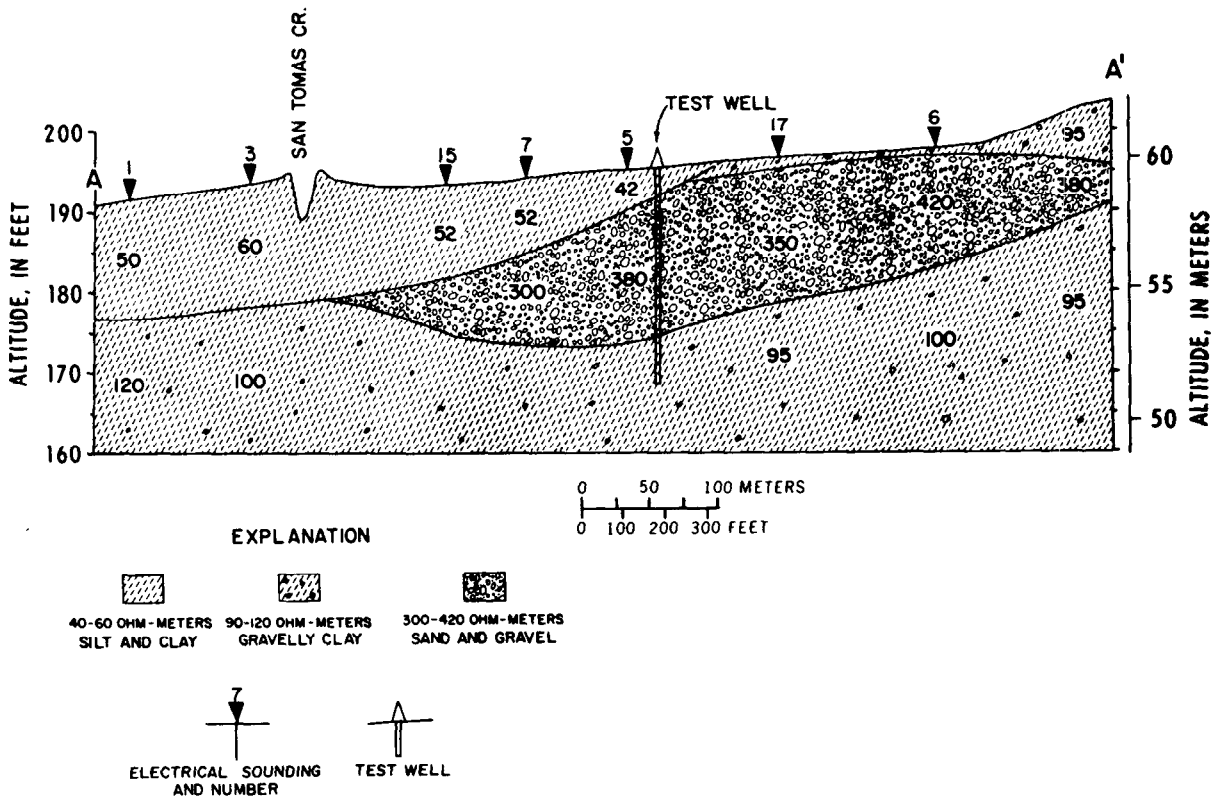

Figure 41.—Geoelectric section and drilling results near Campbell, Calif. Numbers in layers designate interpreted true resistivities. (Unpub. data obtained by Zohdy, 1964.)

by making horizontal profiling using the Schlumberger AB profile technique (see fig. 10a). In this survey the AB line was 4,000 m (13,120 feet) long. Eleven parallel profiles spaced 100 m (328 feet) apart were made, each of which consisted of 111 measurements spaced at 100 m (328 feet) intervals. The apparent-resistivity map obtained from this survey (fig. 44) was used to delineate the traces of the faults.

In New Zealand, Banwell and MacDonald (1965) and Hatherton and others (1966) reported on the successful use of Wenner sounding and horizontal profiling for delineating geothermal areas. Figure 45 shows an apparent-resistivity map prepared from Wenner horizontal profiling data using an electrode spacing of $a = 549$ m (1,800 feet). The two low-resistivity areas outlined by the 5 ohm-meter contour are believed to delineate the hottest ground. The northern area at the Wairakei Geyser Valley was already noted for its geothermal power production, but the large low-resistivity area southeast of Wairakei and northeast of Taupo was discovered by resistivity measurements. A test well (well 225) was drilled in that area, and a temperature of 220°C was recorded at a depth of 256.2 m (840 feet) where a well-marked structural discontinuity is encountered between relatively impermeable mudstones and a permeable pumice breccia. The geothermal power potential in this newly discovered area is probably considerable.

Other studies of geothermal areas were made in Italy by Alfano (1960) and by Breusse and Mathiez (1956).

Mapping Fresh-Salt Water Interfaces

From 1965 to 1969, the U.S. Geological Survey made several resistivity surveys in the southwestern United States where fresh-salt water interfaces were mapped successful-

ly with Schlumberger and equatorial electrical soundings. The apparent-resistivity map (fig. 46) was obtained with $\overline{AB}/2 = 305$ m (1,000 feet) in the White Sands Missile Range area (Zohdy and others, 1969). The apparent-resistivity contour of 10 ohm-m delineates, qualitatively, the area where mineralized groundwater is to be expected at shallow depth. Quantitative interpretation of the electrical sounding curves, using a digital computer for calculation of multilayer curves, resulted in the map shown in figure 47. The isobath lines on the map indicate depths at which the true resistivity of the rocks is less than 10 ohm-m (saline ground water) or more than 500 ohm-m (crystalline basement). Examples of electrical soundings obtained in the White Sands Missile Range area are shown in figure 48.

The literature is rich with case histories of areas in many parts of the world where the resistivity method was successfully used for mapping the fresh-salt water interface (Breusse, 1950; Flathe, 1967, 1968; Flathe and Pfeiffer, 1964; Van Dam and Meulenkamp, 1967; Zohdy, 1969a).

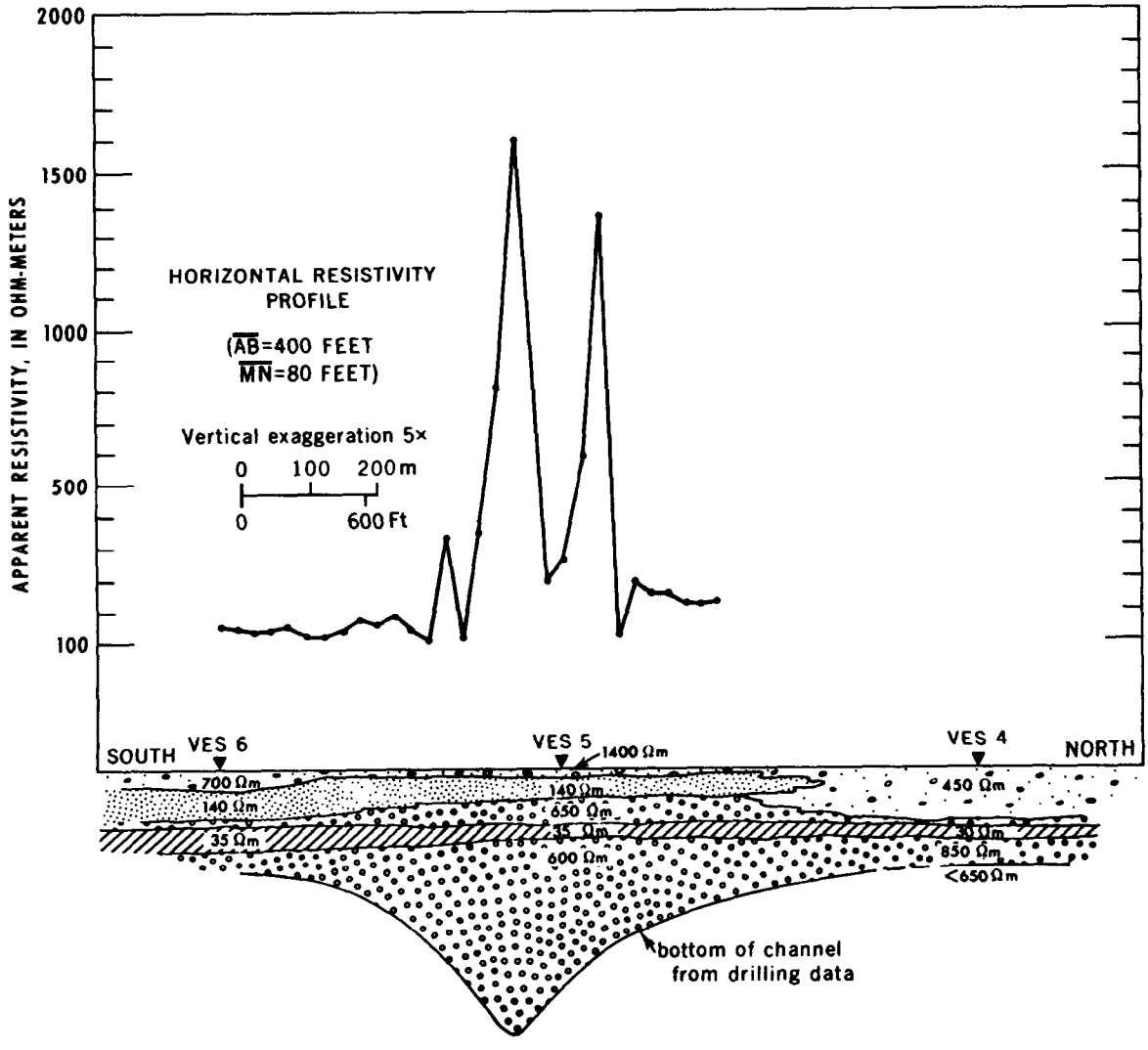

Figure 42.—Apparent-resistivity profile and geologic interpretation over buried channel, near Salisbury, Md. Data obtained by Zohdy and Jackson in 1966.

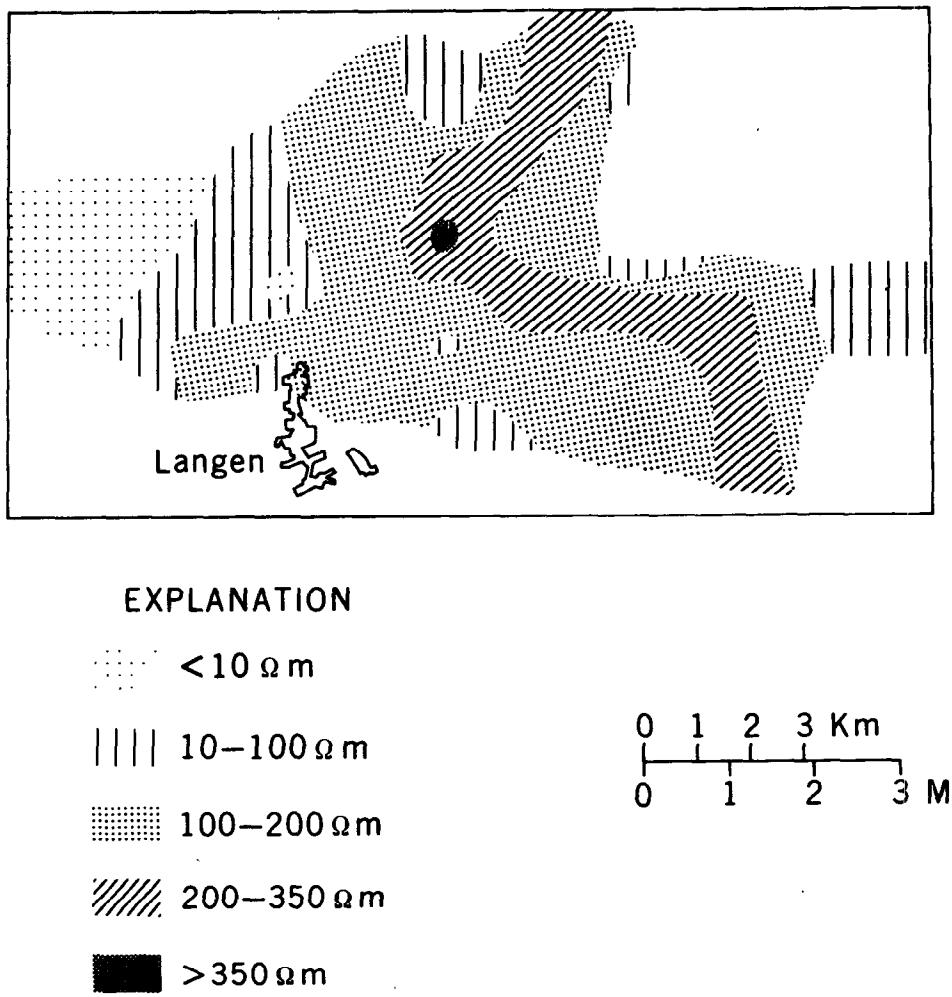

Figure 43.—Buried stream channel near Bremerhaven, West Germany, mapped from electrical sounding (after Hallenbach, 1953). Resistivities of more than 200 ohm-m were interpreted to be within the buried channel. Reproduced with permission of "Geophysical Prospecting."

Mapping the Water Table

Unlike the mapping of the fresh-salt water interface, the determination of the depth to the water table is generally a more difficult problem. Deppermann and Homilius (1965) investigated the geoelectric conditions where the water table can be detected on an electrical sounding curve. Wherever the water table is overlain and underlain by several layers of different resistivities, its detection on a sounding curve may be virtually impossible. Under favorable conditions the water table can be detected on a sounding curve as a conductive layer.

On the island of Hawaii, Zohdy and Jackson (1969) made several deep electrical soundings to determine the depth to low-resistivity layers that may represent basaltic lava saturated wih water. They concluded that the minimum depth to such a layer is of the order of 900 m (3,000 feet) (the survey was made at an average elevation of about 1,900 m (6,200 feet) above sea level). A block diagram based on the interpretation of electrical soundings in the Pohakuloa-

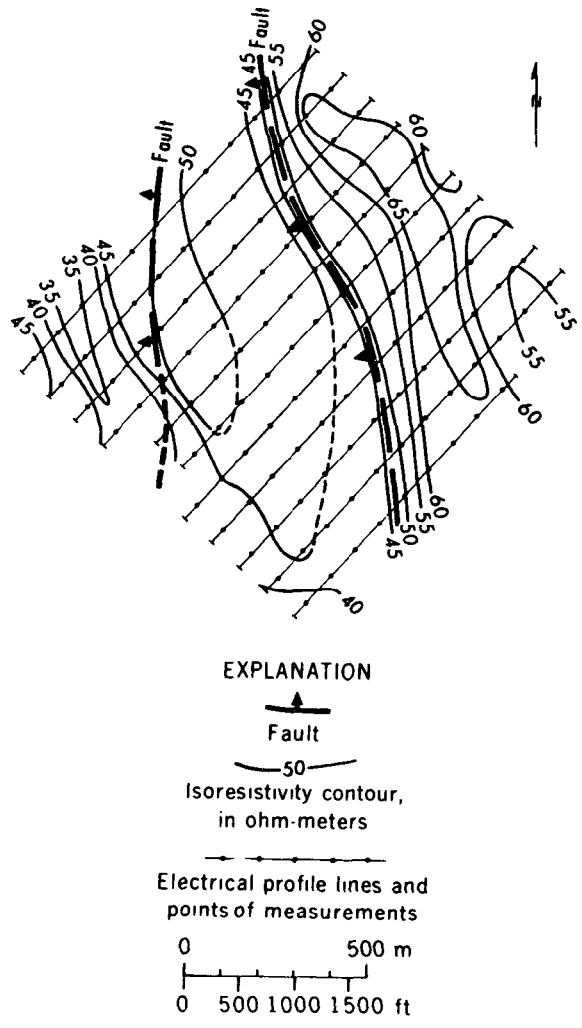

Figure 44.—Map of apparent resistivity in the Bad-Krozingen geothermal area, Germany. AB = 4,000 m (13,120 feet) (after Breusse and Astier, 1961).

Humuula area is shown in figure 49. The top of the layer with resistivity of less than 1,000 omh-m presumably may represent the water table. The ground water in this part of the island probably is partly impounded by dikes.

Mapping Clay Layers

Near Bowie, Ariz., a blue-clay layer separates two aquifers. The lower aquifer is artesian. The resistivity of this clay was found to be in the range of 0.5–7.0 ohm-m. The cross section shown in figure 50 is based on the interpretation of electrical soundings in that area. In places near VES 7 (fig. 51) where the clay is covered by less than 9 m (30 feet) of soil, and where it has very low resistivity (<1 ohm-m) and great thickness 275 m (900 feet), the lower aquifer acts as an electric basement.

Electromagnetic Methods

Electrical surveys also are made using a time-varying electromagnetic field as an energy source. These electromagnetic or induction methods generally use frequencies in the range between 100 and 5,000 Hz, but radio waves of higher frequencies are also used.

The magnetic field is produced by passing an alternating current through a wire loop. When this primary field is imposed on Earth materials a flow of electrical current results. The amount of current flow, as in other electrical surveys, depends on the conductivity of the layers. The current flow produces a secondary magnetic field which has the same frequency as the primary field, but not the same phase or direction. The secondary magnetic field can be detected at or above the ground surface by measuring the voltage induced in another loop of wire, the receiver.

Electromagnetic surveys can be made either on the ground or from a low-flying aircraft. The effective depth at which conductive bodies can be detected with electromagnetic methods is dependent upon both the frequency and spacing between the transmitter and the receiver loops. Thus, electromagnetic measurements can be used in the same manner as resistivity measurements to obtain horizontal profiles and depth soundings. In general, electromagnetic surveys lack the resolution and depth penetration of resistivity surveys but have the advantage of being rapid and less expensive. Results of electromagnetic surveys generally are presented in profile form. Measurements may be made at one or several frequencies. Interpretation usually is accomplished by curve matching or modeling. The technique is very effective in locating conductive bodies within

a few hundred feet of the surface, but has found only limited use in ground-water investigations. The technique has been used effectively in mapping buried channels where the channel-filling material has a resistivity contrast with the enclosing medium (Collett, 1967).

In recent years several powerful radio transmitters have begun broadcasting at frequencies of a few tens of kilo-Hertz. Radio waves at these frequencies penetrate the Earth to sufficient depths to be of use in geophysical exploration. Both ground and airborne detection systems have been developed. The measurements consist of one or more components of the electrical and magnetic fields. This method, which is undergoing rapid development, has proved effective in detecting near-surface highly conductive deposits, but quantitative interpretation techniques are not yet available.

A description of inductive methods is contained in Keller and Frischknecht (1966).

Induced Polarization Method

The induced electrical polarization method is widely used in exploration for ore bodies, principally of disseminated sulfides. Its use in ground-water exploration has been limited. The origin of induced electrical polarization is complex and is not well understood. This is primarily because several physico-chemical phenomena and conditions are responsible for is occurrence.

Conrad Schlumberger (Dobrin, 1960) probably was first to report on the induced polarization phenomenon, which he called "provoked polarization." While making conventional resistivity measurements, he noted that the potential difference, measured be-

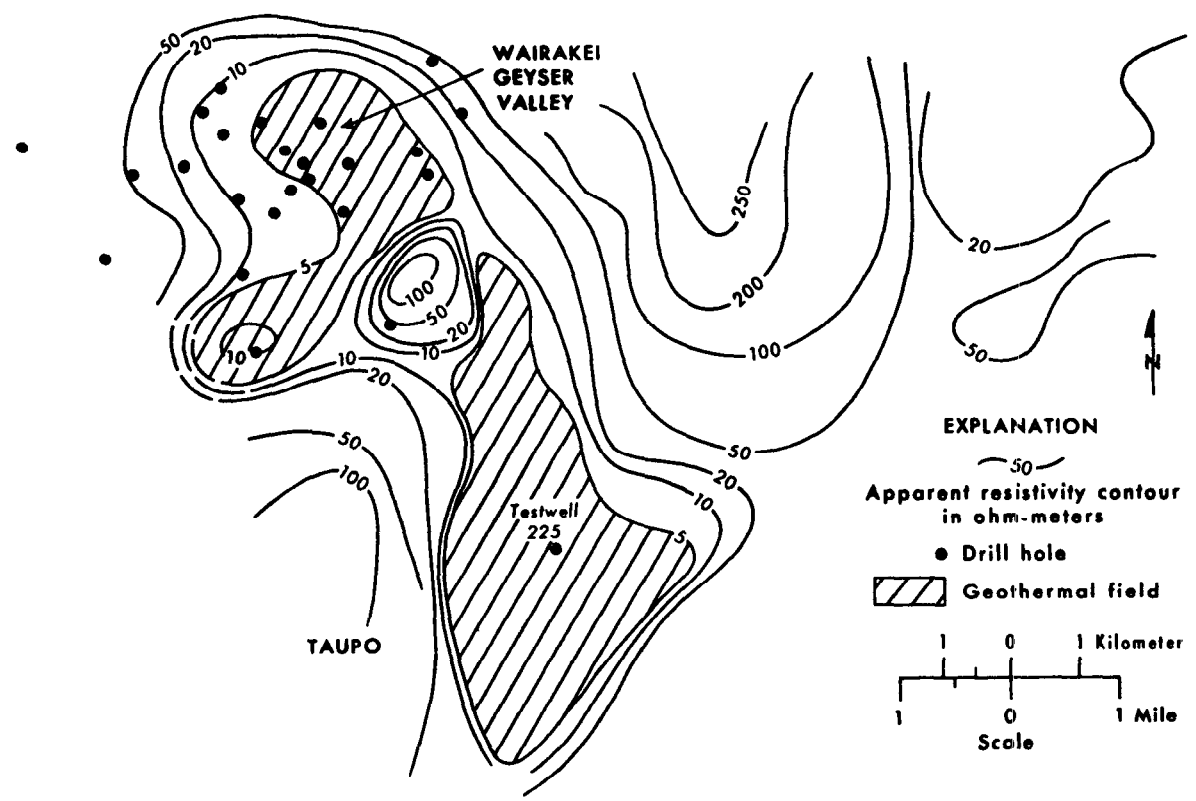

Figure 45.—Map of apparent resistivity in geothermal areas in New Zealand. Wenner spacing a = 549 m (1,800 feet). After Banwell and MacDonald (1965). Reproduced with permission of Commonwealth Mining and Metallurgical Congress.

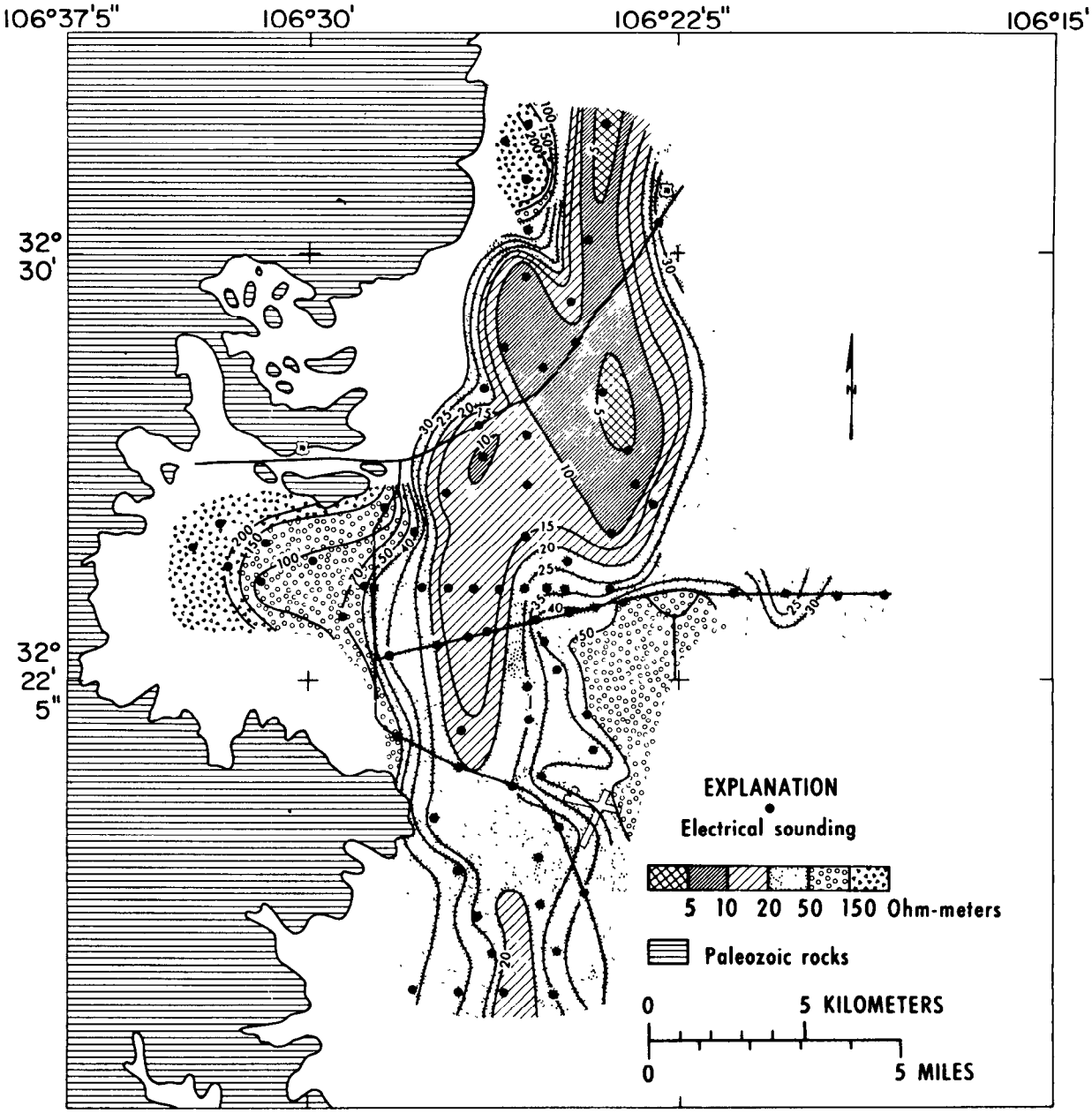

Figure 46.—Map of apparent resistivity in White Sands area, New Mexico, for electrode spacing $\overline{AB}/2 = 305$ m (1,000 feet) (after Zohdy and others, 1969).

tween the potential electrodes, often did not drop instantaneously to zero when the current was turned off. Instead, the potential difference dropped sharply at first, then gradually decayed to zero after a given interval of time. Certain layers in the ground became electrically polarized, forming a battery when energized with an electric current; upon turning off the polarizing current, the ground gradually discharged and returned to equilibrium.

The study of the decaying potential difference as a function of time is now known as the study of IP (induced polarization) in the "time domain." This type of study requires heavy and generally bulky equipment in the

field; to avoid this limitation, mining geophysicists began to study the effect of alternating currents on the measured value of resistivity. This is known as IP in the "frequency-domain."

Ground-water studies generally have been made with time-domain IP. In the time-domain IP, several indices have been used to define the polarizability of the medium. Seigel (1959) defined the "chargeability" (in seconds) as the ratio of the area under the decay curve (in millivolt-seconds) to the potential difference (in millivolts) measured before switching the current off. Komarov and others (1966) define the "polarizability" as the ratio of the potential difference after a given time from switching the current off to the potential difference before switching the current off. The polarizability is expressed as a percentage.

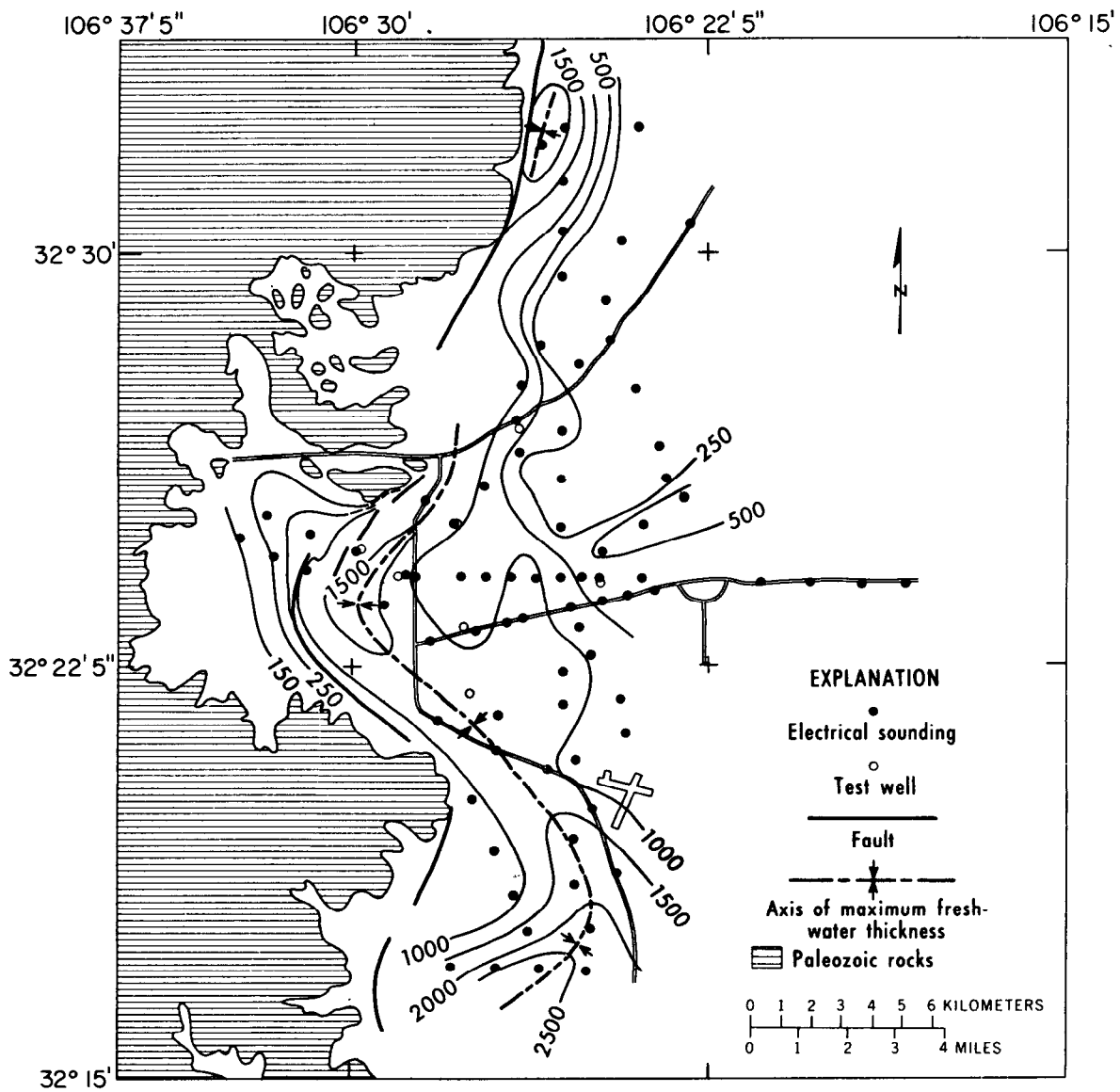

Figure 47.—Map of White Sands area, New Mexico, showing isobaths of the lower surface of fresh-water aquifer. Datum is land surface (after Zohdy and others, 1969).

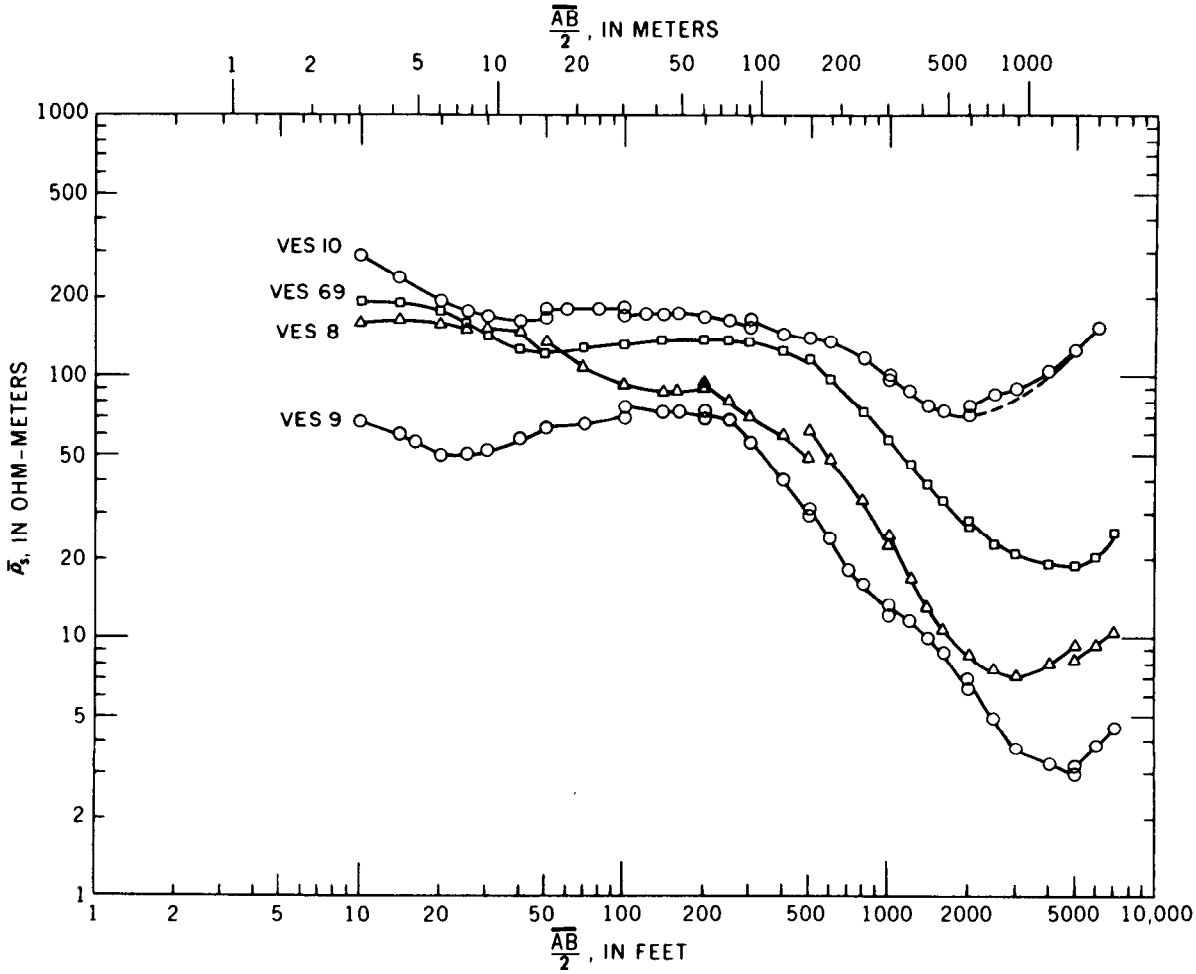

Figure 48.—Examples of Schlumberger sounding curves obtained in the White Sands area, New Mexico (after Zohdy and others, 1969).

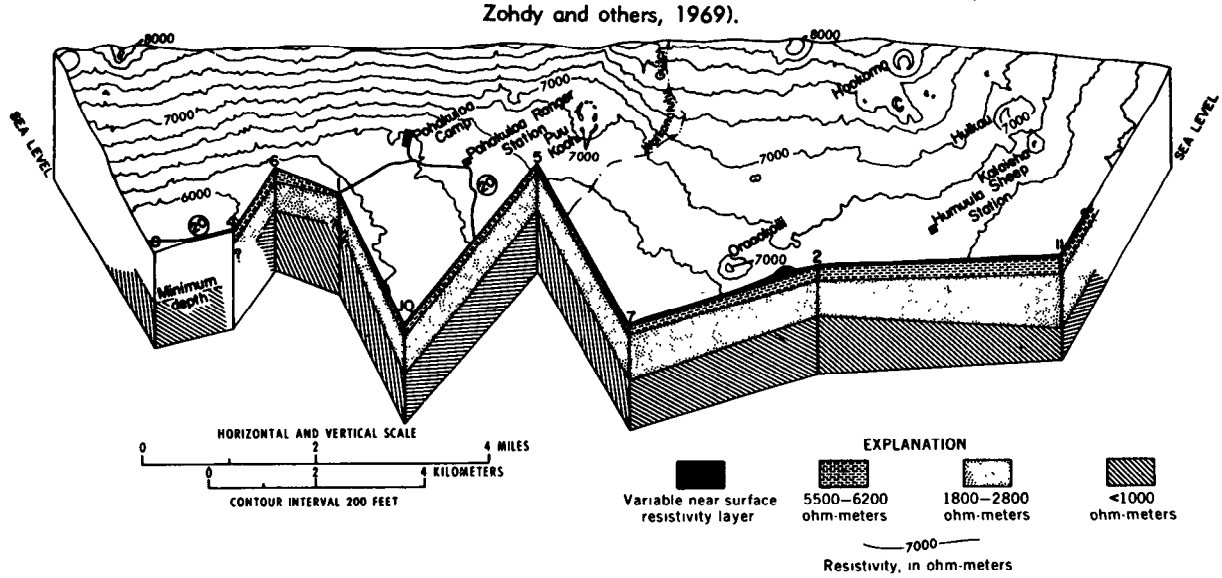

Figure 49.—Block diagram of Pohakuloa-Humuula area, Hawaii (after Zohdy and Jackson, 1969). Reproduced with permission of "Geophysics."

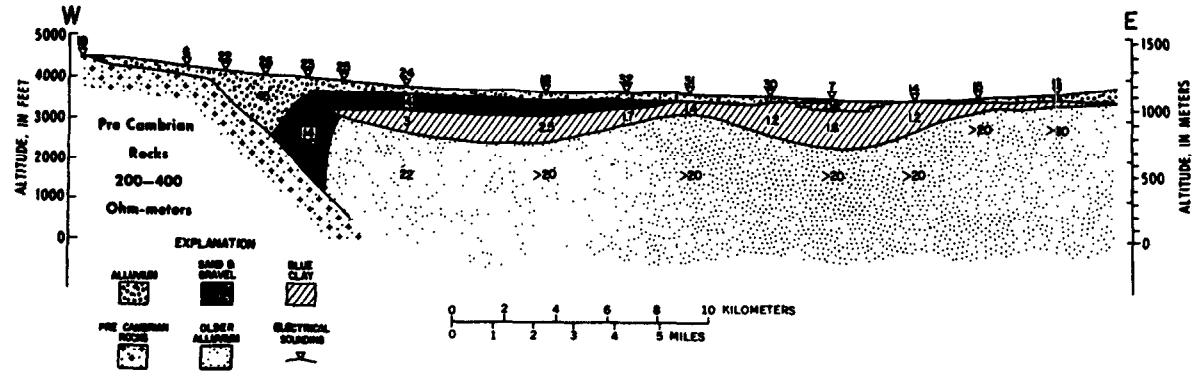

Figure 50.—Geoelectric section north of Bowie, Ariz. Numbers in layers designate true resistivities. Data obtained by Zohdy and Eaton, 1969.

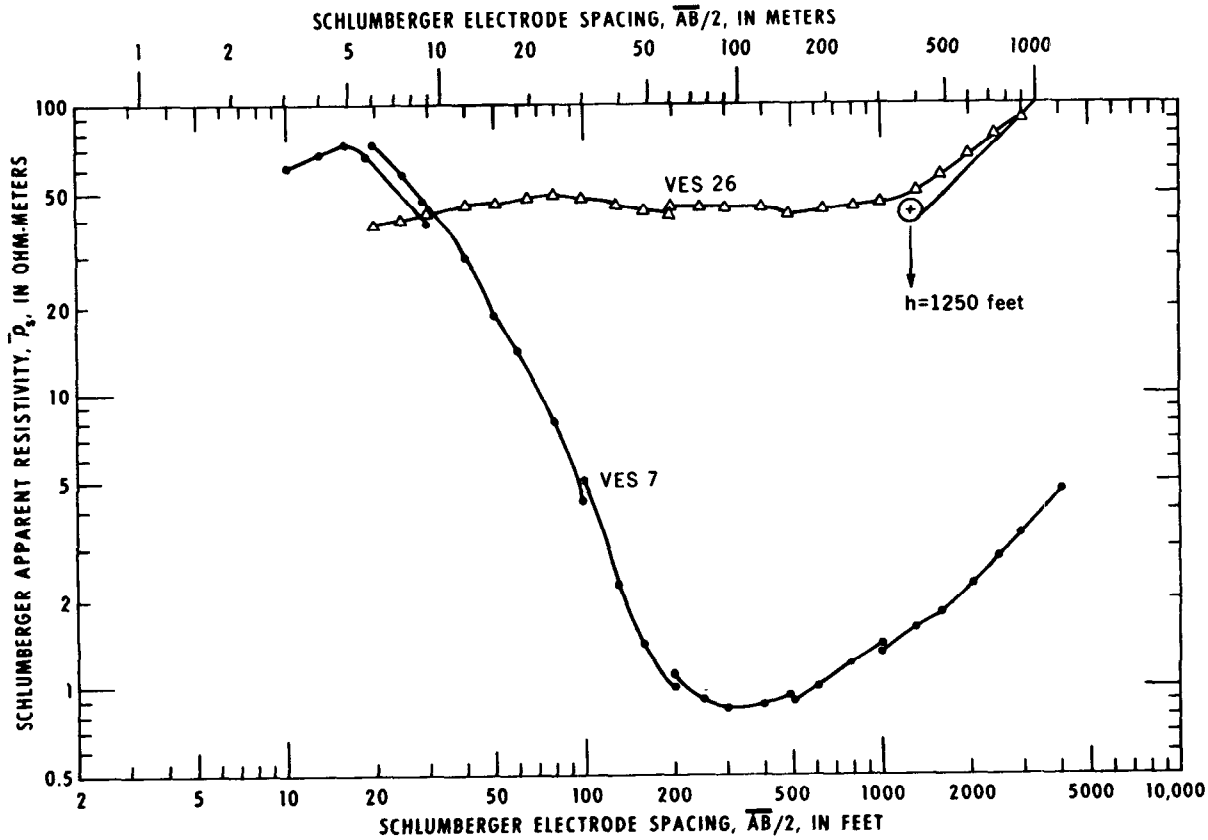

Figure 51.—Examples of Schlumberger sounding curves obtained near Bowie, Ariz. VES 26 shows homogeneous sediments (45 ohm-m) underlain by high resistivity Precambrian rocks at a depth of about 380 m (1,250 feet). VES 7 shows the presence of a thick section 275 m (900 feet) of low resistivity clay (<1 ohm-m). Data obtained by Zohdy and Eaton, 1969.

Relationship between apparent chargeability and apparent resistivity

Seigel (1959) showed that over a heterogeneous medium comprised of n different materials, the apparent chargeability, $\overline{\eta}$, is related to the apparent resistivity by

$$\overline{\eta} = \sum_{i=1}^{n} \eta_i \frac{\partial \log \overline{\rho}}{\partial \log \rho_i}, \qquad (1)$$

where η_i and ρ_i are the chargeability and resistivity of the i^{th} material. He also showed that the relation

$$\sum_{i=1}^{n} \frac{\partial \log \overline{\rho}}{\partial \log \rho_i} = 1, \qquad (2)$$

is valid. From equations 1 and 2 we can write the useful formula:

$$\frac{\overline{\eta}}{\overline{\eta}_1} = 1 + \sum_{i=2}^{n} \frac{\partial \log \overline{\rho}}{\partial \log \rho_i}\left(\frac{\eta_i}{\eta_1} - 1\right). \qquad (3)$$

If the theoretical expression for the apparent resistivity, $\overline{\rho}$, is known, then the corresponding expression for the reduced apparent chargeability $\frac{\overline{\eta}}{\eta_1}$, can be derived easily.

Induced Polarization Sounding and Profiling

The techniques of sounding and profiling, used in resistivity measurements, are also used in the IP method. IP sounding can be made using the Schlumberger, or Wenner array (in time-domain measurements). The apparent chargeability, $\overline{\eta}$, versus the electrode spacing, $\overline{AB}/2$ or $\overline{AB}/3$, is plotted on logarithmic coordinates. The IP sounding curve is interpreted by curve matching procedures using sets of IP sounding master curves.

At present, only a few two-layer master curves (for the Wenner array) have been published in the United States (Seigel, 1959; Frische and von Buttlar, 1957) but three-layer and four-layer curves have been published in the Soviet Union.

An IP sounding curve can be of significant value in complementing a resistivity sounding curve. For example, the resistivity and IP sounding curves for the following four-layer geoelectric section are shown in figure 52:

Layer	Thickness (m)	Thickness (ft)	Resistivity (ohm-m)	Chargeability (seconds)
1	10	32.8	10	1
2	10	32.8	160	1
3	5	16.4	40	10
4	∞	∞	160	1

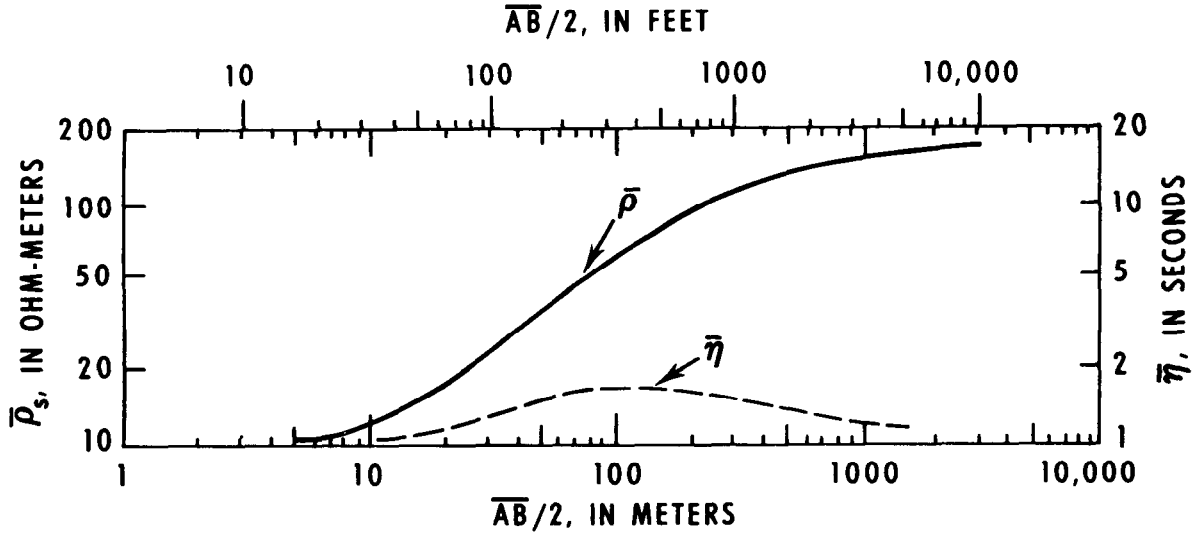

Figure 52.—Apparent resistivity and apparent chargeability (IP) sounding curves for a four-layer model (modified after Vanyan and others, 1961).

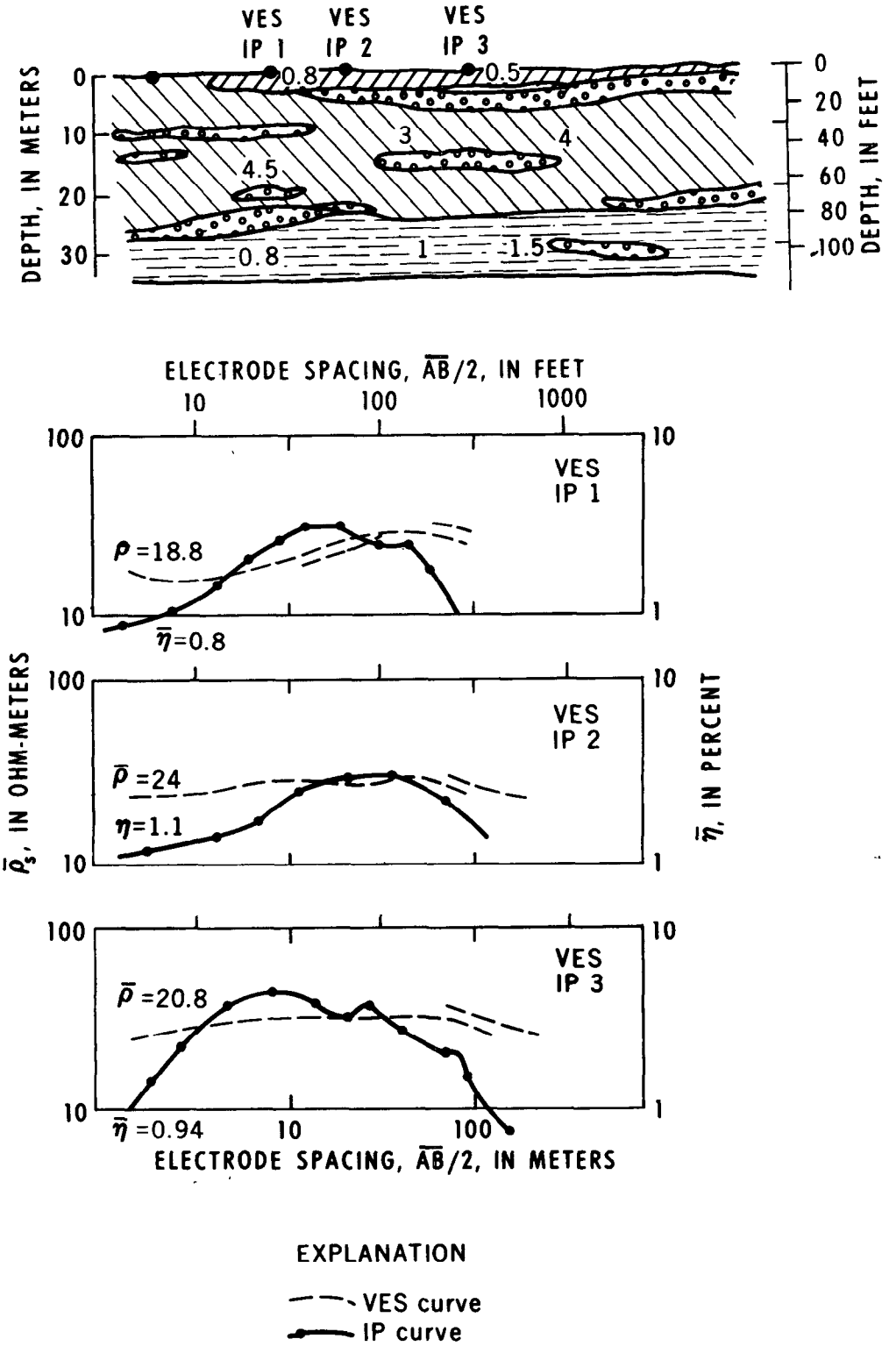

Figure 53.—Geoelectric section, VES and IP sounding curves of alluvial deposits in Crimea (after Kuzmina and Ogil'vi, 1965).

It is obvious that layer 3 cannot be distinguished on the four-layer resistivity curve (which resembles a two- or three-layer curve). But layer 3 is characterized by a different chargeability from the surrounding layers and its presence is indicated clearly by the IP sounding curve.

Applications of Induced Polarization in Ground-Water Surveys

Only a few IP surveys have been made for ground-water exploration, but there are three noted examples in the literature: Vacquier and others (1957); Kuzmina and Ogil'vi (1965); and Bodmer and others (1968). Kuzmina and Ogil'vi reported on work done near the Sauk-Soo river in Crimea and in the Kalinino region of Armenia. In Crimea the IP work consisted essentially of IP sounding (time domain) using the Wenner array. The alluvial deposits in the studied area were poorly differentiated by their resistivities, but three horizons were clearly distinguished by their polarizabilities (fig. 53). The section consisted of a top layer of weak polarizability (h_1 = 2–4 m (6.5–13 ft); η_1 = 0.8–1.5 percent), which represents a dry loamy layer; a second layer of strong polarizability (h_2 = 18–20 m (60–64 ft), η_2 = 3–5 percent), which represented a clayey sand layer saturated with fresh water; and a third layer of weak polarizability ($h_3 \rightarrow \infty$, η_3 = 1 percent), which represents impervious siltstones. The survey in this area demonstrates that the IP work provided more complete information about the ground-water occurrence than did the resistivity soundings alone.

References Cited

Abdullaev, R. A., and Dzhafarov, Kh. D., 1964, Theory and practice of the interpretation of geophysical observations (in Russian): Baku, Azerbaydzh. Gosudarst. Izd. (State press of Azerbaydzhan), p. 117–119.

Alfano, Luigi, 1959, Introduction to the interpretation of resistivity measurements for complicated structural conditions: Geophys. Prosp., v. 7, p. 311–366.

——— 1960, Geoelectric exploration for natural steam near Monte Amiata: Quaderni de Geophysica Applicata, v. 21, p. 3–17.

Al'pin, L. M., 1950, The theory of dipole sounding: Moscow, Gostoptekhizdat, 89 p. [Translation *in* Dipole methods for measuring earth conductivity]: New York, Plenum Press, 1966, p. 1–60.

——— 1958, Transformation of sounding curves: Prikladuaya Geofizika, v. 19, p. 23–46. [Translation *in* Dipole methods for measuring earth conductivity]: New York, Plenum Press, 1966, p. 61–78.

Banwell, C. J., and MacDonald, W. J. P., 1965, Resistivity surveying in New Zealand thermal areas: Eighth Commonwealth Mining and Metallurgical Congress, Australia and New Zealand, New Zealand Section, paper no. 213, 7 p.

Barnes, H. E., 1952, Soil investigations employing a new method of layer value determination for earth resistivity investigation: Highway Research Board Bull. 65, p. 26–36.

Barnes, H. E., 1954, Electrical subsurface exploration simplified: Roads and Streets, v. 97, p. 81–84.

Berdichevskii, M. N., 1957, On the determination of the total longitudinal conductance of sediments above a basement (in Russian): Razved. i promysl. geofiz., v. 19, p. 25–28. English translation by A. Zohdy, 1967, U. S. Geol. Survey Library, Denver, 7 p.

——— 1960, Electrical surveying by means of telluric currents: Moscow, Gostoptekhizdat. (English translation by Bradley, J. E. S., 1963, Boston Spa, England, National Lending Library; also by Keller, G. V., 1965, Quarterly of the Colorado School of Mines, v. 60, no. 1, 216 p.)

Berdichevskii, M. N., and Petrovskii, A. D., 1956, Methods of bilateral equatorial sounding: Prikladnaya Geofizika, v. 14, p. 97–114. [Translation by Ivan Mittin, U.S. Geol. Survey Library, Denver, 37 p.].

Berdichevskii, M. N., and Zagarmistr, A. M., 1958, Problems of interpretation of bilateral dipole electrical soundings of dipole arrays: Prikladnaya Geofizika, v. 19, p. 57–108. [Translation *in* Dipole methods for measuring earth conductivity: Plenum Press, 1966, p. 79–113.]

Bhattacharya, P. K., and Patra, H. P., 1968, Direct current geoelectric sounding, principles and interpretation: New York, Elsevier, 135 p.

Blokh, I. M., 1957, Dipole electroprofiling (in Russian): Moscow, Gosgeoltekhizdat, 191 p.

——— 1962, The resistivity method of electroprofiling (in Russian): Moscow, Gosgeoltekhizdat, 239 p.

Bodmer, René, Ward, S. H., and Morrison, H. F., 1968, On induced electrical polarization and

ground water: Geophysics, v. 33, no. 5, p. 805–821.

Breusse, J. J., 1950, La prospection électrique appliquée aux recherches hydrologique dans la presequ'île de Dakar: Internat. Geol. Cong., pt. V, p. 16–25.

——— 1961, Ground water geological surveys of the area east of Rome: Bull. de D'Association International des Hydrologeolgues, Rome Convention, Aug. 1961, 11 p.

——— 1963, Modern geophysical methods for subsurface water exploration: Geophysics, v. 28, no. 4, p. 633–657.

Breusse, J. J., and Mathiez, J. P., 1956, Application of electrical prospecting to tectonics in the search for natural steam at Larderello (Italy): Geophysical Case Histories, v. 2, p. 623–630.

Breusse, J. J., and Astier, J. L., 1961, Etude des diapirs en Alsace et Baden-Wurtemberg par la method du rectangle de resistivite: Geophys. Props., v. 9, p. 444–458.

Cagniard, Louis, 1953, Basic theory of the magnetotelluric method of geophysical prospecting: Geophysics, v. 18, p. 605–635.

——— 1956, Electricité tellurique, *in* Encyclopedia of Physics: Berlin, Springer-Verlag, v. 47, p. 407–469.

Collett, L. S., 1967, Resistivity mapping by electromagnetic methods: Mining and Groundwater Geophysics/1967, Geol. Survey of Canada, Economic Geology Rept. 26, p. 615–624.

Compagnie Générale de Géophysique, 1955, Abaques de sondage électrique: Geophys. Prosp., v. 3, supplement 3.

——— 1963, Master curves for electrical sounding (2nd revised edition): Leiden, Eur. Assoc. of Explr. Geophys.

Dakhnov, V. N., 1953, Electrical prospecting for petroleum and natural gas deposits: Moscow, Gostoptekhizdat, 497 p.

Denozière, P., Hirtz, J. M., Astier, J. L., Millot, G., and Simler, L., 1961, Étude hydrogeologique par prospection électrique du cône de déjection de L'Andlau (environs d'Anlau, Bas-Rhin): Strasbourg, Bull. Serv. Carte géol. Als. Lorr., v. 14, pt. 2, p. 27–37.

Deppermann, Karl, 1954, Die Abhangigkeit des scheinbaren Widerstandes von Sondenabstand bei der Vierpunkt-Method: Geophys. Prosp., v. 2, p. 262–273.

Deppermann, Karl, and Homilius, Joachim, 1965, Interpretation geoelektrischer Sondierungskurven bei Tiefliegender Grundwasseroberfläche: Geologisches Jahrbuch, v. 83, p. 563–573.

Dobrin, M. B., 1960, Introduction to geophysical prospecting (2nd edition): New York, McGraw-Hill Book Co., Inc., 446 p.

Dzhafarov, Kh. D., and Bairamova, R. A., 1965, The interpretation of four-layer VES curves of the HK-type (in Russian): Razvedochnaya Geofizika, v. 3, p. 78–82. English translation by Rhoda Robinson, U.S. Geol. Survey Library, Denver, 8 p.

Evjen, H. M., 1938, Depth factors and resolving power of electrical measurements: Geophysics, v. 3, p. 78–98.

Flathe, H., 1955, A practical method of calculating geoelectrical model graphs for horizontally stratified media: Geophys. Prosp., v. 3, p. 268–294.

Flathe, H., 1958, Geoelectrical investigations on clay deposits in Western Germany: Leiden, European Assoc. Explor. Geophysicals. Geophysical surveys in mining, hydrological, and engineering projects, p. 170–185.

——— 1963, Five-layer master curves for the hydrogeological interpretation of geoelectric resistivity measurements above a two-story aquifer: Geophys. Prosp., v. 11, p. 471-508.

——— 1964, New ways for the interpretation of geoelectrical resistivity measurements in the search for and delimitation of aquifers: Internat. Assoc. of Sci. Hydrology Bull. 9th year, no. 1, p. 52–61.

——— 1967, Interpretation of geoelectrical resistivity measurements for solving hydrogeological problems: Mining and Groundwater Geophysics/1967, Geol. Survey of Canada, Econ. Geol. Report 26, p. 580–597.

——— 1968, Geoelecktrische Untersuchung der Grundwasserversalzung im südlichen Jordantal: Geologisches Jahrbuch, v. 85, p. 767–782.

Flathe, Herbert, and Pfeiffer, D., 1964, Outlines on the hydrology of the isle of Madura (Indonesia): Internat. Assoc. of Sci. Hydrology, Berkeley, 1963, no. 64, p. 543–560.

Frische, R. H., and Von Buttlar, Haro, 1957, A theoretical study of induced electrical polarization: Geophysics, v. 22, no. 3, p. 688–706.

Genslay, R., and Rouget, F., 1937, Sur l'anisotropie électrique des terrains et la pseudo-anisotropie: World Petroleum Cong. 2d, p. 723–731.

Ghosh, D. P., 1971, Inverse filter coefficient for the computation of apparent resistivity standard curves for a horizontally stratified earth: Geophys. Prosp., v. 19, no. 4, p. 769–775.

Golovtsin, V. N., 1963, Elecktrorazvedka (Electrical prospecting): Kiev, Akademiya Nauuk Ukrainiskoi, SSR, 361 p.

Hallenbach, F., 1953, Geo-electrical problems of the hydrology of West German areas: Geophys. Prosp., v. 1, no. 4, p. 241–249.

Hansen, H. J., III, 1966, Pleistocene stratigraphy of the Salisbury area, Maryland, and its relationship to lower eastern shore: a subsurface approach: Maryland Geol. Survey, report of investigations no. 2, 27 p., 5 tables.

Hatherton, T., Macdonald, W. J. P., and Thompson,

G. E. K., 1966, Geophysical methods in geothermal prospecting in New Zealand: Bull. Volcanol., v. 29, p. 485–498.

Hedstrome, H., 1932, Electrical prospecting for auriferous quartz veins and reefs: Mining Mag., v. 46, p. 201–213.

Homilius, J., 1961, Über die Auswertung geoelektrischer Sondierungskurvon im Falle eines vielfach geschichteten Untergrundes: Zeitschrift für Geophysik, v. 27, p. 282–300.

——— 1969, Geoelectrical investigations in East Afghanistan: Geophys. Prosp., v. 17, p. 449–487.

Hummel, J. N., 1932, A theoretical study of apparent resistivity in surface potential methods: Trans. A.I.M.E., Geophys. Prosp., v. 97, p. 392–422.

Jakosky, J. J., 1950, Exploration Geophysics: Los Angelos, Trija, 1,195 p.

Kalenov, E. N., 1957, Interpretation of vertical electrical sounding curves: Moscow, Gostoptekhizdat, 472 p.

Keller, G. V., 1968, Discussion on "An inverse slope method of determining absolute resistivity" by P. V. Sanker Narayan and K. R. Ramanujachary (Geophysics, v. 32, p. 1036–1040, 1967): Geophysics, v. 33, p. 843–845.

Keller, G. V., and Frischknecht, F. C., 1966, Electrical methods in geophysical prospecting: New York, Pergamon Press, 519 p.

Komárov, V. A., Pishpareva, H. N., Semenov, M. B., and Khloponina, L. S., 1966, (Sheinmanna, S. M., editor), Theoretical fundamentals for interpretation of survey data obtained with the induced polarization method: Leningrad, Isdatel'stov "Nedra," 203 p.

Kreines, I. I., 1957, On the distortion of VES curves in the presence of a vertical electrical contact separating different media: Prikladnaya Geofizika, v. 17, p. 152–161.

Kunetz, Géza, 1955, Einfluss vertikaler Schischten auf elektrische Sondierungen: Zeitschr. Geophysik, v. 21, p. 10–24.

——— 1957, Les courants telluriques et leur application á la prospection: Ciel et Terre, LXXIII[e] année, no. 7–8, July-August issue, 32 p.

——— 1966, Principles of direct current resistivity prospecting: Berlin, Gebrüder Borntraeger, 103 p.

Kuzmina, E. N., and Ogil'vi, A. A., 1965, On the possibility of using the induced polarization method to study ground water: Razvedochnaya i Promyslovaya Geofizika, no. 9, p. 47–69.

Lasfargues, Pierre, 1957, Prospection électrique par courants continus: Paris, Masson et Cie, 290 p.

Logn, O., 1954, Mapping nearly vertical discontinuities by earth resistivities: Geophysics, v. 19, p. 739–760.

Maillet, R., 1947, The fundamental equations of electrical prospecting: Geophysics, v. 3, p. 529–556.

Matveev, B. K., 1964, Methods of graphical construction of electrical sounding curves: Moscow, [Publishing house] Nedra, 72 p. [English translation by I. Mittin, 1967, U.S. Geol. Survey Library, Denver, Colorado, 116 p.]

Migaux, León, 1946, A new method of applied geophysics: prospecting by telluric currents (in French): Annales Geophysique, v. 2, p. 131–146.

——— 1948, Practical applications of the telluric method (in French): Internat. Geol. Cong. Proc., pt. V, p. 85–95.

Migaux, León, Bouchon, R., and Repal, S. N., 1952, Telluric study in the Hodna Basin (in French): Internat. Geol. Cong. Proc., pt. IX, p. 231–243.

Migaux, León, and Kunetz, Géza, 1955, Apports des methodes electriques de surface a la prospection petroliere: World Petroleum Cong., 4th, Proc., Sec. I, p. 545–574.

Mooney, H. M., and Wetzel, W. W., 1956, The potentials about a point electrode and apparent resistivity curves for a two-, three-, and four-layer earth: Minneapolis, University of Minnesota Press, 145 p., 243 plates.

Mooney, H. M., Orellana, Ernesto, Pickett, Harry, and Tornheim, Leonard, 1966, A resistivity computation method for layered earth models: Geophysics, v. 31, p. 192–203.

Moore, W., 1945, An empirical method of interpretation of earth resistivity measurements: A.I.M.E. Geophys. Prosp. Trans., v. 164, p. 197–223.

——— 1951, Earth resistivity tests applied to subsurface reconnaissance surveys: Am. Soc. for Testing Materials, Spec. Tech. Publ. 122, p. 89–103.

Muskat, M., 1933, Potentials about an electrode on the surface of the earth: Physics, v. 4, p. 129–147.

——— 1945, The interpretation of earth resistivity measurements: A.I.M.E. Geophys. Prosps. Trans., p. 224–231.

Muskat, M., and Evinger, H. H., 1941, Current penetration in direct current prospecting: Geophysics, v. 6, p. 297–427.

Ogilvy, A. A., Ayed, M. A., and Bogorlovsky, V. A., 1969, Geophysical studies of water leakages from reservoirs: Geophys. Prosp., v. 27, no. 1, p. 36–62. [Netherlands].

Orellana, Ernesto, 1960, Algunas cuestiones de prospeccion geolectrica: Revista de Geofisica, v. 19, p. 13–28.

——— 1961, Criterios erróneos en la interpretación de sondeos eléctricos: Revista de Geofísica, v. 20, p. 207–227.

——— 1966, Notas sobre a la interpretacion de

sondeos electricos verticalés: Revista de Geofísica, v. 25, p. 1–40.

Orellana, Ernesto, and Mooney, H. M., 1966, Master tables and curves for vertical electrical sounding over layered structures: Madrid Interciecia, 150 p., 66 tables.

Page, L. M., 1968, The use of the geoelectric method for investigating geologic and hydrologic conditions in Santa Clara County, California: Jour. Hydrology, v. 7, no. 2, p. 167–177.

Rabinovich, B. I., 1965, Fundamentals of the method of field difference [in Russian]: Prikladnaya Geofizika, v. 43, p. 47–59. [English translation by I. Mittin, U.S. Geol. Survey Library, Denver, Colorado, 21 p.]

Schlumberger, Marcel, 1939, The application of telluric currents to surface prospecting: Am. Geophys. Union, Trans. part 3, p. 271–277.

Seigel, H. O., 1959, Mathematical formulation and type curves for induced polarization: Geophysics, v. 24, no. 3, p. 547–565.

Stefanesco, S. S., Schlumberger, Conrad, and Schlumberger, Marcel, 1930, Sur la distribution electrique potentielle autor d'une prix de terre ponctuelle daus un terrain a couche horizontales, homogenes et isotrope: Jour. de Physique et le Radium, v. 11, no. 1, p. 132–140.

Unz, M., 1963, Relative resolving power of four point resistivity configurations: Geophysics, v. 28, p. 447–456.

Vacquier, Victor, Holmes, C. R., Kintzinger, P. R., and Lavergne, Michel, 1957, Prospecting for ground water by induced electrical polarization: Geophysics, v. 12, no. 3, p. 660–687.

van Dam, J. C., 1964, A simple method for the calculation of standard graphs to be used in geoelectrical prospecting: Delft, Uitgeverij Waltman, 87 p.

——— 1965, A simple method for the calculation of standard graphs to be used in geo-electrical prospecting: Geophys. Prosp., v. 13, no. 1, p. 37–65.

van Dam, J. C., and Meulenkamp, J. J., 1967, Some results of the geo-electrical resistivity method in ground water investigations in the Netherlands: Geophys. Prosp., v. 15, no. 1, p. 92–115.

Van Nostrand, R. G., and Cook, K. L., 1966, Interpretation of resistivity data: U.S. Geol. Survey Prof. Paper 499, 310 p.

Vanyan, L. L., Morozova, G. M., and Lozhenitsyna, L. V., 1961, On the theoretical curves of the induced polarization method [in Russian]: Geologiya i Geofizika, no. 10, p. 118–123.

Vedrintsev, G. A., and Tsekov, G. D., 1957, Procedure for obtaining multilayer theoretical VES curves by the decomposition method in conjunction with the graphical method [in Russian]: Razvedochnaya i Promyslovaya Geofizika, v. 20, p. 36–46. [English translation by A. A. R. Zohdy and R. Robinson, 1968, U.S. Geol. Survey Library, Denver, Colorado, 19 p.]

Wantland, Dart, 1951, Geophysical measurements of the depth of weathered mantle rock: Am. Soc. Testing and Materials Spec. Tech. Pub. 122, p. 115–135.

Weaver, W., 1929, Certain applications of the surface potential method: A.I.M.E. Geophys. Prosp. Trans., v. 81, p. 68–86.

Weaver, K. N., and Hansen, H. J., III, 1966, An ancient buried river channel is discovered: The Maryland Conservationist, v. 43, no. 2, p. 9–11.

Wenner, Frank, 1916, A method of measuring earth resistivity: U.S. Bureau of Standards Bull., v. 12, p. 469–478.

Yungul, S., 1968, Measurement of telluric "relative ellipse area" by means of vectograms: Geophysics, v. 33, no. 1, p. 127–131.

Zagarmistr, A. M., 1957, Utilization of the increased resolving power of dipole-axial soundings in investigating a "Type-H" section (in Russian): Prikladnaya Geofizika, v. 16, p. 130–144. [Translation by Ivan Mittin, U.S. Geol. Survey Libraray, 1966, Denver, Colorado, 21 p.]

Zohdy, A. A. R., 1964, Earth resistivity and seismic refraction investigations in Santa Clara County, California: Unpub. Ph.D. thesis, Stanford Univ., 132 p.

——— 1965a, The auxiliary point method of electrical sounding interpretation, and its relationship to the Dar Zarrouk parameters: Geophysics, v. 30, p. 644–660.

——— 1965b, Geoelectrical and seismic refraction investigations near San Jose, California: Ground Water, v. 3, no. 3, p. 41–48.

——— 1968a, A rapid graphical method for the interpretation of A- and H-type electrical soundings: Geophysics, v. 33, p. 822–833.

——— 1968b, The effect of current leakage and electrode spacing errors on resistivity measurements, *in* Geological Survey Research 1968: U.S. Geol. Survey Prof. Paper 600–D, p. D258–D264.

——— 1969a, The use of Schlumberger and equatorial soundings in ground-water investigations near El Paso, Texas: Geophysics, v. 34, p. 713–728.

——— 1969b, A new method for differential resistivity sounding: Geophysics, v. 34, p. 924–943.

——— 1970, Variable azimuth Schlumberger sounding and profiling near a vertical contact: U.S. Geol. Survey Bull. 1313–B, 22 p.

Zohdy, A. A. R., and Jackson, D. B., 1969, Application of deep electrical soundings for ground water exploration in Hawaii: Geophysics, v. 34, p. 584–600.

Zohdy, A .A. R., Jackson, D. B., Mattick, R. E. and Peterson, D. L., 1969, Geophysical surveys for ground water at White Sands Missile Range, New Mexico: U.S. Geol. Survey open file rept., 31 p.

Seismology

By G. P. Eaton

Applied seismology has, as its basis, the timing of artificially-generated pulses of elastic energy propagated through the ground and picked up by electromechanical transducers operating as detectors. These detectors, or geophones as they are more commonly called, respond to the motion of the ground, and their response, transformed into electric signals, is amplified and recorded on magnetic tape or film on which timing lines are also placed. The geophysicist is interested in two parameters which affect the elapsed time of transmission of this pulse—the propagation velocity (or velocities) and the geometry of the propagation path. The determination of these parameters is a complex task, both in practice and in theory. Energy generated at the source travels in several types of waves simultaneously, and each wave has a different transmission velocity. Furthermore, each of these waves may travel to the geophones by more than one path. For example, the first energy to arrive at a geophone near the source may arrive via the direct wave; that is, the energy travels parallel to the surface in the layer in (or on) which the source and receiver are located. Another geophone, located farther away, may record the arrival of a refracted wave first. When such a wave impinges on a sub-horizontal discontinuity where there is an abrupt change in elastic properties, reflection or refraction of the wave will lead to the generation of additional waves. Thus a compressional wave can give rise to both a reflected and refracted compressional wave and a shear wave. Lastly, energy travelling into the ground may return to the surface via reflections or refractions from several different interfaces of varying depth. The geophysicist must be able to recognize and sort out from the complex wave train arriving at the geophones those impulses in which he is interested and must translate their times of transmission into geological information.

Elastic wave energy can be imparted to the ground in a variety of ways. The most commonly used method is that of firing a charge of explosives with high detonation velocity in a tamped hole. Such charges may be fired on the surface or a short distance above it. The amount of charge used depends on the length of the propagation path and the attenuation characteristics of the earth materials along the path. Although crude rules-of-thumb for estimating the explosives requirements for a given shot have been formulated, there is enough variation in attenuation characteristics from area to area that the requirements at a given locale are best determined by trial and error; so also are the depth-of-shot requirements. In some areas, and for some kinds of records, the seismologist may require a drilled or augered hole below the water table. In others, he may be satisfied to place the charge in a shallow, hand-dug hole and tamp it with a shovelful of soil. In still others, he may wish to excavate a hole of intermediate depth, say 3–5 m (10–15 feet), with a backhoe and then refill the hole with earth. In general, the deeper the target, the larger the charge, and the larger the charge, the greater depth of implantation. The bulk of the explosive energy should be consumed in producing elastic waves. If much energy is spent in the process of venting, the shot probably will not be efficient and the desired results will not be obtained. For very shallow work (20 m (65 feet) or less) adequate energy sometimes can be generated by a hammer blow on a steel plate. Analogous sources of energy

in larger amounts are produced by weight dropping or by impacting the ground with a plate driven hydraulically.

Elementary Principles

The theory of elasticity on which we base our understanding of elastic wave propagation treats materials as homogeneous and isotropic. Although naturally occurring rocks, in place, do not fit either specification very well in many areas, this theory has proved to be extremely useful in understanding seismic phenomena. Actually, what are sought in seismic prospecting are the very discontinuities which make the crust inhomogeneous. These discontinuities, between bodies of unlike elastic properties, are studied and interpreted in terms of their nature, depth, location, and configuration. In most earth models they correspond to significant geological boundaries. In some settings, however, they do not, and this poses an additional problem for the interpreter.

According to the theory of elasticity, a homogeneous, isotropic, elastic solid can transmit four kinds of elastic waves. Two of these, the compressional (or longitudinal) wave and the shear (or transverse) wave, are body waves. They are transmitted through the interior of the solid. In the passage of a compressional wave, particle motion in the medium is parallel to the direction of propagation, like that of a sound wave in air. The particle motion created by a shear wave is perpendicular to the direction of propagation. The other two waves, known as Rayleigh waves and Love waves, are confined to a region near the free surface of the medium; their amplitudes decrease with depth in the medium. They are also referred to as surface waves. The particle motion created by these surface waves is complex; Love waves, for example, require a surface layer with elastic constants different from those of the rest of the solid. Very little use has been made of the propagation of shear waves or surface waves in hydrogeology. However, suggestions have been made as to how they might be used to advantage in ground-water studies (Eaton and Watkins, 1970). Nothing more will be said of shear or surface waves in the paragraphs that follow—all reference to elastic wave propagation from this point on is concerned with compressional waves. These waves have the highest velocity of the four types discussed and, therefore, the shortest traveltime for a given propagation path.

Elastic energy moves outward from a point source in a series of waves with curved fronts. For illustration, the path which the energy follows from source to geophone is most easily defined by a ray, a line drawn normal, or nearly normal, to the wavefront, depending on whether or not the medium is isotropic. The ray-paths which seismic energy follows are constructed by the method of geometrical optics.

The paths of four rays emanating from a point source of energy at the surface are shown in figure 54. The model is that of a horizontally layered earth, where the seismic wave velocity, V_1, of the upper medium, is less than the velocity of the underlying medium, V_2. These four rays are:

1. The direct ray, which travels a horizontal path from source to receiver.
2. The totally reflected ray, which is generated when a ray strikes the boundary between the two media at an angle of incidence i_1 greater than the critical angle i_c, and all of the energy is reflected back toward the surface.
3. A ray striking the boundary at precisely the critical angle of incidence i_c, part of the energy being reflected back toward the surface and part refracted, the latter travelling parallel to the interface with velocity V_2.
4. A ray striking the interface at an angle of incidence i'_1, less than the critical angle, part of the energy being reflected upward and part being refracted in the lower medium away from the normal to the surface, at angle r. The magnitude of r is a function of the ratio

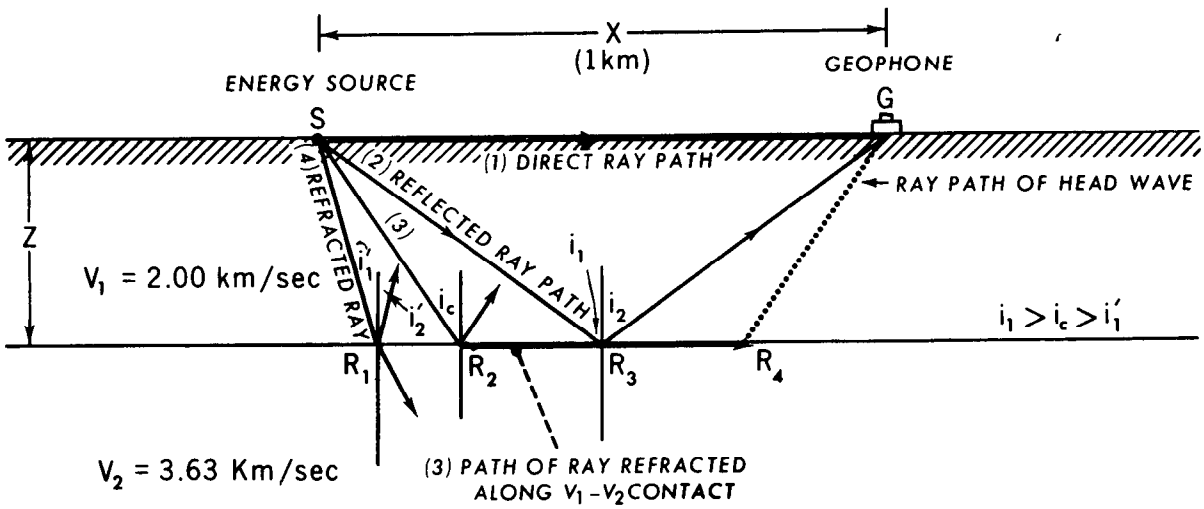

Figure 54.—Schematic ray-path diagram for seismic energy generated at source S and picked up at geophone G. Traveltimes for the various rays are as follows: t_1 = 0.500 sec, t_2 = 0.630 sec, and t_3 = 0.588 sec.

of the two velocities and the angle of incidence (see eq. 1). Division of the incident energy between reflected and refracted waves depends on the angle of incidence and the contrast in velocities and densities of the two media.

As the pulse of energy travelling ray-path 3 moves along the interface between the two media at velocity V_2, it generates a small disturbance or pulse in the lowermost part of the upper medium. Energy from this disturbance eventually reaches the surface of the ground where it is picked up by the geophone.

The angular relationships among the various parts of the ray-paths just described are as follows:

For ray-path 2,

$$i_1 = i_2 \ . \qquad (1)$$

For the reflected branch of ray-path 4, $i_1' = i_2'$, and for the refracted branch

$$\frac{\sin i_1'}{\sin r} = \frac{V_1}{V_2} \quad \text{(Snell's Law)}. \qquad (2)$$

At the critical angle of incidence, the angle of refraction r is 90° and $\sin r = 1$. Thus, the critical angle can be defined in terms of the two velocities as

$$i_c = \arcsin\left(\frac{V_1}{V_2}\right). \qquad (3)$$

These simple equations, plus that expressing the relationship between velocity, distance, and time, constitute the basis for the interpretation of seismic data.

As an example, consider the reflected ray-path $\overline{SR_3G}$. The relationship between the velocity, V_1, the length of the propagation path, $\overline{SR_3G}$, and the transmission time, t is:

$$V_1 = \frac{\overline{SR_3} + \overline{R_3G}}{t}. \qquad (4)$$

Now according to equation 1, $i_1 = i_2$; thus we can rewrite equation 4 as

$$V_1 = \frac{2\,\overline{RS_3}}{t}. \qquad (5)$$

Because

$$\overline{SR_3} = \sqrt{(X/2)^2 + Z^2}\ ,$$

then

$$V_1 = \frac{2\sqrt{(X/2)^2 + Z^2}}{t}.$$

Rearranging terms, and solving for Z:

$$Z = \tfrac{1}{2}\sqrt{V_1^2t^2 - X^2}\ . \qquad (6)$$

The distance X in this equation is predetermined by the placement of the geophone, and the transmission time t is read from the seismogram. Thus, in equation 6 if the velocity V_1, of the upper medium is known from independent measurement, we can calculate the depth to the interface, Z.

Reflection Versus Refraction Shooting

Determination of depth by the means just described is referred to as a seismic reflection measurement. The reflection method is one of two general types of seismic measurements in common use, the other being the refraction method.

The refraction method is illustrated schematically by ray-path 3 in figure 54. The propagation path of ray 3 consists of three branches, $\overline{SR_2}$, $\overline{R_2R_4}$, and $\overline{R_4G}$, but we have not yet indicated why there should be a branch like $\overline{R_4G}$. It was mentioned earlier that energy from the disturbance travelling along path $\overline{R_2R_4}$ eventually reaches the surface. The head wave, which is the name given to the wave carrying energy upward from the disturbance at the interface, is a physical representation of Huygens' principle, which states that each point on an advancing wave front in an ideal elastic body is a source of secondary spherical waves. The wave front of these new waves at a later instant of time is defined by a surface tangent to the newly-generated spherical waves. This is illustrated in figure 55, where a, b, and c represent successive crests of a disturbance moving parallel to the interface with velocity V_2. They are, according to Huygens' principle, sources of secondary waves which will move upward in the disturbed upper medium with velocity V_1. The arcs in figure 55 represent a succession of spherical waves emanating from each of these points and the thin lines tangent to them are the wave fronts normal to which the rays travel. As a disturbance with velocity V_2 travels parallel to the interface from a to c, energy radiating upward from it travels from a to d at velocity V_1. These two paths, $\overline{ac}$ and $\overline{ad}$, define the angle ω. Thus,

$$\sin\omega = \frac{\overline{ad}}{\overline{ac}} = \frac{V_1 t}{V_2 t} = \frac{V_1}{V_2}. \qquad (7)$$

A comparison of equation 7 with equation 3 indicates that the the angle ω is the same as the critical angle i_c. The significance of this in figure 54 is that the right hand branch of ray-path 3 or $\overline{R_4G}$ is a mirror image of the left-hand or incident branch $\overline{SR_2}$. It follows that the relationship between the velocities V_1 and V_2, the length of the propagation path $\overline{SR_2R_4G}$, and the transmission time t can be written

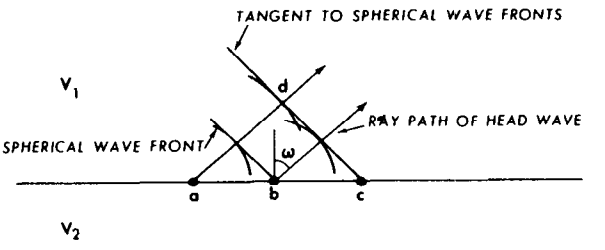

Figure 55.—Huygens' construction for a head wave generated at the V_1–V_2 interface.

$$t = \frac{\overline{2SR_2}}{V_1} + \frac{\overline{R_2R_4}}{V_2}. \qquad (8)$$

The geometry of figure 54 allows us to make the following substitutions:

$$\overline{SR_2} = Z/\cos i_c \qquad (9)$$

and

$$\overline{R_2R_4} = X - 2Z\tan i_c. \qquad (10)$$

Substituting these expressions and that of equation 3 in equation 8 leads to

$$t = \frac{X}{V_2} + \frac{2Z\cos i_c}{V_1}. \qquad (11)$$

After rearranging terms, and substituting an expression containing V_1 and V_2 for $\cos i_c$:

$$Z = \frac{V_1V_2}{2\sqrt{V_2^2 - V_1^2}}\left(t - X/V_2\right). \qquad (12)$$

As before, the distance X is predetermined by the placement of the geophone and the transmission time t is read from the seismogram. Substitutions of these values, plus those for V_1 and V_2, in equation 12 leads to a value for the depth Z to the interface.

In making calculations of depth from reflection measurements, the velocity values

used must be determined by independent means. In contrast, refraction measurements yield values for the velocities of the formations directly, provided certain conditions are realized. Although a discussion of these conditions is beyond the scope of the manual, it may be instructive to show how the values for velocities V_1 and V_2 are a product of the refraction measurement itself.

Figure 56 shows a model of a two-layered, horizontally-stratified Earth. The compressional wave velocities of each of the layers is indicated at the right. On the surface are ten geophones recording direct and refracted wave energy from a source at the left. Directly above the model is a time-distance plot. The abscissa of this plot is horizontal distance, measured from the shot point, and the ordinate is time elapsed since the shot instant. The measured elpased time of the first arrival of energy recorded by each geophone is plotted as a point directly above the geophone. Straight lines drawn through these points constitute branches of a traveltime curve. The slope of each branch is the reciprocal of the velocity of the layer it represents. This is most readily understood from the following argument:

At distances less than X_c, the "critical distance," at which the two branches of the traveltime curve intersect, the first arrival of energy is via the direct wave. At distances greater than X_c, the first arrival is via the refracted wave. The refracted wave travels a longer path than the direct wave, but at distances beyond X_c the fraction of its total path occurring along the high velocity bed is sufficiently great to compensate for the effect of this extra distance of travel. The traveltimes indicated on the first branch of the plot (to the left of X_c) are the result of direct wave arrivals, and as such are given by the equation for direct traveltime:

$$t = X/V_1 \qquad (13)$$

Differentiating this equation with respect to X gives

$$\frac{dt}{dX} = \frac{1}{V_1}. \qquad (14)$$

From this it is seen that

$$V_1 = 1/(dt/dX) = 1/\text{(slope of first segment of plot)}. \qquad (15)$$

The traveltimes indicated on the second segment of the plot correspond to first arrivals that reached the geophone via the refracted wave path. As such, they are given by equation 11,

$$t = \frac{X}{V_2} + \frac{2Z\cos i_c}{V_1}. \qquad (11)$$

Differentiating this equation with respect to X gives

$$\frac{dt}{dX} = \frac{1}{V_2}, \qquad (16)$$

since Z, i_c, and V_1 are constants,or

$$V_2 = 1/(dt/dX) = 1/\text{(slope of second segment of plot)}. \qquad (17)$$

The thin lines in the model (fig. 56), both curved and straight, represent successive positions of wave fronts for those waves travelling to the surface by the fastest, or minimum-time, paths. The straight segments are those representing the head wave; curved segments represent direct and refracted waves. The dotted line separating the straight and curved parts of the wave fronts is an envelope of points for which the travel times of direct and head-wave pulses are the same. The diagram has been simplified by deleting those parts of the curved-wave front below the envelope and those parts of the plane-wave front above it. The omitted parts of each wave front exist and their ar-

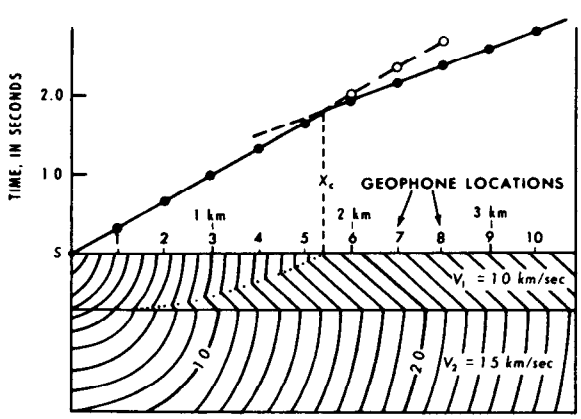

Figure 56.—Seismic wave fronts and traveltime plot for an idealized horizontally layered model. Heavy dots represent first arrivals of energy; open dots represent later arrivals. X_c represents the critical distance for the V_1–V_2 interface.

rival at the geophones constitutes a later arrival of real energy. Thus one may see on the seismogram at geophones 6, 7, and 8, an instant after the head-wave arrival, pulses that represent the arrival of a direct wave travelling with velocity V_1. These are shown in figure 56 as open circles falling on a prolongation of the V_1 traveltime branch. Such pulses are known as second arrivals. Because the amplitude of a head wave usually is much smaller than that of a direct wave, it very rarely is observed on the seismograms at distances less than the critical distance.

Comparison of the Reflection and Refraction Seismic Methods in Practice

In the preceding paragraphs, simple techniques of depth measurement by both the reflection and refraction methods have been described. How does one go about deciding which method to use in a given situation? The differences between reflection and refraction methods go far beyond the differences in ray-path geometry. These differences include geophone array (the refraction method uses much longer spreads), accuracy, resolution, depth, size and shape of the target, number of discontinuities to be mapped, vertical succession of velocity values, and cost. The great bulk of all applied seismic work done today is done by the reflection method. It offers higher accuracy and resolution, allows the mapping of a larger number of horizons, requires smaller amounts of energy, uses shorter geophone spreads (simplifying their layout and minimizing problems associated with the communication of the shot instant), and is more amenable to routine field operation. In addition it does not require, as does the refraction method, that each succeeding layer have a velocity higher than that of the layer above it. In light of all these advantages, it is reasonable to inquire why the refraction method is used at all. This is an especially relevant question here, because most seismic measurements made in hydrogeology are refraction measurements. It is in petroleum exploration that the reflection method is so extensively used.

The reasons for use of the refraction method are several. In some areas it is almost impossible to obtain good reflection records. A typical example is an area of thick alluvial or glacial fill. In this setting optimum reflection prospecting would require the drilling of deep shot holes. Such an area lends itself admirably to the refraction method and is precisely the kind of setting in which the hydrogeologist might be interested. A downward increase in velocity can be reasonably expected in such an area and abrupt increases in velocity might be encountered both at the water table and at the base of the sediments, if they overlie consolidated bedrock. No prior knowledge of velocity is required in reconnaissance refraction measurements and the velocity information obtained in the course of the work may help in identifying the rock types involved. In reflection shooting special measurements of velocity to be made, either by greatly expanding an occasional geophone spread or by shooting at a well into which a geophone has been lowered. In the exploration of a large alluvial basin such wells may not be available to the seismologist. The reflection method works best when continuous line coverage is possible and when the line or lines can be tied to a few points of velocity control. A single reflection profile, or a series of them individually isolated and spread over many square kilometers of an alluvial basin, are not as useful as a series of isolated refraction profiles.

In areas where steeply dipping boundaries are encountered, the refraction method is better suited for exploration than the reflection method. Typical examples include a fault-bounded valley or a buried valley with steeply sloping sides.

The sophisticated equipment used in reflection work today, the relatively large size of the crews required, and the benefits derived from continuous coverage, are all difficult to justify in relation to the objectives and budget of a typical ground-water study.

The geometric subtlety of the target and the ultimate economic returns from successful exploration for petroleum do justify its use in the oil industry.

Seismic Refraction Measurements in Hydrogeology

Effect of Departures From the Simple Stratified Model

The models shown in figures 54 and 56 are highly simplified. The ground surface is perfectly plane and horizontal, the surface of the refractor with velocity V_2 is also plane, and the two surfaces are parallel. In addition, there is but one velocity discontinuity to map and there are no lateral or vertical variations of velocity within either layer. The ray-path geometry and the equations for calculating depths to the lower refractor are therefore equally simple. Such simplicity is seldom encountered in nature. The complications of real systems can be illustrated by some hypothetical models and time-distance plots.

Figure 57 shows 10 models which depart in significant ways from the simple models of figures 54 and 56. Immediately above each model is a schematic time-distance plot typical of the type that the model would generate. Ray paths are shown for models A through E, and also for model H.

The Multilayered Model

Figure 57A

Although this model is a simple extension of the horizontal two-layer model, its interpretation is fraught with practical difficulty. The thickness of each succeeding layer must be calculated individually employing a series of formulas into which one substitutes values derived for the layer immediately above it. Small errors in each step of the analysis have a multiplier effect which carries over to the calculations on each succeeding layer. This model also requires that each layer have a velocity higher than the one above it (see fig. 57H) and that each be thick enough to produce a separate branch of the traveltime curve (see fig. 57G).

Effect of a Regular Increase of Velocity With Depth

Figure 57B

If the layers in A become vanishingly thin, they would approximate, as a group, a continuous velocity increase with depth. The result is the generation of a curved ray path in the upper medium. Such a situation is realized in thick sections of young, semiconsolidated sedimentary rocks which display increasing compaction and lithification with depth. Several velocity-depth functions have been proposed by investigators for different areas (Dobrin, 1960, p. 77; Kaufmann, 1953, table 1). The mathematics required for the calculation of depth to a lower bedrock refractor using these equations are simple enough for analytical treatment in some situations.

Effect of Dipping Layers

Figure 57C

This model illustrates the effect of a refractor that is not parallel to the surface of the ground. Geologically, this model corresponds to a series of dipping beds or to a sloping bedrock surface. In this situation the slopes of the separate branches of the traveltime curves give reciprocal values of velocity for the uppermost layer (V_1) only. In figure 57C, the slopes of the second and third branches of the traveltime curves are not reciprocals of velocities V_2 and V_3. These slopes also are not the same for the two directions of shooting (left to right, or updip, and right to left, or downdip). If a seismic profile in a geologic setting like this one were not reversed; that is, if it were not shot first from one end of the geophone spread and then from the other, there would be no way of recognizing the dip nor the erroneous values for V_2 and V_3. By reversing the pro-

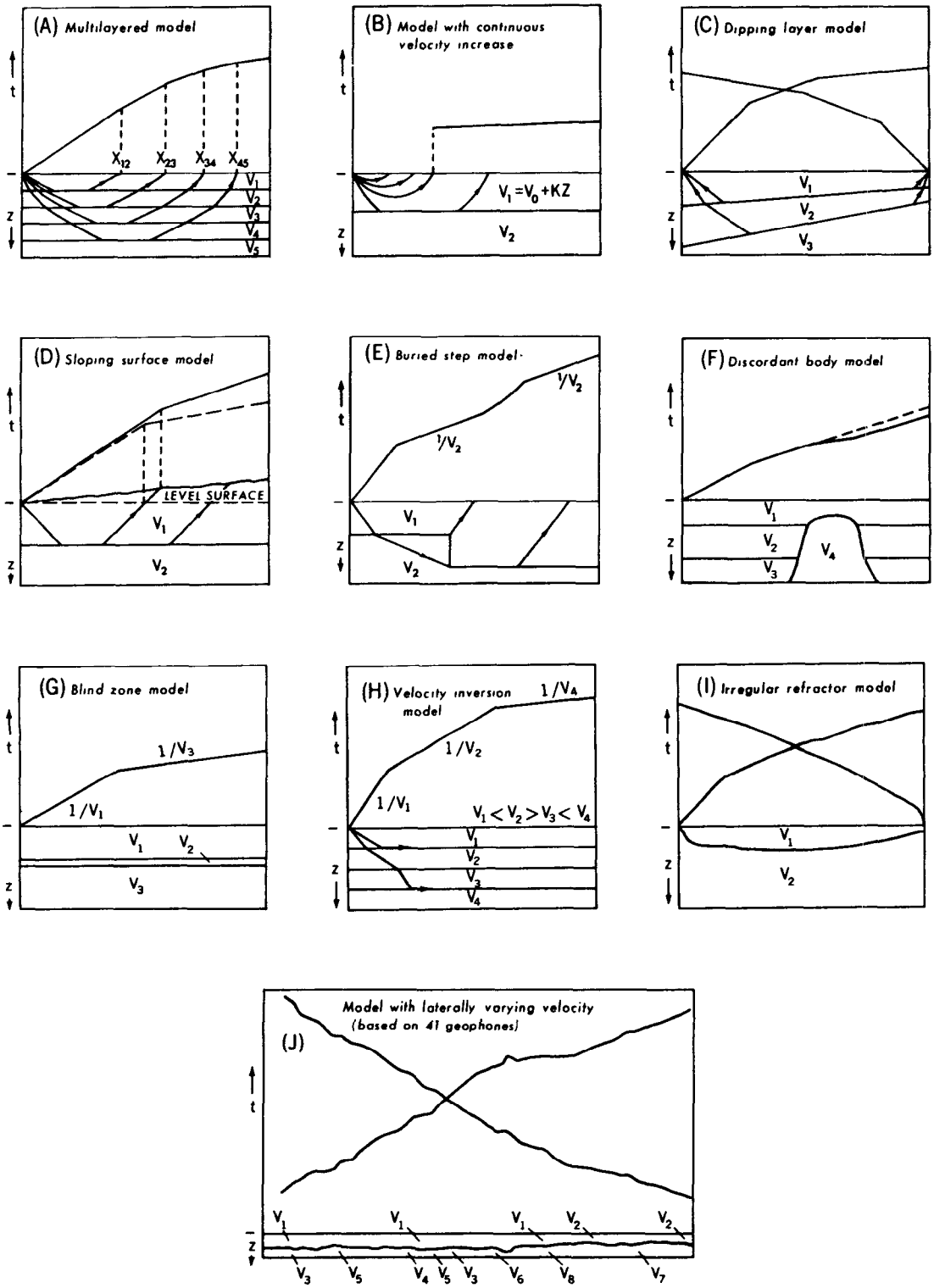

Figure 57.—Schematic traveltime curves for idealized nonhomogenous geologic models.

file, that is shooting from both ends of the geophone spread, the existence of dip is readily apparent and the dip angle can be calculated. The equations used in the calculation of dip include intermediate steps that lead to a derivation of the true values of V_2 and V_3. For a typical solution see Slotnick (1959, p. 103–118).

Effect of a Sloping Ground Surface

Figure 57D

The effect of shooting along a sloping ground surface above a horizontal refractor is somewhat analogous to that of a dipping refractor below a horizontal surface (fig. 57C). In both models the path length of rays in the upper medium varies with horizontal distance. The effect of this variation is shown in an exaggerated fashion in the time-distance plot, where the observed data are shown as solid lines, and the plot that would have been obtained if the shot and geophones had been on a horizontal surface is shown by dashed lines. Unlike the dipping refractor example, however, the slope of the ground is known before shooting and corrections can be applied to the observed arrival times. The method is discussed briefly in the section entitled "Corrections applied to seismic refraction measurements."

Effect of a Buried Steplike Refractor

Figure 57E

This model illustrates the effect of an abrupt vertical offset in a buried refractor. Geologically this could be a buried and faulted bedrock surface or a buried erosional step. Note that the two parts of the V_2 branch of the traveltime curve are parallel, but displaced from one another. This displacement is a measure of the increase in path length for rays travelling upward from the downthrown block and it can be used to calculate the vertical offset of the refractor.

Effect of a Discordant Steep-sided Body

Figure 57F

Steep-sided discordant bodies like the one illustrated may represent igneous stocks, broad dikes, or salt diapirs intrusive into bedded sedimentary rocks. Alternatively, they might represent a buried bedrock ridge. Such a body commonly has higher velocity than the other layers and causes seismic waves travelling through it to arrive earlier than they would have otherwise. A somewhat similar time-distance plot would be obtained from figure 57E if it were shot in the opposite direction (that is, from right to left).

Effect of a Thin Refractor

Figure 57G

This illustration shows a simple three-layered model in which each layer has a velocity higher than the one above it. However, there is no traveltime branch corresponding to the layer with velocity V_2. Its absence results from the layer's thinness in relation to its depth. This condition poses a problem in interpretation if only first arrivals of energy are used in preparing the time-distance plot. What happens, in effect, is that the head wave from the thin layer is overtaken by the head wave from the higher velocity layer below it. If second arrivals are recorded, then the head wave from this layer might be seen on the seismogram. Digital seismic timers of the sort commonly used in engineering geophysics, where the arrival of a single pulse of energy is all that is recorded, would be useless in the study of a setting like this one. A layer of the V_2 type is referred to in geophysics as a blind zone. Where unrecognized, it causes error in the calculation of the depth to refractors below it. In addition, lack of knowledge of its existence may prove detrimental to the very objectives of the survey. A hydrogeologic example of this last point was illustrated by Soske (1959, fig. 6) using data from Nevada. In the area he studied, the ground consisted of consolidated bedrock with a velocity of 3.2 km/sec overlain by saturated alluvium with a velocity of approximately 2.0 km/sec. Above the water table was a zone of unsaturated alluvium with a velocity of 1.0 km/sec. The water table was at a depth of 60 meters and the bedrock at 90 meters. The

saturated zone, which was only 30 meters thick, could not be recognized from first arrivals. The presence of the saturated zone was not apparent on the time-distance plot and it appeared as though bedrock were overlain by unsaturated alluvium only.

Effect of a Velocity Inversion at Depth

Figure 57H

In this model the sequence of layer velocities from the surface downward is V_1–V_2–V_3–V_4, where V_3 is less than both V_2 and V_4. Layer V_3 constitutes a velocity inversion. The effect of this inversion is illustrated by the ray path in layer V_3. It is refracted downward, away from the land surface. As a result, there is no V_3 branch on the traveltime curve, for no head wave is generated by refraction below the V_2–V_3 boundary. Thus, calculations of depth to the top of layer V_4 will be in error, for the unrecognized V_3 layer will be treated as though it had the higher velocity, V_2. The result will be an overestimate of the depth to the top of layer V_4. Independent knowledge of the existence of a velocity inversion must be known from either velocity logging in a well penetrating the section, or at least suspected from resistivity measurements or knowledge of the stratigraphy, if the inversion is to be taken into account during the interpretation.

Effect of a Refractor of Irregular Configuration

Figure 57I

All the models discussed so far consist of plane refractors, either horizontal, dipping, or vertically stepped. In hydrogeologic investigations many refractors are curved and irregular. A typical example is that of a buried bedrock channel. Such a channel is illustrated schematically in figure 57I. The time-distance plot above it is irregular and lacks straight second branches that might provide a direct measure of velocity according to the methods described above. A time-distance curve of this type cannot be analyzed by customary means to extract depth information. Much of the seismic refraction equipment manufactured for shallow or moderately deep refraction measurements includes tables, nomograms, or formulas designed to reduce depth calculations to cookbook simplicity. None of these aids is applicable to a geologic setting similar to that illustrated in figure 57I, for all of them assume an idealized geometry. The reader interested in interpreting irregular time-distance curves should consult Hawkins (1961) or Willmore and Bancroft (1960) for techniques of data processing that will lead to accurate estimates of depth.

Effect of Laterally Varying Velocities

Figure 57J

The model shown in this illustration was taken from a real example (Hawkins, 1961, fig. 6) and constitutes what might well be regarded as the general case. It is essentially a two-layer model, in which unconsolidated sediment overlies consolidated bedrock, but the boundary is irregular and the velocities in both layers vary considerably. The resulting time-distance plot is exceedingly complex. Analytical solutions of depth based on plane sloping refractors and homogeneous elastic properties would be doomed to failure under these conditions. Curves of this type are amenable to solution, however, and the hydrogeologist concerned with a geologic setting of this type is strongly advised to seek the aid of an expert in seismic refraction interpretation.

Corrections Applied to Seismic Refraction Measurements

Arrival times recorded in refraction work must be corrected to remove unwanted time variations. These variations are due to differences in elevation between individual geophones and the energy source and the presence of an irregular, near-surface layer of low velocity. The latter is referred to

commonly as the weathered layer, although this name may or may not be strictly correct geologically.

Elevation Correction

The simplest means of correcting for differences in elevation between the geophones and the shot is to convert them all to a common elevation datum by subtracting or adding the times that elastic waves would take to travel from the datum to the actual geophone or shot locations. A schematic example is shown in figure 57D. This requires knowledge of the elevation of shot and geophones and of the velocity of the medium between them and the datum. The velocity is readily obtained from refraction shooting.

Weathered-layer Correction

If an irregular low-velocity layer exists immediately beneath the surface, but is not taken into account in correcting the travel-time data, the effect will be to produce artifical variations in depth to a mapped refractor such as the buried bedrock surface. The simplest means for making this correction is to shoot it with short geophone spreads and calculate its thickness and velocity by conventional methods. This information then can be used to calculate the time delays which the weathered layer causes along those parts of the ray path near the surface, both at the shot point and at the geophones.

Errors in Seismic Refraction Measurements

A figure commonly quoted in the literature concerning the magnitude of error involved in seismic refraction depth calculations is 10 percent. Eaton and Watkins (1970) appear to substantiate this oft-quoted value with a comparison between seismically predicted depths and drilled depths at 97 drill-hole sites (fig. 58). It is notable, however, that there are 8 points in this plot which represent errors of at least 30 percent and three of these represent errors in excess of 100 percent. Such data do not reflect incompetence on the part of the geophysicists who published them, rather they represent an attempt at intellectual honesty and a willingness to reveal how far off some geophysical predictions can be. Because there is a general tendency on the part of most investigators to publish only their successful results, the data shown in figure 58 may be regarded as representing a biased sample. It is probable that the average error in most seismic refraction work is somewhat greater than 10 percent.

There are, on the other hand, published examples in which average errors in depth prediction are as small as 5 percent. The difference between these extremes of 5 and 100 percent stems, in part, from the availability of independent geologic information or other kinds of geophysical data. It should be emphasized that the more information of a stratigraphic nature the hydrogeologist can give to the seismologist, the better the seismic interpretations will be. The geophysicist, like the surveyor, benefits from being able to close on one or more control points in the form of a borehole or well. In the total absence of independent geologic or geophysical information, the interpretations can be no better than the assumptions made concerning probable conditions below the surface.

Inspection of figure 58 indicates that those depth measurements which are in error by 30 percent or more are all on the high side; the seismic method overestimated depths to the refractors. A common cause of overestimation is illustrated by figure 57H. If unrecognized velocity inversions exist in the section, an overestimate of depth is inevitable. The thickness of the slow layer and the velocity difference between it and the layer above determine the magnitude of the error.

Other sources of error pertinent to hydrogeologic studies include (1) discontinuous and abrupt lateral variations of velocity, (2) pronounced velocity anisotropy, (3) blind

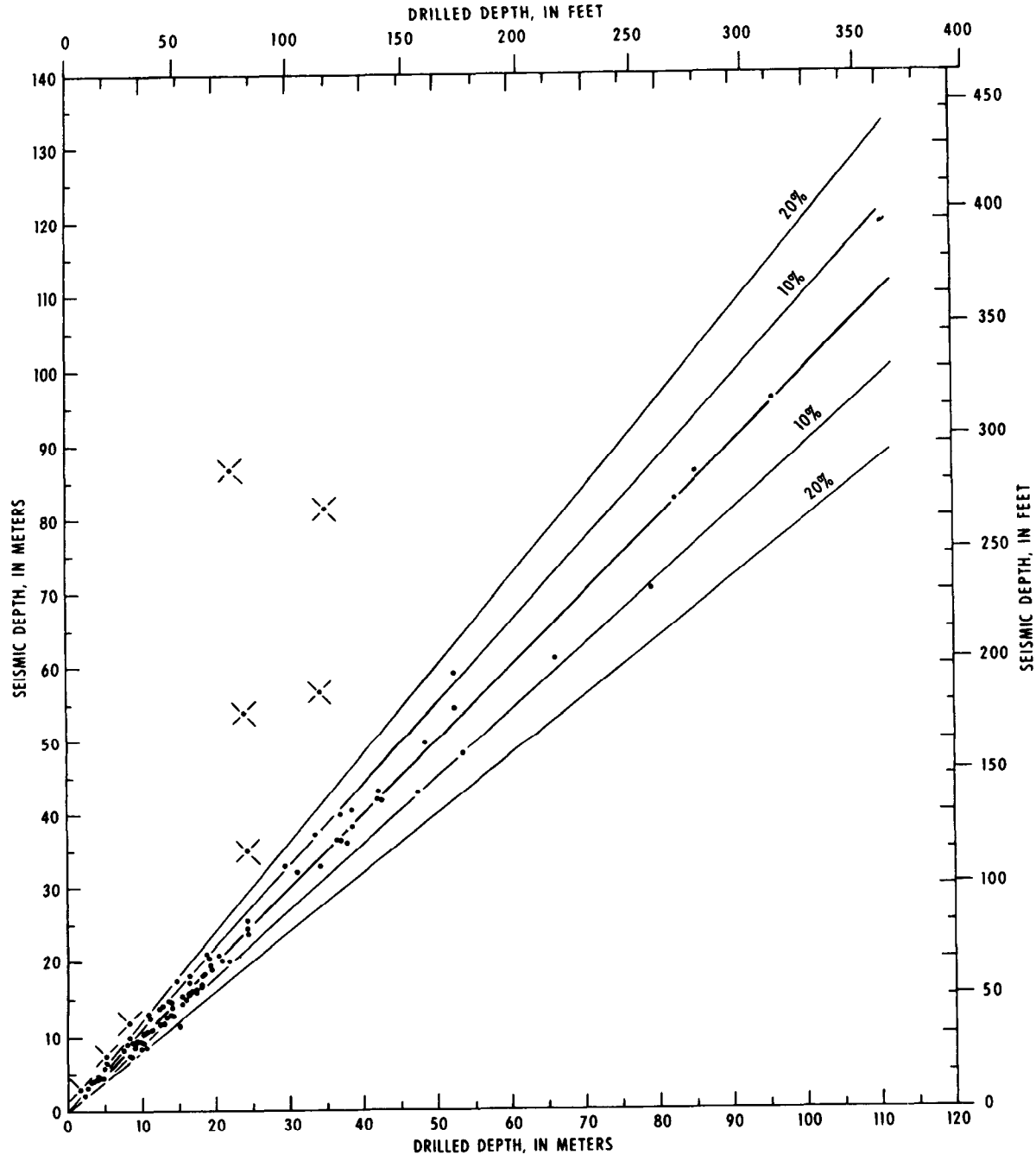

Figure 58.—Comparison of 97 seismic refraction depth determinations versus drill-hole depths at the same localities. Heavy line represents envelope of error-free determinations; labelled lines represent envelopes for errors of 10 percent and 20 percent (after Eaton and Watkins, 1970). Reproduced by permission of "Information Canada."

zones, (4) a highly fractured or weathered bedrock surface, and (5) hydrologically significant interfaces that do not display velocity contrasts large enough for seismic detection.

Applications of Seismic Refraction Measurements in Hydrogeology

Mapping Buried Channels

The most common use of the seismic method in hydrogeology is in the determination of the thickness of sediments which overlie essentially non-water-bearing consolidated bedrock. The surface of the bedrock may be plane or irregular, but it is of special hydrologic interest where it occurs in the form of a channel filled with silt, sand, and gravel. Typical examples include the fluvial sediments of present-day river valleys and valley-train deposits in old water courses. Models of this type are particularly well adapted for seismic study if there is an appreciable contrast in velocity between the sediments and the bedrock.

A characteristic example, drawn from a study by Peterson, Yeend, Oliver, and Mattick (1968, fig. 9) is shown in figure 59. The location of this study is in northern Nevada County, California. The channel is carved in Paleozoic and Mesozoic igneous and metamorphic rocks and is filled with gravel, sand, and clay of Tertiary age. The length of the seismic refraction profile across the channel, as shown in figure 59, is 1.28 km (0.8 mile). An average geophone spacing of 30.5 meters (100 ft) was employed, and charges were fired in five shot holes ranging in depth from 1.5 to 5.0 meters (5 to 16 ft) and approximately equally spaced. All spreads were reversed.

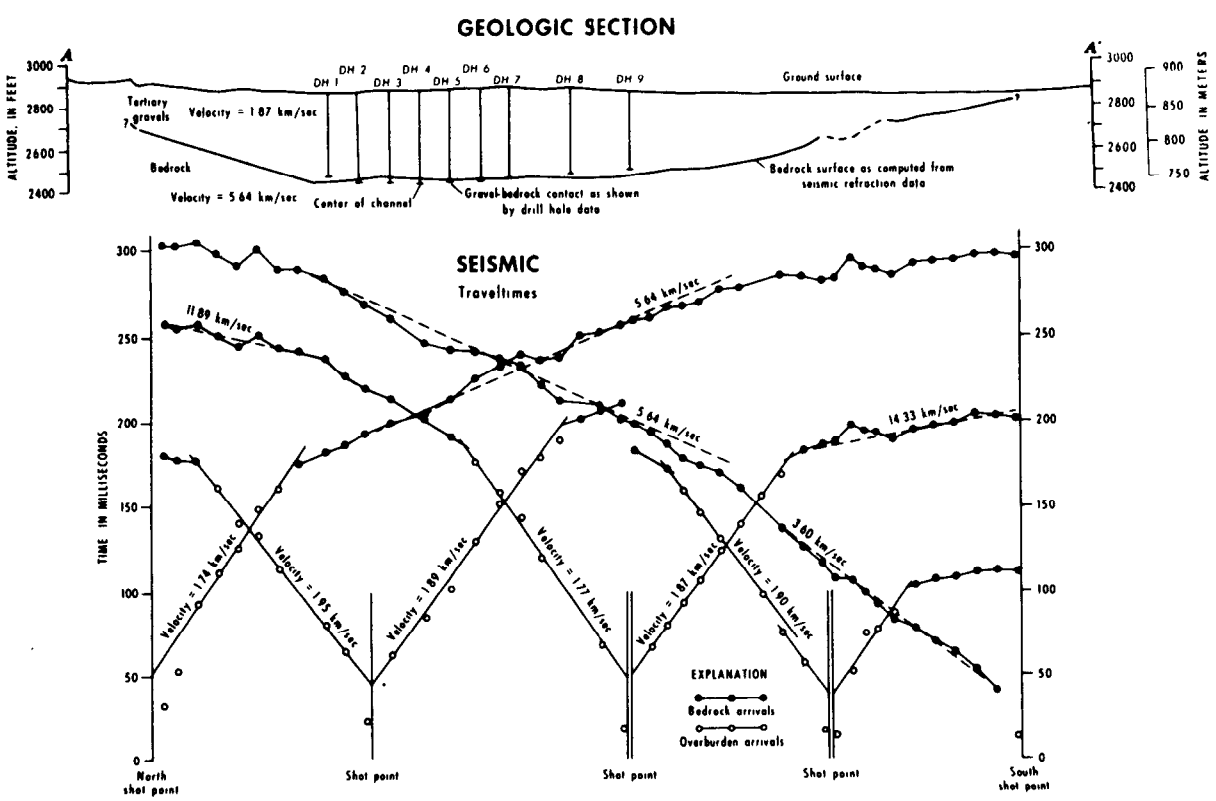

Figure 59.—Seismic cross section, drill-hole data, and traveltime curves for a buried Tertiary stream channel in northern Nevada County, California (after Peterson and others, 1968).

Dynamite charges ranged from 25 to 90 kg each. The elevations of all shot holes and geophone locations were determined to the nearest 3.0 cm (0.1 ft).

The velocity in the gravel was found from the seismic data to average 1.87 km/sec (1.16 mile/sec) and the velocity in the bedrock was 5.64 km/sec (3.51 mile/sec). On the extreme northern and southern branches of the traveltime curves, apparent velocities in excess of 11 km/sec (6.84 mile/sec) were recorded. These values are artificial and reflect the fact that the bedrock refractor is dipping toward the shot point at either end. A schematic model of a dipping refractor and its effect on the traveltime curves was shown in figure 57C.

Above the traveltime curves is a geologic cross section (fig. 59) based entirely on the seismic refraction work. Superimposed on it are vertical lines representing nine drill holes which penetrated to the buried bedrock surface. The correspondence between the two sets of bedrock depths, determined independently, is excellent. The average error in computed seismic depth for the nine holes was 4.6 percent and the maximum error, at a single hole, 8.6 percent.

A second example of a seismic refraction study of a buried valley is the work of Bonini and Hickok (1958) in northern New Jersey. This study differed from the one just described in that many more shot holes and geophone spreads were used and essentially complete areal coverage was achieved. The seismic measurements were tied closely to drill-hole control, as well.

The results of the New Jersey study are shown in figure 60, as a contour map of the buried bedrock surface. The geology of the area consists of unconsolidated glacial, alluvial, and lacustrine sediments in a buried bedrock channel carved from Triassic sedimentary rocks. Velocities in the unconsolidated sediments were found to range from 0.27 to 2.07 km/sec (0.17 to 1.29 miles/sec), and those in the bedrock, from 3.23 to 5.00 km/sec (2.00 to 3.11 miles/sec). The average error in seismic depth determinations in this study was approximately 7 percent and the maximum error, at a single hole, was 11 percent. The present-day Passaic River follows the buried bedrock channel along this reach rather closely and probably provides recharge to the aquifer.

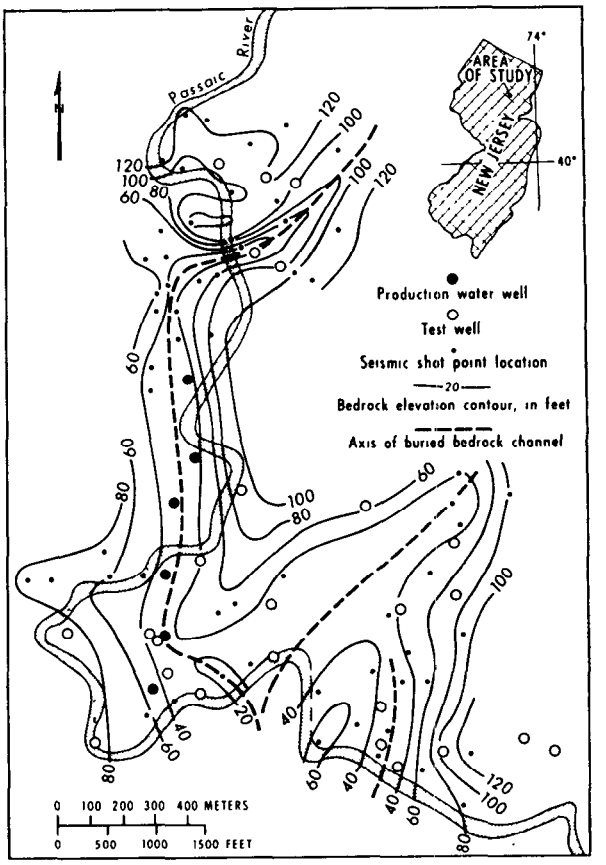

Figure 60.—Structure contours on the buried bedrock surface of the Passaic River Valley, northern New Jersey, based on seismic refraction and drill-hole measurements (after Bonini and Hickok, 1958). Reproduced with permission of Society of Mining Engineers of AIME.

Measuring Depths to the Water Table

Seismic refraction measurements of semiconsolidated or unconsolidated clastic deposits reveal that compressional wave velocities increase abruptly at the water table. The velocity in saturated continental sediments generally is about 1.50 km/sec (0.92 miles/sec) and is sufficiently higher than that in unsaturated sediments so that the zone of

saturation acts as a refractor. Observed velocities in unsaturated sediments generally are less than 1.00 km/sec (0.6 miles/sec), but rarely may be as high as 1.40 km/sec (0.9 miles/sec). According to Levshin (1961) the minimum observed difference in velocity across the water table occurs in fine-grained sediments and exceeds 100 to 150 meters/sec (330 to 500 ft/sec). In aquifers composed primarily of gravel he noted differences as large as 1.00 km/sec (0.62 miles/sec).

Whether or not the water table can be recognized seismically depends on the thickness of the saturated zone above the bedrock. In the discussion of figure 57G, it was noted that if the saturated zone is too thin in relation to its depth it will not appear as a separate branch on a traveltime curve prepared from first arrivals only.

Determining the Gross Stratigraphy of an Aquifer

If some of the velocity discontinuities in unconsolidated or semiconsolidated deposits represent stratigraphic breaks in the sedimentary section, seismic refraction measurements can be used, under optimum conditions to unravel the gross stratigraphy of a deposit. If these breaks further represent significant hydrologic boundaries, such as those between water-producing formations and non-water-producing formations, the seismic work may have special hydrogeologic interest. A typical example, provided by the work of Arnow and Mattick (1968), is shown in figure 61. The setting is the area between Salt Lake City, Utah, and Great Salt Lake. The study was done to determine the thickness of the valley fill so that the amount of ground water discharged toward Great Salt Lake could be estimated. The surface is underlain by Quaternary deposits of silt, sand, and clay exceeding 150 meters (500 ft) in thickness. The seismic refraction study revealed an irregular, buried bedrock surface at depths ranging from 270 meters (900 ft) to 1,460 meters (4,800 ft) below the surface. Overlying it, along part of the seismic section, is a thick section of sediments believed to be semiconsolidated sediments of Tertiary age. The velocity of these sediments is enough higher than that of the Quaternary sediments overlying them to suggest markedly different physical properties. Therefore they probably have different water-bearing properties. These older sediments would have to be taken into account in attempting to calculate the cross section of the area through which effective discharge is taking place.

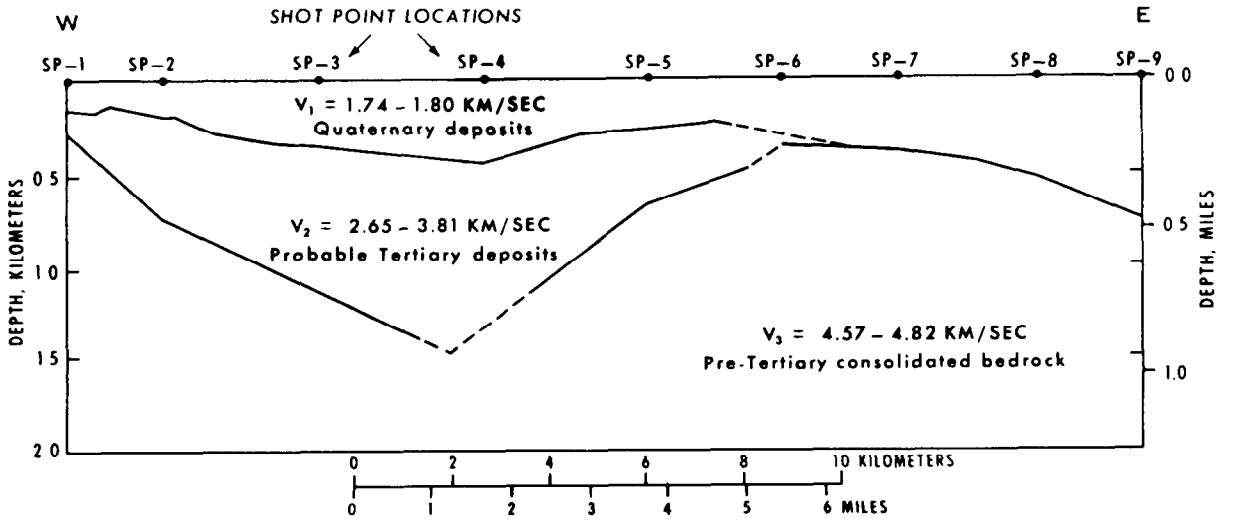

Figure 61.—Seismic cross section of the Jordan Valley east of Great Salt Lake, Utah (after Arnow and Mattick, 1968).

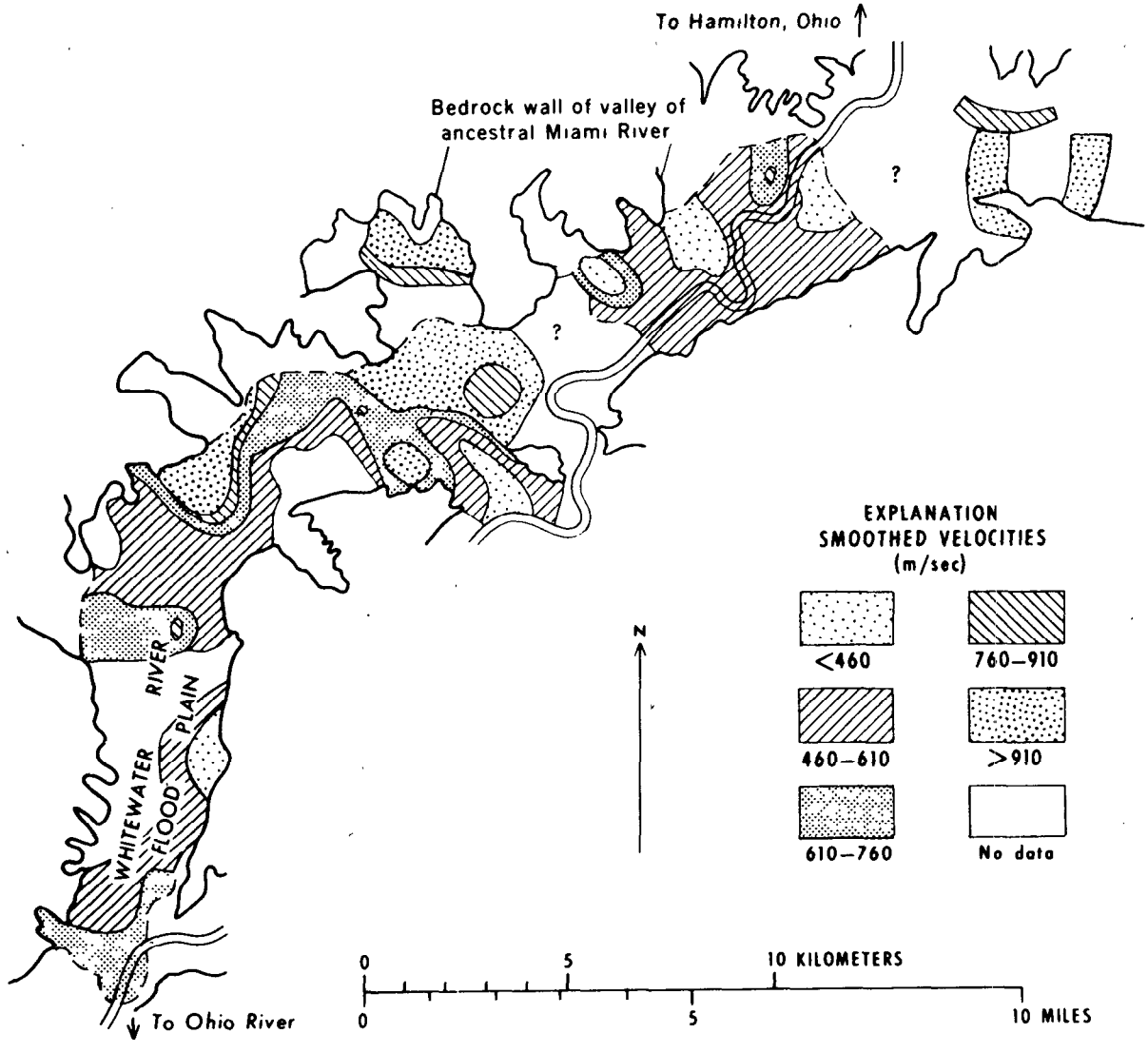

Figure 62.—Distribution of observed compressional wave velocities in unsaturated sediments of the ancestral Miami River Valley, Ohio (after Eaton and Watkins, 1970). Reproduced by permission of "Information Canada."

Another example of this kind of use of seismic refraction data is illustrated by Johnson's (1954) study of Pleistocene sediments in Illinois. Careful measurements tied to stratigraphic control at wells made it possible to distinguish drift of Wisconsin age from that of Illinoian age. In addition, water-bearing strata of sand and gravel were recognized in the section from their effect, as delayed arrivals, on the traveltime curves.

Mapping Lateral Facies Variations in an Aquifer

Seismic refraction measurements in areas where a large number of geophone spreads and shot points are employed, may reveal systematic lateral variations in the velocity of unconsolidated deposits. These variations reflect measurable variations in the physical properties of the deposits, which in turn stem from fundamental variations in lithology. Many geologic factors contribute to variations in the compressional wave velocity of unconsolidated and semiconsolidated sediments. Among these are geologic age, average grain size, grain-size distribution, composition, degree and nature of cementation, confining pressure, degree of saturation, and porosity.

A paper by Eaton and Watkins (1970)

shows the distribution of compressional wave velocities in unsaturated outwash sand and gravel in the valley of the ancestral Miami River in southwestern Ohio (fig. 62). The velocity variations represent lithofacies variations in the upper 30 to 100 meters (100 to 300 ft) of the valley fill. A correlation of water wells of high productivity with areas of a given velocity value would allow use of the seismic velocity map for locating additional well sites of potential high productivity.

Estimating Porosity from Seismic Wave-Velocity Values

Many investigators have noted a pronounced correlation between porosity and compressional wave velocity in clastic sediments, velocity increasing with decreasing porosity (fig. 63). Similarly, there is a correlation between velocity and density, velocity increasing with increasing density. These correlations of porosity and density with seismic wave velocity are interdependent, as bulk density can be defined by three parameters: porosity, grain density, and pore-fluid density. For a group of sediments with the same average mineralogical composition and saturated with ground water of approximately uniform composition, variations in bulk density are a function primarily of variations in porosity. If a small amount of cementing material is present in the pores, it would diminish total porosity but at the same time increase bulk density. Assuming the composition, and more particularly the grain density, of the cement to be approximately the same as that of the clastic constituents, its presence would not materially affect the relationship between density and porosity. In such a situation, the cement could be regarded macroscopically as one of the mineral constituents of the sediment. If its composition is grossly different from that of the clastic grains, however, variations in the degree of cementation would result in variations in the average grain density of the sediment, and the simple relationship between porosity and bulk density would not hold. Neither would that between porosity and velocity. Other factors, such as the degree of

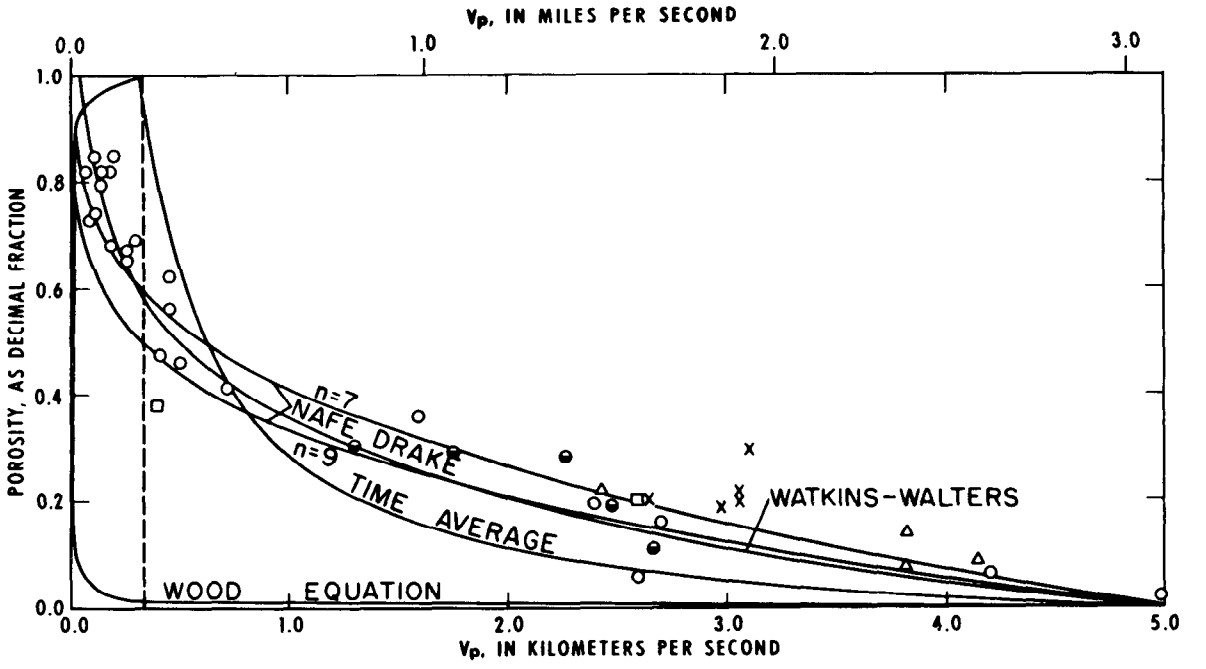

Figure 63.—Plot of observed porosity versus compressional wave velocity for unconsolidated sediments (after Eaton and Watkins, 1970). Reproduced by permission of "Information Canada."

fracturing in a semiconsolidated rock, also influence velocity, the greater the volume density of fractures, the lower the velocity. To some extent, however, fractures contribute to the total porosity, so their effect on the velocity-porosity relationship is not always pronounced. The net result is that velocity values can be used to predict total average porosity, within certain limits, for unconsolidated sediments and weakly consolidated sedimentary rocks.

Experimental data bearing on the systematic relationship between velocity and porosity (fig. 63) include rocks and sediments of a wide variety of compositions. The smooth curves drawn through the data points are empirically derived mathematical functions relating the two properties. Curves such as these could be used in conjunction with mapped velocities like those in figure 62 to produce maps illustrating areal variations in porosity for uniform sediments in a given area. Although the standard deviation of porosity determined in this way would be high, the maps might nevertheless serve a useful purpose in evaluating the relative water-storage potential of the sediments.

References Cited

Arnow, Ted, and Mattick, R. E., 1968, Thickness of valley fill in the Jordan Valley east of the Great Salt Lake, Utah, *in* Geological Survey Research 1968: U.S. Geol. Survey Prof. Paper 600–B, p. B79–B82.

Bonini, W. E., and Hickok, E. A., 1958, Seismic refraction method in ground-water exploration: Am. Inst. Mining Metall. Engineers Trans., v. 211, p. 485–488.

Dobrin, M. B., 1960, Introduction to geophysical prospecting: 2d ed. New York, N. Y., McGraw-Hill Book, Co., Inc., 446 p.

Eaton, G. P., and Watkins, J. S., 1970, The use of seismic refraction and gravity methods in hydrogeological investigations, p. 544–568 *in* Morley, L. W., ed., Mining and Groundwater Geophysics, 1967: Geol. Survey Canada, Economic Geol. Rept. 26, 722 p.

Hawkins, L. V., 1961, The reciprocal method of routine shallow seismic refraction investigations: Geophysics, v. 26, p. 806–819.

Johnson, R. B., 1954, Use of the refraction seismic method for differentiating Pleistocene deposits in the Arcola and Tuscola quadrangles, Illinois: Illinois State Geol. Survey Rept. Inv. 176, 59 p.

Kaufmann, H., 1953, Velocity functions in seismic prospecting: Geophysics, v. 18, p. 289–297.

Levshin, A. L., 1961, Determination of groundwater level by the seismic method: Akad. Nauk. SSSR IZU. Ses. Geofiz, no. 9, p. 857–870.

Peterson, D. W., Yeend, W. E., Oliver, H. W., and Mattick, R. E., 1968, Tertiary gold-bearing channel gravel in northern Nevada County, California: U.S. Geol. Survey Circ. 566, 22 p.

Slotnick, M. M., 1959, Lessons in seismic computing: Soc. Exploration Geophysicists, Tulsa, 268 p.

Soske, J. L., 1959, The blind zone problem in engineering geophysics: Geophysics, v. 24, p. 359–365.

Willmore, P. L., and Bancroft, A. M., 1960, The time term approach to refraction seismology: Royal Astron. Soc. Geophys. Jour. (London), v. 3, p. 419–432.

Gravimetry

By G. P. Eaton

Gravimetry is the geophysical measurement of the acceleration of gravity and has, as its basis, two well-known laws of elementary physics. The Law of Universal Gravitation states that every particle of matter exerts a force of attraction on every other particle that is directly proportional to the product of their masses and inversely proportional to the square of the distance between them. Thus,

$$F = G\frac{m_1 m_2}{r^2} \qquad (1)$$

where G is a constant of proportionality (the gravitational constant), m_1 and m_2 are the particle masses, and r is the distance between the particles. The other law is Newton's second law of motion, which may be stated in the form: when a force is applied to a body, the body experiences an acceleration that is directly proportional to the force and inversely proportional to the body's mass. Thus,

$$a = F/m \qquad (2)$$

where a is the acceleration of the body in the direction in which the force is acting.

Because the Earth is approximately spherical and because the mass of a sphere can be treated as though all of it were concentrated at a point at the center, any object with mass m_o, resting on the Earth's surface, will be attracted to the Earth by a force.

$$F \cong G\frac{m_o m_e}{R^2} \qquad (3)$$

where m_e is the mass of the Earth and R, its average radius. This force of attraction between the object and the Earth is the object's weight.

If the object is lifted a short distance above the Earth and allowed to fall, it will do so with a gravitational acceleration,

$$g^* = F/m_o \cong G\frac{m_e}{R^2}. \qquad (4)$$

This acceleration is the force per unit mass acting on the object. It is a function of both the mass of the Earth and the distance to its center. The principle is the same, however, when the attracting body is something other than the Earth as a whole, and it is on this principle that gravimetry, as a geophysical method, is based.

In gravimetric studies, the local vertical acceleration of gravity (the standard cgs unit of which is the gal, after Galileo) is measured. A gal is equivalent to an acceleration of 1 cm/sec/sec. Most gravity variations associated with geologic bodies in the outer several miles of the Earth's crust are measured in mgals (milligals). The maximum gravity difference between the Earth's normal field (the main gravity field of the reference spheroid) and that actually observed on the surface and corrected for altitude and latitude is of the order of several hundred mgals. This difference, known as a gravity anomaly, reflects lateral density variations in rocks extending to a depth of several tens of miles.

Two types of instruments are used in making gravity measurements in the field: (1) the gravity pendulum, which operates on the principle that the period of a free-swinging pendulum is inversely proportional to a simple function of gravitational acceleration, and (2) the gravity meter, or gravimeter, which is a highly sensitive spring balance with which differences in acceleration are measured by weighing, at different points, a small internal mass suspended from a spring. Because this mass

* Most textbooks of elementary physics denote acceleration with the symbol a, as in equation 2. It is customary in geophysics, however, to use the symbol g to signify gravitational acceleration.

does not change, differences in its weight at different points on the Earth reflect variations in the acceleration of gravity (eq. 4).

The gravity meter rather than the gravity pendulum is used in exploration geophysics because it is light in weight, easily portable, highly accurate, and rapidly read. The modern gravity meter measures, with great accuracy and precision, differences in gravity between points, but does not measure the absolute value of gravity itself at any point. What is measured is the vertical component of the acceleration of gravity rather than the total vector, which may depart slightly from the vertical. The last point is illustrated in figure 64 and discussed below.

The total gravitational attraction of a body M, at point P, can be calculated by subdividing it into a series of vanishingly small elementary masses (fig. 64). One of these is shown in figure 64 as dm. The summed effect of all of the elemental masses contained within body M represents the total attraction.

The gravitational acceleration due to mass dm measured in the direction of r, is

$$dg_r = G\frac{dm}{r^2}. \qquad (5)$$

An instrument designed to measure the vertical component of this attraction will experience an acceleration, dg_z, that is a function of the angle ϕ

$$dg_z = G\frac{dm}{r^2}\cos\phi. \qquad (6)$$

A summation of dm over the entire body yields the vertical component of the total attraction due to M at point P:

$$g_z = G\int_m \frac{dm}{r^2}\cos\phi. \qquad (7)$$

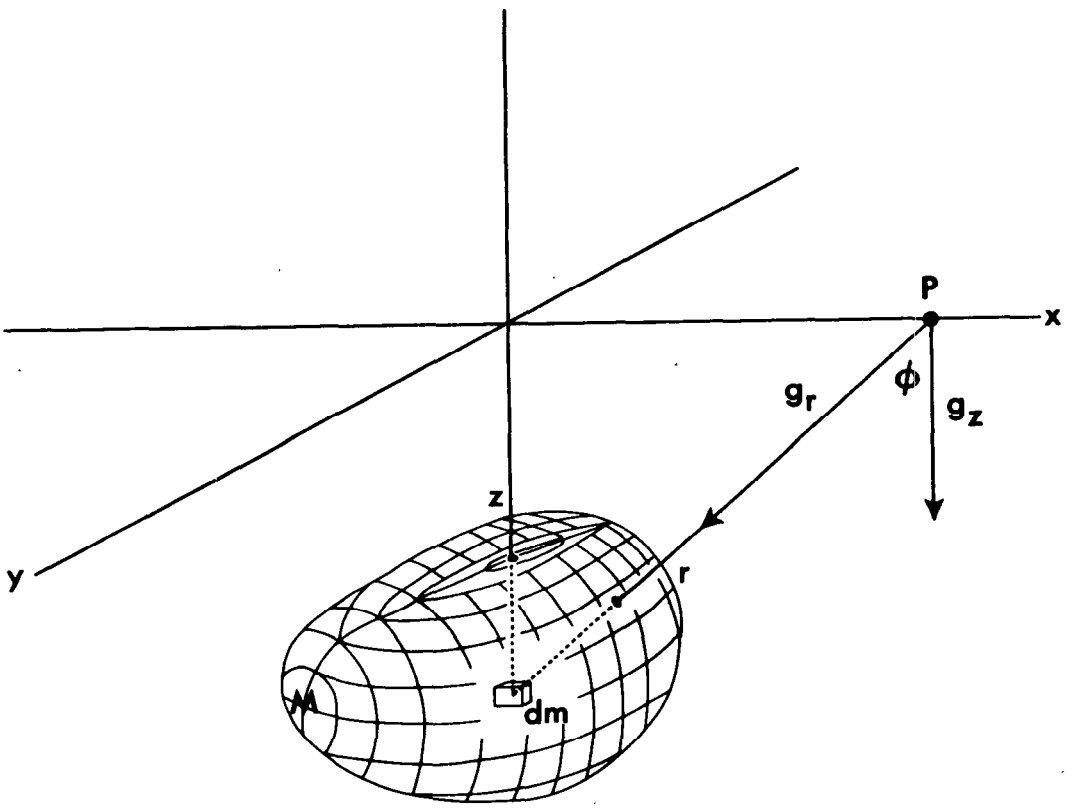

Figure 64.—Gravitational attraction at point P due to buried mass dm.

If the density of body M is homogeneous and has the value ρ, we can rewrite equation 7 as:

$$g_s = \rho G \int_v \frac{dv}{r^2} \cos \phi \qquad (8)$$

where dv represents the volume of dm and the integration is performed over the entire volume. Equation 8 is the basic equation of gravimetry. An exact solution for the integral can be obtained if the body has a simple analytical shape; for example, a sphere, a right circular cylinder, or an infinite, uniformly thick plate. If, however, the body is irregular in shape, as most geologic bodies are, then the total attraction must be calculated by graphical integration or by numerical summation, using a digital or analog computer.

Although the gravitational attraction of any geologic body is a function of its mass, the total gravitational attraction measured by a gravimetric device on the surface above it represents the sum of the attractions of both the body and the rest of the Earth, as a whole. In geophysical prospecting, we are interested only in that part of the gravity field due to the body; therefore, we generally need be concerned only with the excess or deficiency of mass that the body represents, rather than with its absolute mass. Under these circumstances, the body can be described quantitatively in terms of its density contrast with its surroundings. Observed gravity variations, when corrected for nongeologic effects, reflect contrasts in density within the Earth, particularly, lateral contrasts in density. The symbol ρ in equation 8 can be taken to represent the density contrast between a geologic body and its surroundings, rather than the actual density of the body.

Reduction of Gravity Data

Several corrections must be applied to raw gravity data collected in the field before they can be used for geological interpretation. Some of these corrections have a practical effect on the design of a gravity survey and the applicability of gravimetry to the hydrogeological problem at hand.

The theoretical foundations for gravity data reduction have been worked out in rigorous detail but need not be presented here. The interested reader is referred to Dobrin (1960) or Grant and West (1965) for the details and mathematical derivation of the corrections.

Reference to figure 65 should provide a qualitative understanding of the origin and nature of the various effects necessitating the corrections. In figure 65A is a spherical geologic body, the center of which lies 6.1 km (3.8 mi) below the Earth's surface. This surface, which is perfectly flat in our example, bounds a rigid, stationary, homogeneous Earth of semi-infinite extent. The buried body, with a density that is 0.50 gm/cm^3 greater than that of the rest of the Earth, represents the only departure from homogeneity affecting the total gravitational field. The gravity anomaly associated with the buried sphere is shown immediately above the model. It represents a local departure from the otherwise featureless gravity field associated with the hypothetical Earth, and is what we would see if we were to make a series of measurements with a gravity meter in the area and plot them, without modification, on a sheet of graph paper. The maximum amplitude of the anomaly is 3.7 mgals. Although spherical masses such as this one are an imprecise representation of most real geologic bodies, they are ones for which the analytical computation of gravity anomalies is relatively simple, hence in the pages that follow the sphere will be used to illustrate several properties of gravity fields. Actually the Earth model we have chosen is far more unrealistic than is the sphere, insofar as a representation of nature is concerned. The real Earth is not flat, it is spheroidal, and its surface is far from plane. In addition, it is neither rigid, stationary, nor homogeneous.

A more accurate representation of the real Earth is shown in figure 65B. The Earth depicted there is a rotating, nonrigid, spheroid within the gravitational influence of other

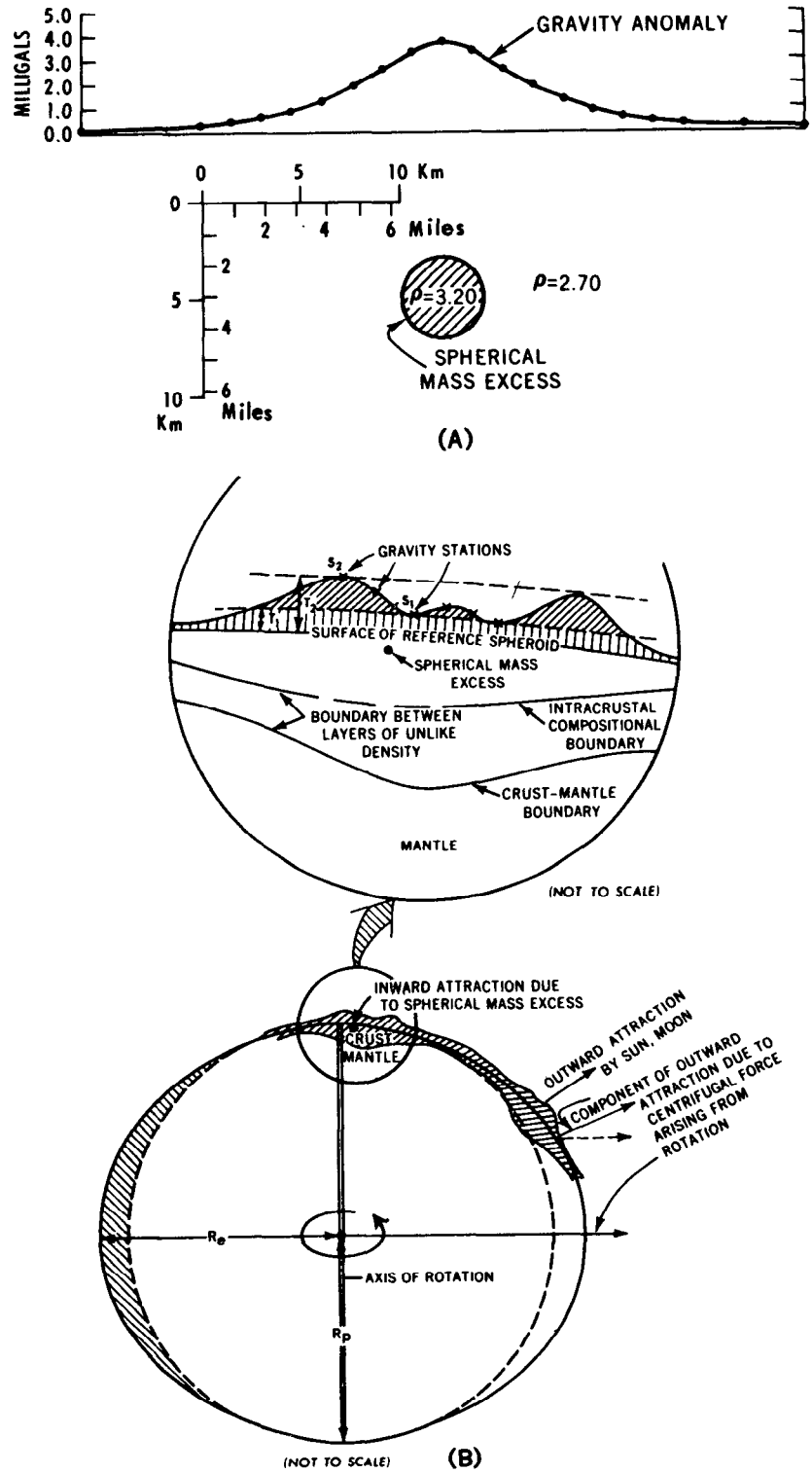

Figure 65.—A, Observed gravity profile for a buried sphere in a homogeneous rigid nonrotating Earth. B, Sources of variation present in gravitational measurements made in the search for a buried sphere in a schematic, but real, Earth model.

celestial bodies, with a compositionally nonhomogeneous crust of geographically varying thickness, and with a topographically rugged surface. Gravity measurements made on the surface of this Earth over a buried sphere would, if plotted as observed, display a scatter of points seemingly distributed without reason or order.

The reduction of gravity data refers to the removal of all unwanted effects that tend to mask or distort the gravity field caused by the object of interest. Several steps in the reduction process can be treated as mathematical routines, making them mechanically simple to execute. Others require judgment based on a knowledge of the local geology.

Latitude Correction

Gravitational acceleration measured on the Earth's surface varies systematically with latitude because the Earth rotates, is not perfectly rigid, and its shape is not precisely that of a sphere. At the poles the distance to the center of the Earth (radius R_P) is less than it is at the equator (radius R_e), and there is no component of centrifugal force, as there is at the equator, acting outward. Both these effects tend to reduce gravity at the equator relative to that at the poles. The effect of a somewhat greater thickness of rock (with consequent greater mass) between the equator and the Earth's center tends to reduce very slightly the effect of the first two factors, but the net result is that gravity at the poles is approximately 5 gals greater than it is at the equator. This latitudinal variation can be expressed as a trigonometric function of latitude. For this reason the latitude correction is both simply and routinely determined, either from table of values at discrete increments of latitude or by high-speed machine computation.

If an accuracy of 0.1 mgal in reduced gravity data is desired, the latitude of each station must be known to within 150 meters (500 feet) of its actual location. If an accuracy of 0.01 mgal is needed (which is approaching the limits of precision of the modern field instrument), locations must be known to within 15 meters (50 feet). With most modern topographic maps published at a scale of 1:62,500 or larger, this is not a serious problem. The correction is made by subtracting from the value for observed gravity, the value of theoretical gravity on the reference spheroid at sea level at the same latitude. For gravity surveys of limited latitudinal extent, the variation of gravity with latitude can be treated as though it were a linear function of surface distance north or south of an arbitrary base line drawn through the area of study. For the continental United States this variation of gravity ranges from approximately 0.6 mgal/km (0.96 mgal/mile) to 0.8 mgal/km (1.29 mgal/mile) and is greatest at 45° north latitude.

Tidal Correction

The Sun and Moon both exert an outward-directed attraction on the gravity meter, just as they do on large bodies of water as evidenced by tides. This attraction varies both with latitude and time. Although its magnitude is small, there are some hydrologic applications of gravimetry where tidal variations must be taken into account. The maximum amplitude of the tidal effect is approximately 0.2 mgal and its maximum rate of change is about 0.05 mgal/hour. If accuracy of this order of magnitude is not required in a gravity survey, the tidal effect may be neglected.

Several routes are open to the geophysicist in making tidal corrections; perhaps the one most commonly used is to monitor tidal variations, empirically, along with instrument drift, by returning every 2 hours or so to a gravity base station. Details of this approach are discussed under the heading "Drift Correction."

Altitude Corrections

Two corrections for station altitude must be made in the data-reduction process. One of these is the free-air correction and the other is the Bouguer correction.

Free-Air Correction

As the gravity meter is moved from hill to valley over the irregular surface of the Earth, the distance to the center of mass of the Earth varies. Equation 4 indicates that variation in the value of R (the distance to the center of the Earth's mass) will cause variations in the measured acceleration of gravity. This effect is known as the free-air effect.

The average value for the free-air gradient of gravity is —0.3086 mgal/m (—0.0941 mgal/foot). This value varies with both latitude and altitude but the variations are very small—less than one percent over most of the Earth's surface from sea level up to altitudes as great as 9,000 meters (31,000 feet). Variations in the free-air gradient of gravity also may be caused by large gravity anomalies arising from the outer part of the Earth. Departures in the measured value of this gradient have been found, under exceptional circumstances, to exceed 10 percent of the average value of —0.3086 mgal/m (—0.091 mgal/foot). Knowledge of the exact local free-air gradient of gravity is not important in most gravity surveys. For some hydrogeologic applications, however, it may be necessary to measure the local value. Measurement of the local free-air gradient, should it be required at any locality, is not an insurmountable problem, but the necessity for doing so should be thoroughly evaluated by the geophysicist.

Bouguer Correction

The Bouguer correction is necessitated by the presence of rock between the gravity station and the elevation datum (commonly mean sea level) to which the observations are to be reduced. Referring to 65B, there is, at gravity station S_1, a mass of rock of thickness T_1, between the station and the elevation datum, which causes an additional downward attraction that would not be sensed had we been able to suspend the gravity meter in free space at the same elevation. This attraction varies with station elevation and has a value at station S_2 different from that at station S_1.

The standard procedure for making the Bouguer correction is to assume that an infinite slab of rock, of thickness equal to the height of the station above the datum, is present beneath the station. For a station in relatively flat country this approximation is a reasonable one, but for areas of rugged topography it is not. For example, in figure 65B, the infinite slab approximation is good for station S_1, but poor for station S_2. An adjustment is made for the relatively poor fit of the infinite slab model in topographic situations such as that of station S_2 when one makes the terrain correction described below.

The gravitational acceleration due to an infinite horizontal slab of uniform density ρ is:

$$g_z = 2\pi G\rho T \qquad (9)$$

where T is the thickness of the slab. Note that the gravitational acceleration is not dependent on the distance of the point of measurement from the surface of the slab, but only on the slab's thickness and density. Thus the gravitational acceleration caused by a given slab of homogeneous rock would be the same whether measured on its surface, or on a tower several hundred feet above its surface. This apparent peculiarity of the gravitational field of an infinite slab has great utility in gravity exploration, both for data reduction and data interpretation, as will be apparent later.

Two parameters in equation 9 are needed to make the Bouguer correction, density and thickness. In many gravity surveys, particularly those of regional extent, mean sea level is chosen as the elevation datum. The value of T is then the elevation of the gravity station. Likewise, ρ routinely is assigned a constant value of 2.67 gm/cm^3. These choices, though they have some theoretical and practical foundation, are essentially arbitrary and may not be appropriate for use in some areas or in certain hydrogeologic studies. When subtle gravitational variations are being sought it is important to use true

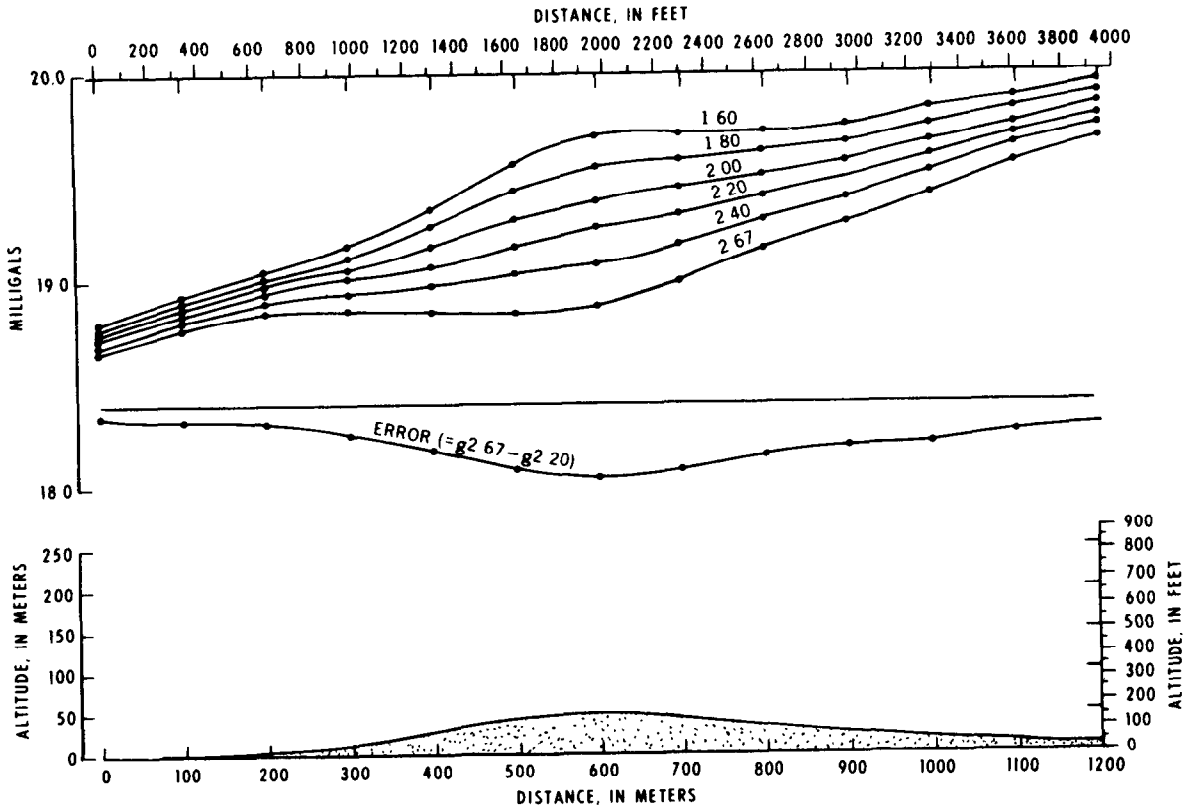

Figure 66.—Bouguer gravity profiles across a low ridge based on six different densities employed in calculating the Bouguer correction. The proper value for density is 2.20 gm/cm³.

rock density values and to use a local elevation datum.

The effect of the use of an incorrect density value in making the Bouguer correction is shown in figure 66. In the lower part of figure 66 is a topographic profile of a broad ridge. This ridge is underlain by young sedimentary rocks that have a uniform density of 2.20 gm/cm³. A regional gravity gradient slopes downward across the area from right to left. It is caused by a deep-seated density variation. The gravity anomaly curve labelled 2.20 is the one that would be obtained if tidal, latitude, free-air and Bouguer corrections were made, using in the Bouguer correction a density of 2.20 gm/cm³.

If there were no data on local rock densities and an assumed value of 2.67 gm/cm³ were used, the reduced gravity data would provide the curve labelled 2.67. This curve, which mirrors the topography, is in error. It displays an artificial local anomaly, superimposed on the regional gradient. The curve labelled "ERROR" represents the algebraic difference between the correct Bouguer gravity curve, based on the true density 2.20 gm/cm³, and the erroneous one created by assuming a density of 2.67 gm/cm³.

If the density data were based on cores recovered in an area a few miles away, where the local near-surface density was 1.60 gm/cm³, and this value were used to make the Bouguer correction, an artificial anomaly in the form of an upward convexity superimposed on the regional gradient (curve 1.60) is created.

In summary, knowledge of the correct local rock density is essential to the correct reduction of gravity data. If incorrect values are used, artificial gravity anomalies related to topography are created. Hills or ridges

produce artificial gravity highs if the density value used is smaller than the actual value and they produce gravity lows if the density value is too high.

In many regions the geology is sufficiently complex that the assumption of a single uniform density is not warranted. When seeking targets with very small differences in density, variable density values must be used in making the Bouguer correction. In effect, this amounts to making a correction for the near-surface geology. The more that is known about the local distribution of rock types and their densities, the less chance there is of introducing artificiality and error in the result. For regional surveys of a reconnaissance nature this kind of sophistication usually is not justified. For highly detailed studies, with closely spaced gravity stations and subtle targets, it is.

If local rock densities are poorly known, or if the densities vary vertically, it is advisable to use a datum as close to the great bulk of the station elevations as possible. Either of two options can be employed. A frequency diagram of all station elevations can be plotted, and the modal elevation value for the datum selected or the elevation of the lowest station in the survey area can be used as datum. Doing either minimizes the chance of errors resulting from imperfect knowledge of the geology between the station and the datum.

Because the free-air and Bouguer corrections are both simple functions of the elevation of the gravity station above the datum, they are combined, for computation, into a single correction referred to as the combined elevation correction. The algebraic form of the combined elevation correction is Kh, where h is the height of the station above the datum and K is a function of the free-air gradient and the rock density. Examination of the magnitude of K for varying values of density and a fixed value for the free-air gradient of —0.3086 mgal/m (—0.0941 mgal/foot), illustrates the magnitude of the errors incurred when station elevations are imperfectly known:

Rock density (gm/cm³)	*K value*	*Approximate error, in mgal, created by an elevation error of 3 meters (9.84 ft)*
1.7	0.2375	0.71
1.9	.2291	.69
2.1	.2207	.66
2.3	.2123	.64
2.5	.2040	.61
2.7	.1956	.59

The errors in the right-hand column are larger than can be tolerated in certain kinds of ground-water investigations. In those studies where anomalies of several hundredths to a few tenths of a milligal are sought, elevations must be known to the nearest 3 cm (0.1 ft). Precision levelling is required for station elevations of this accuracy.

Terrain Correction

It is apparent that some correction must be made for the topographic masses situated above the level of the gravity station. Hills that project above that level exert an upward gravitational attraction, reducing the gravity value read at the station. Similarly, valleys represent topographic depressions which are filled with rock computationally in making the Bouguer correction (fig. 65). Just as a correction is needed for positive masses projecting above the station, one also is needed for negative masses that are created artificially below it. The algebraic sign of the terrain correction therefore is always positive, whether for hills or valleys.

A terrain correction generally requires the existence of good topographic maps. If they are not available, the cost of obtaining the necessary topographic information is generally prohibitive. The topographic detail required depends on the accuracy sought in the reduced values and on the proximity of topographic irregularities to the stations. For example, if the topography enclosed within two concentric circles about a given station, the inner circle, with a radius of 17 m (56 feet), and the outer one, with a radius of 53 m (174 feet), differs in elevation from the station by an average of 8 m (26

feet), and if the rock density is 2.67 gm/cm^3, a terrain correction of approximately 0.13 mgal is required. To estimate this elevation difference accurately, a topographic map at a scale of close to 1 : 25,000 or better and with a contour interval of 3–5 m (10–15 feet) is required. In the absence of this kind of topographic detail it is better not to locate the station where the terrain is varied enough to create effects of this size when high accuracy is sought. Balance between the detail and accuracy sought from the survey and the topographic detail available must be considered in designing the survey. For a study of an intermontane valley with dimensions of 25 by 65 km (15.5 by 40.4 miles), and filled with 2,000 m (6,500 feet) of late Cenozoic sediments, the expectable maximum amplitude of the associated gravity anomaly will be several tens of milligals. If one is interested only in the gross configuration of the buried bedrock floor of this valley, and in a quantitative estimate of the depth to bedrock, errors of a milligal or so can be tolerated. This means that the topographic detail needed for the terrain corrections is not nearly as limiting as it is for a buried outwash channel only 160 m (525 feet) deep and 1 km (0.62 mile) across. The maximum amplitude of the anomaly for the buried channel will not exceed 5 mgal. If the channel contains clay-rich glacial till, the anomaly may be only a few tenths of a milligal. Here the accuracy of each correction must be kept as high as possible and errors should not be allowed to exceed a few hundredths of a milligal.

Terrain corrections are made by arbitrarily subdividing the region about the station into a series of rectangles or curvilinear cells and estimating the average topographic elevation of each. Mathematical computations are then made to determine the correction for each cell and the results summed to obtain the total correction for the station. Either of two schemes may be used. One, a manual method, consists of centering a transparent graticule on the station, subdividing it into compartments by radii, and estimating the compartment elevations by eye. The other, usually justified only by a relatively large number of gravity stations, consists of digitizing the topography of the surrounding region on a rectangular grid, and performing the necessary calculations with a high-speed digital computer. The computer program in use in the Geological Survey allows terrain correction computations to be extended to a distance of 166.7 km (104 miles) from the station. In most hydrologic applications computations to this distance are unnecessary. Terrain corrections are rarely extended beyond 25 km (16 miles) when the calculations are made by hand. The judgment of a person experienced in making gravity terrain corrections is advisable, although not absolutely necessary for efficient design of the reduction program.

Drift Correction

Because the materials of construction of most, if not all, gravity meters are susceptible to both elastic and inelastic strains when subjected to thermal or mechanical stresses, reoccupation of the same gravity station at different times with a given meter may reveal differences in the readings obtained. The observed differences may be caused by tidal effects, but some result from stresses or shock to the internal components of the instrument. Gravity differences resulting from these stresses are referred to as instrument drift. In practice, instrument drift and tidal effects usually are monitored together by returning to a base station every 2 hours or so during the course of a survey. It is assumed that variations between reoccupations of the base are time-dependent. Corrections for readings at field stations occupied in the interim are scaled from a plot of drift versus time.

Regional Gradients

All the corrections described thus far are designed to eliminate nongeologic effects such as those caused by variations in elevation and latitude, topographic irregularities,

or other extraneous sources. The resulting contoured gravity field is known as a complete Bouguer gravity anomaly map and displays features that theoretically are due only to lateral variations in rock density below the elevation datum. An analysis of the gravity field in terms of this geology is presumably the reason for making the survey in the first place. From a practical standpoint, things are not quite so simple. Usually a target of geologic interest is quite specific at the outset and the gravity field arising from it is the objective sought. The problem which arises results from the fact that rarely do we see the gravity field of a given geologic body in isolation. Usually, the anomaly of interest is distorted or partly masked by the gravity fields of other bodies. As a result, the geophysicist is faced with the problem of sorting out those parts of a total gravity field caused only by the object of immediate interest. Basically he knows only the magnitude and shape of the total Bouguer gravity field, but he hopes to be able to subtract from it the contributions caused by geologic bodies of unknown shape, density, and location, in order to isolate the residual anomaly of interest. A simple example, and one for which the isolation process is usually rather simple, can be seen in figure 65B. The target here is the spherical body. Interfering with the gravity field of the sphere is another which arises from variation in density between the lower part of the crust and the mantle beneath it. The interface between the crust and mantle is not concentric with the reference spheroid and hence it constitutes a lateral density contrast that will be sensed by the gravity meter. Because it is a broad deep-seated feature, its gravitational effect will be that of a gentle areally-extensive undulation. If the center of the anomaly sought is well up on one flank of this undulation, the regional effect will be that of a continuous gradient extending across the survey area for a distance many times greater than the width of the target anomaly. We refer to this part of the total field as the regional gradient and in order to make a quantitative interpretation of the anomaly caused by the target alone, we must somehow subtract the effect of the regional gradient. (See fig. 71 and related text for an actual example of a regional gradient). Many schemes have been proposed for doing this. The interested reader may want to read Nettleton (1954) for a nonmathematical discussion of the methods in use today.

Bouguer Anomaly

If the value of absolute gravity is known at a station by virtue of having tied it directly, or indirectly with a gravity meter, to a base station where pendulum measurements of gravity have been made, the calculated corrections can be added algebraically to this value to obtain what is known as the complete Bouguer gravity anomaly. This anomaly is defined as follows:

Observed gravity plus drift and tidal correction plus combined elevation correction plus terrain correction minus theoretical gravity on the reference spheroid (latitude correction).

If the terrain corrections have not been made, the results are referred to as simple Bouguer anomaly values.

In gravimetric prospecting it is not necessary to know the value of absolute gravity at any point in the survey area. The concern is principally with variations in Bouguer gravity from point to point and an arbitrary value can be assigned to the base station. The resulting field differs from the true Bouguer anomaly field by a constant amount everywhere. Knowing the value of absolute gravity at the base provides the means of tying the gravity survey to others and for this reason it is common practice to relate each survey to the same absolute datum.

Interpretation of Gravity Data

Ambiguity

In its simplest form, the interpretation of gravity data consists of constructing a hypothetical distribution of mass that would give

rise to a gravity field like the one observed. Models are constructed graphically or mathematically and their gravity effects calculated from equation 8 by numerical summation or graphical integration. The difficulty lies in the fact that a large number (theoretically, an infinity) of hypothetical models will produce the same gravity anomaly. The known quantity g_z is a complex function of three unknowns: density, shape, and depth of the causative body. It is apparent, even without knowledge of an exact solution for the volume integral in equation 8, that one could substitute, simultaneously, a variety of values for the parameters ρ, r, ϕ, and $\int_v dv$ in such a way as to maintain a constant value for g_z at point P on the surface.

If we had enough information in a given

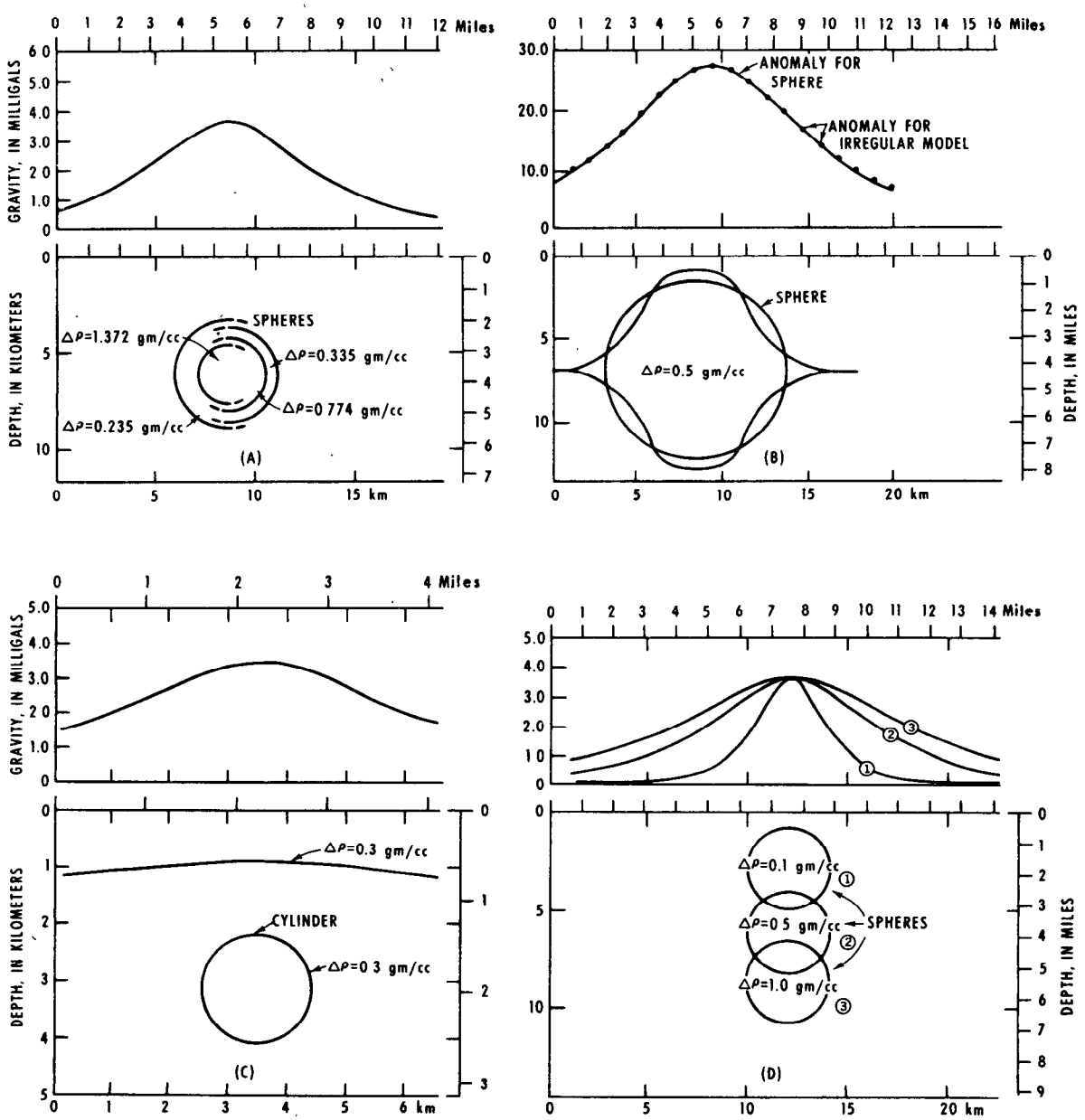

Figure 67.—Schematic models and associated Bouguer gravity anomalies for idealized geologic bodies.

situation to know that we were dealing with a spherical body with its center buried at a specific depth, we still could not make a unique interpretation of the gravity anomaly in terms of size and density (fig. 67A). The gravity anomalies for these four spheres are identical. This results from the fact that the mass of a sphere can be treated as though it were concentrated at a point at the center. In figure 67A, the radius and density of the spheres have been adjusted to keep the total mass constant. The geologic implication is clear.

In addition, the gravity field of a sphere does not have a unique configuration (fig. 67B). Thus the shape of a body cannot be determined from its gravity anomaly alone, even when the density contrast and center of gravity are known. In figure 67B the anomaly arising from the sphere is shown as a smooth curve and the field due to an irregular body of different rotational shape, with coincident center and density, is shown by dots. The two curves match one another very closely.

Bodies of other shape also produce non-unique anomalies (fig. 67C). The gravity anomaly of a horizontal right circular cylinder buried at a depth slightly in excess of 3 km (1.9 miles) can be matched by that of a gently convex basement surface at a depth of approximately 1 km (0.6 mile) when the density contrast between basement and overburden matches that of the sphere and its surroundings.

In summary, the non-uniqueness is pronounced. The fact that gravimetry has been successfully employed as an exploration technique for many decades indicates that ambiguity is not an insurmountable interpretation problem. For example, the individual masses and gravity fields of the spheres of different size shown in figure 67A were kept constant by holding the product ρR^3 constant. The maximum range of bulk densities for common, naturally occurring consolidated rocks and unconsolidated sediments is well known. Reference to Clark (1966, Sec. 4) and Manger (1963) indicates that the limits of the range are approximately 1.70 and 3.00 gm/cm^3. These limits represent well sorted, unconsolidated clastic sediments of high porosity and massive basalt, respectively. There are a few earth materials with densities outside this range, but they are not common. This range places an upper limit on the magnitude of the density contrast that one might expect to encounter in nature and constitutes the maximum density contrast (1.30 gm/cm^3) that can be used in modelling. In most geologic settings the contrast is less than 1.00 gm/cm^3. Greater restriction can be placed on the density contrast in an actual setting from a knowledge of the local geology.

Other boundary conditions can be imposed as well. Consider a typical valley-fill aquifer. It consists of unconsolidated or semiconsolidated sediments resting uncomformably on older, and usually more consolidated (and therefore, denser), rocks. Geologic mapping determines the approximate surface location of the interface between the aquifer and the rocks on which it rests. If, in addition, the top of the aquifer is coincident with the surface of the ground, this fact constitutes an additional boundary condition. Further limits on the interpretational model can be achieved by making measurements of the average bedrock density and the density of the uppermost part of the valley fill. It can be reasonably assumed that the fill density probably increases with depth and that the walls of the valley probably slope inward in the subsurface. Thus severe limitations have been placed upon the conceptual model. Several different models that will produce the observed anomaly probably can still be constructed, but the differences between the models may not be significant. If they are, however, we might be able to bring other data to bear that would furnish still further constraints and thus allow a more nearly unique interpretation. The greater the amount of geologic data that can be used in establishing limits or constraints on the model, the more unique will be the interpretation.

Another facet of the interpretation process

that is of aid in the early stages of data analysis is shown in figure 67D. Three spheres of the same size at different depths have had their densities adjusted so as to keep the maximum amplitude of their anomalies the same. At horizontal distances that are several times the depth of burial of the spheres, all three anomalies asymptotically approach zero because the vertical component of gravity at this distance is negligible. Between the regions of zero and maximum amplitude, however, the three curves are notably different. The greater the depth of burial of a given body, the gentler are the gradients of the flanks of its anomaly. The gradients of any anomaly are also a function of the shape of the producing body because two bodies at distinctly different depths may produce anomalies with the same gradients. There is, however, a limit to the depth to which we can push a model and still maintain anomaly gradients at or above a fixed value. For example, there is no infinitely-long, horizontal body of any cross-sectional shape that can be buried with its upper surface at a depth of 3 km (1.9 miles) or more and still produce an anomaly that has flanking gradients as steep as those shown in figure 67D. There are some general formulas, based on potential theory, that allow determination of the maximum possible depth to the top of anomaly-producing body from the ratio of the maximum amplitude to the maximum gradient of its flanks (Bott and Smith, 1958; Bancroft, 1960). These formulas are useful for a rough fix on maximum depth to the top of a body in the early stages of modelling.

Interpretation Techniques

The basic technique of gravity interpretation is field matching. A model is constructed and its gravity field calculated for comparison with the observed field.

Several methods of calculation are open to the investigator and the one chosen depends on the factors of accuracy and detail sought, the shape and complexity of the model, and the time and equipment available. All of the methods represent some form of integration or summation. Computation of the model field is followed by a comparison of the results with the observed anomaly. The model is then changed and its anomaly recalculated, until the desired fit between observed and theoretical anomalies is achieved.

In its crudest form, the body under study may be assumed to have a constant density and an analytical shape (that is, a sphere, cylinder, or plate), its field being calculated by appropriate substitutions in equation 8. In its most sophisticated form the body can be given an irregular three-dimensional form, with a spatially continuous or discontinuous distribution of density, and its field calculated by digital computer. The computer can be instructed to follow an iterative routine, wherein it makes the comparison between the observed and calculated data, institutes certain changes in the model that will lead to a better fit, recomputes the field, makes a second comparison, and so on.

Presentation of details of the various interpretation methods currently in use is relevant, but not appropriate here. The interested reader is referred to Dobrin (1960, p. 253–262) and Grant and West (1965, p. 268–305). Two points should be stressed however; they are: (1) The solution for a given gravity anomaly is never unique and the use of highly sophisticated and elegant mathematical methods of interpretation does not make it so, and (2) the quality and uniqueness of the interpretation are, in part, a function of the kind and amount of geologic information available to the interpreter.

Significance and Use of Density Measurements

The interpretation of gravity data necessitates accurate knowledge of rock densities in the area surveyed. Because variations in rock density produce the potential field differences we observe after data reduction, this property is of fundamental importance.

There are several ways in which the geophysicist may obtain the density values to be used in handling the data for a given area.

The cost of the method selected should be in rough proportion to the significance of the problem. Eight methods are described briefly below. They are listed approximately in order of increasing significance and accuracy.

1. Assumption of a constant density value of 2.67 gm/cm^3.
2. Assignment of density values on the basis of lithology. Because of the wide variability of rock composition and rock density within a lithologic classification, values assigned on this basis can be in error by as much as 40 percent.
3. Estimates of density based on sound-wave velocities in rocks. Compressional wave velocities and densities of rocks are a function of some of the same lithologic factors. Because of this, they show a pronounced correlation. Approximately three-fourths of the data points in figure 68 fall within 0.1 gm/cm^3 of the regression curve fitted to them.
4. In situ gamma-gamma logging. A gamma-gamma borehole logging device measures radiation that originates from a source in the sonde and travels through a shell of rock adjacent to the borehole. The decrease in strength of the returning signal is approximately proportional to the density of the rock. However, the borehole diameter, the presence of borehole fluids, mudcake on the hole walls, mud-filtrate invasion, and the roughness of the hole all adversely affect the results. A separation of the logging tool from contact with the rock by as little as 0.7 cm (0.3 in) can cause a significant error in the density value.
5. Density measurements on handspecimens collected at the outcrop. If care is taken to procure unweathered material, if the sampling statistics are adequate, and if the samples are large and geologically representative, the results of this method are usually quite accurate. This probably is the method most frequently used today.
6. Density profiling with the gravity meter. If a topographic feature such as a hill or valley is underlain by rocks of laterally homogeneous density and if the topography is not an expression of geologic structure, the data from a gravity profile can be used to measure the average bulk density. The principle is illustrated in figure 66, where the Bouguer anomaly curve computed using the correct density of 2.20 gm/cm^3 shows the least tendency to mirror the topography. The advantage of this method is that it samples, in place, a very large volume of rock.
7. Laboratory measurements of drill-core samples of consolidated rocks. This method provides a means of sampling below the zone of weathering and, if recovery is good, it also provides the basis for computing geologically-weighted means for the section. Recent tests (McCulloh, 1965) indicate that when proper care is taken in handling the cores, the accuracy of this method is high. However, a borehole represents a single vertical traverse of the rocks in an area. If there are pronounced lateral variations in density, cores from a single hole may not suffice.
8. Logging with a borehole gravity meter. A gravity meter lowered in a borehole can be used to measure the in situ density of rocks directly. Its ability to do so stems in large part from the relationship expressed in equation 9. The difference in the acceleration of gravity between two points in a borehole, separated vertically by the distance T, is a function of the product $4\pi G\rho T$. At the top of the interval downward attraction is $2\pi G\rho T$ and at the base, $-2\pi G\rho T$ (the same attraction acting upward, or in a negative sense). T can be measured and the measured value of the gravity difference, Δg_z, can be used to calculate the density, ρ. The radius of the region of rock that is sampled is roughly five

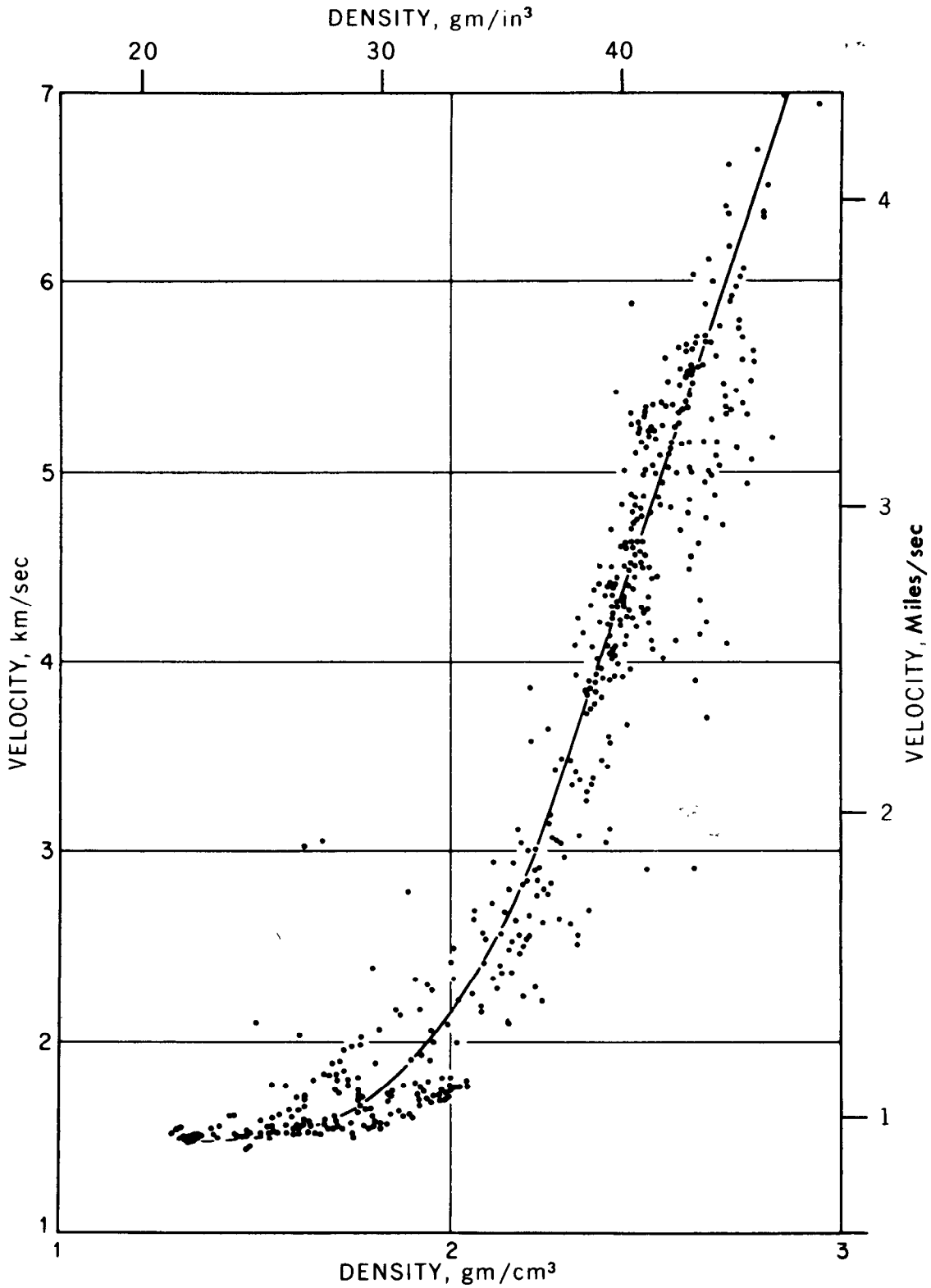

Figure 68.—Plot of observed compressional wave velocities versus density for sediments and sedimentary rocks (after Grant and West, 1965). Reproduced with permission of McGraw-Hill Book Company.

times the length of the vertical interval, T. A typical borehole gravity meter log of a thick section of alluvium is shown in figure 72.

Application of Gravimetry to Hydrogeology

Aquifer Geometry

The gravity method is a rapid, inexpensive means of determining the gross configuration of an aquifer, providing an adequate density contrast between the aquifer and the underlying bedrock exists. It is useful in locating areas of maximum aquifer thickness, in tracing the axis of a buried channel (fig. 69A), and in locating a buried bedrock high that may impede the flow of ground water (fig. 69B).

In figure 69A, the irregular belt of unconsolidated sediments that runs from the northwest corner of the map to the south-central part consists of buried outwash or ice-contact deposits resting in a glacially-overdeepened, preglacial bedrock channel of the Connecticut River. Well data (Cushman, 1964) defined the course of this buried channel, and its axis coincides with the axis of the gravity trough shown. Thus the gravity data reflect the locus of maximum thickness of the unconsolidated sediments. The success of the gravity method in defining the geometry of the aquifer in this area is due to the high density contrast between the unconsolidated fill and the bedrock, which consists of dense Paleozoic metamorphic rocks and Triassic sedimentary rocks. In areas where the contrast is lower, the definition of a narrow buried valley, such as the one shown here, becomes more difficult. If the density contrast is zero, the gravity method is useless for defining or mapping buried channels.

The San Gorgonio Pass area in southern California (fig. 69B) is bounded on the north and south by high mountain ranges consisting of Pre-Cenozoic metamorphic and igneous rocks. These rocks have a relatively high density. Deformed sedimentary rocks of late Tertiary age are exposed east and west of the map area along the north side of the pass. Recent sand and gravel underlie the central part of the area. Water levels measured in the spring of 1961 in two wells (A and B) define a water table sloping gently eastward with a gradient of about 5.7 m/km (30.1 feet/mile), in agreement with other well data west of the map area. In the vicinity of well B, however, the water table drops abruptly from an elevation of 345 m (1,130 ft) to 160 m (525 ft) in well C.

Contours of complete Bouguer gravity reveal that the cause of the discontinuity in the water table is a subsurface continuation of the exposed bedrock ridge which projects northward from the south side of the pass. This ridge rock is virtually impermeable and serves as a ground-water barrier. Aside from its visible expression on the south side of the pass, there is no surface evidence of its presence. The gravity method thus provides a means for recognizing its existence.

Estimating Average Total Porosity

Surface Method

Figure 70A shows the distribution of outcrops of granitic rocks bordering Perris Valley, Calif. Also shown are structure contours on the buried bedrock surface, as defined by well data. The structure contours reveal a large buried channel in the vicinity of Perris Boulevard. The land surface in this area is at an altitude of approximately 1,400 feet, which means that the maximum thickness of the unconsolidated sediments filling the buried valley is approximately 800 feet.

Figure 70B shows a Bouguer gravity map of the same area. The gravity map mimics the bedrock topography of the buried channel almost perfectly. Because of this high degree of correlation and the unusual amount of well control available from the area, estimation of the average in situ sediment porosity from surface gravity measurements

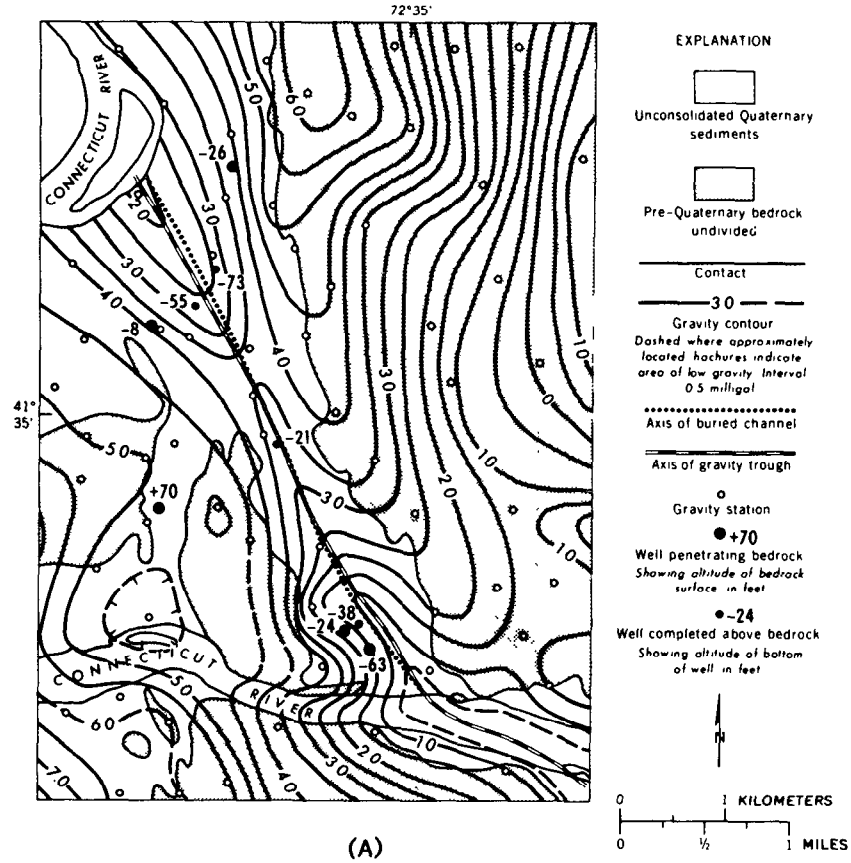

(A)

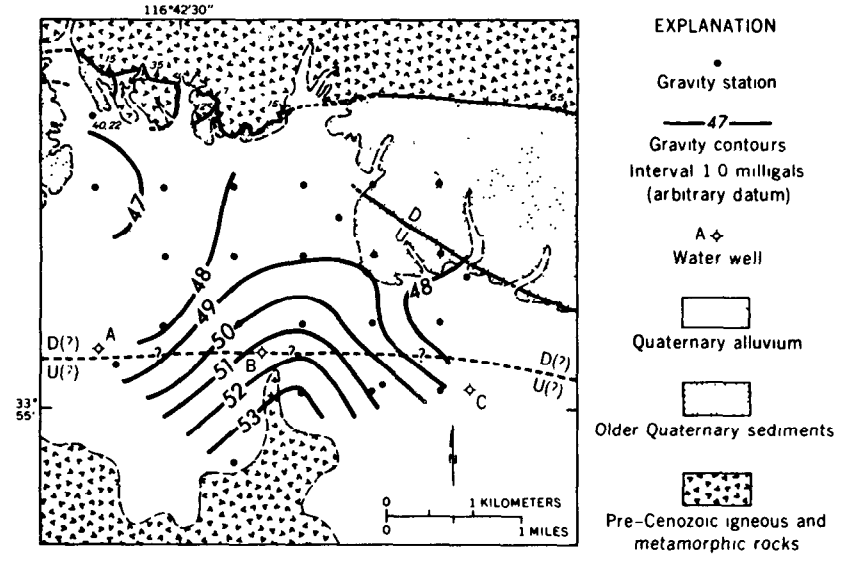

(B)

Figure 69.—A, Complete Bouguer-gravity map of a buried pre-glacial channel of the Connecticut River (after Eaton and Watkins, 1970). B, Complete Bouguer-gravity map of part of San Gorgonio Pass, California (after Eaton and others, 1964).

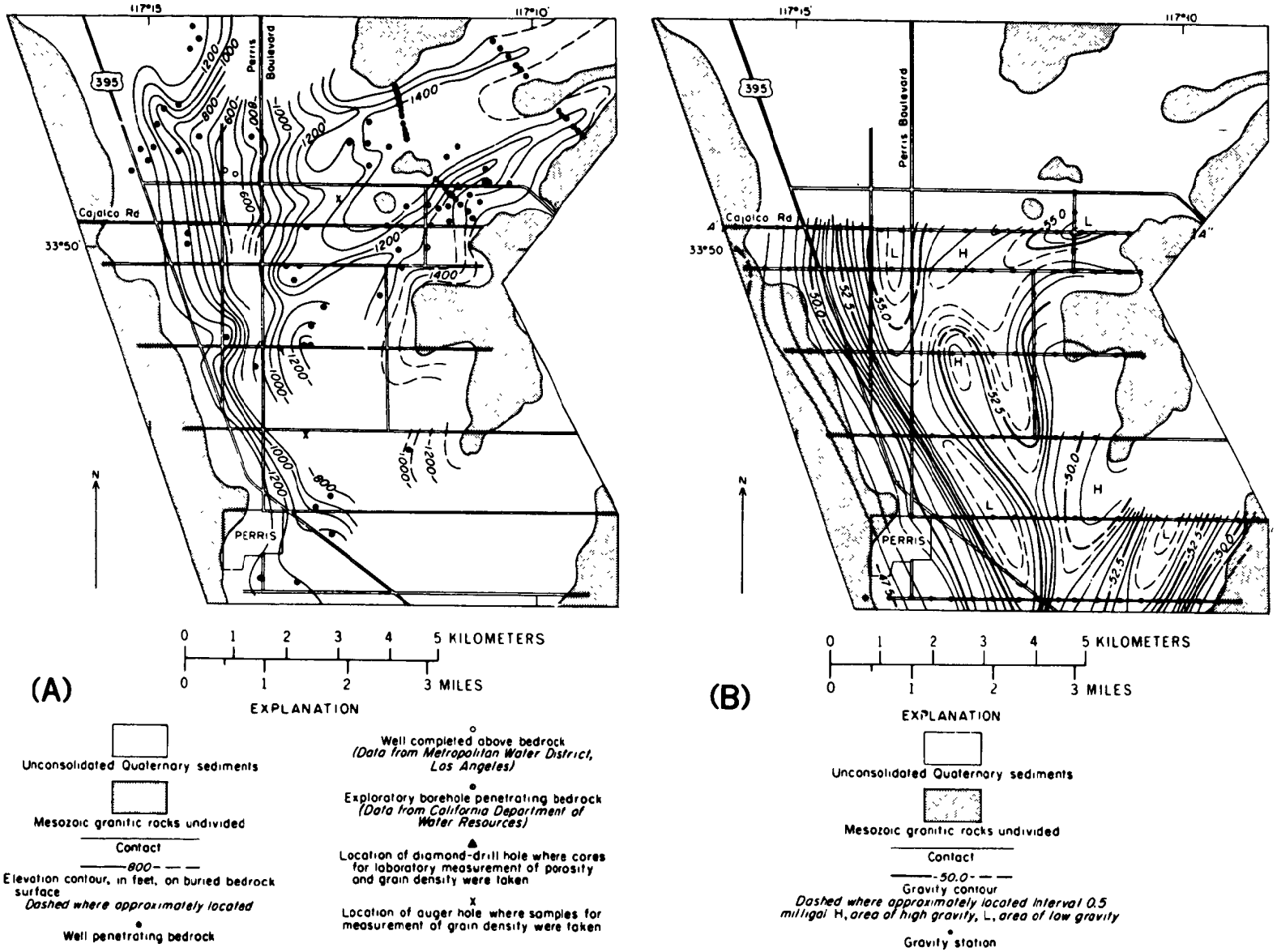

Figure 70.—A, Distribution of outcrops and structure contours on the buried bedrock surface, Perris Valley, Calif. B, Bouguer-gravity map of Perris Valley, Calif. (after Eaton and Watkins, 1970). Reproduced by permission of "Information Canada."

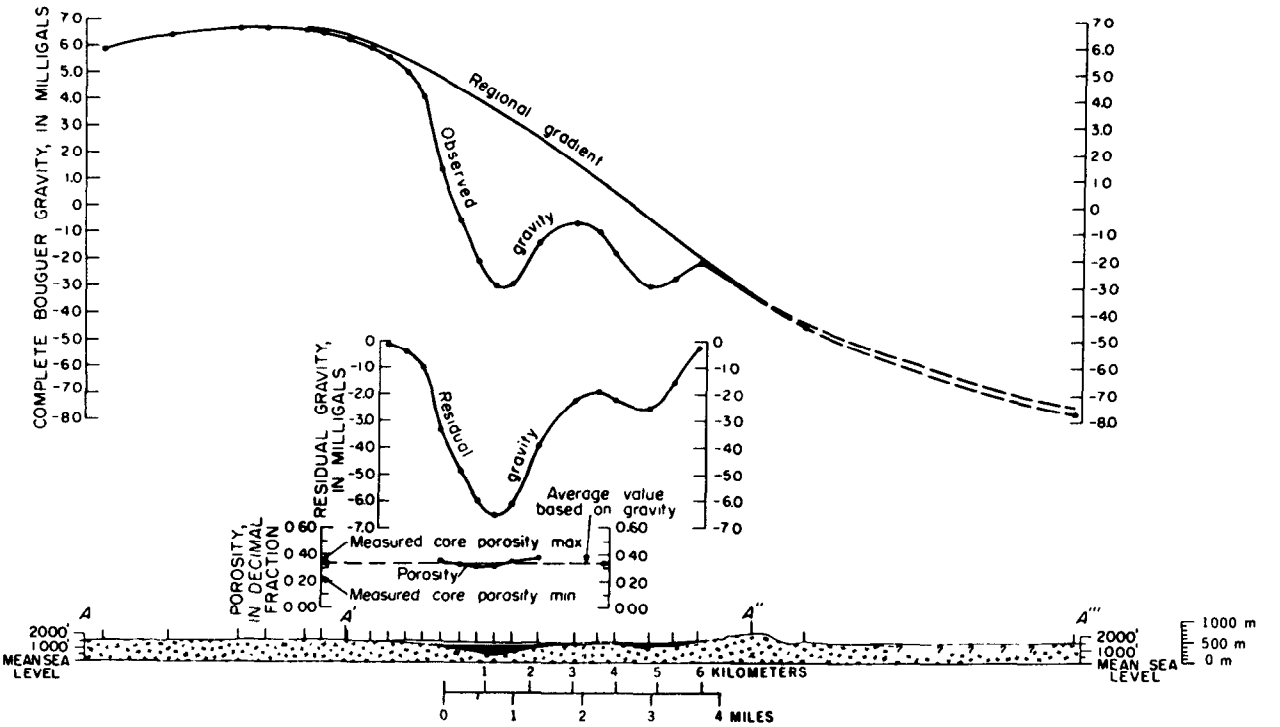

Figure 71.—Profiles of observed Bouguer gravity, residual gravity, and calculated porosity for Perris Valley, Calif. (after Eaton and Watkins, 1970). Reproduced by permission of "Information Canada."

was undertaken (Eaton and Watkins, 1970). A long gravity profile was extended beyond the borders of the map at the latitude of Cajalco Road in order to study the regional gradient. In making this profile (fig. 71), a different datum was employed from that on which the map was based. Hence the gravity values in figures 70B and 71 are different. Bedrock of fairly uniform composition (granitic rock of the southern California batholith) is exposed for many miles east and west of the valley so the eastern and western branches of the observed gravity curve were used for the regional gradient, the residual anomaly due to the low density valley fill being restricted to the central part of the area. If this gravity survey were part of a study of the batholith, or individual lithologic units within the batholith, it would have been necessary to define a different regional gradient and interpret the shape of a residual anomaly that would have included part of the regional gradient as defined here. A regional gradient is defined arbitrarily by the objective or target, which means that one must have at least an approximate idea concerning its size and nature to begin with. All parts of the observed gravity field in figure 71 have geologic origins, but we are interested in focusing our attention only on that part arising from sources close to the surface. Hence we concern ourselves with that part of the curve having the steepest gradients.

The residual gravity curve was calculated by subtracting the regional gradient from the observed gravity curve and was used, in conjunction with the geologic cross section shown below it, to calculate the average total porosity of the alluvial fill. Basically, the fill was weighed by the gravity meter, and, when its average bulk density had been determined from the gravity measurements, its porosity was calculated from the bulk density value and additional measured values of average grain density. Porosity values were calculated at six gravity stations over the central part of this valley. The results are shown in figure 71 on a porosity profile,

where the average porosity is seen to be 33 percent. For comparison, 10 samples of the fill were collected at depths ranging from 6 to 82 meters (20 to 270 feet) in a borehole nearby and found to have porosities ranging from 23 to 35 percent. No significance is attached to the convexity of the porosity profile because the resolving power of the method is not great enough to distinguish real differences as small as those shown.

Borehole Method

An in situ density log (fig. 72) of a section of unconsolidated sediments in Hot Creek Valley, Nev., was made using the U.S. Geological Survey—LaCoste and Romberg borehole gravity meter system (McCulloh and others, 1967) and shows a remarkably systematic increase in bulk density with depth in the alluvium. At a depth of approximately 975 m (3,200 feet) the sediments have a maximum density of 2.34 gm/cm^3 and remain at or near this value to a depth of 1,280 m (4,200 feet), where lake beds underlie the alluvium. The reading interval of the gravity meter in this study was fairly coarse—61 m (200 feet)—which means that the slab of material contributing to each calculation extended horizontally away from the hole to a distance of some 300 m (985 feet). A gamma-gamma log of the same hole would have sampled a zone of sediments surrounding the well that was only a few centimeters thick and it could not have been used in a cased hole. If cores or cuttings had been taken from the well in which the density log of figure 72 was run, a highly detailed, vertical profile of porosity could have been calculated. Such a profile would be clearly superior to a single, averaged value of porosity as determined in the manner shown in figure 71, but the difference in cost between these two methods is considerable.

Surface gravity measurements are used primarily in a regional search and evaluation study. Borehole gravity meter measurements are warranted only in the case of a detailed site evaluation study and require a well or borehole with a diameter of approximately 18 cm (7 in) or more in order to accept the sonde.

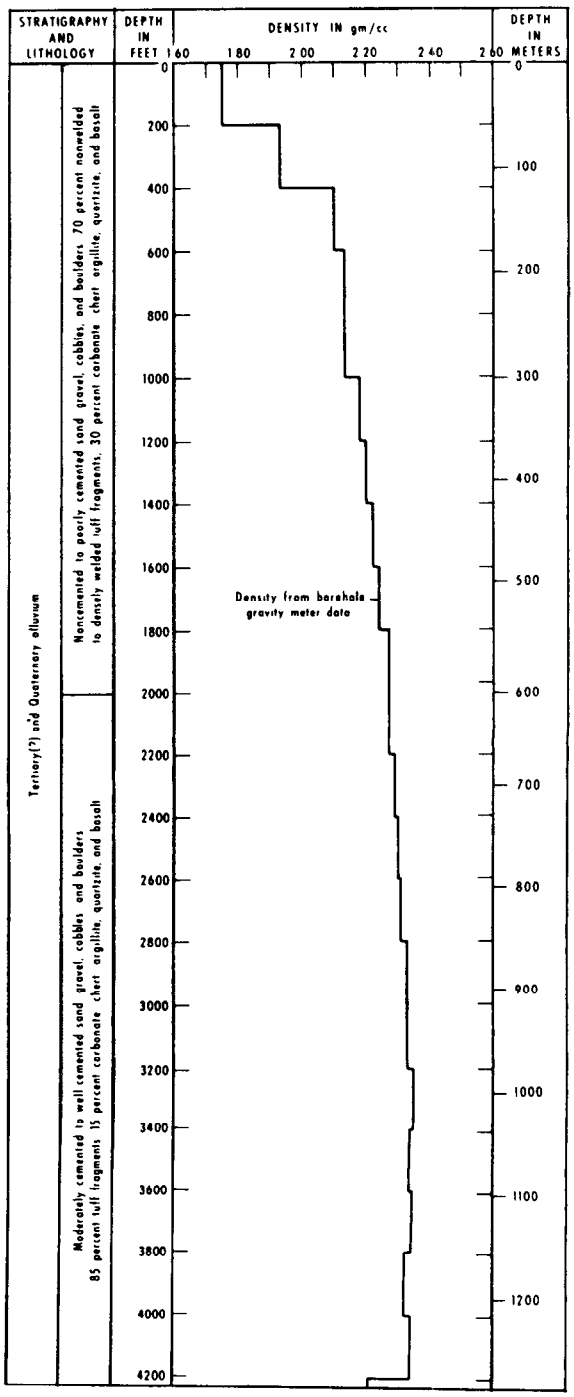

Figure 72.—In situ density log determined with a borehole gravity meter; drill hole UCe–18, Hot Creek Valley, Nev. (after Healey, 1970).

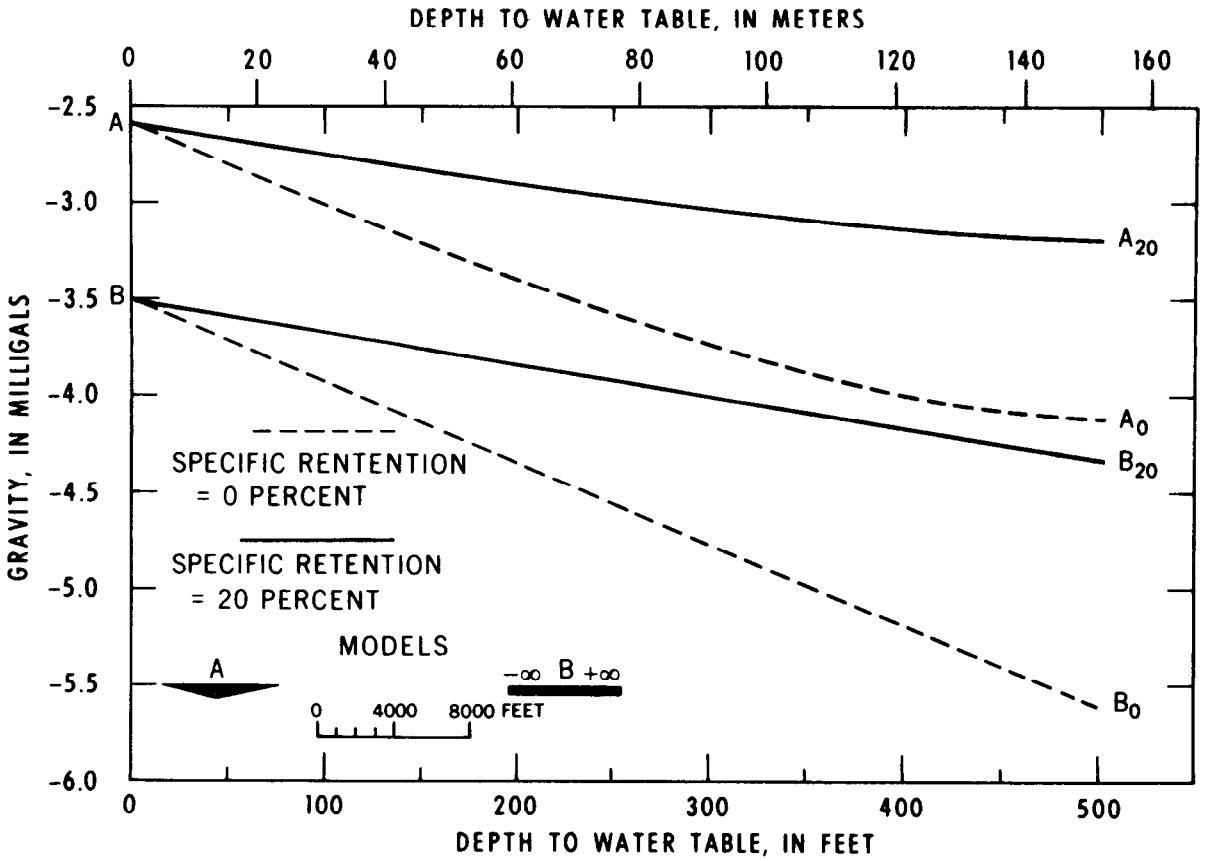

Figure 73.—Plots of gravity values versus depth to the water table for aquifers having a porosity of 33 percent and specific retentions of 0 percent and 20 percent, respectively. A, triangular aquifer, and B, infinitely extensive sheetlike aquifer.

Effect of Ground-Water Levels on Gravity Readings

Water in the interstices of a rock contributes to the total mass of the rock and if porosity is moderate or high, this effect is detectable with a gravity meter. For example, gravity effects resulting from changes of water level in two different aquifers are shown in figure 73. One of these aquifers is an idealized buried stream channel with triangular cross section and the other is a sheetlike deposit of unconsolidated sediment. The gravity effects plotted in this figure are the largest that would be observed, which, for the buried channel, are measured over its center. The physical properties of the rocks employed in calculating the gravity effects displayed by this model were as follows: bedrock density, 2.67 gm/cm^3; bedrock porosity, 0 percent; dry bulk density of the unconsolidated material, 1.79 gm/cm^3; porosity, 33 percent. Curves for two different values of specific retention (0 and 20 percent) in the unsaturated zone are shown. Curves for materials with intermediate values of specific retention fall between the two curves shown in the figure.

A water table decline of approximately 30 meters (100 feet) in a sheetlike aquifer produces a maximum gravity change of 0.42 mgal if the specific retention of the deposit has the limiting value of zero. If the specific retention is 20 percent, a more realistic value, the gravity change is only 0.17 mgal. Because of the peculiarity of the gravitational field of an infinite sheet, its gravity effect is the same regardless of the distance to the point of measurement, that is, the depth to the water table. Furthermore, the slopes of

the curves from this model are linear and are a function of the specific yield. If water-level declines in a water-table aquifer of this configuration are monitored with a gravity meter the results can be translated into a measure of the aquifer's specific yield. In areas of long-period water-table decline, repeated gravity measurements, coupled with water-level observations at a few wells, would suffice for a calculation of specific yield, independent of well tests.

This use of the gravity method requires the utmost in precision and accuracy. A gravity difference of 0.17 mgal is a small one to measure accurately and its achievement depends on accuracy at every stage of the data reduction process.

References Cited

Bancroft, A. M., 1960, Gravity anomalies over a buried step: Jour. Geophys. Research, v. 65, p. 1630–1631.

Bott, M. H. P., and Smith, R. A., 1958, The estimation of the limiting depth of gravitating bodies: Geophys. Prospecting, v. 6, p. 1–10.

Clark, S. P., Jr., ed., 1966, Handbook of physical constants (revised edition): Geol. Soc. America Mem. 97, 587 p.

Cushman, R. V., 1964, Ground-water resources of north-central Connecticut: U.S. Geol. Survey Water-Supply Paper 1752, 96 p.

Dobrin, M. B., 1960, Introduction to geophysical prospecting: New York, N.Y., McGraw-Hill Book Co., Inc., 446 p.

Eaton, G. P., Martin, N. W., and Murphy, M. A., 1964, Application of gravity measurements to some problems in engineering geology: Engineering Geology, vol. 1, no. 1, p. 6–21.

Eaton, G. P., and Watkins, J. S., 1970, The use of seismic refraction and gravity methods in hydrogeological investigations: Proc. Canadian Centennial Conf. Mining and Ground-Water Geophysics, Ottawa.

Grant, F. S., and West, G. F., 1965, Interpretation theory in applied geophysics: New York, N.Y., McGraw-Hill Book Co., Inc., 583 p.

Healey, D. L., 1970, Calculated in situ bulk densities from subsurface gravity observations and density logs, Nevada Test Site and Hot Creek Valley, Nye County, Nevada: U.S. Geol. Survey Prof. Paper 700-B, p. 52–62.

Manger, G. E., 1963, Porosity and bulk density of sedimentary rocks: U.S. Geol. Survey Bull. 1144–E, 55 p.

McCulloh, T. H., 1965, A confirmation by gravity measurements of an underground density profile based on core densities: Geophysics, v. 30, p. 1108–1132.

McCulloh, T. H., LaCoste, L. J. B., Schoellhamer, J. E., and Pampeyan, E. H., 1967, The U.S. Geological Survey—LaCoste and Romberg precise borehole gravimeter system—Instrumentation and support equipment, *in* Geological Survey Research 1967: U.S. Geol. Survey Prof. Paper 575–D, p. D92–D100.

Nettleton, L. L., 1954, Regionals, residuals and structures: Geophysics, v. 19, p. 1–22.

Schwennesen, A. T., 1917, Ground water in San Simon Valley, Arizona and New Mexico, *in* Contributions to the Hydrology of the United States, 1917: U.S. Geol. Survey Water-Supply Paper 425, p. 1–35.

White, N. D., 1963, Analysis and evaluation of available hydrologic data for San Simon Basin, Cochise and Graham Counties, Arizona: U.S. Geol. Survey Water-Supply Paper 1619–DD, p. DD1–DD33.

Magnetic Methods

By D. R. Mabey

The magnetic method of geophysical exploration involves measurements of the direction, gradient, or intensity of the Earth's magnetic field and interpretation of variations in these quantities over the area of investigation. Magnetic surveys can be made on the land surface, from an aircraft, or from a ship. Most exploration surveys made today measure either the relative or absolute intensity of the total field or the vertical component. Measurements of magnetic intensity can be made with simple mechanical balances or with elaborate electronic instruments.

The unit of magnetic intensity used almost exclusively in exploration geophysics is a gamma (γ). A gamma is defined as 10^{-5} oersted; an oersted is the magnetic intensity at a point that will exert a force of 1 dyne on a unit magnetic pole. The intensity of the magnetic field on or above the surface of the Earth is dependent upon the location of the observation point in the primary magnetic field of the Earth and local or regional concentrations of magnetic material. The intensity of the Earth's undisturbed magnetic field ranges from a minimum of about 25,000 γ at the magnetic equator to more than 69,000 γ near the magnetic poles. Over the United States, exclusive of Hawaii, the range is from 49,000 to 60,000 γ.

Magnetic anomalies are distortions of the magnetic field produced by magnetic material in the Earth's crust or perhaps upper mantle. Magnetic anomalies of geologic interest are of two types: induced anomalies and remanent anomalies. Induced anomalies are the result of magnetization induced in a body by the Earth's magnetic field. The anomaly produced is dependent upon the geometry, orientation, and magnetic properties of the body, and the direction and intensity of the Earth's field. Because of the dependence on the direction of the Earth's field, magnetic anomalies produced by similar bodies may differ widely with geographic location. Remanent anomalies are the result of "permanent" magnetization of a body and are controlled by the direction and intensity of remanent magnetization and the geometry of the disturbing mass. Most magnetic anomalies are a combination of the two types, but usually one type of magnetization is dominant and the other can be ignored in the approximate interpretation of results.

Several types of information can be obtained from magnetic surveys. The character of a magnetic anomaly is often indicative of the type of rock producing the anomaly, and an experienced interpreter can identify a general rock type on the basis of character of the magnetic anomalies observed. Quantitative interpretation of individual magnetic anomalies yields information on the depth of burial, extent, structure, and magnetic properties of rock units. The most common use of magnetic data in ground-water studies is to map the depth to the magnetic basement rock.

Sedimentary rocks are the most common aquifers. However, most sedimentary rocks are essentially nonmagnetic and thus not amenable to direct study by magnetic methods. A few clastic rocks, such as some stream deposits and beach sands, do contain magnetic minerals and can be studied directly.

Igneous and metamorphic rocks generally contain a larger proportion of magnetic minerals and are therefore more magnetic than sedimentary rocks but of less interest in

ground-water investigations; however, determination of the configuration of the surface of a basement complex composed of igneous and metamorphic rock underlying water-bearing sediments is important in nearby ground-water studies. In general the darker, more basic, rocks are more magnetic than the light colored, acidic rocks. Some volcanic rocks, particularly basalts in the northwestern United States, are important aquifers.

Magnetic Surveys

Magnetic surveys may be very simple or very complex, depending on the objectives of the survey. The amplitude of magnetic anomalies range from less than 1 γ to several thousand gammas; horizontally the extent of these anomalies ranges from less than 1 m to tens of kilometers. The anomalies of larger amplitude can be defined with simple instruments and procedures; the small anomalies may require complex ones.

The simplest instruments for measuring magnetic intensity involve balancing the force exerted by the vertical component of the Earth's magnetic field on a magnet against the force of gravity. The simplest of these instruments, the dip needle, can be used to map the location of anomalies with amplitudes of several hundred gammas. With the Schmidt-type vertical balance, sensitivity of a few gammas can be obtained. Torsion instruments of comparable sensitivity also are available. Most types of mechanical instruments used to measure magnetic intensity are simple to operate and, if protected from mechanical damage, are trouble free. Generally, the higher the sensitivity of a mechanical instrument for measuring magnetic intensity, the more care and time required to orient the instrument and complete an observation.

Several nonmechanical methods for measuring magnetic intensity are in common use. The fluxgate (magnetic saturation) magnetometers can be made sensitive to less than 1 γ, but most handheld units have sensitivities of a few tens of gammas. Proton-precession magnetometers range in sensitivity from less than 1 gamma to a few gammas. Optical-absorption magnetometers are capable of measuring magnetic fields to 0.01 γ. All these instruments can be adapted for use on a moving platform, and pairs of the optical-absorption magnetometers can be used to measure gradients.

The design of a magnetic survey is based on the character of the magnetic anomalies expected and the type of interpretation to be made of the magnetic data. Airborne magnetic surveys measuring variations in the total magnetic intensity are the most common methods of obtaining magnetic data. To minimize magnetic disturbances from the aircraft, the magnetic sensor normally is towed from the aircraft or mounted in a boom extending from the aircraft. Magnetic data are obtained continuously along a flight path. Although low-level flights may be prohibited in populated areas, access is usually not a major problem in airborne surveys. Continuous magnetic measurements also can be made from a motor vehicle or boat if the sensor can be located a few feet from the parts of the vehicle containing large masses of iron.

Time variations in the magnetic field, which must be corrected for, are important in some surveys. Secular variations are long term changes and usually can be ignored, but in special situations must be considered. Of much greater importance are variations with a period of a day or less and with amplitudes ranging from less than 50 γ for a normal day to 1,000 γ in high latitudes during magnetic storms. A correction for solar diurnal variations with an average range of about 30 γ usually can be made by repeated observations of a magnetometer station or profile during a surveying day. If accuracy of a few gammas or less is to be obtained, a continuous record of the magnetic variations at a location within or near the survey area is required.

For most exploration purposes it is only necessary to measure relative magnetic in-

tensity over the area of interest. Thus, an arbitrary magnetic datum can be used for each map or profile.

Magnetic Properties

The magnetic susceptibility and remanent magnetization of rocks are the properties of interest in magnetic surveys. Susceptibility is a measure of the ability of a rock to acquire a magnetization in the presence of a magnetic field. Remanent magnetization is the permanent magnetization of rock and is not dependent on any contemporary external field. The ratio of the remanent magnetization to induced magnetization is the Q ratio.

Induced magnetization is defined by the formula $M = KH_o \times 10^{-5}$ where K is the susceptibility in cgs units and H_o is the intensity of the applied field in gammas. Susceptibility of a rock is primarily dependent upon the composition and internal structure of the rock. The magnetic susceptibility of most rocks depends primarily on the content of magnetite and pyrrhotite, the two most common magnetic minerals.

Although remanent magnetization can be acquired by a rock in several ways, thermoremanent magnetization is the most important type. As an igneous rock cools through the Curie temperature (585°C for magnetite), it acquires a magnetization parallel to the Earth's field. This thermoremanent magnetization is usually stable and remains with the rock through subsequent changes in the direction of the Earth's field. Most volcanic rocks are magnetic and many have strong remanent magnetization. Over near-surface volcanic rocks the magnetic intensity may vary widely over short distances, and detailed observations are required to define the magnetic field near the surface. Although in many places the presence of volcanic rocks can be inferred from the character of the magnetic field, the geologic significance of many of the very local magnetic features over volcanic rocks is not determined easily.

Design of Magnetic Surveys

The precision of the measurements, the detail obtained, and, with airborne surveys, the flight level, determine the cost of the survey as well as the usefulness of the data. Ideally a magnetic survey should define the major features of the magnetic field at a level which will resolve all anomalies of interest; however, the cost of obtaining this detail may be prohibitive. A more realistic objective in areas of complex geology is to obtain sufficient data to resolve the major geologic uncertainties. Where rock type is to be determined, a survey that indicates the general character of the field without defining individual anomalies may be adequate, and where approximate depth to basement rock is to be determined, gradients along profiles may be adequate data.

Detailed data along a single profile may be more useful than isolated observations distributed over the entire area of interest because most quantitative magnetic interpretation methods involve analysis of details of a magnetic anomaly (such as the extent of a uniform gradient, location of inflection points, or the position or amplitude of highs or lows).

Planning a magnetic survey involves three major decisions:

1. Can the data be best obtained by a ground or airborne survey? For all except extremely detailed work, most geophysicists prefer airborne data to ground data. However, the minimum cost of an airborne survey may be prohibitive.
2. What precision is required? This determination will be based on the nature of the anomalies anticipated and the methods of interpretation to be attempted. For a ground survey this will determine the selection of a magnetometer, and the method used to correct for diurnal magnetic variations. Most magnetometers used in airborne surveys are capable of sufficient precision for most needs. However, if anomalies

of very small amplitude are significant, the use of an optical-absorption magnetometer may be required.

3. What detail is required? This consideration will govern the station spacing for ground surveys and the flightline spacing and flying height for airborne surveys. The problems relating to detail are discussed in the section on interpretation.

Data Reduction

The reduction of magnetic data is relatively simple. Proton-precession and optical-absorption magnetometers measure the absolute value of the Earth's field. Other magnetometers provide a relative measure. The readings from the latter may be in gammas or may require adjustment by a scale factor. Ground magnetometers generally are referenced to a base station or a stationary magnetometer. If a base magnetometer is operated, the difference between the reading of the base magnetometer and the survey magnetometer at the observation time multiplied by the appropriate calibration constants will be the value for the station. If repeat readings at a base station are used as the method for determining diurnal variations, enough repeat readings must be obtained to construct a curve showing the variations of magnetic intensity with time.

In most airborne surveys, continuous or nearly continuous observations are made. The data are recorded on a paper chart or magnetic tape. The flight path of the aircraft is recorded in some manner, most commonly by photographing the path or by electronic navigation systems. The flight path is plotted and the data adjusted for variation in aircraft speed, instrument drift, and diurnal magnetic variations.

Magnetic data can be presented in profile form or as contour maps. Although magnetic contours provide an effective way of illustrating many magnetic features, some of the information that is available on continuous profiles cannot be illustrated on a contour map. Therefore, profiles commonly are used in making detailed interpretations.

Interpretation of Magnetic Data

The magnetization of most major rock units is complex and the details of the magnetic anomalies are also complex. This, coupled with the inherent ambiguity, makes the comprehensive interpretation of magnetic anomalies a complex art.

The two major applications of magnetic surveys to ground-water studies have been the study of magnetic aquifers, mainly basalt, and the determination of the configuration of the basement rock underlying the water-bearing sediments. The study of magnetic aquifers involves the identification of rock type and, in some studies, the determination of geometry and magnetic properties. The study of basement-rock configuration generally involves determining the depth to the surface of the basement at several points and perhaps contouring the depths, but may also include determining relief on the basement surface, such as displacement across a fault.

Major magnetic rock units commonly produce magnetic anomalies with characteristics that can be identified and used to infer the presence or absence of the rock. Volcanic rocks may produce high amplitude magnetic variations of very local extent. Negative magnetic anomalies produced by permanent magnetization in a direction approximately opposite to the Earth's magnetic field may be associated with volcanic rocks. Large igneous intrusives produce anomalies with a wide range of amplitudes, but generally of greater extent and less complex than the anomalies associated with volcanic rocks, and often approach the theoretical anomaly produced by simple geometric forms. Metamorphic rocks may produce complex patterns and pronounced lineaments are common. Most sedimentary rocks are nonmagnetic, but magnetite-bearing sands and gravels are a notable exception.

An experienced interpreter generally can identify rock type by inspection of the magnetic anomalies; however, such an interpretation is necessarily subjective. Contacts between units of differing magnetic properties can be identified on magnetic maps and profiles or traced in the field by dip needle or simple magnetometer surveys.

To determine the thickness of nonmagnetic sedimentary rock overlying a magnetic basement, we assume that an observed anomaly is produced by a magnetic mass extending upward to the surface of the basement. Several features of such an anomaly, such as the extent of the steepest gradient and the distance between various identifiable points on the anomaly, are used. Assumptions must be made concerning the geometry of the disturbing mass, but these assumptions generally are not critical. No assumption need be made on the physical properties of the rocks involved. Several procedures are used in this type of interpretation, and it is beyond the scope of this report to describe the methods. Vacquier and others (1951) describe a widely used technique for determining depths from magnetic anomalies and also illustrate a variety of anomalies. As a generalization, the closer the level of observations to a disturbing mass, the steeper the magnetic gradients and the smaller the extent of major features on the anomaly.

Under optimum conditions depth estimates made by a skilled interpreter are within 10 to 20 percent of the actual depths, and, in many sedimentary basins, good contour maps on the basement surface have been prepared from magnetic data. Aeromagnetic surveys have proven especially effective and valuable in reconnaissance surveys of sedimentary basins where large areas must be explored quickly and where access on the surface is a problem. In some basins the sedimentary rock thicknesses obtained from magnetic data are more reliable than can be obtained by any other geophysical method.

The ambiguities inherent in the interpretation of magnetic data limit the extent to which the magnetic data can be used to infer the geometry of a disturbing mass. However, if detailed magnetic data are available, curve-matching techniques can be used effectively in identifying simple geometric forms that could produce an observed anomaly. The character of many magnetic anomalies will indicate the form and the attitude of the disturbing mass. For example, the anomaly produced by steeply dipping tabular bodies can be identified as reflecting a tabular body, and, by assuming the direction of magnetization (generally parallel to the Earth's magnetic field), the position, strike, and approximate dip of the body can be inferred. In some situations the width and magnetic properties also can be inferred. Bodies of more complex geometry are also amenable to modeling or curve matching, but as the geometric complexity increases, the uncertainties of the interpretation become greater. In most curve-matching or modeling procedures, uniform magnetization of the disturbing mass, as well as the enclosing material, is assumed. For large bodies this assumption may not be justified, and the resulting interpretation is subject to large errors.

Some magnetic anomalies reflect variation in thickness or surface elevation of a magnetic unit. Computations of these thickness or elevation changes require the assumption of magnetic properties. Thus, the location of these features may be inferred, but the thickness or relief may be uncertain if information is not available on the magnetic properties.

Albums of computed magnetic anomalies for masses of simple geometry and magnetization are being produced. Probably the best albums currently available are Vacquier and others (1951) and Andreasen and Zietz (1969).

Examples of Magnetic Surveys

Gem Valley, Idaho

Magnetic surveys have been used in the study of basalt aquifers in several areas,

particularly in the Snake River Plain and Columbia Plateau, with varying degrees of success. Magnetic data from Gem Valley in southeastern Idaho illustrate some of the potentials and limitations of magnetic surveys in the study of volcanic rocks (Mabey and Oriel, 1970).

Gem Valley is an intermontane basin about 56 km (35 miles) long and as much as 13 km (8 miles) wide. The enclosing ranges are Paleozoic sedimentary rocks. Much of the valley floor consists of Cenozoic basalt flows from vents in the southeastern part of the valley and from an extensive volcanic field northeast of the valley. The basalt flows inundated a surface of unknown relief on the older Cenozoic sediments. Post-basalt sediments overlap the basalt in several areas but in most of the valley the basalt is overlain by a thin cover of windblown soil. Water is pumped from basalt in several parts of the valley and information on the extent, thickness, and structure of the basalt is important to ground-water investigations in the valley.

The first magnetic observations in the valley consisted of measurements with a magnetometer mounted on a 1-m tripod. The magnetic field in areas where the basalt was within a few feet of the surface varied several hundred gammas over distances of a few meters. These abrupt variations reflect the magnetization of the upper few meters of the basalt and were of little value in determining the thickness or gross structure of the flows, so the survey was abandoned. The method could have been used to locate the edge of the basalt where it was at shallow depths.

An aeromagnetic profile (fig. 74) flown across the valley about 230 m (755 feet) above the surface defines a complex magnetic pattern, but broad features are apparent and the edge of the basalt is apparent at the ends of the profile. A survey made about 1,200 m above the valley (fig. 75) reveals anomalies that appear to reflect the thickness of the basalt except in the area of anomaly B, which is a large anomaly associated with eruptive centers. Of particular significance to the ground-water investigations is the high magnetic trend A. Three wells indicated that the base of the lowest basalt flow in this area was about 100 m (330 feet) below the surface and that about 70 percent of the material above this level was basalt and 30 percent interbedded sediments. Using this as control, a two-dimensional form that would produce the shape of the measured anomaly was computed using a digital computer and the magnetization of the basalt necessary to produce the amplitude of the measured anomaly was calculated. The magnetic anomaly could be produced by a prism of basalt about 1,000 m (3,300 feet) wide and parallel to the trend of the anomaly. The western edge of the prism, which presumably is a pre-basalt river channel, was inferred along with the thickness of basalt east of the channel. Subsequent resistivity soundings have confirmed the existence of the channel.

Using the magnetization determined in the above analysis, computations were made of the approximate thickness of basalt that would produce the measured anomalies in other parts of the valley. In the area of the large positive anomaly B, the magnetic field appears to be strongly affected by intrusive units relating to the eruptive centers, and the magnetic data cannot be used to infer the thickness of basalt in this area.

Gem Valley is not a typical example of the application of magnetic surveys in the

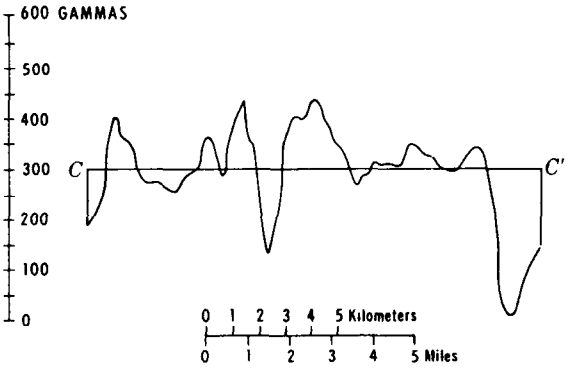

Figure 74.—Aeromagnetic profile at 230 m (755 feet) above Gem Valley, Idaho. Location of profile shown in figure 75.

study of volcanic aquifer problems, but it does illustrate some of the possible applications and limitations: (1) Magnetic surveys generally are effective in detecting and determining the extent of concealed volcanic rocks, and the approximate depth of burial of the volcanic rock can be inferred; and (2) quantitative interpretations of the thickness and structure of volcanic rock can be made in some simple situations, but generally cannot be made where a thick sequence of flows occurs or where the volcanic rocks are underlain by strongly magnetic rocks.

Antelope Valley, California

If a sedimentary basin is underlain by magnetic basement rock, magnetic surveys may be an effective tool in studying the structure of the basin. An example of this application of magnetic measurements is an aeromagnetic profile in eastern Antelope Valley, Calif. (fig. 76). The basement in this part of Antelope Valley is igneous rock of approximately quartz monzonite composition. A Cenozoic basin several thousand feet deep has been defined by drilling and gravity measurements on the south side of Rosamond Lake (Mabey, 1960). Figure 76 illustrates the aeromagnetic and gravity profiles across the basin, and the configuration inferred from the gravity data and one deep drill hole (not along the profile) that did not penetrate the basement rock.

On the southern half of the profile are three local magnetic anomalies produced by lithologic variations in the basement rock. The character of these anomalies, which is better revealed on a contour map, is typical of anomalies over quartz monzonite in this part of the Mojave Desert. A skilled interpreter would infer from these anomalies that the rock producing the anomalies is similar to the quartz monzonite exposed a few miles to the east. Depths determined for sources of anomalies A and B were used to supplement the gravity data as control for the base of basin fill along the southern part of the profile. This interpretation involved assumptions on the geometry of the disturbing mass, which were not critical, and the assumption that the top of the disturbing mass extended to the top of the basement. However, because the determination of depths from these magnetic anomalies does not involve assumptions of physical properties or the removal of a regional gradient as do the gravity data, the magnetic depths for this part of the profile are more reliable than the depths determined from the gravity data. The magnetic data provide only two depths and do not provide a continuous indication of the depth to basement along the profile.

Near the north end of the profile is a double-peaked magnetic high. The extent of the gradients on this high indicate an elevation of the top of the magnetic mass consistent with the elevation of the basement surface inferred from the gravity. The contrast in character between this anomaly and the anomalies at the south end of the profile suggests a difference in magnetic properties of the rock producing the anomalies, although all the anomalies probably are produced by intrusive rocks.

The magnetic low near the center of the profile is over the deepest part of the basin, but the lowest value is produced by the steeply dipping interface, probably a fault on the south side of the basin. The location of the fault and also a crude approximation of the vertical displacement could be inferred from the magnetic anomaly. Over the deepest part of the basin no local magnetic anomalies suitable for precise depth analysis were recorded; therefore, the thickness of the basin fill in this area could not be determined from the magnetic data. Variations in the general level of magnetic intensity over the central and southern part of the profile, computed assuming a susceptibility contrast of 1.7×10^{-3} cgs units, agree with the measured intensity. Along most of the southern part of the profile the computed intensity is higher than the measured level, suggesting that the rock underlying this area has a lower susceptibility than the rock to the south.

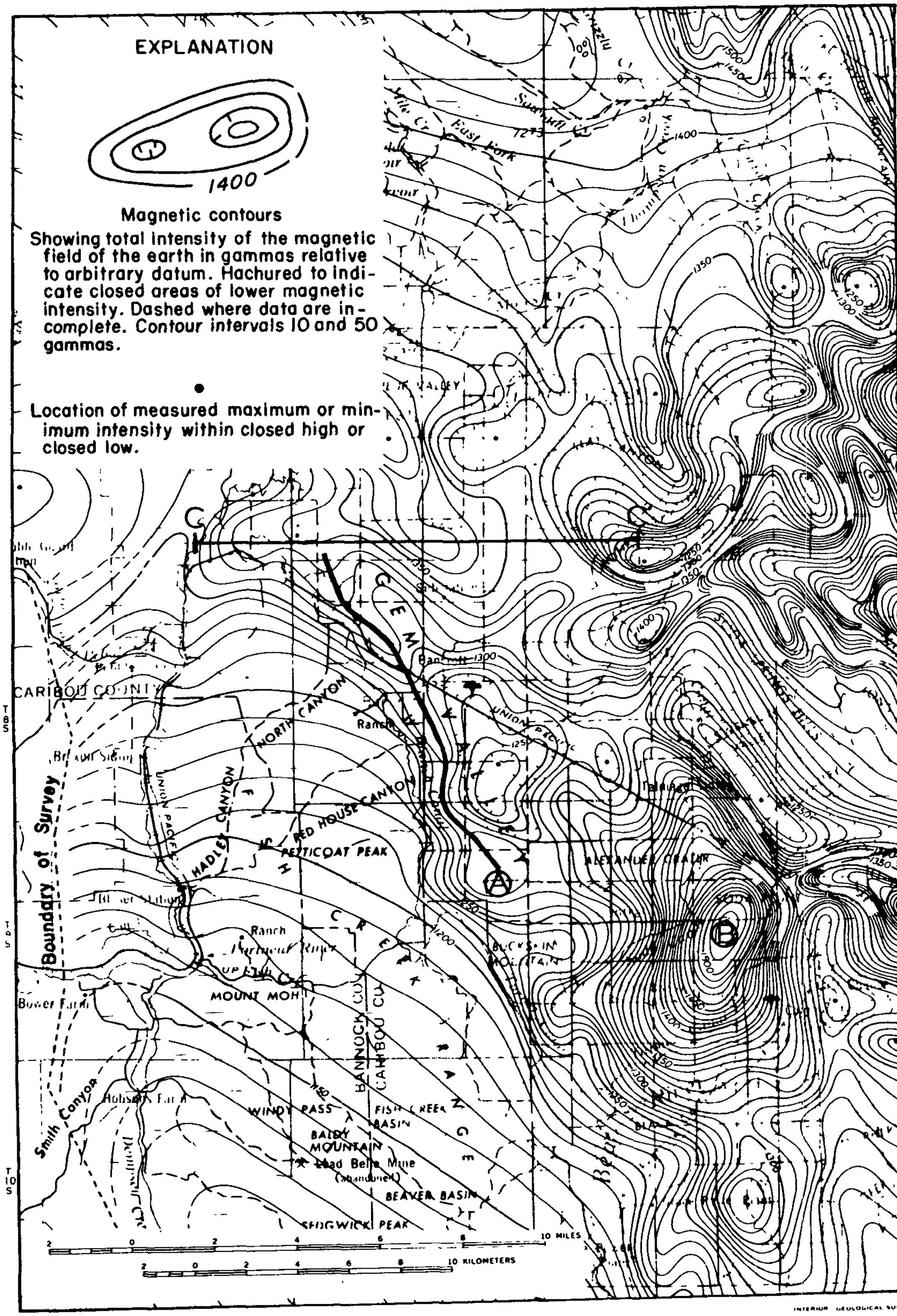

Figure 75.—Aeromagnetic map of Gem Valley and adjoining areas, Idaho. Survey flown at 2,700 m (8,900 feet) above sea level along east-west flightlines 1.6 km (1 mile) apart. The valley floor is about 1,700 m (5,600 feet) above sea level.

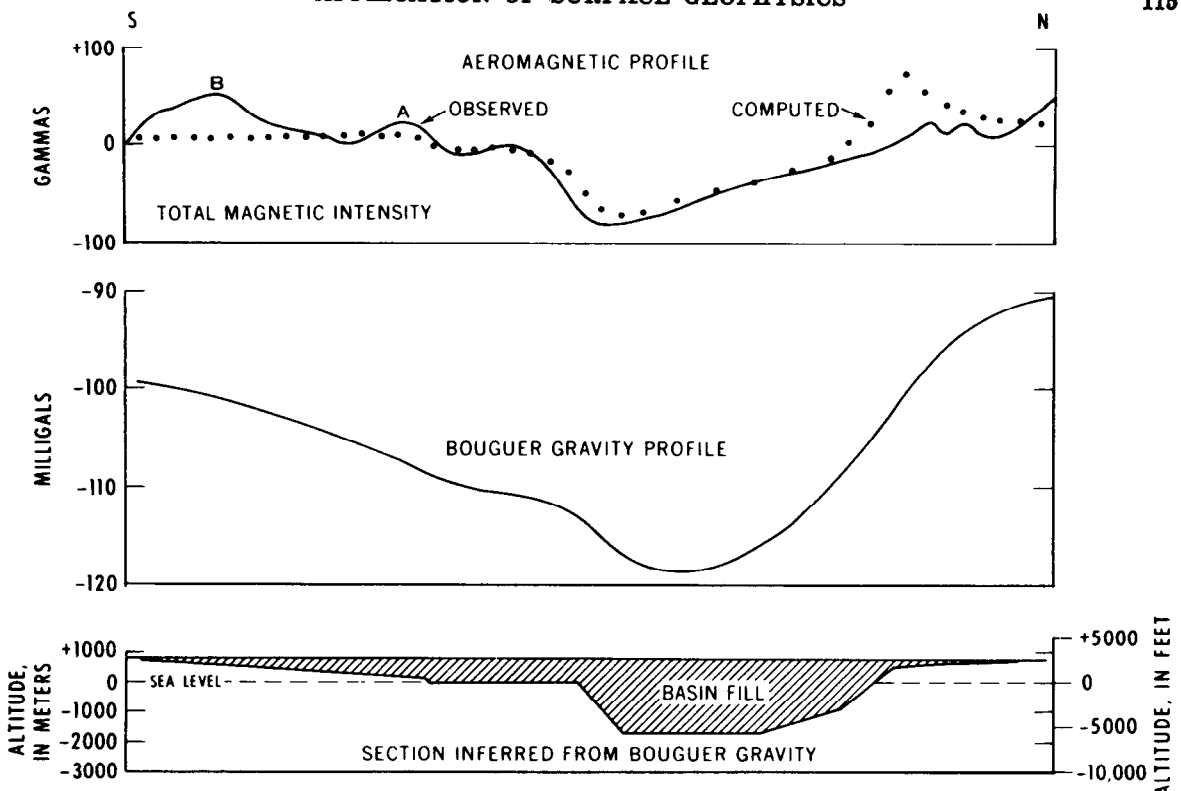

Figure 76.—Gravity and aeromagnetic profiles across Cenozoic basin in Antelope Valley, Calif. Aeromagnetic profile flown at 150 m (500 feet) above ground level.

The application of magnetic surveys to the study of sedimentary basins can be summarized as follows:

1. The basement rock underlying the sedimentary basin must be magnetic and the basin sediments nonmagnetic in order to make basement depth determinations. Lithologic contrasts within most metamorphic and igneous basement complexes produce magnetic anomalies that can be analyzed to determine approximate depth to the top of the basement.
2. Accurate depths can be determined only where anomalies amenable to depth analysis occur; therefore, depth information may not be evenly distributed and may be completely lacking in some areas.
3. Anomalies caused by relief on a magnetic basement generally can be used to locate structures but may not be amenable to quantitative interpretation.

References Cited

Andreasen, G. E., and Zietz, Isidore, 1969, Magnetic fields for a 4×6 prismatic model: U.S. Geol. Survey Prof. Paper 666, p. 9.

Mabey, D. R., 1960, Gravity survey of the western Mojave Desert, California: U.S. Geol. Survey Prof. Paper 316–D, p. 51–73.

Mabey, D. R., and Oriel, S. S., 1970, Gravity and magnetic anomalies from the Soda Springs region, southeastern Idaho: U.S. Geol. Survey Prof. Paper 646–E, 15 p.

Vacquier, Victor, Steenland, N. C., Henderson, R. G., and Zietz, Isidore, 1951, Interpretation of aeromagnetic maps: Geol. Soc. America Mem. 47, 151 p.

Cost of Geophysical Surveys in 1970

Electrical Methods

Deep resistivity surveys normally are made with a 6-man crew, equipment costing between $5,000 and $10,000, and two vehicles. Two of the crew members should be technically trained, but the other positions require no special training. The major cost of the field operation is the salary and expenses of the crew. The average cost of one crew-month including preliminary data interpretation is about $10,000. Under normal conditions in one month a crew could make about 50 soundings to a depth of 900 m (3,000 feet), 100 soundings to 150 m (500 feet), or 80 km (50 miles) of profiling to 150 m (500 feet).

The cost of induced-polarization surveys is somewhat greater than resistivity surveys. Electromagnetic surveys are usually less expensive and the coverage may be more rapid.

Telluric and magneto-telluric surveys are generally experimental and generalizations on cost and coverage are not meaningful.

Gravity Surveys

The cost of gravity surveying varies widely, depending on the station density required, the accessibility of the stations, and the presence or absence of adequate elevation control. In detailed studies of near-surface effects, where the station spacing is measured in terms of hundreds of feet, the cost, exclusive of elevation surveying, can be as low as $5 per station with the data reduced and interpreted in preliminary fashion. If the elevations in such a study must be established independently, the cost will be approximately double. At the other extreme, for widely scattered stations in mountainous or hilly terrain, where backpacking or helicopter support is required, the cost may rise to $25 or $30 per station. The nature of the problem will dictate the required station spacing, at least approximately, and estimates of cost are best made after a preliminary assessment of the problem, a study of the terrain, and a check on the avability of elevation control.

Seismic Surveys

The cost of seismic refraction surveys, including interpretation, varies from $600 to $750 per linear mile of coverage, depending on the geophone spacing. Shallow soundings, with short geophone spacings, are the more expensive, but provide more detailed information than do deeper soundings. If the objective (for example, the basement surface) is as much as 3,000 m (10,000 feet) below the surface, geophone spreads several miles long will be required to define the surface. The completed cost for a single depth determination may be as much as $2,500 to $3,000. On the other hand, for a refractor at a depth of 300 m (1,000 feet), only a mile or so of shooting would be required for definition and the consequent cost would be somewhere in the neighborhood of $700.

Magnetic Surveys

Aeromagnetic surveys, which measure total magnetic intensity, normally cost between $5 and $15 per flightline mile depending primarily on the size of the area to be surveyed. This cost includes the preparation of a contour map and profiles along flightlines. The major cost of a ground survey is the salary and expenses for the crew (one or two men) and transportation. Using electronic magnetometers, a magnetometer observation can be made in less than 1 minute.